

ABSTRACT

FEESE, ELKE. Development of Novel Photosensitizers for Photodynamic Inactivation of Bacteria. (Under the direction of Dr. Reza A. Ghiladi).

In the age of rising bacterial drug resistance against currently marketed antibiotics, new and supplemental treatment regimens are desperately needed. This particular work is motivated by the current public health threat posed by infection with *Mycobacterium tuberculosis*, the causative agent of tuberculosis. Tuberculosis is one of the world's leading causes of death due to a single disease with 9.2 million new infections and 1.7 million deaths reported for 2006 alone. Efforts to control tuberculosis infection have been hampered by the rise of multiple drug-resistant strains, thereby sparking a new round of interest in alternative treatment options, novel drug targets, as well as a more profound understanding of the origins and mechanisms involved in the development of drug-resistance.

Chapter 2 investigates the feasibility of photodynamic inactivation (PDI) as an alternative approach to current drug-based tuberculosis treatments. Significant advances made in the past decade in treating several forms of cancer with photodynamic therapy suggest that photodynamic inactivation of localized bacterial infections might allow for the development of a valuable alternative or supplemental option to the current antibiotic-based treatments. PDI employs a localized, light-activated photosensitizer that generates cytotoxic species, particularly singlet oxygen, upon illumination with visible light. The non-pathogenic *M. smegmatis* was employed as a surrogate for *M. tuberculosis* and the reduction in colony forming units was examined as a function of both the type of photosensitizer and the light dose used. Photodynamic inactivation of *M. smegmatis* was found to be highly efficient in reducing the number of viable cells *in vitro* when cationic photosensitizers were employed.

The trends established in Chapter 2 allowed us to propose a targeting strategy for bacteria with an outer cell membrane such as myco- or Gram-negative bacteria. Successfully targeted photosensitizers are the crucial milestone in order to move this area closer to clinical application. Chapter 3 describes the synthesis, characterization, toxicity, and PDI-profiles of water soluble, cationic porphyrin-peptide conjugates in order to investigate bacterial-targeted photosensitizers for the selective inactivation of bacteria. Our targeting strategy aims at exploiting the membrane binding capabilities of highly positively-charged antimicrobial peptides that are known for their affinity to bacterial cell membranes. The novel porphyrin-peptide conjugates discussed in this chapter were found to be excellent photosensitizers while being non-toxic in the dark and non-hemolytic against red blood cells in the relevant concentration range for PDI.

Bacterial infection transmitted through contaminated surfaces, particularly in hospitals, poses an increasingly deadly health threat. Therefore, research presented in Chapter 4 pursues the goal of developing alternative materials (fabrics, plastics or coatings) with antimicrobial properties under intense lighting conditions. The synthesis and characterization of cellulose nanocrystals that were surface modified with a cationic porphyrin, and the ability of this material to inactivate a variety of bacteria, was demonstrated. Cellulose-based materials, such as paper or fabrics might prove useful in the health care, food preparation, or other industries where prevention of unintended bacterial contamination is crucial for the protection of human health.

Chapter 5 discusses the synthesis and characterization of our first generation, porphyrin-based, small molecule model complexes of the KatG active site, the enzyme that activates the most commonly prescribed anti-tuberculosis drug, isoniazid. It is our goal to

utilize these model complexes in a biomimetic approach to gain an understanding of the mechanisms of KatG's failure to activate isoniazid. Together with the characterization of these model complexes and the synthetic strategies developed in Chapter 3, we are now able to synthesize porphyrin-peptide mimics of the KatG active site.

© Copyright 2011 Elke Feese.

All rights reserved.

Development of Novel Photosensitizers for Photodynamic Inactivation of Bacteria

by
Elke Feese

A dissertation submitted to the Graduate Faculty of
North Carolina State University
in partial fulfillment of the
requirements for the degree of
Doctor of Philosophy

Chemistry

Raleigh, North Carolina

2011

APPROVED BY:

Dr. Reza A. Ghiladi,
Committee Chair

Dr. Jonathan S. Lindsey

Dr. Tatyana I. Smirnova

Dr. Lucian Lucia

DEDICATION

This work is dedicated to

*Detlef Lück, for sparking my love for chemistry and all the help along the way on my journey
in science;*

Erika Lück, for her unconditional love and support;

George Feese, for being my partner in life and making it worthwhile.

BIOGRAPHY

Elke Feese was born in September 1978. She was raised in Berlin, Germany, and witnessed the fall of the Berlin Wall on November 9th 1989. From an early age, Elke was very active in her local sports club, practicing Rhythmic Gymnastics starting as an athlete, and then later moving into coaching and judging roles. After graduating from high school with her German “Abitur” she spent a year as an au-pair, taking care of three teenage children in a New Jersey household and travelling the United States. Upon return to Germany she followed her passion for Chemistry and enrolled as a student at Freie Universität Berlin. She conducted her research thesis under the supervision of Prof. Dr. Jürgen-H. Fuhrhop in the field of organic chemistry and graduated with her diploma in Chemistry (M.Sc. equivalent) in March 2005.

In the fall of 2005, she moved to the United States with her husband, where she lived at Fort Benning, GA “Home of the Infantry” until she joined the chemistry PhD program at North Carolina State University in 2006. For the past five years, Elke has been conducting her doctoral research under the supervision of Prof. Dr. Ghiladi. During her time at NCSU she has received several honors and awards, including a GSK Graduate Fellowship, the C. J. Muddiman Award for Creativity and Excellence in Research, the Berman Family Award for Excellence in Teaching, and several poster and travel awards. In her free time she enjoyed participation and leadership positions in organizations including PLU (Beta Lambda Chapter), UGSA and the NC-ACS Women Chemists committee.

Upon graduation with her PhD in March 2011, Elke will work for BASF in their Professional Development Program.

ACKNOWLEDGMENTS

I would like to express my deepest gratitude for everyone who has supported me during my time at North Carolina State University. Most importantly, I am very thankful to my advisor, Dr. Reza Ghiladi, who accepted me into his group as one of his first students. He has placed an enormous amount of trust in me and has given me the freedom to explore new fields in synthesis and biology. Besides the science, I thank him for being such a generous and patient person, and giving me the opportunity to get engaged in many extracurricular activities. Further, I would like to thank the members of my advisory committee, Dr. Jonathan Lindsey, Dr. Christian Melander, Dr. Tatyana Smirnova and Dr. Lucian Lucia, for contributing to my education in chemistry and for providing scientific advice during my graduate career. In addition, I express my sincere appreciation for the mentorship I have received from Dr. Maria Oliver-Hoyo. I thank her for helping me “separate the wheat from the chaff” on a personal and professional level and for providing me so much motivation during our conversations.

I would like to thank Dr. Dimitris Argyropoulos and Dr. Hasan Sadeghifar, both from the Department of Forest Biomaterials (NCSU), for fruitful collaboration on the cellulose-porphyrin conjugate work. Further, I thank Dr. Hanna Gracz for taking the time to teach me more about advanced NMR techniques.

Further, I am very appreciative of my current and past fellow Ghiladi group members for their friendship and comradery while battling lab work every day: Especially, Rania Dumarieh for being the calming center in our group, Jennifer D’Antonio for teaching me

about enzymes and spicing up the lab environment with some Latin rhythms, and lastly, David Barrios for energizing discussions about science and life in general, or simply said, for keeping me sane during the past two years.

I am also very thankful for the fellowship and fun times I have shared with Dr. Douglas Young, Dr. Wesleigh Georgianna and Dr. Virginia Burns particularly while getting started at North Carolina State University and while sharing PLU duties. Further, I am also indebted to Dr. Ana Muresan, Dr. Dilek Dogutan, Dr. Masahiko Taniguchi and Dr. Marcin Ptaszek for their indispensable advice regarding porphyrin chemistry. I also owe thanks to Dr. Steven Rogers for assistance with biological assays and click chemistry. I would like to also thank my fellow PLU officers of 2009-2010 (Jennifer D'Antonio, Joe DeSousa, Christine Cade and Dr. Wesleigh Georgianna) for productive teamwork and a job well done.

From the bottom of my heart, I feel endless appreciation for my parents, who have expressed their love, encouragement and support of me without condition on this journey of life. They have shaped the person I am today in so many ways regardless of the ocean between us.

My final words are dedicated to my husband George. I am so grateful for the beauty, excitement and challenge he has brought to my life. I thank him for loving me, showing me other perspectives in life, for challenging me to be a better person inside and outside the lab, and for the endless support, commitment and patience he has given me since we have been together.

TABLE OF CONTENTS

LIST OF TABLES	x
LIST OF FIGURES	xii
LIST OF ABBREVIATIONS.....	xvi

CHAPTER 1

GENERAL INTRODUCTION.....	1
Tuberculosis – a Global Health Threat	1
Challenges in Anti-TB Treatment and PDT as a New Perspective	5
Mechanism of Photodynamic Inactivation	7
Photosensitizers.....	10
Mycobacterium Genus	12
Other Bacteria Relevant to This Work.....	17
Bacteria-targeted Photodynamic Inactivation.....	21
Antimicrobial Peptides.....	23
Overview.....	27
References.....	29

CHAPTER 2

HIGHLY EFFICIENT <i>IN VITRO</i> PHOTODYNAMIC INACTIVATION OF <i>MYCOBACTERIUM SMEGMATIS</i>	45
--	----

Abstract.....	45
Introduction.....	45
Results.....	47
Discussion.....	62
Experimental Methods.....	64
References.....	69

CHAPTER 3

TOWARDS MICROBE-TARGETED PHOTSENSITIZERS: SYNTHESIS, CHARACTERIZATION AND PHOTODYNAMIC ACTIVITY OF PORPHYRIN-PEPTIDE CONJUGATES.....	72
Abstract.....	72
Introduction.....	73
Results.....	79
Discussion.....	110
Outlook	115
Experimental Methods - Synthesis	116
Experimental Methods - Biology.....	156
Acknowledgements.....	159
References.....	161

CHAPTER 4

TOWARDS PHOTOBACTERICIDAL MATERIALS: SYNTHESIS, CHARACTERIZATION AND PHOTODYNAMIC ACTIVITY OF PORPHYRIN-CELLULOSE NANOCRYSTALS.....	172
Abstract.....	172
Introduction.....	173
Results.....	177
Discussion.....	198
Experimental Methods.....	204
Acknowledgements.....	212
References.....	213

CHAPTER 5

TOWARDS SMALL MOLECULE MODEL COMPLEXES OF THE KATG ACTIVE SITE.....	222
Abstract.....	222
Introduction.....	223
Results.....	231
Summary and Outlook.....	246
Experimental Methods.....	251
References.....	267

APPENDIX	274
X-Ray Crystallography of 3.1 – Details on disorders	275
Copyright Permissions	277

LIST OF TABLES

Table 2.1	TMPyP (2.1) mediated photodynamic inactivation of <i>M. smegmatis</i> in the presence of the singlet oxygen quencher NaN ₃54
Table 2.2	recovery (nM) from lysed cell suspensions after 1-3 PBS washing steps ^{a,b} ...55
Table 2.3	Photodynamic inactivation of <i>E. coli</i> by TMPyP (2.1) and TNMAP (2.2)61
Table 2.4	Published Values for Photophysical Properties of employed Photosensitizers.....62
Table 3.1	Summary of Crystal Data for 3.182
Table 3.2	Selected bond length for 3.1 in Å84
Table 3.3	Initial survey of conditions for Click reaction of 3.485
Table 3.4	Photodynamic inactivation with 3.11 and 3.12 against <i>M. smegmatis</i> , 60 mW/cm ²105
Table 3.5	Light sensitivity of selected porphyrin compounds. The % decrease of Soret absorption band is displayed as a function of varying illumination times (60 mW/cm ²)107
Table 3.6	Hemolysis assay with 10% defibrinated sheep blood. % hemolysis at varying concentrations of the photosensitizer is listed108
Table 3.7	Minimum Inhibitory Concentrations for porphyrins and selected antimicrobial peptides against <i>M. smegmatis</i> as determined by broth microdilution109
Table 3.8	RP-HPLC conditions for 3.1123
Table 3.9	RP-HPLC conditions for 3.5125

Table 3.10	RP-HPLC conditions for 3.7	128
Table 3.11	RP-HPLC conditions for 3.11	133
Table 3.12	RP-HPLC conditions for 3.12-prot.	135
Table 3.13	RP-HPLC conditions for 3.12	136
Table 3.14	RP-HPLC conditions for 3.14-prot.	138
Table 3.15	RP-HPLC conditions for 3.14	139
Table 3.16	RP-HPLC conditions for 3.15-prot.	141
Table 3.17	RP-HPLC conditions for 3.15	142
Table 3.18	RP-HPLC conditions for 3.16-prot.	144
Table 3.19	RP-HPLC conditions for 3.16	145
Table 3.20	RP-HPLC conditions for 3.17-prot.	147
Table 3.21	RP-HPLC conditions for 3.17	148
Table 3.22	RP-HPLC conditions for 3.19	150
Table 3.23	RP-HPLC conditions for 3.18	154
Table 4.1	Molecular weight distributions of benzoylated derivatives of CNC-N ₃ (4.3) and CNC-Por (4.4) in THF	184
Table 4.2	Estimated diffusion coefficients D determined from PFGSE ¹ H-NMR	188
Table 4.3	Light control experiments with azide surface-modified CNC-N ₃ (4.3).....	196
Table 4.4	Results of PDI studies with the water soluble porphyrin 3.1 as a function of different bacteria, PS and light doses.....	198
Table 5.1	Chemical shifts for β -pyrrole hydrogens in heme complexes	236

LIST OF FIGURES

Figure 1.1	MDR-TB among new and previously treated cases; adapted from Anti-Tuberculosis Drug Resistance in the World Report No. 4, WHO.....	3
Figure 1.2	Structures of Moxifloxacin and PA 824	6
Figure 1.3	Mechanism of photodynamic inactivation	8
Figure 1.4	Photoreactions relevant in PDT; PS: photosensitizer, Sub: substrate.....	9
Figure 1.5	Cell envelope model for the mycobacterium genus.....	15
Figure 1.6	Typical mycolic acid in <i>M. tuberculosis</i>	16
Figure 1.7	Proposed structure of the symmetric outer membrane by Hoffmann et al.: A) mycolic acids fully integrated into the bilayer, B) mycolic acid only partially integrated into the bilayer.	17
Figure 1.8	Cell envelopes of (a) Gram-positive and (b) Gram-negative bacteria.....	18
Figure 1.9	Action of antimicrobial peptides.....	26
Figure 2.1	Photosensitizers employed in this study	48
Figure 2.2	Photodynamic inactivation of <i>M. smegmatis</i> using photosensitizers 2.1-2.6 ..	50
Figure 2.3	Fluorescence spectra of 5 μ M PhCS (2.6) in different ratios of PBS buffer (0.05% tween) and cell lysate from 10^8 CFU/mL bacterial cell suspension ...	56
Figure 2.4	Photodynamic inactivation of <i>E. coli</i> using photosensitizers 2.1-2.6	58
Figure 3.1	Synthesis of the ethynylphenyl porphyrins 3.1 and 3.5	81
Figure 3.2	ORTEP drawing of the 3.1 cation.....	82

Figure 3.3	Initial survey of reaction conditions for the Click reaction of 3.1 or 3.4 with (azidomethyl)benzene	85
Figure 3.4	Porphyrin-peptide synthesis on the solid support	87
Figure 3.5	Overview of synthetic routes to porphyrin-peptide conjugates	88
Figure 3.6	Formation of porphyrin-amino acid conjugate 3.11	89
Figure 3.7	Synthesis of porphyrin-peptide conjugate 3.12	91
Figure 3.8	Total correlation (TOCSY) NMR spectrum of PPC 3.12	92
Figure 3.9	Synthesis of PPCs 3.14-3.17 via Route B.....	93
Figure 3.10	Route C for porphyrin-peptide conjugates attached via the C-terminus.....	95
Figure 3.11	Synthesis of porphyrin 3.19	96
Figure 3.12	Photodynamic inactivation of <i>M. smegmatis</i> using photosensitizers 2.1 , 3.1 , 3.5 , 3.14-3.17 , 3.19	99
Figure 4.1	A) TEM image of CNC (4.1), B) Cross-sectional representation of the cellulose nanocrystal indicating the surface accessible reaction sites	178
Figure 4.2	Synthesis of cellulose nanocrystal-porphyrin conjugate CNC-Por (4.4).....	178
Figure 4.3	IR spectra of CNC (4.1), CNC-tos (4.2), and CNC-N ₃ (4.3).....	180
Figure 4.4	IR spectra of CNC-N ₃ (4.3) and CNC-Por (4.4).....	182
Figure 4.5	Gel permeation chromatography of benzoylated derivatives of CNC-N ₃ (4.3) and CNC-Por (4.4) in THF	184
Figure 4.6	Pulsed field gradient spin echo ¹ H-NMR spectra of acetylated CNC-Por.....	187
Figure 4.7	Pulsed field gradient spin echo ¹ H-NMR control experiments of a mixture of porphyrin 3.1 and acetylated CNC-N ₃	187

Figure 4.8	Graphical representation of the loss in proton signal intensity for PFGSE ^1H -NMR experiments comprised from data shown in Figures 4.6 and 4.7	188
Figure 4.9	Thermal gravimetric analysis of CNC-Por (4.4).....	189
Figure 4.10	Photodynamic inactivation of A) <i>E. coli</i> , B) <i>M. smegmatis</i> C) <i>S. aureus</i> using 20 μM CNC-Por (4.4) as the photosensitizer	192
Figure 4.11	Concentration dependence of PDI for <i>M. smegmatis</i> and <i>S. aureus</i> using CNC-Por (4.4) at constant incubation (30 min) and illumination times (15 min).....	196
Figure 5.1	Crystal structures of A) the KatG active site of <i>M. tuberculosis</i> , and B) the Met-Tyr-Trp crosslink.	225
Figure 5.2	Activation of INH by KatG.....	226
Figure 5.3	Proposed mechanism for the activation of isoniazid by KatG.....	228
Figure 5.4	Target model complexes of the KatG active site	231
Figure 5.5	Synthesis of model complexes 5.1 and 5.2	235
Figure 5.6	^1H -NMR spectra of $\text{TMPyPFe}^{\text{II}}$ (5.1)	238
Figure 5.7	^1H -NMR spectra of $\text{TMImpFe}^{\text{II}}$ (5.2)	239
Figure 5.8	^1H -NMR spectra of A) $\text{TMPyPFe}^{\text{II}}$ (5.1), B) its dioxygen adduct, and C) the ferric-hydroxy decomposition product in $\text{THF-}d_8$, -80°C	241
Figure 5.9	^1H -NMR spectra of A) $\text{TMImpFe}^{\text{II}}$ (5.2), B) its dioxygen adduct, and C) the ferric-hydroxy decomposition product in $\text{THF-}d_8$, -80°C	242
Figure 5.10	Synthesis of partially β -pyrrole deuterated porphyrin analogs	244
Figure 5.11	^2H -NMR spectrum of 5.7-d_2 in CHCl_3	244

Figure 5.12	Route to fully β -pyrrole deuterated porphyrins, 5.3-d_8 and 5.4-d_8245
Figure 5.13	Proposed mechanism for formation of the Met-Tyr-Trp crosslink in KatG..248
Figure 5.14	Planned 2 nd generation model complexes250

LIST OF ABBREVIATIONS

ADS	Albumin dextrose saline
AFB	Acid-fast bacillus
AMIM-Cl	1-ally-3-methylimidazoliumchloride, ionic liquid
AMP	Antimicrobial peptide
Arg	Arginine
BCG	Bacillus Calmette-Guérin
Boc	<i>tert</i> -Butoxy carbamate, protecting group
Br	Broad
C	Carbon or cysteine
Calcd.	Calculated
CDC	The Centers for Disease Control and Prevention
CFU	Colony forming units from a single bacterial cell
CNC	Cellulose Nanocrystal
¹³ C-NMR	Carbon Nuclear Magnetic Resonance
conc.	Concentration or concentrated
COSY	Correlation spectroscopy
d	Doublet
DCM	Dichloromethane
dd	Doublet of doublets
DIEA	Diisopropylethylamine

DNA	Deoxyribonucleic acid
DMF	<i>N,N</i> -dimethylformamide
DMSO	Dimethyl sulfoxide
DS	Degree of substitution
EDTA	Ethylene diamine tetraacetic acid tetrasodium salt dihydrate
ESI	Electrospray ionisation
EtOH	Ethanol
F	Phenylalanine
Fmoc	Fluorenylmethyloxycarbonyl group
FT	Fourier transform
G	Glycine
Gln	Glutamine
H	Hydrogen or histidine
h	Hour
HCTU	1-[Bis(dimethylamino)methylen]-5-chlorobenzotriazolium 3-oxide hexafluorophosphate
HIV	Human immunodeficiency virus
HMBC	Heteronuclear Multiple Bond Correlation
¹ H-NMR	Proton Nuclear Magnetic Resonance
HP	Hematoporphyrin
HPD	Hematoporphyrin derivative
HPLC	High performance liquid chromatography

HRMS	High resolution mass spectrometry
HSQC	Heteronuclear Single Quantum Coherence
IR	Infrared
K	Lysine
<i>J</i>	Coupling constant
L	Leucine
LB	Luria-Bertani
Leu	Leucine
Lys	Lysine
m	Multiplet
MALDI	Matrix assisted laser desorption ionization
MB	Methylene Blue
MDR	Multidrug-resistant
MeCN	Acetonitrile
MeOH	Methanol
MHz	Megahertz
MIC	Minimum inhibitory concentration
min	Minutes
MRSA	Methicillin-resistant <i>Staphylococcus aureus</i>
MS	Mass spectrometry
N ₃	Azide group
NEt ₃	Triethylamine

OAc	Acetate group
obsd.	Observed
OD ₆₀₀	Optical density at 600 nm
OTf	Triflate group
<i>P</i>	Probability
Pbf	2,2,4,6,7-Pentamethyldihydrobenzofurane protecting group
PBS	Phosphate buffered saline
PFGSE	Pulsed field gradient spin echo
PDI	Photodynamic Inactivation
PDT	Photodynamic Therapy
pH	Measure of acidity/basicity of a solution
PhCS	Phthalocyanine tetrasulfonic acid
Phe	Phenylalanine
Por	Porphyrin
PPC	Porphyrin-peptide conjugate
ppm	Parts per million
PS	Photosensitizer
q	Quartet
Q	Glutamine
QSAR	Quantitative structure-activity relationship
quart.	Quarternary atom
R	Arginine

Ref	Reference
RP	Reverse phase
RT	Room temperature
s	Singlet
S	Serin
S.D.	Standard deviation
Ser	Serine
TB	Tuberculosis
^t Bu	<i>tert</i> -Butyl group
TCPP	5,10,15,20-Tetrakis(4-carboxyphenyl)porphyrin
TEA	Triethylamine
TEM	Transmission electron microscopy
Temp.	Temperature
TFA	Trifluoroacetic acid
THF	Tetrahydrofurane
TMPyP	5,10,15,20-Tetrakis(1-methyl-4-pyridinyl)porphyrin tetratosylate
TNMAP	5,10,15,20-Tetrakis(4-N,N,N-trimethylanilinium)porphyrin tetrachloride
TOCSY	Total correlation spectroscopy
TOF	Time of flight
tol	Toluene
TosCl	4-Toluenesulfonyl chloride

TSPP	5,10,15,20-Tetrakis(4-sulfonatophenyl)porphyrin
Trp	Tryptophan
Trt	Triphenylmethyl protecting group
UV	Ultraviolet
vis	Visible
W	Tryptophan
WHO	World Health Organization
XDR	Extremely drug-resistant
Y	Tyrosine

CHAPTER 1

General Introduction

Tuberculosis – A Global Health Threat

Tuberculosis (TB) is one of the leading causes of death due to a single disease, comprising 2.5% of the global burden of disease with 9.2 million new infections and 1.7 million deaths reported for 2006 alone.¹ With approximately one third of the world's population currently infected, experts estimate that nearly 1 billion people will be newly infected, over 125 million people will get sick, and 30 million will die of TB in the next 20 years if control is not further strengthened. On average, 10% of those infected will develop an active case of TB (AFB smear-positive), whereas HIV co-infection increases that likelihood 50 times.² TB is a highly communicable airborne pathogen and patients with active TB, on average, infect 10-15 people annually.³ TB affects mostly young people in their productive years and most commonly in countries of the developing world.

In 1991, the World Health Organization (WHO) recognized TB as a global public health problem and declared the detection of at least 70% of all AFB smear-positive TB cases (most infectious form of TB) and treatment of at least 85% of all detected cases as the central goals in an effort to battle TB. These goals, which have been met for the first time in 2006,² are being achieved by implementing and expanding programs like “Stop TB Partnership” and “Directly Observed Treatment, Short Course” (DOTS), which encompasses

the following elements: “i) *political commitment with increased and sustained financing*, ii) *case detection through quality-assured bacteriology*, iii) *standardized treatment with supervision and patient support*, iv) *an effective drug supply and management systems*, v) *monitoring and evaluation system and impact measurement*”.¹ As of 2006, the goal for global TB control as part of the Millennium Development Goals (MDG 6 target 6.C) “*to have halted and begun to reverse the incidence [by 2015]*” is also on target in most regions. In all areas monitored by the World Health Organization (WHO), the annual incidence rates peaked between 2003 and 2004 and are currently falling except for Europe, where the rate of incidences remains unchanged. Furthermore, significant successes have been achieved in both incidence and death rates, which fell by 2.8% (219 per 100,000 population) and 2.6% (25 per 100,000 population) between 2005 and 2006, respectively.²

While a number of antibiotics are effective in treating TB, the rise in drug-resistant strains poses an austere threat to the advances made in controlling TB. Drug-resistance, primarily a man-made problem, is due to improper or incomplete drug therapy, poor drug quality or insufficient drug supply. These three factors often lead to a so-called acquired resistance: improper treatment causes only suppression of drug-susceptible forms of *M. tuberculosis*, the causative agent of TB, while drug-resistant strains will proliferate and accumulate, rendering the patient drug-resistant. Primary resistance occurs if a person is newly infected with drug-resistant *M. tuberculosis* without prior treatment. Patients with multiple drug-resistant (MDR)-TB show resistance to the most common first line drugs, isoniazid and rifampicin, rendering the standard six-month treatment ineffective. MDR-TB can be treated using a two-year therapy with second line drugs, which are significantly more

expensive, toxic and less effective. The highest rates of MDR-TB ever recorded were published by the WHO for 2006: Globally 5.3% of all newly detected TB cases were MDR-TB, with areas in the former Soviet Union peaking over 35%, and both China and India carrying the biggest burden in the absolute number of new MDR-TB cases (Figure 1.1).⁴ Forty-five countries have reported at least one case of extensively drug-resistant TB (XDR-TB), which is defined by the WHO Global Task Force on XDR-TB as resistance to isoniazid, rifampicin and to at least one of the injectable drugs amikacin, kanamycin or capreomycin. Estimations, based on the data collected by the WHO suggest an occurrence of 40,000 XDR-TB cases annually.⁵

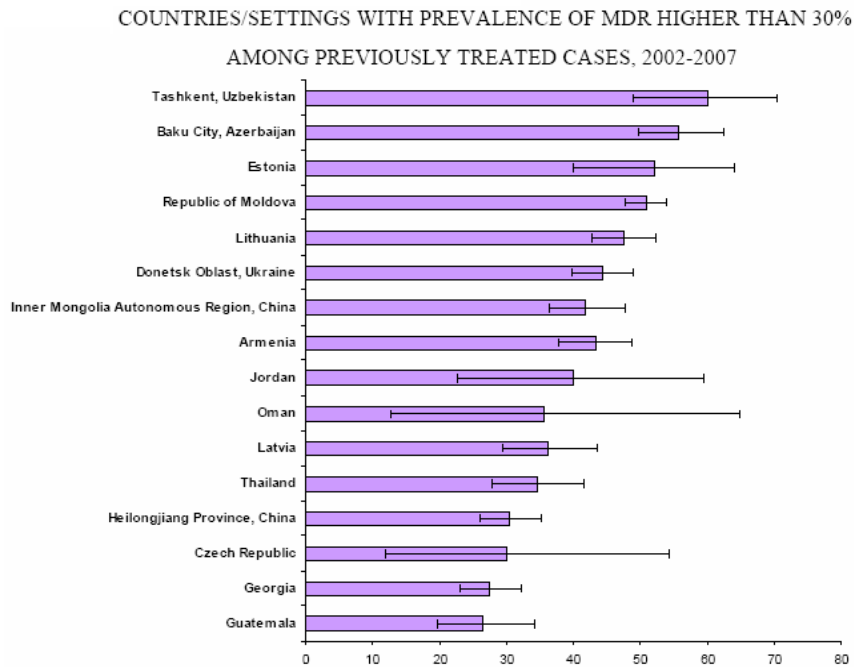


Figure 1.1: MDR-TB among new and previously treated cases (Adapted with permission from Ref [4]. Copyright 2008 WHO).

The grave situation outlined above has sparked a new round of interest in antitubercular treatments.^{6,7} The chemist's ability to advance knowledge and tools necessary to combat TB lies especially in the areas of developing new and more potent drugs, alternative drug targets, effective vaccines, and additional treatment options to the current antibiotic-based therapy. The work described in the following chapters attempts to enrich the discussion about combating TB, and bacteria in general, by addressing the following aspects:

- Investigation of photodynamic inactivation of non-pathogenic *M. smegmatis* as a surrogate for *M. tuberculosis* to determine the efficacy of photodynamic therapy (PDT) as an alternative TB treatment option (Chapter 2).
- Development of antimicrobial peptide inspired porphyrin-peptide conjugates as mycobacteria-targeted photosensitizers (Chapter 3).
- Application of photodynamic therapy employing novel materials with photobactericidal properties towards reducing the spread of bacteria through contaminated surfaces (Chapter 4).
- Characterization of small molecule model complexes of the KatG active site, an enzyme involved in the activation of the most commonly prescribed anti-TB drug isoniazid, in order to elucidate structure-function relationships and their connections to the failure of the enzyme in drug resistant *M. tuberculosis* (Chapter 5).

Challenges in Anti-TB Treatment and PDT as a New Perspective

In light of the global situation concerning TB outlined in the general introduction, the necessity for a vigorous search for alternative treatments, novel drugs, as well as new drug targets is clearly justified along with intensification of efforts to control spread of the disease. It has been approximately 35 years since a new class of tuberculosis drugs has been found.^{7, 8} This is mostly due to the very restrictive requirements necessary for a successful anti-TB drug. New drug candidates should significantly shorten the standard six-month treatment by showing high activity against bacilli in low metabolic states (persistent bacteria), be specific for *M. tuberculosis*, compatible with existing anti-TB drugs (TB treatment includes a mix of different antibiotics), be compatible with HIV treatment regimens due to the high degree of HIV/TB co-infections, show activity against resistant and non-resistant strains, and have low toxicity as well as low production costs in order to be marketable in developing countries. Several derivatives of established TB drugs have been investigated in the last decades. Moxifloxacin, a fluoroquinolone,⁹⁻¹³ in phase III, and PA 824, a nitroimidazole,^{11, 14} in phase II clinical trials are currently the most promising new drug candidates (Figure 1.2).⁸ Long culturing periods (up to 4 weeks) and the necessity to handle *M. tuberculosis* under Bio-Safety level Category 3 physical containment further complicate efficient high throughput screening of possible drug candidates.

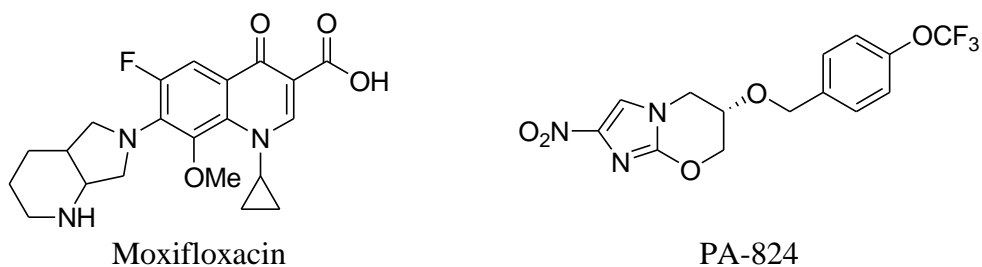


Figure 1.2: Structures of Moxifloxacin and PA 824.

Several alternative drug targets have been suggested in the literature,⁷ but will not be discussed further in this introduction. Rather, we suggest the investigation of a different approach, which directly attacks and eradicates living cells: Photodynamic Therapy.^{15, 16} PDT uses three key components: light, oxygen and a photosensitizer (PS). The therapeutic effect of light was already known in ancient civilizations in Egypt, India and China thousands of years ago,¹⁷⁻¹⁹ but in 1900, the German medical student Oscar Raab in the laboratory of H. von Tappeiner first observed the cytotoxic effect on *Paramecium caudatum* upon treatment with a combination of light and acridine.^{20, 21} Later, Tappeiner and A. Jesionek introduced the term “photodynamic action”.²² Interestingly, Niels Finsen was awarded the Noble Prize in 1903 for his contribution to the treatment of dermal TB infection, lupus vulgaris, with light.²³ Finsen attributed the curing effect to UV irradiation, but recent investigations point to photodynamic actions of endogenous porphyrins.²⁴ The synthesis of hematoporphyrin (HP) and its derivatives (HPD) from dried blood²⁵ provided the next step in the development of photodynamic therapy. Historically, HPD photosensitization was first observed in mice by W. Hausmann,¹⁸ but it wasn't until the sixties when the accumulation of HPD in tumors was investigated as a diagnostic tool by Lipson and Baldes.²⁶ In the seventies, T. Dougherty

conducted the first clinical studies in humans using PDT for cancer treatment.^{15, 27} The approval of Photofrin[®], an HPD derivative, in 1999 was followed by several others over the past decade. The treatment of various forms of cancers (basal-cell carcinoma, cervical cancer, endobroncheal cancer, gastric cancer, head, neck and papillary bladder cancer) with PDT is well established in clinical application in many countries in the world today.¹⁹ Advances made in the treatment of cancer,^{28, 29} age related macular degeneration,³⁰ as well as in the sterilization of contaminated blood³¹ using PDT suggest that photodynamic treatment of localized bacterial infections (termed Photodynamic Inactivation, PDI) might also be feasible, and possibly circumvent problems occurring with drug-resistance in antibiotic-based treatments.³²⁻³⁵ Wound infections, psoriasis, acne vulgaris, and oral disease are some of the areas currently under intensive investigation towards the applicability of antimicrobial photodynamic inactivation.³⁶⁻³⁸ The efficacy of PDI against bacteria like *Escherichia coli*, *Staphylococcus aureus* (including methicillin resistant strains), *Acinetobacter baumannii*, *Pseudomonas aeruginosa* and others using a wide variety of conditions and photosensitizers has been investigated extensively *in vitro*, whereas the records of *in vivo* studies are rather limited.^{33, 39}

Mechanism of Photodynamic Inactivation

Bacterial inactivation is achieved by short incubation of the bacteria (5-15 minutes) with a photosensitizer, a light absorbing agent which is either uptaken or localizes within the bacterial cell wall. Irradiation of the bacteria with visible light causes oxidative damage to

biomolecules and eventually leads to cell death.^{15, 16} The photosensitizer is excited by illumination with low intensity visible light (1-100 mW/cm²) using a large variety of light sources ranging from lasers to tungsten light bulbs.

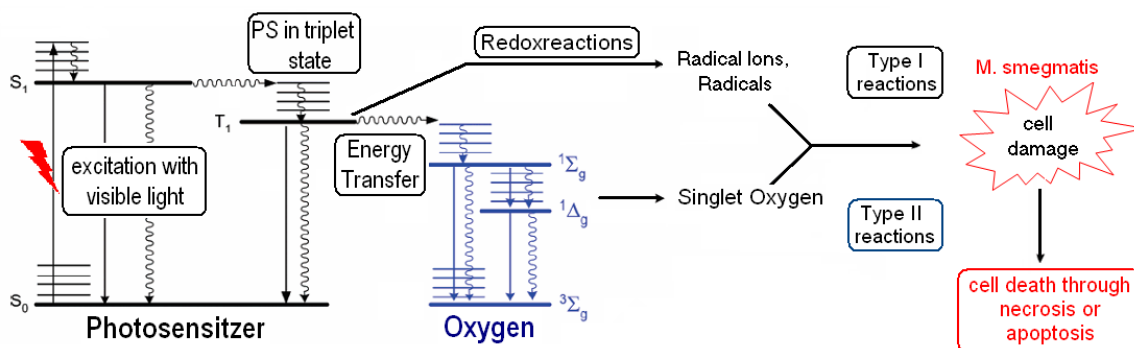


Figure 1.3: Mechanism of photodynamic inactivation (Modified with permission from Ref [40]. Copyright 2005 American Chemical Society).

Upon light absorption and excitation into the first excited singlet state the photosensitizer can relax back to the ground state by photon emission or by radiationless decay (Figure 1.3). The crucial pathway to efficient photodynamic therapy is the formally forbidden intersystem crossing (ISC) to the lower lying excited triplet state, which exhibits a lifetime in aqueous media ranging from 2-4 μ s. A lifetime of this magnitude is sufficient to initiate the two main pathways relevant for PDT/PDI (Figure 1.4):¹⁶

1. Electron Transfer/Redox reactions (Type I mechanism): The photosensitizer, in its triplet state, undergoes electron transfer reactions with suitable substrates such as cellular

biomolecules, solvent molecules or dioxygen, forming cytotoxic free radicals and superoxide.

2. Energy transfer (Type II mechanism): Molecular oxygen (triplet ground state) has a low lying singlet excited state, which is accessible by energy transfer from the excited triplet state of the photosensitizer. Singlet oxygen is highly reactive due to pairing of two electrons in one π^*_{2p} antibonding orbital. Because of its lifetime of approximately 2 μ s in aqueous media, singlet oxygen causes only highly localized damage.¹⁶

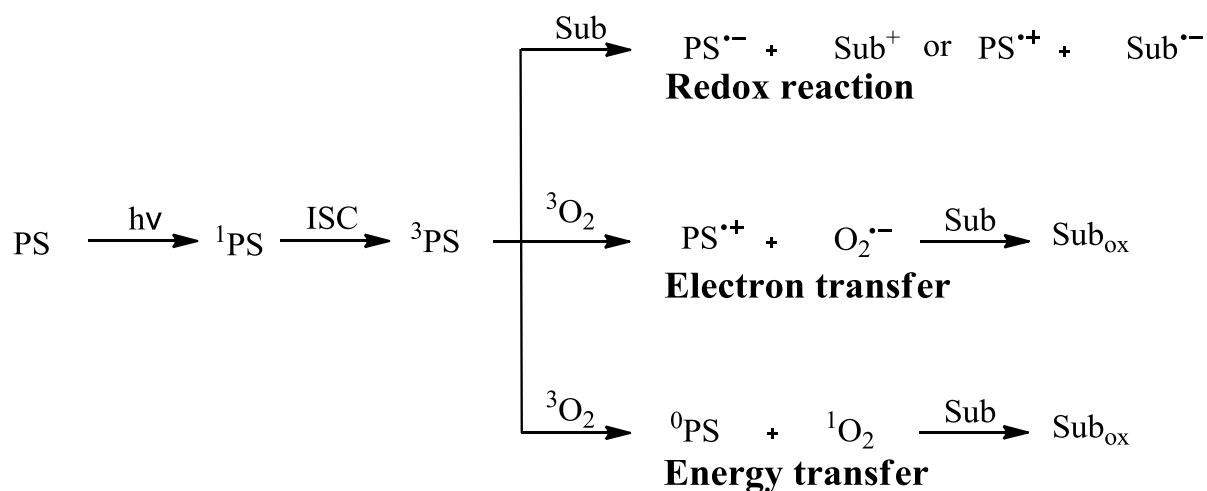


Figure 1.4: Photoreactions relevant in PDT; PS: photosensitizer, Sub: substrate.

Although factors like the nature of the PS, energies and lifetimes of the excited states, subcellular localization, and concentration may favor either of the two mechanisms, oxidative cell damage, typically, is predominantly caused by the Type II pathway in aerated media,⁴¹ ultimately leading to cell death by apoptosis or necrosis.^{42, 43} Experimental data

suggests that photodamage initially occurs at the cytoplasmic membrane, allowing leakage of cell contents and the diffusion of the photosensitizer inside the bacterium,⁴⁴ where singlet oxygen will cause lethal damage.

In general, photodynamic inactivation of bacteria can be achieved independently of the resistance patterns that plague traditional antibiotic treatments.^{33, 45} Development of bacterial resistance towards the PDI process is currently under debate.^{33, 37, 45} Although there are several reports of the lack of photoresistance after repeated treatments,³⁷ a loss in photosensitizer affinity due to structural changes in the cell wall or more efficient efflux systems are imaginable.^{46, 47} Changes in cell wall thickness, crosslinking patterns in the peptidoglycan or a reduction in overall charge of the lipopolysaccharides on the cell surface,⁴⁸ as well as a change in slime production that has been observed for a case of *Staphylococcus aureus*,⁴⁹ all could result in a less effective binding or uptake of the PS, consequently leading to loss of PDI efficiency. It is generally agreed that initial and major cell damage is induced at the cell membrane, and that DNA damage is not a relevant process under most conditions. Therefore, the risk for mutagenesis initiated by illumination is considered low.^{50, 51}

Photosensitizers

Currently there are four classes of drugs approved for use in PDT cancer treatments.⁵² Photofrin[®] was the first drug licensed for clinical use. Photofrin is synthesized by the

treatment of hemin with 5% sulfuric acid and contains a mixture of up to 60 compounds of hematoporphyrin and oligomeric derivatives. The major drawback of Photofrin[®] is its accumulation in the skin of the patient, evoking photosensitivity even several weeks after PDT treatment. Aminolevulinic acid and its methylester derivative are marketed under the names Levulan[®] and Metvix[®]. Both are prodrugs, which are converted enzymatically to the PS protoporphyrin IX. Foscan[®] [5,10,15,20-tetrakis(*m*-hydroxyphenyl)chlorin], is being administered to treat head and neck cancers. Lastly, Visudyne[®], a benzoporphyrin derivative, is approved for the treatment of wet age-related macular degeneration. As mentioned earlier, photodynamic treatment of bacterial infections is still in its infancy and not yet in clinical application. Nonetheless, a large variety of different photosensitizers and experimental conditions have been investigated towards their potency in PDI against bacteria.³³

In general terms, the ideal photosensitizer possesses the following characteristics: It should be chemically well defined and synthetically affordable. It is also necessary for the PS to display low dark toxicity along with high phototoxicity at pharmacologically useful concentrations. The most useful therapeutic window with the deepest penetration of visible light into tissue is between 600-900 nm. Therefore, an intense absorption band in this region is desirable. Other photophysical parameters, such as a high quantum yield of the triplet state as well as a long triplet life time, can significantly increase PDI efficiency. Furthermore, one of the major challenges is specific localization of the PS in the bacteria in order to minimize damage of the host tissue upon illumination. Lastly, rapid clearance from the infected patient is necessary in order to avoid photosensitivity as a side effect.

In general, porphyrins,⁵³ phthalocyanines,⁵⁴ porphycenes⁵⁵ and phenothiazines⁵⁶ have been thoroughly investigated *in vitro*. Most photosensitizers do not meet all the criteria mentioned above, but significant advances have been made in certain aspects. Tetraphenylporphyrins possess weak absorption in the therapeutic window for effective tissue illumination, but diverse synthetic possibilities allow access to a great number of derivatives, which makes them an obvious choice when investigating and evaluating structure-function relationships.⁵³ Bacteriochlorins, porphycenes, and phthalocyanines, on the other hand, have absorption bands with high molar absorptivities between 600-800 nm, optimal for clinical application. Palladium complexed porphyrins have been shown to exhibit especially high quantum yields of triplet state formation and long triplet state lifetimes in deoxygenated aqueous media.⁵⁷⁻⁵⁹ Recently, it has been demonstrated that selective inactivation of bacterial cells over mammalian cells is feasible: Soncin et al. were able to use various Zn-phthalocyanines to selectively inactivate wild-type as well as methicillin-resistant *S. aureus*, while sparing human fibroblasts and keratinocytes.⁶⁰ By using short irradiation times, they exploited the different rates of PS uptake, resulting in the predominant accumulation of the PS in bacterial cells over mammalian cells.

Mycobacterium Genus

The causative agent of tuberculosis is infection with *M. tuberculosis*, a Gram-positive bacterium.⁶¹ With historically documented incidences of TB in Egypt dating back as far as 5,000 years,⁶² it is estimated that the genus *Mycobacterium* emerged about 150 million years

ago.⁶³ Although Benjamin Martin suggested in 1720 that TB might be caused by “*minute living creatures*”,⁶⁴ it was Robert Koch in 1882 who first isolated and demonstrated the infectiousness of *M. tuberculosis* and pioneered what has become modern medical microbiology.^{61,65}

M. tuberculosis is only one out of many species in the Mycobacterium genus, which belongs to the phylum Actinobacteria. Mycobacteria such as *M. tuberculosis*, *M. leprae* and *M. africanum* cause disease in humans, whereas *M. avium*, *M. marinum*, *M. kansasii*, *M. fortuitum*, and *M. chelonae* are considered atypical mycobacteria with a much lower virulence towards humans and might only cause disease in immunologically compromised patients. Furthermore, mycobacteria are grouped into slow (doubling time of days) or fast growers (doubling time of hours).⁶⁶

M. smegmatis has been shown to be a valuable surrogate for the pathogenic *M. tuberculosis*, and was therefore employed in the PDI studies presented in Chapters 2-4.⁶⁷⁻⁶⁹ Recently, *M. smegmatis* was specifically suggested as an effective screening model in the search for new anti-TB drugs.⁶⁷ *M. smegmatis* is a fast growing mycobacterium, whereas *M. tuberculosis* is slow growing, allowing initial results to be produced within a reasonable time frame (days instead of weeks). *M. smegmatis* is especially advantageous due to its non-pathogenicity, circumventing the need to handle the organism under Bio-Safety Level Category 3 conditions as required for *M. tuberculosis*.

Mycobacteria are aerobic, rod shaped, acid-fast bacteria, and since they do retain the Gram stain, are categorized as Gram-positive.⁶⁶ However, the cell envelope of mycobacteria is significantly different from the one typically found in Gram-positive bacteria (Figure 1.5)

and imparts exceptional persistence and resistance to this genus. Further, genome analysis indicates that mycobacteria might be more closely related to Gram-negative rather than Gram-positive bacteria.⁷⁰ Mycobacteria have a relatively thick cell wall skeleton, which acts as an efficient permeability barrier, allowing the bacteria to fall into a dormant state, where they are capable of surviving without nutrients for many years. Generally, mycobacteria are resistant to the most commonly used antibiotics, chemotherapeutica, many typical disinfectants and dry conditions. Susceptibility to broadly applied antibiotics is only observed toward streptomycin, rifampicins, and among the chemotherapeutic agents fluoroquinolones.⁷¹ Their cell surface contains relatively few porin channels for hydrophilic reagents, and are 100-1000 times less permeable when compared to *Escherichia coli*.⁷² The waxy and densely packed cell envelope also displays a comparably low permeability for hydrophobic molecules. Nevertheless, the fact that hydrophobic antibiotics are more effective against mycobacteria than more hydrophilic analogs shows the significance of the uptake pathway through the lipid bilayer.⁷³⁻⁷⁵

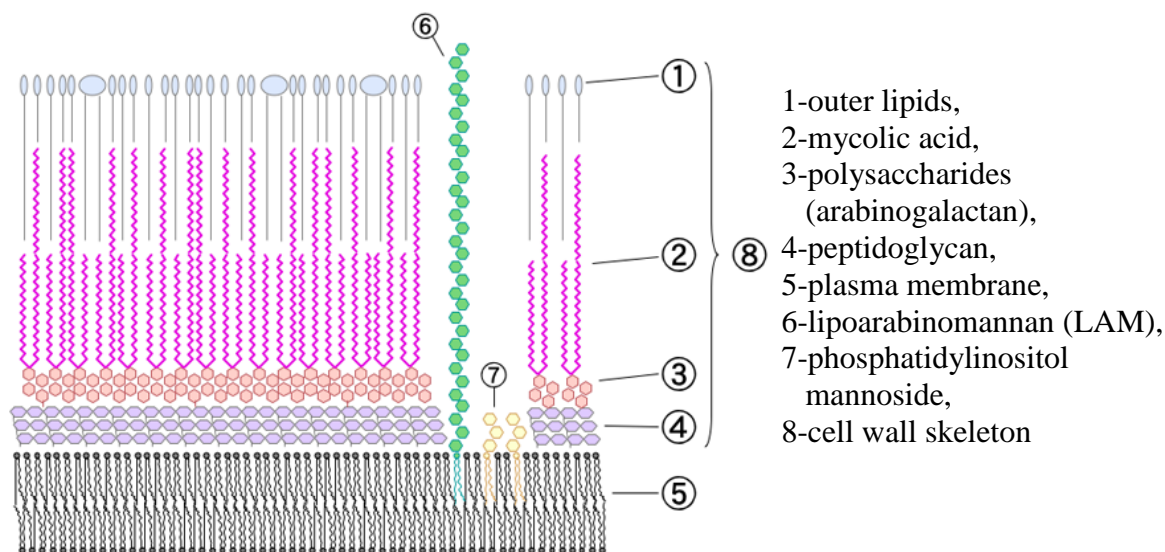


Figure 1.5: Cell envelope model for the mycobacterium genus (Reprinted with permission from Ref [76]).

Figure 1.5 shows the cell envelope model suggested by Minnikin, which, however, was never verified directly by microscopic techniques.⁷⁷ The cell wall skeleton, an asymmetric bilayer, contains the peptidoglycan (4) covalently bound to an arabinogalactan layer (3), which is esterified with exceptionally long fatty acids, the so-called mycolic acids (2).⁶⁶ Mycolic acids are unique for mycobacteria and the *Corynebacterium*-*Mycobacterium*-*Nocardia* branch of Actinobacteria. Mycolic acids are typically 70-90 carbon atoms in length and contain several double bonds, cyclopropane units, and hydroxyl groups in the meromycolic branch (Figure 1.6). The outer leaflet of the asymmetric double layer is comprised of extractable medium length (C_{14} - C_{18}) as well as longer (C_{30} - C_{40}) fatty acids. Evidence for the waxy lipid bilayer comes from freeze-fracture experiments.⁷⁸ X-ray crystallographic data identified the parallel aligned structure of the mycolic acids

perpendicular to the cytoplasmic membrane, as well as an area of very low fluidity in the region of the inner leaflet.⁷⁹ In this area, the α - and meromycolic branches are very densely packed, contributing to the low permeability of the cell wall, and consequently to the intrinsic natural resistance to many antibiotics. According to X-ray data, the outer lipid is more fluid, which is supported by the observation of an increased permeability caused by surfactants capable of interacting with the membrane.⁸⁰

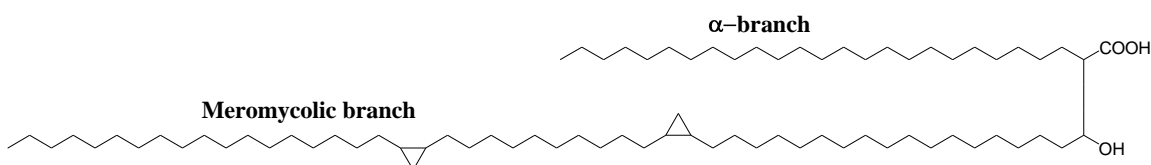


Figure 1.6: Typical mycolic acid in *M. tuberculosis*.

Hoffmann et al. have recently challenged the asymmetric bilayer picture.⁸¹ Using cryo-electron tomography, an inner and an outer cell membrane consisting of what appears to be a morphologically symmetric lipid bilayer was made visible - a structure comparable to the Gram-negative cell envelope (Figure 1.8). Investigations with a mycolic acid deficient mutant of *Corynebacterium glutamicum*, a close relative of mycobacteria, revealed the necessity for the presence of mycolic acid for the formation of the symmetric mycobacterial outer cell wall. Based on their findings, and consistent with earlier experimental data, Hoffmann et al. proposed the structure for the mycobacterial outer membrane shown in Figure 1.7. The location of the mycolic acid (displayed in red) could not yet be identified, leading to the two possibilities A and B.

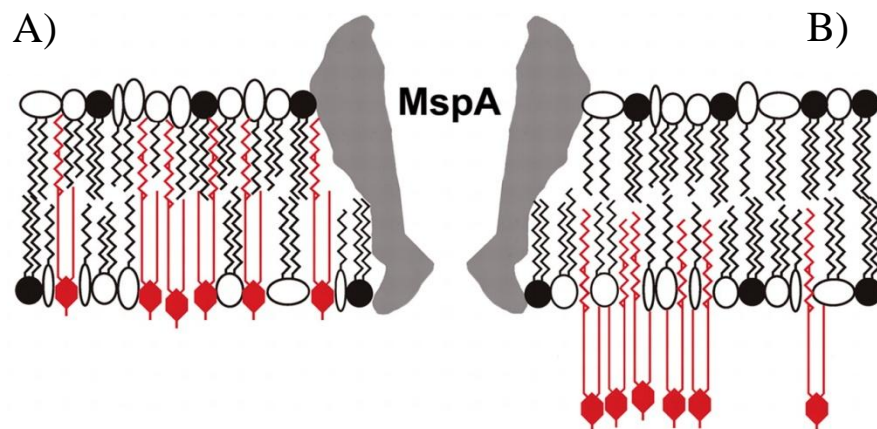


Figure 1.7: Proposed structure of the symmetric outer membrane by Hoffmann et al.: A) mycolic acids fully integrated into the bilayer, B) mycolic acid only partially integrated into the bilayer [mycolic acid (red), polar headgroups (filled symbols), apolar headgroups (open symbols), porin in *M. smegmatis* (MspA)] (Adapted from Ref [80] with Permission from PNAS publishing. Copyright 2008 PNAS publishing).

Other Bacteria Relevant to This Work

Bacteria can be grouped as Gram-positive or Gram-negative using Gram staining. In the early days of antimicrobial photodynamic inactivation, researchers found a decisively different susceptibility of Gram-positive and Gram-negative bacteria. The findings were rationalized by considering the distinctive cell envelope composition of Gram (+/-) bacteria (Figure 1.8 a).⁸² In Gram-positive bacteria, a relatively porous layer of peptidoglycan and lipoteichoic acid surrounds the cytoplasmic membrane,^{83, 84} which can easily be crossed by positively, negatively and neutrally charged photosensitizers, resulting in a high susceptibility to PDI.^{85, 86}

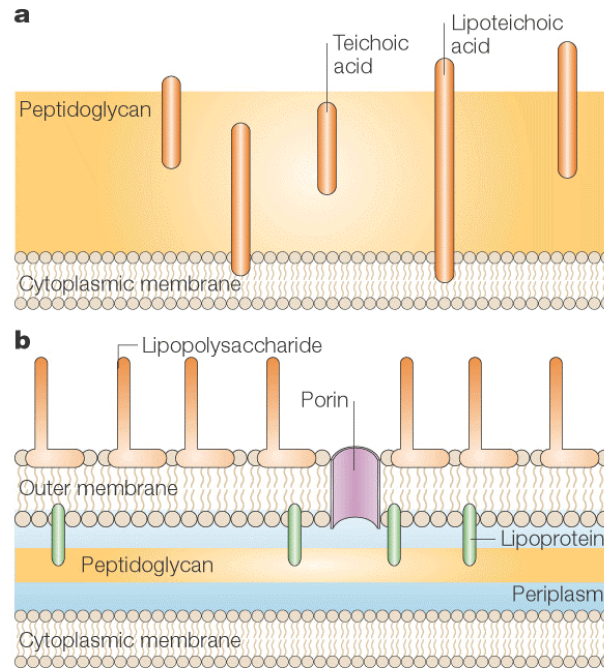


Figure 1.8: Cell envelopes of (a) Gram-positive and (b) Gram-negative bacteria (Reprinted with permission from Macmillan Publishers Ltd: Nature Reviews Microbiology from Ref [83]. Copyright 2005).

Gram-negative bacteria, on the other hand, have an enhanced physical permeability barrier consisting of an inner and outer membrane with an intermediate peptidoglycan-containing periplasm (Figure 1.8 b). Anionic photosensitizers can bind to the outer cell wall, but do not inactivate the bacteria.⁸⁵ However, Nitzan and coworkers observed susceptibility to photodynamic inactivation upon addition of a polycationic peptide, polymyxin B, which increases permeability of the anionic PS by disturbing the cell wall.⁸⁷ Disruption of the cell wall is also procured with EDTA as a co-reagent.⁴⁴ In contrast, both Padova and Brown achieved photodynamic inactivation of Gram-negative bacteria without cell wall disrupting

agents by using positively charged porphyrins and phthalocyanines.^{88, 89} It is now generally agreed upon that cationic PSs bind to the negatively charged cell surface (caused by exposed phospholipids) efficiently. Uptake of cationic photosensitizers is hypothesized to occur via the self-promoted uptake pathway across the outer membrane of Gram-negative bacteria.⁹⁰

Escherichia coli is a Gram-negative, rod-shaped bacterium that can be found in the intestines of many animals and humans. Most strains are non-pathogenic and even benefit the host, i.e., production of vitamin K₂ or prevention of intestinal colonization with pathogenic bacteria.^{86, 91} Pathogenic strains such as O157:H7 can cause serious food poisoning, neonatal meningitis, urinary tract infection, gastroenteritis and diarrhea.⁹² Spread of pathogenic *E. coli* commonly occurs via unhygienic food preparation, manure fertilization, irrigation of crops with and consumption of contaminated water, contact with dairy and beef cattle as well as by flies.⁹³⁻⁹⁸ Antibiotics including amoxicillin, cephalosporins, carbapenems, aztreonam, ciprofloxacin and aminoglycosides are active against *E. coli*, however the development of antibiotic resistance driven by the high rate of adaptive mutations is of major concern.⁹⁹ *E. coli* is also able to transfer drug resistance plasmids to bacteria like *S. aureus*, as well as receive genes such as the one encoding the Shiga toxin in *E. coli* O157:H7.¹⁰⁰ Due to its ease of genetic manipulation, *E. coli* also plays an important role in laboratory culture and biotechnology.¹⁰¹ *E. coli* was the first organism with a completed genome sequence,¹⁰² and the creation of recombinant DNA using plasmids and restriction enzymes was developed using *E. coli*, pioneering the development of modern biotechnology.¹⁰³ Today, *E. coli* can be

found in industrial applications such as in protein synthesis, human insulin production, vaccine development and bioremediation.¹⁰⁴⁻¹⁰⁶

Staphylococcus aureus is a Gram-positive, golden-colored bacterium that grows in grape-like clusters. Although 30-50% of healthy adults are carriers of the bacterium, it does cause a wide range of diseases encompassing simple skin infection, but also life-threatening conditions such as pneumonia, meningitis, bacteremia (blood infection), osteomyelitis (bone infection), endocarditis (infection of the inner lining of the heart), abscesses in internal organs and toxic shock syndrome.¹⁰⁷ *S. aureus* infection is generally contracted by contact with a person, surgical procedures, or via invasive medical or prosthetic devices. The Centers for Disease Control and Prevention estimate that two million patients in the United States receive infections related to health care in hospitals every year, amongst which *S. aureus* infections are within the top five causes.¹⁰⁸ Mortality rates for staphylococcal blood infections range from 11-43%, whereas *S. aureus* induced endocarditis rates of mortality varies from 20-44%.¹⁰⁷ Drug resistance is a major obstacle in the fight against nosocomial infection. Today, 95% of all patients with staphylococcal infections do not respond to first-line antibiotics such as penicillin and ampicillin, and additionally, 55% of strains are now methicillin-resistant.^{109, 110} The rate of methicillin-resistant *S. aureus* infections has doubled in intensive care units from 1987 to 1997, and is now endemic to hospitals globally.¹⁰⁷ *S. aureus* has been found to be able to survive for weeks and months under dry conditions on cotton and polyester fabrics used in the hospital environment.^{111, 112}

Bacteria-targeted Photodynamic Inactivation

The ability of photosensitizers in the photodynamic treatment to damage host cells is a significant disadvantage of photodynamic therapy as well as photodynamic inactivation. Therefore, the development of malignant cell-targeted photosensitizers is of great value. Targetable photosensitizers will not only protect the host tissue, but might also lower the PS dose needed due to improved binding, and possibly allow lower light doses because of less light absorption by unbound PS. Targeting of PS to cancerous cells for photodynamic therapy has been investigated in some detail.^{113, 114} Explored targeting technologies include PS-antibody conjugates for recognition of tumor associated antigens,¹¹⁵⁻¹¹⁸ PS-polymer conjugates for improved pharmacokinetics and biodistribution,^{119, 120} a variety of PS-ligand conjugates for ligand recognition by over-expressed receptors on the cancer cells (lipoprotein,¹²¹ estradiol,^{122, 123} epidermal growth factor,¹²⁴ insulin,¹²⁵⁻¹²⁸ transferring cycle,^{129, 130} saccharides¹³¹), and PS-scavenger conjugates for specific recognition by macrophages.¹³² Comparatively fewer strategies for microbe-targeted photosensitizers can be found in the literature. Such approaches include bacteriophage delivery,¹³³ antibody^{116, 134-136} and polylysine^{49, 137-141} conjugation, exploitation of specific drug-resistance mechanisms,¹⁴² and the use of cell penetrating peptide conjugation.¹⁴³ In photodynamic inactivation of bacteria, most commonly it is the cell wall (particularly for Gram-negative bacteria) that is the major target for photosensitizers. As an example, bacteriochlorophyll conjugates with the immunoglobulin G successfully targeted *S. aureus* strains rich in the surface protein A.¹³⁵ A tin (IV) chloride- immunoglobulin G conjugate was also able to inactivate *S. aureus* and *E. coli* in a strain and growth phase-dependent manor.^{136, 144} Hamblin and co-workers developed

the hypothesis that polylysine containing PS should be able to inactivate gram-positive and gram-negative bacteria.¹¹⁴ Because of the size of the conjugate, temporal selectivity of PS binding/uptake by the bacteria in comparison to mammalian cells should be achievable due to the slower endocytosis mechanism for uptake into mammalian cells. Hamblin and co-workers demonstrated this by selective inactivation of *Actinomyces viscosus* (Gram-positive) and *Porphyromonas gingivalis* (Gram-negative), both oral pathogens, with a chlorin e₆-polylysine conjugate (20 lysine units) while sparing epithelial cells.¹³⁷ More recently, they conducted a study on the influence of the length of the polylysine chain on the inactivation efficiency. Best results against Gram-positive and Gram-negative bacteria were obtained with 37 lysine units.¹⁴¹ Polylysine-chlorin conjugates have also been investigated in infected wounds on mouse models.¹⁴⁵⁻¹⁴⁷ Jori and co-workers demonstrated that porphycene- and cationic porphyrin-polylysine conjugates were also able to inactivate *E. coli* or *S. aureus*.^{139,}¹⁴⁸ In a very recent publication, Zheng et al. described selective photodynamic inactivation of methicillin-resistant *S. aureus* (MRSA) by exploiting a specific drug-resistance pathway of this bacterium.¹⁴² The photosensitizer prodrug consisted of two phenothiazinium photosensitizer units linked by the β -lactam containing cephalosporin derivative. Singlet oxygen production in the prodrug was minimized by quenching due to the close proximity of the two photosensitizer units. The β -lactamases expressed by MRSA (and other β -lactam drug-resistant bacteria) were shown to be able to cleave the β -lactam of the prodrug, thereby releasing the phenothiazinium photosensitizers and relinquishing the quenching effect, followed by photodynamic inactivation of MRSA.¹⁴² While our work was in progress, Bourre et al. presented a study employing a porphyrin-cell penetrating peptide conjugate.¹⁴³ They

used a peptide sequence (GRKKRRGRRRGYKC) derived from the HIV-1 Tat mammalian cell penetrating protein and demonstrated inactivation of Gram-positive and Gram-negative bacteria. However, binding/uptake rates of the PPC by bacteria versus mammalian cells were not reported.

Antimicrobial Peptides

A disadvantage of several of the targeting techniques described in the previous section is the specificity of the approaches towards a particular target, particular strain, or bacterial genus. In the work described in Chapter 3, we set out to contribute to and expand the repertoire of methodologies for targeting bacteria, particularly keeping applicability towards different bacterial genera in mind and using mycobacteria as a specific example. Our targeting strategy is based upon the ability of antimicrobial peptides (AMP) to bind efficiently to the Gram-negative bacterial cell wall.

Antimicrobial peptides are low-molecular-weight peptides (12-50 amino acids) which have recently gathered significant attention in light of the search for new mechanisms combating bacterial infections.¹⁴⁹⁻¹⁵¹ AMPs are part of the human innate immune system, but are also found throughout the animal and plant kingdoms.¹⁵² AMPs were first discovered in the skin of frogs in the 1980s,^{153, 154} and today over 900 naturally occurring defense peptides have been identified.¹⁵⁵ Besides their typical broad-spectrum antibacterial properties, AMPs have been also found to have antiviral,¹⁵⁶ antifungal,^{157, 158} antitumor¹⁵⁹ and immunomodulatory^{160, 161} properties. AMPs can be grouped into four major categories: i) linear,

mostly helical, without cysteine, ii) linear peptides without cysteine, but possessing a composition high in certain amino acids such as proline or arginine, iii) one disulfide bond, or iv) two or more disulfide bonds, β -sheet type structures.¹⁶² AMPs are generally amphiphatic with positively charged and hydrophobic regions.¹⁶³ QSAR analysis of small synthetic peptides shows that the amino acid composition rather than the specific sequence is correlated to the degree of antimicrobial activity.^{164, 165} Generally, AMPs have a net positive charge and contain a high degree of arginine (R), lysine (K) and histidine (H) amino acids. Further, it has been shown that the hydrophobic content of AMPs is correlated to the antibacterial activity.¹⁶⁶ Typically, $\geq 30\%$ hydrophobic amino acids such as tryptophan (W), phenylalanine (F) or tyrosine (Y) are necessary.^{152, 166} More specifically, a multitude of highly active AMPs contain arginine-tryptophan rich motifs and their role has been investigated intensively.^{164, 167, 168}

The mechanism of action of AMPs has been investigated over a decade, but is still not entirely understood. However, the consensus opinion is that the outer bacterial cell membrane is the first point of attack regardless whether AMPs have proposed intracellular targets.^{162, 169, 170} Many small AMPs may lack structure in aqueous media, but take on an α -helical arrangement exposing a cationic and a hydrophobic domain in the presence of a lipid membrane.¹⁶⁸ Amongst many interactions in the AMP-membrane binding process, the cationic side chains electrostatically bind to the phosphate groups of the phospholipids, whereas the hydrophobic groups anchor into the hydrophobic portions of the membrane. The special role of arginine and tryptophan in AMPs can be explained by the ability of arginine, contrary to lysine, to engage in cation π -interactions with tryptophan while maintaining

hydrogen bonding capabilities.¹⁷¹ In addition, tryptophan, with its bulky, paddle-shaped indole side chain, seems to have a particular affinity towards the interfacial layer of phospholipid membranes.¹⁷²

The most prominently discussed bacterial cell death mechanisms include the “carpet” or “barrel-stave” mechanisms (Figure 1.9), whereas other models such as electroporation, or the sinking raft model have received less attention.^{162, 173-175} In the “carpet” mechanism, the hydrophobic side of the helix interacts with the cell membrane, whereas the hydrophilic part is exposed to the medium. Crossing of a threshold concentration results in permeation of the membrane. In the “barrel-stave” mechanism, the AMPs are suggested to aggregate and form pores in the cell membrane, which results in the disruption of vital ion gradients and leakage of cell contents. Preferential attack of bacterial cells by AMPs is driven by electrostatic interactions, not prevalent for zwitterionic mammalian cell surfaces, between the cationic AMP and the anionic bacterial cell surface.

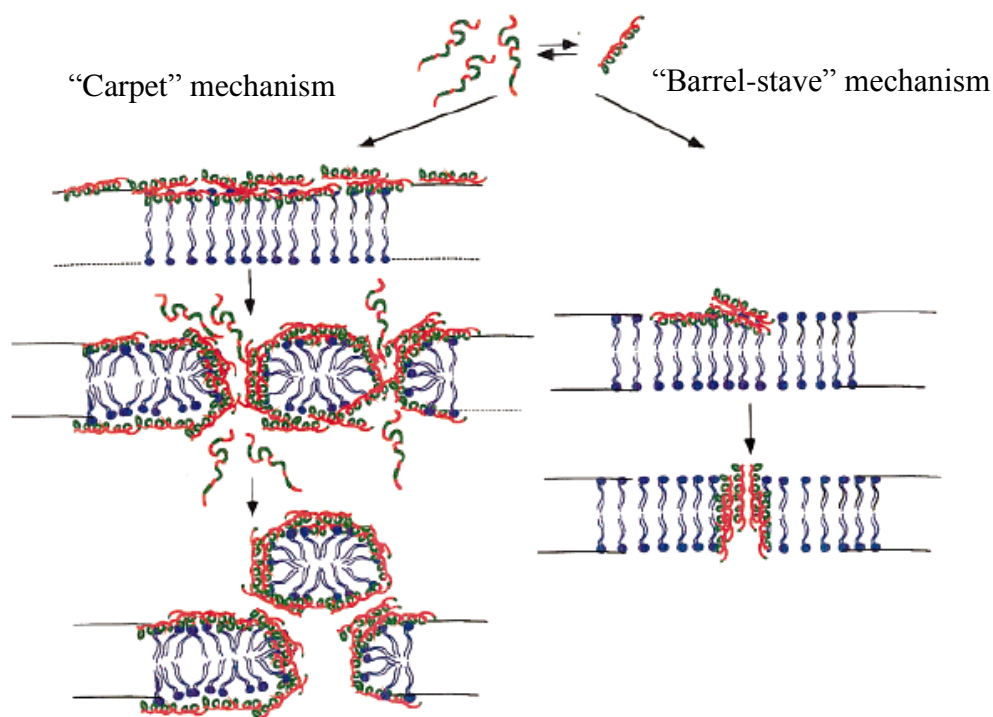


Figure 1.9: Action of antimicrobial peptides (Modified from Ref [163] with permission from John Wiley and Sons. Copyright 1998 John Wiley and Sons).

Driven by the search for alternative therapeutics and new antibiotics for the treatment of bacterial infections, a large number of small synthetic peptides with antimicrobial properties have been investigated.¹⁷⁶⁻¹⁸⁰ Even very short peptide sequences (2-7 amino acids) can display high broad-spectrum antimicrobial activities, making these compounds economically attractive for novel treatments.^{164, 176, 178, 181} For example, Kallenbach and co-workers recently investigated a series of $(RW)_n$ ($n = 1-5$) peptides and found increasing bactericidal (against *S. aureus* and *E. coli*) and hemolytic activities with elongation of the peptide chain.¹⁶⁷ They concluded that $(RW)_3$ provided the optimal cost efficiency with minimal hemolytic activity.

Several natural AMPs have been identified to be active against *M. tuberculosis* and *M. smegmatis*.¹⁸² They include NK-lysin, fragments gran F2 and G13 of granulysin, protegrin PG-39 (residues 1-26) and human neutrophil α -defensin.¹⁸³⁻¹⁸⁶ Antimycobacterial activity of AMPs caused by weakening of the cell wall has been demonstrated by Sharma et al.¹⁸⁷ Related to this study, the membrane weakening ability of AMPs towards the hard to penetrate mycobacterial cell envelope also rationalizes synergistic effects observed for combination treatments of AMPs with common antimycobacterial drugs.^{188, 189} Interestingly, a potential role for AMPs in the development of new tuberculosis vaccines has been discussed.¹⁸²

Overview

Based on the threat of increasingly more difficult to treat diseases caused by bacterial infections, we have set out to investigate the possibility of employing bacteria targeted photodynamic therapy for the eradication of bacteria. In this work, we are employing mycobacteria (with their difficult to penetrate cell envelope) driven by the dire outlook in tuberculosis treatment options and a surging increase in multidrug resistant strains of this bacterium. In particular we have focused here on *M. smegmatis*, a surrogate for *M. tuberculosis* as our model microbe.

In Chapter 2 we present our study demonstrating for the first time the feasibility of the inactivation of *M. smegmatis* using photodynamic inactivation *in vitro*. Techniques and procedures necessary to conduct photodynamic inactivation studies as part of our research

program were developed and optimized using a set of commonly employed commercially available photosensitizers.

The trends established in Chapter 2 allowed us to propose a targeting strategy for bacteria with an outer cell membrane such as myco- or Gram-negative bacteria. In our opinion, successfully targeted photosensitizers are the crucial milestone in order to move this area closer to clinical application. As described in Chapter 3, we developed the synthesis of cationic porphyrin-peptide conjugates. The peptide portion of the conjugate photosensitizers contained peptide sequences mimicking antimicrobial peptides as described earlier in this introduction. We envisioned combining the ability of the porphyrin core to produce singlet oxygen with the ability of antimicrobial peptides to efficiently and preferentially bind to a bacterial cell surface for cell specific targeting.

To enhance the scope and applicability of our photodynamic research, in Chapter 4 we further developed cellulose-porphyrin conjugates in collaboration with Prof. Dimitris S. Argyropoulos of the Department of Forest Biomaterials. Such compounds, based on the structurally well defined and renewable resource cellulose, might find application as components in cotton fibers in fabrics and papers in the food preparation and health care sectors, where prevention of unintended bacterial contamination is crucial for the protection of human health.

REFERENCES

1. *World Health Organization, Tuberculosis Fact Sheet, No 104*. World Health Organization: 2008.
2. *Global tuberculosis Control 2008 surveillance, planning, financing*. World Health Organization: Geneva, 2008.
3. Dye, C.; Watt, C. J.; Bleed, D. M.; Hosseini, S. M.; C.Raviglione, M., Evolution of tuberculosis control and prospects for reducing tuberculosis incidence, prevalence and deaths globally. *Journal of the American Medical Association* **2005**, 293, 2767.
4. *Anti-Tuberculosis Drug Resistance in the World Report No. 4*. The WHO/IUALTD Global project on anti-tuberculosis drug resistance surveillance: Geneva, 2008.
5. *Tuberculosis MDR-TB & XDR-TB Fact Sheet*. World Health Organization: Geneva, 2008.
6. Moore, M.; Onorato, I. M.; McCray, E.; Castro, K. G., Trends in Drug-Resistant Tuberculosis in the United States, 1993-1996. *Journal of the American Medical Association* **1997**, 278, 833.
7. Duncan, K.; Sacchettini, J. C., Approaches to Tuberculosis Drug Development. In *Molecular Genetics of Mycobacteria*, Hatfull, G. F.; William R. Jacobs, J., Eds. ASM Press: Washington DC, 2000; pp 297.
8. Silva, P. A. d.; Ainsa, J. A., Chapter 18: Drugs and Drug Interactions. In *Tuberculosis 2007 from basic Science to patient care*, Palomino, J. C.; Leao, S. C.; Ritacco, V., Eds. 2007.
9. Nuermberger, E. L.; Yoshimatsu, T.; Tyagi, S.; O'Brien, R. J.; Vernon, A. N.; Chaisson, R. E.; Bishai, W. R.; Grosset, J. H., Moxifloxacin-containing Regimen Greatly Reduces Time to Culture Conversion in Murine Tuberculosis. *American Journal of Respiratory and Critical Care Medicine* **2004**, 169, (3), 421.
10. Tortoli, E.; Dionisio, D.; Fabbri, C., Evaluation of Moxifloxacin Activity In Vitro Against Mycobacterium tuberculosis, Including Resistant and Multidrug-Resistant Strains. *Journal of Chemotherapy* **2004**, 16, (4), 334.
11. Onyebujoh, P.; Zumla, A.; Ribeiro, I.; Rustomjee, R.; Mwaba, P.; Gomes, M.; Grange, J. M., Treatment of tuberculosis: present status and future prospects. *Bulletin of the World Health Organization* **2005**, 83, 857.

12. Hu, Y.; Coates, A. R. M.; Mitchison, D. A., Sterilizing Activities of Fluoroquinolones against Rifampin-Tolerant Populations of Mycobacterium tuberculosis. *Antimicrobial Agents and Chemotherapy* **2003**, 47, (2), 653.
13. Ji, B.; Lounis, N.; Maslo, C.; Truffot-Pernot, C.; Bonnafous, P.; Grosset, J., In Vitro and In Vivo Activities of Moxifloxacin and Clinafloxacin against Mycobacterium tuberculosis. *Antimicrobial Agents and Chemotherapy* **1998**, 42, (8), 2066.
14. Barry, C. E.; Boshoff, H. I. M.; Dowd, C. S., Prospects for Clinical Introduction of Nitroimidazole Antibiotics for the Treatment of Tuberculosis. *Current Pharmaceutical Design* **2004**, 10, 3239.
15. Henderson, B. W.; Dougherty, T. J., *Photodynamic Therapy*. Marcel Dekker Inc.: New York, 1992.
16. Macdonald, I. J.; Dougherty, T. J., Basic principles of photodynamic therapy. *Journal of Porphyrins and Phthalocyanines* **2001**, 5, 105.
17. Spikes, J. D., The historical development of ideas on applications of photosensitized reactions in health sciences. In *Primary Photoprocesses in Biology and Medicine*, Bergasson, R. V.; Jori, G.; Land, E. J.; Truscott, T. G., Eds. Plenum Press: New York, 1985; pp 209.
18. Moan, J.; Peng, Q., An Outline of the Hundert-Year History of PDT. *Anticancer Research* **2003**, 23, 3591.
19. Dolmans, D. E. J. G. J.; Fukumura, D.; Jain, R. K., Photodynamic therapy for cancer. *Nature Reviews Cancer* **2003**, 3, (5), 380.
20. Raab, O., Ueber die Wirkung fluoreszierender Stoffe auf Infusorien. *Zeitschrift fuer Biologie* **1900**, 39, 524.
21. von Tappenheimer, H.; Jodlbauer, A., Ueber die Wirkung fluoreszierenden Stoffe auf Infusorien. *Muenchner Medizinische Wochenschrift* **1900**, 47, 5.
22. Jesionek, A.; von Tappeiner, H., Zur Behandlung der Hautcarcinome mit fluoreszierenden Stoffen. *Archiv for Klinische Medizin* **1905**, 82, 223.
23. Roelandts, R., A new light on Niels Finsen, a century after his nobel prize. *Photodermatology, Photoimmunology & Photomedicine* 2005, p 115.
24. Moeller, K. I.; Kongshoj, B.; Philipsen, P. A.; Thomsen, V. O.; Wulf, H. C., How Finsen's light cured lupus vulgaris. *Photodermatology, Photoimmunology & Photomedicine* **2005**, 21, (3), 118.

25. Scherer, H., Chemical-physiological investigations. *Annalen der Chemie und Pharmazie* **1841**, 40, 1.
26. Lipson, R. L.; Baldes, E. J.; Olsen, A. M., Further Evaluation of the Use of Hematoporphyrin Derivative As a New Aid for the Endoscopic Detection of Malignant Disease. *Disease of the Chest* **1964**, 46, (6), 676.
27. Dougherty, T. J., Photodynamic therapy (PDT) of malignant tumors. *Critical Reviews in Oncology/Hematology* **1984**, 2, (2), 83.
28. Stables, G. I.; Ash, D. V., Photodynamic therapy. *Cancer Treatment Reviews* **1995**, 21, (4), 311.
29. Ochsner, M., Photophysical and photobiological processes in the photodynamic therapy of tumours. *Journal of Photochemistry and Photobiology B: Biology* **1997**, 39, (1), 1.
30. Hunt, D.; Margaron, P., Status of therapies in development for the treatment of age-related macular degeneration. *J Drugs* **2003**, 6, 464.
31. Grellier, P.; Santus, R.; Mouray, E.; Agmon, V.; Maziere, J.-C.; Rigomier, D.; Dagan, A.; Gatt, S.; Schrevel, J., Photosensitized Inactivation of Plasmodium falciparum- and Babesia divergens-Infected Erythrocytes in Whole Blood by Lipophilic Pheophorbide Derivatives. *Vox Sanguinis* **1997**, 72, (4), 211.
32. Wainwright, M., Photodynamic antimicrobial chemotherapy (PACT). *Journal of Antimicrobial Chemotherapy* **1998**, 42, (1), 13.
33. Hamblin, M. R.; Hasan, T., Photodynamic therapy: a new antimicrobial approach to infectious disease? *Photochemical & Photobiological Sciences* **2004**, 3, (5), 436.
34. Jori, G.; Brown, S. B., Photosensitized inactivation of microorganisms. *Photochemical & Photobiological Sciences* **2004**, 3, (5), 403.
35. O'Riordan, K.; Akilov, O. E.; Hasan, T., The potential for photodynamic therapy in the treatment of localized infections. *Photodiagnosis and Photodynamic Therapy* **2005**, 2, (4), 247.
36. Maisch, T., Anti-microbial photodynamic therapy: useful in the future? *Lasers in Medical Science* **2007**, 22, (2), 83.
37. Maisch, T.; Szeimies, R.-M.; Jori, G.; Abels, C., Antibacterial photodynamic therapy in dermatology. *Photochemical & Photobiological Sciences* **2004**, 3, (10), 907.

38. Jori, G.; Coppellotti, O., Inactivation of Pathogenic Microorganisms by Photodynamic Techniques: Mechanistic Aspects and Perspective Applications. *Anti-Infective Agents in Medicinal Chemistry* **2007**, 6, 119.
39. Demidova, T. N.; Hamblin, M. R., Photodynamic Therapy Targeted to Pathogens. *International Journal of Immunopathology and Pharmacology* **2004**, 17, (3), 245.
40. Szacilowski, K.; Macyk, W.; Drzewiecka-Matuszek, A.; Brindell, M.; Stochel, G., Bioinorganic Photochemistry: Frontiers and Mechanisms. *Chemical Reviews* **2005**, 105, (6), 2647.
41. Weishaupt K R; Gomer C J; Dougherty, T. J., Identification of singlet oxygen as the cytotoxic agent in photo-inactivation of a murine tumor. *Cancer Research* **1976**, 36, 2326-2329.
42. Chen, G. G.; Sin, F. L. F.; Leung, B. C. S.; Ng, H. K.; Poon, W. S., Differential role of hydrogen peroxide and staurosporine in induction of cell death in glioblastoma cells lacking DNA-dependent protein kinase. *Apoptosis* **2005**, 10, (1), 185.
43. Oleinick, N. L.; Morris, R. L.; Belichenko, I., The role of apoptosis in response to photodynamic therapy: what, where, why, and how. *Photochemical & Photobiological Sciences* **2002**, 1, (1), 1.
44. Bertolini, G.; Rossi, F.; Valduga, G.; Jori, G.; van Lier, J., Photosensitizing activity of water- and lipid-soluble phthalocyanines on Escherichia coli. *FEMS Microbiology Letters* **1990**, 71, (1-2), 149.
45. Jori, G., Inactivation of Pathogenic Microorganisms by Photodynamic Techniques: Mechanistic Aspects and Perspective Applications. *Anti-Infective Agents in Medicinal Chemistry* **2007**, 6, (2), 119.
46. Masuda, N.; Church, G. M., Escherichia coli Gene Expression Responsive to Levels of the Response Regulator EvgA. *Journal of Bacteriology* **2002**, 184, (22), 6225.
47. Maisch, T., Revitalizes Strategies Against Multidrug-Resistant bacteria: Anti-microbial Photodynamic Therapy and Bacteriophage Therapy. *Anti-Infective Agents in Medicinal Chemistry* **2007**, 6, (2), 145.
48. Vaara, M.; Vaara, T.; Jensen, M.; Helander, I.; Nurminen, M.; Rietschel, E. T.; Mäkelä, P. H., Characterization of the lipopolysaccharide from the polymyxin-resistant pmrA mutants of Salmonella typhimurium. *FEBS Letters* **1981**, 129, (1), 145.
49. Gad, F.; Zahra, T.; Hasan, T.; Hamblin, M. R., Effects of Growth Phase and Extracellular Slime on Photodynamic Inactivation of Gram-Positive Pathogenic Bacteria. *Antimicrobial Agents and Chemotherapy* **2004**, 48, (6), 2173.

50. Smijs, T. G. M.; Nivard, M. J. M.; Schuitmaker, H. J., Development of a Test System for Mutagenicity of Photosensitizers Using *Drosophila melanogaster*. *Photochemistry and Photobiology* **2004**, 79, (4), 332.
51. Evans, H. H.; Horng, M.-F.; Ricanati, M.; Deahl, J. T.; Oleinick, N. L., Mutagenicity of Photodynamic Therapy as Compared to UVC and Ionizing Radiation in Human and Murine Lymphoblast Cell Lines. *Photochemistry and Photobiology* **1997**, 66, (5), 690.
52. Stockert, J. C.; Canete, M.; Juarranz, A.; Villanueva, A.; Horobin, R. W.; Borrell, J. I.; Teixido, J.; Nonell, S., Porphycenes: Facts and Prospects in Photodynamic Therapy of Cancer. *Current Medicinal Chemistry* **2007**, 14, (9), 997.
53. Sternberg, E. D.; Dolphin, D.; Brückner, C., Porphyrin-based photosensitizers for use in photodynamic therapy. *Tetrahedron* **1998**, 54, (17), 4151.
54. Dei, D.; Chiti, G.; Filippis, M. P. d.; Fanetti, L.; Giuliani, F.; Giuntini, F.; Giulio, M.; Fantetti, L.; Giuliani, F.; Giuntini, F.; Soncin, M.; Jori, G.; Roncucci, G., Phthalocyanines as photodynamic agents for the inactivation of microbial pathogens. *Journal of Porphyrins and Phthalocyanines* **2006**, 10, 147.
55. Rubio, N.; Prat, F.; Bou, N.; Borrell, J. I.; Teixido, J.; Villanueva, A.; Juarranz, A.; Canete, M.; Stockert, J. C.; Nonell, S., A comparison between the photophysical and photosensitising properties of tetraphenyl porphycenes and porphyrins. *New Journal of Chemistry* **2005**, 29, (2), 378.
56. Harris, F.; Chatfield, L. K.; Phoenix, D. A., Phenothiazinium Based Photosensitisers - Photodynamic Agents with a Multiplicity of Cellular Targets and Clinical Applications. *Current Drug Targets* **2005**, 6, (5), 615.
57. Mitra, S.; Foster, T. H., Photochemical Oxygen Consumption Sensitized by a Porphyrin Phosphorescent Probe in Two Model Systems. *Biophysical Journal* **2000**, 78, (5), 2597.
58. Brun, A. M.; Harriman, A., Energy- and Electron-Transfer Processes Involving Palladium Porphyrins Bound to DNA. *Journal of the American Chemical Society* **1994**, 116, (23), 10383.
59. Eastwood, D.; Gouterman, M., Porphyrins: XVIII. Luminescence of (Co), (Ni), Pd, Pt complexes. *Journal of Molecular Spectroscopy* **1970**, 35, (3), 359.
60. Soncin, M.; Fabris, C.; Busetti, A.; Dei, D.; Nistri, D.; Roncucci, G.; Jori, G., Approaches to selectivity in the Zn(ii)-phthalocyanine-photosensitized inactivation of wild-type and antibiotic-resistant *Staphylococcus aureus*. *Photochemical & Photobiological Sciences* **2002**, 1, (10), 815.

61. Koch, R., Aetiologie der Tuberculose. *Berliner klinische Wochenschrift* **1882**, 19, (15), 221.
62. Daniel, T. M., The history of tuberculosis. *Respiratory Medicine* **2006**, 100, (11), 1862.
63. Hayman, J., Mycobacterium ulcerans: An infection from Jurassic time? *The Lancet* **1984**, 324, (8410), 1015.
64. Doetsch, R. N., Benjamin Marten and His "New Theory of Consumptions". *Microbiological Reviews* **1978**, 42, (3), 521.
65. Kaufmann, S. H. E.; Schaible, U. E., 100th anniversary of Robert Koch's Nobel Prize for the discovery of the tubercle bacillus. *Trends in Microbiology* **2005**, 13, (10), 469.
66. Goodfellow, M.; Minnikin, D. E., Circumscription of the Genus. In *The Mycobacteria A Sourcebook, Part A*, George P. Kubiccia; Wayne, L. G., Eds. Marcel Dekker, Inc: New York, 1984; pp 1.
67. Chaturvedi, V.; Dwivedi, N.; Tripathi, R. P.; Sinha, S., Evaluation of Mycobacterium smegmatis as a possible surrogate screen for selecting molecules active against multi-drug resistant Mycobacterium tuberculosis. *The Journal of General and Applied Microbiology* **2007**, 53, (6), 333.
68. Jacobs, W. R., Jr.; Hatfull, G. F., *Mycobacterium tuberculosis; a Once Genetically Intractable Organism*. ASM Press, Washington DC, 2000; p 1.
69. Jacobs, W. R.; Tuckman, M.; Bloom, B. R., Introduction of foreign DNA into mycobacteria using a shuttle plasmid. *Nature* **1987**, 327, (6122), 532.
70. Fu, L. M.; Fu-Liu, C. S., Is Mycobacterium tuberculosis a closer relative to Gram-positive or Gram-negative bacterial pathogens? *Tuberculosis* **2002**, 82, (2-3), 85.
71. Brennan, P. J.; Nikaido, H., The Envelope of Mycobacteria. *Annual Review of Biochemistry* **1995**, 64, (1), 29.
72. Trias, J.; Benz, R., Permeability of the cell wall of Mycobacterium smegmatis. *Molecular Microbiology* **1994**, 14, (2), 283.
73. Wallace, R. J., Jr.; Dalovisio, J. R.; Pankey, G. A., Disk diffusion testing of susceptibility of Mycobacterium fortuitum and Mycobacterium chelonae to antibacterial agents. *Antimicrobial Agents and Chemotherapy* **1979**, 16, (5), 611.
74. Haemers, A.; Leysen, D. C.; Bollaert, W.; Zhang, M. Q.; Pattyn, S. R., Influence of N substitution on antimycobacterial activity of ciprofloxacin. *Antimicrobial Agents and Chemotherapy* **1990**, 34, (3), 496.

75. Yajko, D. M.; Sanders, C. A.; Nassos, P. S.; Hadley, W. K., In vitro susceptibility of *Mycobacterium avium* complex to the new fluoroquinolone sparfloxacin (CI-978; AT-4140) and comparison with ciprofloxacin. *Antimicrobial Agents and Chemotherapy* **1990**, 34, (12), 2442.
76. Tambe, Y. Schematic diagram of Mycobacterial cell wall. http://en.wikipedia.org/wiki/File:Mycobacterial_cell_wall_diagram.png (26 February 2011),
77. Minnikin, D. E., In *The Biology of the Mycobacteria*, Ratledge, C.; Stanford, J. L., Eds. Academic: London, 1982; pp 95.
78. Puech, V.; Chami, M.; Lemassu, A.; Laneelle, M.-A.; Schiffler, B.; Gounon, P.; Bayan, N.; Benz, R.; Daffe, M., Structure of the cell envelope of corynebacteria: importance of the non-covalently bound lipids in the formation of the cell wall permeability barrier and fracture plane. *Microbiology* **2001**, 147, (5), 1365.
79. Nikaido, H.; Kim, S.-H.; Rosenberg, E. Y., Physical organization of lipids in the cell wall of *Mycobacterium chelonae*. *Molecular Microbiology* **1993**, 8, (6), 1025.
80. Hui, J.; Gordon, N.; Kajioka, R., Permeability Barrier to Rifampin in Mycobacteria. *Antimicrobial Agents and Chemotherapy* **1977**, 11, (5), 773.
81. Hoffmann, C.; Leis, A.; Niederweis, M.; Plitzko, J. M.; Engelhardt, H., Disclosure of the mycobacterial outer membrane: Cryo-electron tomography and vitreous sections reveal the lipid bilayer structure. *Proceedings of the National Academy of Sciences* **2008**, 105, (10), 3963.
82. Weidenmaier, C.; Peschel, A., Teichoic acids and related cell-wall glycopolymers in Gram-positive physiology and host interactions. *Nat Rev Micro* **2008**, 6, (4), 276.
83. Cabeen, M. T.; Jacobs-Wagner, C., Bacterial cell shape. *Nature Reviews Microbiology* **2005**, 3, (8), 601.
84. Navarre, W. W.; Schneewind, O., Surface proteins of gram-positive bacteria and mechanisms of their targeting to the cell wall envelope. *Microbiology And Molecular Biology Reviews* **1999**, 63, (1), 174.
85. Malik, Z.; Ladan, H.; Nitzan, Y., Photodynamic inactivation of Gram-negative bacteria: Problems and possible solutions. *Journal of Photochemistry and Photobiology B: Biology* **1992**, 14, (3), 262.
86. Reid, G.; Howard, J.; Gan, B. S., Can bacterial interference prevent infection? *Trends in Microbiology* **2001**, 9, (9), 424.

87. Nitzan, Y.; Gutterman, M.; Malik, Z.; Ehrenberg, B., Inactivation of gram-negative bacteria by photosensitized porphyrins. *Photochemistry and Photobiology* **1992**, 55, (1), 89.
88. Merchat, M.; Bertolini, G.; Giacomini, P.; Villaneuva, A.; Jori, G., Meso-substituted cationic porphyrins as efficient photosensitizers of gram-positive and gram-negative bacteria. *Journal of Photochemistry and Photobiology B: Biology* **1996**, 32, (3), 153.
89. Minnock, A.; Vernon, D. I.; Schofield, J.; Griffiths, J.; Howard Parish, J.; Brown, S. B., Photoinactivation of bacteria. Use of a cationic water-soluble zinc phthalocyanine to photoinactivate both Gram-negative and Gram-positive bacteria. *Journal of Photochemistry and Photobiology B: Biology* **1996**, 32, (3), 159.
90. Hancock, R. E. W., Alterations in Outer Membrane Permeability. *Annual Review of Microbiology* **1984**, 38, (1), 237.
91. Bentley, R.; Meganathan, R., Biosynthesis of vitamin K (menaquinone) in bacteria. *Microbiology and Molecular Biology Reviews* **1982**, 46, (3), 241.
92. Nataro, J. P.; Kaper, J. B., Diarrheagenic Escherichia coli. *Clinical Microbiology Reviews* **1998**, 11, (1), 142.
93. Heaton, J. C.; Jones, K., Microbial contamination of fruit and vegetables and the behaviour of enteropathogens in the phyllosphere: a review. *Journal of Applied Microbiology* **2008**, 104, (3), 613.
94. RM, C.; Aird H, B. F., Waterborne Escherichia coli O157. *Symposium series (Society for Applied Microbiology)* **2000**, 29, 142S.
95. Bach, S. J.; McAllister, T. A.; Veira, D. M.; Gannon, V. P. J.; Holley, R. A., Transmission and control of Escherichia coli O157:H7 — A review. *Canadian Journal of Animal Science* **2002**, 82, (4), 475.
96. Sela, S.; Nestel, D.; Pinto, R.; Nemny-Lavy, E.; Bar-Joseph, M., Mediterranean Fruit Fly as a Potential Vector of Bacterial Pathogens. *Applied and Environmental Microbiology* **2005**, 71, (7), 4052.
97. Rahn, K.; Renwick, S. A.; Johnson, R. P.; Wilson, J. B.; Clarke, R. C.; Alves, D.; McEwen, S. A.; Lior, H.; Spika, J., Follow-up Study of Verocytotoxigenic Escherichia coli Infection in Dairy Farm Families. *Journal of Infectious Diseases* **1998**, 177, (4), 1139.
98. Alam, M. J.; Zurek, L., Association of Escherichia coli O157:H7 with Houseflies on a Cattle Farm. *Applied Environmental Microbiology* **2004**, 70, (12), 7578.
99. Perfeito, L. I.; Fernandes, L.; Mota, C.; Gordo, I., Adaptive Mutations in Bacteria: High Rate and Small Effects. *Science* **2007**, 317, (5839), 813.

100. Brussow, H.; Canchaya, C.; Hardt, W.-D., Phages and the Evolution of Bacterial Pathogens: from Genomic Rearrangements to Lysogenic Conversion. *Microbiology and Molecular Biology Reviews* **2004**, 68, (3), 560.
101. Lee, S. Y., High cell-density culture of Escherichia coli. *Trends in Biotechnology* **1996**, 14, (3), 98.
102. Blattner, F. R.; Plunkett, G.; Bloch, C. A.; Perna, N. T.; Burland, V.; Riley, M.; Collado-Vides, J.; Glasner, J. D.; Rode, C. K.; Mayhew, G. F.; Gregor, J.; Davis, N. W.; Kirkpatrick, H. A.; Goeden, M. A.; Rose, D. J.; Mau, B.; Shao, Y., The Complete Genome Sequence of Escherichia coli K-12. *Science* **1997**, 277, (5331), 1453.
103. Russo, E., Special Report: The birth of biotechnology. *Nature* **2003**, 421, (6921), 456.
104. Cornelis, P., Expressing genes in different Escherichia coli compartments. *Current Opinion in Biotechnology* **2000**, 11, (5), 450.
105. Jana, S.; Deb, J. K., Strategies for efficient production of heterologous proteins in Escherichia coli. *Applied Microbiology and Biotechnology* **2005**, 67, (3), 289.
106. Nilsson, J.; Jonasson, P.; Samuelsson, E.; Stahl, S.; Uhlén, M., Integrated production of human insulin and its C-peptide. *Journal of Biotechnology* **1996**, 48, (3), 241.
107. Lowy, F. D., Staphylococcus aureus Infections. *New England Journal of Medicine* **1998**, 339, (8), 520.
108. Klevens, R. M.; Edwards, J. R.; Richards, C. L.; Horan, T. c.; Gaynes, R. P.; Pollock, D. A.; Cardo, D. M., Estimating Health care-associated Infections and Deaths in U.S. Hospitals, 2002. In Prevention, C. f. D. C. a., Ed. Centers for Disease Control and Prevention: 2007; Vol. 122, pp 160.
109. Rubin, R. J.; Harrington, C. A.; Poon, A.; Dietrich, K.; Greene, J. A.; Moiduddin, A., The Economic Impact of Staphylococcus aureus Infection in New York City Hospitals. *Emerging Infectious Diseases* **1999**, 5, (1), 9.
110. System, A. r. f. t. N., National Nosocomial Infections Surveillance (NNIS) System Report, data summary from January 1992 through June 2003, issued August 2003. *American journal of infection control* **2003**, 31, (8), 481.
111. Cimolai, N., MRSA and the environment: implications for comprehensive control measures. *European journal of clinical microbiology & infectious diseases: official publication of the European Society of Clinical Microbiology* **2008**, 27, (7), 481.
112. Neely, A. N.; Maley, M. P., Survival of Enterococci and Staphylococci on Hospital Fabrics and Plastic. *Journal of Clinical Microbiology* **2000**, 38, (2), 724.

113. Hudson, R.; Boyle, R. W., Strategies for selective delivery of photodynamic sensitizers to biological targets. *Journal of Porphyrins and Phthalocyanines* **2004**, 8, 954.
114. Hamblin, M. R., Covalent photosensitizer conjugates for targeted photodynamic therapy. *Trends in Photochemistry & Photobiology* **2002**, 9, 1.
115. Yarmush, M. L.; Thorpe, W. P.; Strong, L.; Rakestraw, S. L.; Toner, M.; Tompkins, R. G., Antibody Targeted Photolysis. *Critical Reviews in Therapeutic Drug Carrier Systems* **1993**, 10, (3), 197.
116. Bhatti, M.; MacRobert, A.; Henderson, B.; Shepherd, P.; Cridland, J.; Wilson, M., Antibody-Targeted Lethal Photosensitization of *Porphyromonas gingivalis*. *Antimicrobial Agents and Chemotherapy* **2000**, 44, (10), 2615.
117. Hamblin, M. R.; Bamberg, M. P.; Miller, J. L.; Hasan, T., Cationic Photoimmunoconjugates Between Monoclonal Antibodies and Hematoporphyrin: Selective Photodestruction of Ovarian Cancer Cells. *Applied Optics* **1998**, 37, (31), 7184.
118. Hamblin, M. R.; Miller, J. L.; Hasan, T., Effect of Charge on the Interaction of Site-specific Photoimmunoconjugates with Human Ovarian Cancer Cells. *Cancer Research* **1996**, 56, (22), 5205.
119. Duncan, R.; Spreafico, F., Polymer Conjugates: Pharmacokinetic Considerations for Design and Development. *Clinical Pharmacokinetics* **1994**, 27, (4), 290.
120. Hamblin, M. R.; Miller, J. L.; Rizvi, I.; Ortel, B.; Maytin, E. V.; Hasan, T., Pegylation of a Chlorin e6 Polymer Conjugate Increases Tumor Targeting of Photosensitizer. *Cancer Research* **2001**, 61, (19), 7155.
121. Jori, G.; Reddi, E., The role of lipoproteins in the delivery of tumour-targeting photosensitizers. *International Journal of Biochemistry* **1993**, 25, (10), 1369.
122. James, D. A.; Swamy, N.; Paz, N.; Hanson, R. N.; Ray, R., Synthesis and estrogen receptor binding affinity of a porphyrin-estradiol conjugate for targeted photodynamic therapy of cancer. *Bioorganic & Medicinal Chemistry Letters* **1999**, 9, (16), 2379.
123. Swamy, N.; James, D. A.; Mohr, S. C.; Hanson, R. N.; Ray, R., An estradiol-Porphyrin conjugate selectively localizes into estrogen receptor-Positive breast cancer cells. *Bioorganic & Medicinal Chemistry* **2002**, 10, (10), 3237.
124. Gijssens, A.; Witte, P. D., Photocytotoxic action of EGF-PVA-Sn(IV)chlorin e6 and EGF-dextran-Sn(IV)chlorin e6 internalizable conjugates on A431 cells. *International Journal of Oncology* **1998**, 13, (6), 1171.

125. Hekrnreiter, M.; Kagan, J.; Chen, X.; Lau, K. Y.; D'Auria, M.; Vantaggi, A., Phototoxicity of (1*H*-indenyl)thiophenes. *Photochemistry and Photobiology* **1993**, 58, (1), 49.
126. Akhlynina, T. V.; Rosenkranz, A. A.; Jans, D. A.; Sobolev, A. S., Insulin-mediated Intracellular Targeting Enhances the Photodynamic Activity of Chlorin e6. *Cancer Research* **1995**, 55, (5), 1014.
127. Akhlynina, T. V.; Jans, D. A.; Rosenkranz, A. A.; Statsyuk, N. V.; Balashova, I. Y.; Toth, G.; Pavo, I.; Rubin, A. B.; Sobolev, A. S., Nuclear Targeting of Chlorin e6 Enhances Its Photosensitizing Activity. *Journal of Biological Chemistry* **1997**, 272, (33), 20328.
128. Akhlynina, T. V.; Jans, D. A.; Statsyuk, N. V.; Balashova, I. Y.; Toth, G.; Pavo, I.; Rosenkranz, A. A.; Naroditsky, B. S.; Sobolev, A. S., Adenoviruses synergize with nuclear localization signals to enhance nuclear delivery and photodynamic action of internalizable conjugates containing chlorin e6. *International Journal of Cancer* **1999**, 81, (5), 734.
129. Wellhoner, H. H.; Neville, D. M.; Srinivasachar, K.; Erdmann, G., Uptake and concentration of bioactive macromolecules by K562 cells via the transferrin cycle utilizing an acid-labile transferrin conjugate. *Journal of Biological Chemistry* **1991**, 266, (7), 4309.
130. Hamblin, M. R.; Newman, E. L., Photosensitizer targeting in photodynamic therapy I. Conjugates of haematoporphyrin with albumin and transferrin. *Journal of Photochemistry and Photobiology B: Biology* **1994**, 26, (1), 45.
131. Chen, X.; Hui, L.; Foster, D. A.; Drain, C. M., Efficient Synthesis and Photodynamic Activity of Porphyrin-Saccharide Conjugates: Targeting and Incapacitating Cancer Cells. *Biochemistry* **2004**, 43, (34), 10918.
132. Hamblin, M. R.; Miller, J. L.; Ortel, B., Scavenger-Receptor Targeted Photodynamic Therapy. *Photochemistry and Photobiology* **2000**, 72, (4), 533.
133. Embleton, M. L.; Nair, S. P.; Heywood, W.; Menon, D. C.; Cookson, B. D.; Wilson, M., Development of a Novel Targeting System for Lethal Photosensitization of Antibiotic-Resistant Strains of *Staphylococcus aureus*. *Antimicrobial Agents and Chemotherapy* **2005**, 49, (9), 3690.
134. Berthiaume, F.; Reiken, S. R.; Toner, M.; Tompkins, R. G.; Yarmush, M. L., Antibody-targeted photolysis of bacteria in vivo. *Biotechnology (NY)* **1994**, 12, (7), 703.
135. Gross, S.; Brandis, A.; Chen, L.; Rosenbach-Belkin, V.; Roehrs, S.; Scherz, A.; Salomon, Y., Protein-A-mediated Targeting of Bacteriochlorophyll-IgG to *Staphylococcus aureus*: A Model for Enhanced Site-Specific Photocytotoxicity. *Photochemistry and Photobiology* **1997**, 66, (6), 872.

136. Embleton, M. L.; Nair, S. P.; Cookson, B. D.; Wilson, M., Selective lethal photosensitization of methicillin-resistant *Staphylococcus aureus* using an IgG-tin (IV) chlorin e6 conjugate. *Journal of Antimicrobial Chemotherapy* **2002**, 50, (6), 857.
137. Soukos, N. S.; Hamblin, M. R.; Hasan, T., The Effect of Charge on Cellular Uptake and Phototoxicity of Polylysine Chlorin(e6)-Conjugates. *Photochemistry and Photobiology* **1997**, 65, (4), 723.
138. Rovaldi, C. R.; Pievsky, A.; Sole, N. A.; Friden, P. M.; Rothstein, D. M.; Spacciapoli, P., Photoactive Porphyrin Derivative with Broad-Spectrum Activity against Oral Pathogens In Vitro. *Antimicrobial Agents and Chemotherapy* **2000**, 44, (12), 3364.
139. Polo, L.; Segalla, A.; Bertoloni, G.; Jori, G.; Schaffner, K.; Reddi, E., Polylysine-porphycene conjugates as efficient photosensitizers for the inactivation of microbial pathogens. *Journal of Photochemistry and Photobiology B: Biology* **2000**, 59, (1-3), 152.
140. Lauro, F. M.; Pretto, P.; Covolo, L.; Jori, G.; Bertoloni, G., Photoinactivation of bacterial strains involved in periodontal diseases sensitized by porphycene-polylysine conjugates. *Photochemical & Photobiological Sciences* **2002**, 1, (7), 468.
141. Hamblin, M. R.; O'Donnell, D. A.; Murthy, N.; Rajagopalan, K.; Michaud, N.; Sherwood, M. E.; Hasan, T., Polycationic photosensitizer conjugates: effects of chain length and Gram classification on the photodynamic inactivation of bacteria. *Journal of Antimicrobial Chemotherapy* **2002**, 49, (6), 941.
142. Zheng, X.; Sallum, U.; Verma, S.; Athar, H.; Evans, C.; Hasan, T., Exploiting a Bacterial Drug-Resistance Mechanism: A Light-Activated Construct for the Destruction of MRSA. *Angewandte Chemie International Edition* **2009**, 48, (12), 2148.
143. Bourre, L.; Giuntini, F.; Eggleston, I. M.; Mosse, C. A.; MacRobert, A. J.; Wilson, M., Effective photoinactivation of Gram-positive and Gram-negative bacterial strains using an HIV-1 Tat peptide-porphyrin conjugate. *Photochemical & Photobiological Sciences* **2010**, 9, (12), 1613.
144. Embleton, M. L.; Nair, S. P.; Cookson, B. D.; Wilson, M., Antibody-Directed Photodynamic Therapy of Methicillin-Resistant *Staphylococcus aureus*. *Microbial Drug Resistance* **2004**, 10, (2), 92.
145. Gad, F.; Zahra, T.; Francis, K. P.; Hasan, T.; Hamblin, M. R., Targeted photodynamic therapy of established soft-tissue infections in mice. *Photochemical & Photobiological Sciences* **2004**, 3, (5), 451.
146. Hamblin, M. R.; Zahra, T.; Contag, C. H.; McManus, A. T.; Hasan, T., Optical Monitoring and Treatment of Potentially Lethal Wound Infections In Vivo. *Journal of Infectious Diseases* **2003**, 187, (11), 1717.

147. Hamblin, M. R.; O'Donnell, D. A.; Murthy, N.; Contag, C. H.; Hasan, T., Rapid Control of Wound Infections by Targeted Photodynamic Therapy Monitored by In Vivo Bioluminescence Imaging. *Photochemistry and Photobiology* **2002**, 75, (1), 51.
148. Tome, J. P. C.; Neves, M. G. P. M. S.; Tome, A. C.; Cavaleiro, J. A. S.; Soncin, M.; Magaraggia, M.; Ferro, S.; Jori, G., Synthesis and Antibacterial Activity of New Poly-S-lysine-Porphyrin Conjugates. *Journal of Medicinal Chemistry* **2004**, 47, (26), 6649.
149. Wang, Z.; Wang, G., APD: the Antimicrobial Peptide Database. *Nucleic Acids Research* **2004**, 32, D590.
150. Wang, G., *Antimicrobial Peptides: Discovery, Design and Novel Therapeutic Strategies*. Wallingford: Oxfordshire, 2010.
151. Boman, H. G., Peptide Antibiotics and their Role in Innate Immunity. *Annual Review of Immunology* **1995**, 13, (1), 61.
152. Zasloff, M., Antimicrobial peptides of multicellular organisms. *Nature* **2002**, 415, (6870), 389.
153. Steiner, H.; Hultmark, D.; Engstrom, A.; Bennich, H.; Boman, H. G., Sequence and specificity of two antibacterial proteins involved in insect immunity. *Nature* **1981**, 292, (5820), 246.
154. Zasloff, M., Magainins, a class of antimicrobial peptides from *Xenopus* skin: isolation, characterization of two active forms, and partial cDNA sequence of a precursor. *Proceedings of the National Academy of Sciences of the United States of America* **1987**, 84, (15), 5449.
155. Tossi, A.; Mitaritonna, N.; Tarantino, C.; Giangaspero, A.; Sandri, L.; Winterstein, K., Antimicrobial Database; <http://www.bbcm.units.it/~tossi/pag1.htm>. In Universitaet Trieste.
156. Andersen, J. H.; Jenssen, H.; Sandvik, K.; Gutteberg, T. J., Anti-HSV activity of lactoferrin and lactoferricin is dependent on the presence of heparan sulphate at the cell surface. *Journal of Medical Virology* **2004**, 74, (2), 262.
157. De Lucca, A. J.; Walsh, T. J., Antifungal Peptides: Novel Therapeutic Compounds against Emerging Pathogens. *Antimicrobial Agents and Chemotherapy* **1999**, 43, (1), 1.
158. Theis, T.; Stahl, U., Antifungal proteins: targets, mechanisms and prospective applications. *Cellular and Molecular Life Sciences* **2004**, 61, (4), 437.
159. Papo, N.; Shai, Y., Host defense peptides as new weapons in cancer treatment. *Cellular and Molecular Life Sciences* **2005**, 62, (7), 784.

160. Jerala, R.; Porro, M., Endotoxin Neutralizing Peptides. *Current Topics in Medicinal Chemistry* **2004**, 4, 1173.
161. McPhee, J. B.; Scott, M. G.; Hancock, R. E. W., Design of Host Defence Peptides for Antimicrobial and Immunity Enhancing Activities. *Combinatorial Chemistry & High Throughput Screening* **2005**, 8, (3), 257.
162. Oren, Z.; Shai, Y., Mode of action of linear amphipathic alpha-helical antimicrobial peptides. *Peptide Science* **1998**, 47, (6), 451.
163. Dathe, M.; Wieprecht, T., Structural features of helical antimicrobial peptides: their potential to modulate activity on model membranes and biological cells. *Biochimica et Biophysica Acta (BBA) - Biomembranes* **1999**, 1462, (1-2), 71.
164. Strøm, M. B.; Rekdal, Ø.; Svendsen, J. S., Antimicrobial activity of short arginine- and tryptophan-rich peptides. *Journal of Peptide Science* **2002**, 8, (8), 431.
165. Giuliani, A.; Pirri, G.; Nicoletto, S., Antimicrobial peptides: an overview of a promising class of therapeutics. *Central European Journal of Biology* **2007**, 2, (1), 1.
166. Chen, Y.; Guarnieri, M. T.; Vasil, A. I.; Vasil, M. L.; Mant, C. T.; Hodges, R. S., Role of Peptide Hydrophobicity in the Mechanism of Action of alpha-Helical Antimicrobial Peptides. *Antimicrobial Agents and Chemotherapy* **2007**, 51, (4), 1398.
167. Liu, Z.; Brady, A.; Young, A.; Rasimick, B.; Chen, K.; Zhou, C.; Kallenbach, N. R., Length Effects in Antimicrobial Peptides of the (RW)_n Series. *Antimicrobial Agents and Chemotherapy* **2007**, 51, (2), 597.
168. Chan, D. I.; Prenner, E. J.; Vogel, H. J., Tryptophan- and arginine-rich antimicrobial peptides: Structures and mechanisms of action. *Biochimica et Biophysica Acta (BBA) - Biomembranes* **2006**, 1758, (9), 1184.
169. Brogden, K. A., Antimicrobial peptides: pore formers or metabolic inhibitors in bacteria? *Nature Reviews Microbiology* **2005**, 3, (3), 238.
170. Papo, N.; Shai, Y., Can we predict biological activity of antimicrobial peptides from their interactions with model phospholipid membranes? *Peptides* **2003**, 24, (11), 1693.
171. Aliste, M. P.; MacCallum, J. L.; Tieleman, D. P., Molecular Dynamics Simulations of Pentapeptides at Interfaces: Salt Bridge and Cation π -Interactions. *Biochemistry* **2003**, 42, (30), 8976.
172. Yau, W.-M.; Wimley, W. C.; Gawrisch, K.; White, S. H., The Preference of Tryptophan for Membrane Interfaces. *Biochemistry* **1998**, 37, (42), 14713.

173. Miteva, M.; Andersson, M.; Karshikoff, A.; Otting, G., Molecular electroporation: a unifying concept for the description of membrane pore formation by antibacterial peptides, exemplified with NK-lysin. *FEBS Letters* **1999**, 462, (1-2), 155.
174. Pokorny, A.; Almeida, P. F. F., Kinetics of Dye Efflux and Lipid Flip-Flop Induced by delta-Lysin in Phosphatidylcholine Vesicles and the Mechanism of Graded Release by Amphipathic, alpha-Helical Peptides. *Biochemistry* **2004**, 43, (27), 8846.
175. Pokorny, A.; Almeida, P. F. F., Permeabilization of Raft-Containing Lipid Vesicles by delta-Lysin: A Mechanism for Cell Sensitivity to Cytotoxic Peptides. *Biochemistry* **2005**, 44, (27), 9538.
176. Blondelle, S. E.; Perez-Paya, E.; Houghten, R. A., Synthetic combinatorial libraries: novel discovery strategy for identification of antimicrobial agents. *Antimicrobial Agents and Chemotherapy* **1996**, 40, (5), 1067.
177. Rathinakumar, R.; Wimley, W. C., Biomolecular Engineering by Combinatorial Design and High-Throughput Screening: Small, Soluble Peptides That Permeabilize Membranes. *Journal of the American Chemical Society* **2008**, 130, (30), 9849.
178. Rathinakumar, R.; Walkenhorst, W. F.; Wimley, W. C., Broad-Spectrum Antimicrobial Peptides by Rational Combinatorial Design and High-Throughput Screening: The Importance of Interfacial Activity. *Journal of the American Chemical Society* **2009**, 131, (22), 7609.
179. Chu, D. T. W.; Plattner, J. J.; Katz, L., New Directions in Antibacterial Research. *Journal of Medicinal Chemistry* **1996**, 39, (20), 3853.
180. Blondelle, S. E.; Houghten, R. A.; James, A. B., Chapter 17. Progress in Antimicrobial Peptides. In *Annual Reports in Medicinal Chemistry*, Academic Press: 1992; Vol. Volume 27, p 159.
181. Mitra, R. N.; Shome, A.; Paul, P.; Das, P. K., Antimicrobial activity, biocompatibility and hydrogelation ability of dipeptide-based amphiphiles. *Organic & Biomolecular Chemistry* **2009**, 7, (1), 94.
182. Méndez-Samperio, P., Role of antimicrobial peptides in host defense against mycobacterial infections. *Peptides* **2008**, 29, (10), 1836.
183. Miyakawa, Y.; Ratnakar, P.; Rao, A. G.; Costello, M. L.; Mathieu-Costello, O.; Lehrer, R. I.; Catanzaro, A., In vitro activity of the antimicrobial peptides human and rabbit defensins and porcine leukocyte protegrin against *Mycobacterium tuberculosis*. *Infection and Immunity* **1996**, 64, (3), 926.

184. Linde, C. M. A.; Hoffner, S. E.; Refai, E.; Andersson, M., In vitro activity of PR-39, a proline-arginine-rich peptide, against susceptible and multi-drug-resistant *Mycobacterium tuberculosis*. *Journal of Antimicrobial Chemotherapy* **2001**, 47, (5), 575.
185. Andreu, D.; Carreno, C.; Linde, C.; Boman, H. G.; Andersson, M., Identification of an anti-mycobacterial domain in NK-lysin and granulysin. *Biochemistry Journal* **1999**, 344, (3), 845.
186. Toro, J. C.; Hoffner, S.; Linde, C.; Andersson, M.; Andersson, J.; Grundström, S., Enhanced susceptibility of multidrug resistant strains of *Mycobacterium tuberculosis* to granulysin peptides correlates with a reduced fitness phenotype. *Microbes and Infection* **2006**, 8, (8), 1985.
187. Sharma, S.; Verma, I.; Khuller, G. K., Biochemical interaction of human neutrophil peptide-1 with *Mycobacterium tuberculosis* H37Ra. *Archives of Microbiology* **1999**, 171, (5), 338.
188. Rastogi, N.; Labrousse, V.; Goh, K. S.; De Sousa, J. P., Antimycobacterial spectrum of sparfloxacin and its activities alone and in association with other drugs against *Mycobacterium avium* complex growing extracellularly and intracellularly in murine and human macrophages. *Antimicrobial Agents and Chemotherapy* **1991**, 35, (12), 2473.
189. Tomioka, H.; Sato, K.; Shimizu, T.; Sano, C., Anti- *Mycobacterium tuberculosis* Activities of New Fluoroquinolones in Combination with Other Antituberculous Drugs. *Journal of Infection* **2002**, 44, (3), 160.

CHAPTER 2

Highly efficient *In Vitro* Photodynamic Inactivation of *Mycobacterium smegmatis*

Abstract

Efforts to control tuberculosis (TB) have been hampered by the emergence of multiple-drug resistant strains, thus necessitating alternative approaches to the current antibiotic-based TB treatments. Herein, we explore the feasibility of photodynamic inactivation (PDI) of mycobacteria as one such alternative. *In vitro* studies employing *M. smegmatis* as a surrogate for *M. tuberculosis* were performed as a function of photosensitizer (PS) type, concentration, and light-dose. Our best results demonstrate that PDI of *M. smegmatis* can achieve a noteworthy 5-6 log unit reduction in colony forming units (99.999+ % viable cell eradication) when cationic PS are employed in the nanomolar concentration range.

Introduction

Tuberculosis (TB) is a significant health threat in the world today, with approximately one third of the world's population currently infected, resulting in 9.2 million new infections and 1.7 million deaths reported for 2006 alone.¹ While a number of antibiotics (isoniazid, rifampicin, ethionamide) are effective against the causative agent *Mycobacterium*

tuberculosis,² a Gram-positive bacterium, the rise in multiple drug resistant (MDR) strains due to improper or incomplete drug therapy has increased dramatically. For 2006, the WHO reported the highest ever recorded global average of MDR-TB among newly detected TB cases at 5%, with areas in the former Soviet Union peaking over 20%.¹ These alarming numbers have sparked a new round of interest in the search for better and alternative anti-tubercular treatments.

Significant advances made in the past decade in treating several forms of cancer with photodynamic therapy (PDT)^{3, 4} suggest that photodynamic inactivation (PDI) of localized bacterial infections such as tuberculosis might also be feasible, thus allowing for the development of a valuable alternative or supplemental option to the current antibiotic-based treatments.⁵⁻⁸ Wound infection, psoriasis, acne vulgaris and oral disease are some of the areas currently under intensive investigation towards the feasibility of antimicrobial photodynamic inactivation.^{9, 10} PDI employs a localized, light-activated photosensitizer (PS) that generates cytotoxic species, particularly singlet oxygen, upon illumination with visible light.^{11, 12} Specifically, inactivation of the bacteria is achieved by incubation (5-15 minutes) with the photosensitizer, which is either uptaken or localizes within the bacterial cell wall, followed by illumination with low intensity visible light (50-200 mW/cm²). The thereby excited photosensitizer in its triplet state produces cytotoxic free radicals (type I mechanism) and singlet oxygen (type II mechanism).^{11, 13} These highly reactive species created through type I and type II mechanisms, consequently, damage the bacterium triggering apoptosis or necrosis. The type II mechanism is thought to be the main pathway invoking cellular death. Development of bacterial resistance against PDI is believed to be unlikely due to the unspecific damage caused by ¹O₂.¹⁴ The efficacy of PDI against *Escherichia coli*,

Staphylococcus aureus (including methicillin-resistant strains), *Acinetobacter baumannii* and *Pseudomonas aeruginosa* has been discussed widely in the literature,⁵ but fundamental *in vitro* studies on mycobacteria are still lacking. In light of this, we have examined the drug- and light-dose dependencies of several photosensitizers on mycobacterial survival using *Mycobacterium smegmatis* mc²155, a widely employed non-pathogenic surrogate for *M. tuberculosis*.^{15, 16} As a point of comparison and validation of methods, analogous experiments using *E. coli*. were also conducted.^{11, 17-19}

Results

Studies with M. smegmatis. To broadly elucidate the scope of photodynamic inactivation, we have screened a small number of commercially available photosensitizers (Figure 2.1) for mycobactericidal PDI. *M. smegmatis* was grown to a concentration of $\sim 10^8$ colony forming units per mL (CFU/mL), re-suspended in PBS-0.05% Tween-80 containing buffer, incubated with the photosensitizer for 5 min and subsequently illuminated with white light (400-700 nm) with a fluence rate of 60 mW/cm² for 1, 5, 15 or 30 min equivalent to 3.4, 18, 54 or 108 J/cm². The percentage survival was determined by the ratio of the colony count from illuminated and non-illuminated control cell suspensions. Light (exposure to light without the PS) and dark (PS treatment in the dark) controls did not show any reduction in CFU/mL in the concentration range examined.

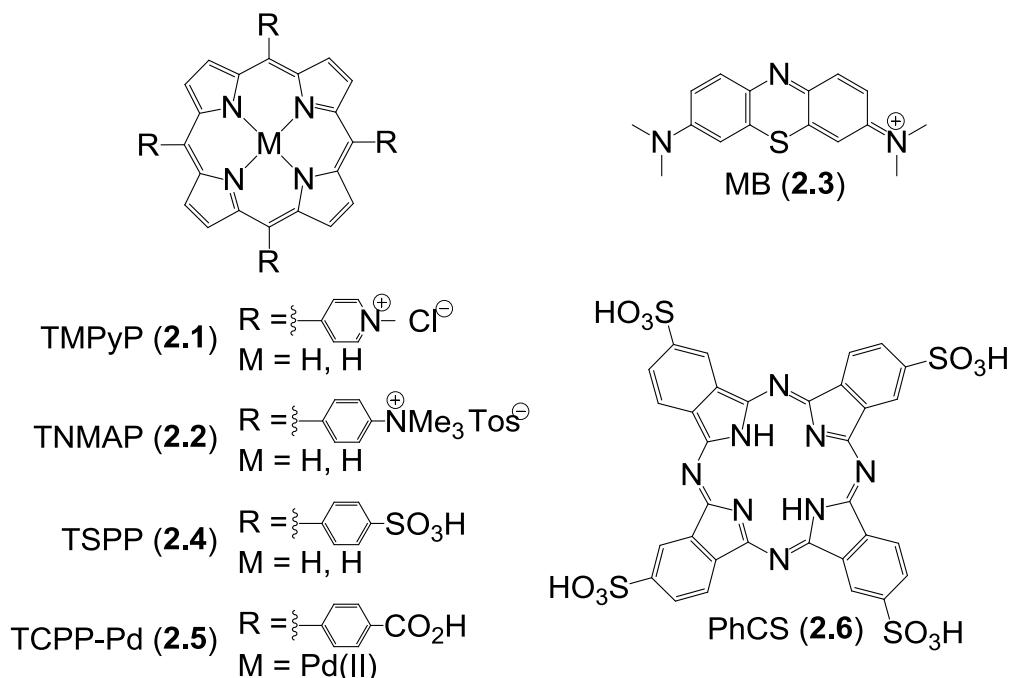


Figure 2.1: Photosensitizers employed in this study (Reprinted from Ref [20] with permission from Oxford University Press. Copyright 2009).

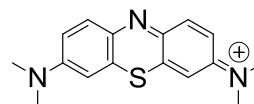
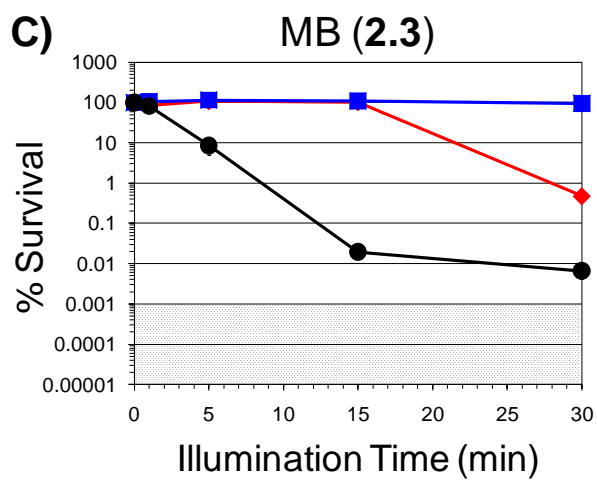
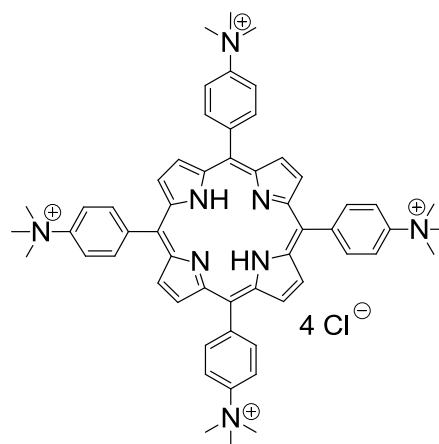
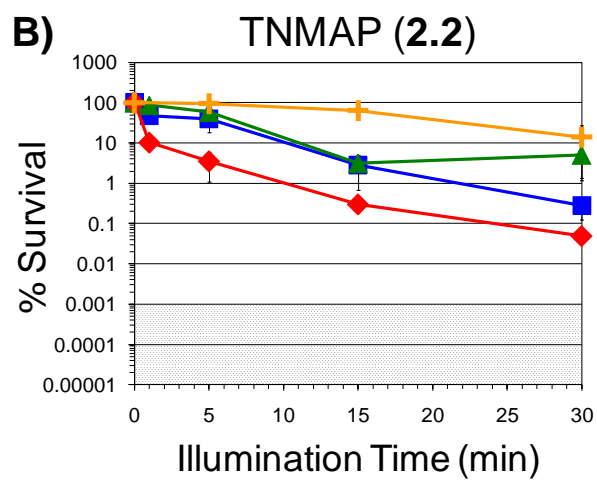
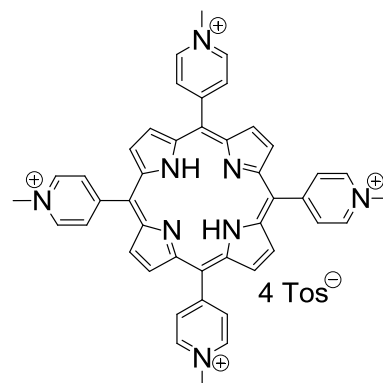
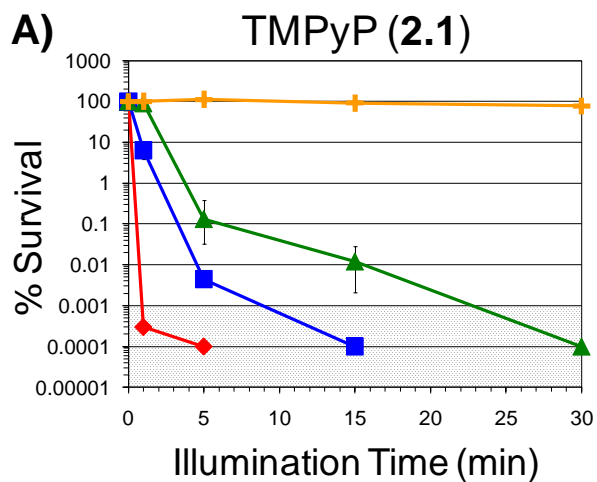
The greatest extent of mycobacterial photodynamic inactivation was observed when employing cationic porphyrins **2.1** and **2.2** as the photosensitizers (Figure 2.2). In the low micromolar concentration range, TMPyP (**2.1**) (Figure. 2.2 A) reduced bacterial survival by 5-6 log units (99.999+ % viable cell eradication, $P < 0.001$), even after illumination times as short as 60 seconds. Excellent anti-mycobacterial activity was also observed for the pharmaceutically relevant concentration of 150 nM: 3, 4 and 5-6 log units reduction in viable cells after 5, 15 or 30 min illumination, respectively ($P < 0.001$). With TNMAP (**2.2**) (Figure 2.2 B), a maximum viable cell reduction of 3.5 log units ($P < 0.001$) occurred after 30 min illumination at 7.5 μM (~300-fold less efficient than with **2.1**). However, **2.2** exhibited the lowest PS concentration (100 nM) for which anti-mycobacterial photodynamic inactivation was achievable (14% survival, 30 min illumination, $P = 0.001$). The results obtained here for

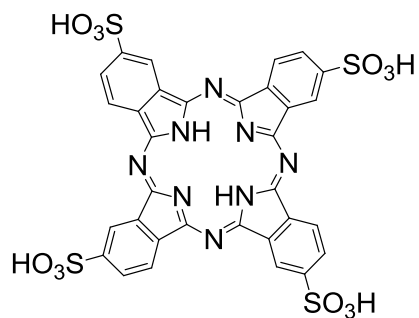
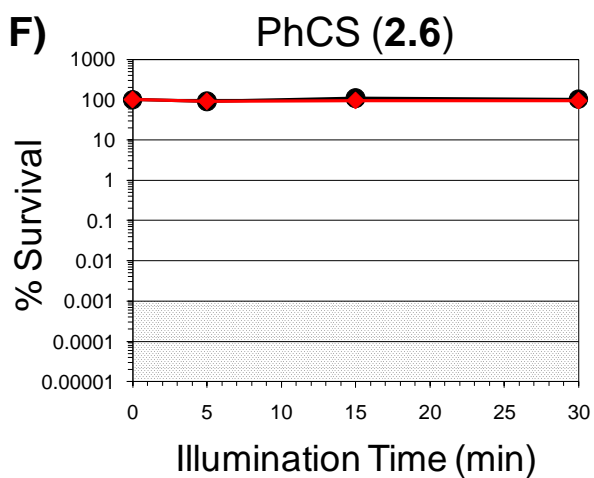
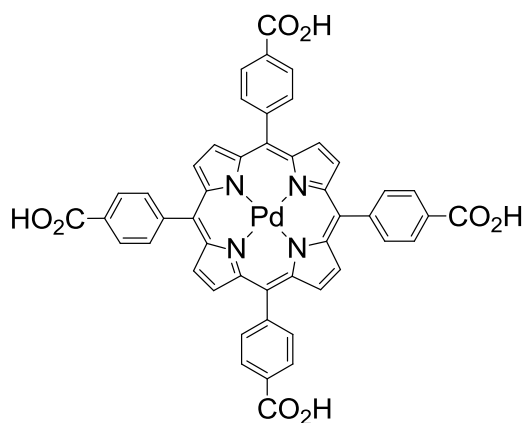
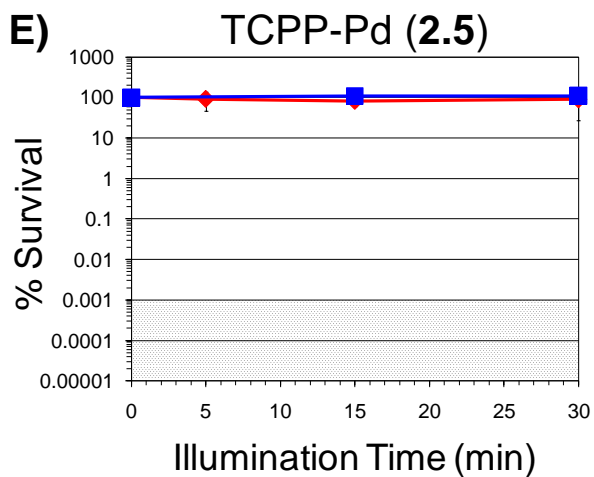
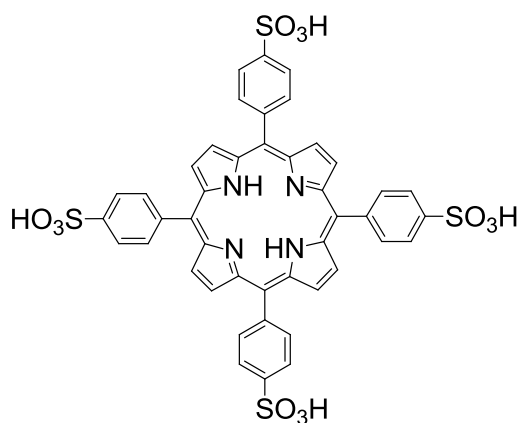
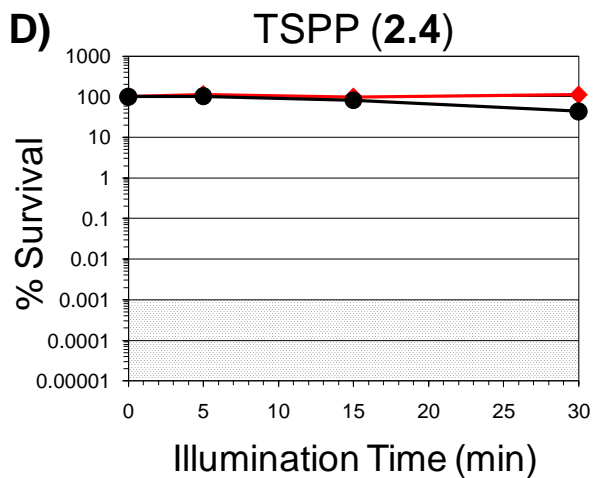
2.1 and **2.2** are significantly better than the only other report of *in vitro* mycobacterial PDI (< 2 log units reduction of *M. bovis* BCG, 5 μ M verteporfin as PS, 60 J/cm², 690 nm).²¹

Methylene blue (**2.3**), a cationic phenothiazine, was only effective at the highest concentrations tested (Figure 2.2 C). At 75 μ M, a 4 log unit reduction ($P < 0.001$) in viable cells was observed after 30 min illumination, but this decreased to a 2 log unit reduction ($P < 0.001$) when a concentration of 7.5 μ M was employed. The poor efficiency of MB when compared to other cationic PS is obvious when one compares identical illumination conditions (15 min): MB exhibits 100 times lower PDI efficacy at 75 μ M than TMPyP (**2.1**) at 750 nM, and is over 300 times less efficient at 7.5 μ M than TNMAP (**2.2**) at the same concentration.

The anionic photosensitizers TSPP (**2.4**), TCPP-Pd(II) (**2.5**) and PhCS (**2.6**) did not mediate any statistically significant ($P < 0.05$) photodynamic inactivation in the concentration range tested (Figures 2.2 D-F). A slight reduction in viable cells ranging from 50% for TSSP ($P < 0.02$) to 10% by TCPP-Pd(II) was observed, but only at the highest concentrations tested, whereas the use of PhCS (**2.6**) did not result in any detectable mycobactericidal activity.

Figure 2.2: Photodynamic inactivation of *M. smegmatis* using photosensitizers **2.1-2.6**. The illumination time was varied over 1, 5, 15, and 30 min, corresponding to total fluences of 3.6, 18, 54, and 108 J/cm², respectively, at 60 mW/cm². PS concentrations are as follows: 75 μM (●), 7.5 μM (◆), 750 nM (■), 150 nM (▲), 100 nM (⊕). Variations in the bacterial concentration of the starter cultures (1-4·10⁸ CFU/mL) resulted in a variation of the detection limit spanning the region of 0.001-0.0001% survival (shaded). As the plating technique employed did not allow for detection of survival rates of < 0.0001%, data points below the detection limit are set to 0.0001% survival for graphing purposes (Reprinted from Ref [20] with permission from Oxford University Press. Copyright 2009).





Photodynamic inactivation is caused by reactive species such as singlet oxygen (Type II mechanism) and/or other reactive oxygen species and radicals (Type I mechanism) produced in the light mediated process. The excited state of the photosensitizer is quenched by either relaxation to the ground state or by spin forbidden formation of the triplet state via intersystem crossing. The lifetime in aqueous media of such a triplet species is on the order of 2-4 μ s, which is sufficient to initiate the two main pathways relevant for PDI: Electron transfer reactions with suitable substrates such as cellular biomolecules, solvent molecules or dioxygen, forming cytotoxic free radicals and superoxide (Type I mechanism) and/or energy transfer to molecular oxygen forming singlet oxygen with an approximate lifetime of 2 μ s in aqueous media (Type II mechanism).¹² In the experiments described in Table 2.1 the main mechanism of action was investigated by addition of sodium azide, a singlet oxygen quencher, and D-mannitol, a superoxide and hydroxyl radical quencher, to the PDI experiment.^{22, 23} Whereas the presence of D-mannitol did not have an effect on the survival of *M. smegmatis* in the PDI experiment, in the presence of 2-20 mM of the singlet oxygen quencher NaN₃, a statistically significant increase in mycobacterial survival was observed when **2.1** was used as the PS (Table 2.1). This data suggests that photodynamic inactivation of *M. smegmatis* is mediated by singlet oxygen production as the major pathway of action.

Table 2.1: TMPyP (**2.1**) mediated photodynamic inactivation of *M. smegmatis* in the presence of the singlet oxygen quencher NaN_3^a (Reprinted from Ref [20] with permission from Oxford University Press. Copyright 2009).

NaN ₃ concentration (mM)	Survival % (avg. \pm S.D.)
0	$<1 \cdot 10^{-4}$
0.2	0.0030 ± 0.0032^b
2	0.0060 ± 0.0023
20	54.8 ± 8.9

^a Conditions: 750 nM TMPyP (**2.1**), 15 min illumination at 60 mW/cm² for a total fluence of 54 J/cm². The control (0 mM NaN₃ added) exhibited no surviving mycobacteria, and was therefore set to the detection limit of less than 1×10^{-4} %.

^b Not statistically significant ($P = 0.26$)

The degree of photosensitizer association (binding or uptake) of *M. smegmatis* was evaluated by analysis of the amount PS recovered from lysed cells by fluorescence spectroscopy (Table 2.2).^{5, 18} Consistent with its efficient photodynamic inactivation at 100 nM (Figure 2.2 B), TNMAP (**2.2**) exhibited the highest amount of PS recovered from lysed cells, suggesting a strong association with *M. smegmatis*. The large drop in recovered PS after the second washing step points to the possibility that a significant portion of **2.2** is only loosely associated with the cell. TMPyP (**2.1**) was found to bind to *M. smegmatis* to a lesser degree than **2.2**, but a number of factors not related to binding, such as differences in photophysical properties, dye aggregation, localization and/or uptake, are likely reasons as to why **2.1** is overall the more efficient photosensitizer. MB (**2.3**) is the least able of the cationic PS to bind to *M. smegmatis*, which helps to rationalize the large difference in PDI mediated by **2.3** compared to **2.2** despite their similar quantum yields of singlet oxygen production (Φ_Δ) (Table 2.4). The anionic PS **2.4** poorly associates with *M. smegmatis* and is not

detectable after three washings, explaining its inability to mediate PDI despite possessing a favorable Φ_{Δ} . Binding of PS **2.5** could not be examined by fluorescence spectroscopy (fluorescence quantum yield of $<10^{-4}$).²⁴ Decreased emission and high background fluorescence did not allow for quantification of PS binding of **2.6** in solutions containing lysed *M. smegmatis* or lysed *E. coli* as demonstrated in Figure 2.3 A and B.

Table 2.2: PS recovery (nM) from lysed cell suspensions after 1-3 PBS washing steps^{a,b} (Reprinted from Ref [20] with permission from Oxford University Press. Copyright 2009).

PS	Number of washing steps prior to lysis		
	1	2	3
TMPyP (1)	168.8 ± 30.7	91.1 ± 31.1	40.4 ± 17.6
TNMAP (2)	413.8 ± 148.5	102.5 ± 18.9	140.3 ± 83.9
MB (3)	84.7 ± 21.4	45.1 ± 10.3	17.2 ± 7.6
TSPP (4)	34.1 ± 9.1	0.2 ± 0.1	n.d.

^a incubation of $1 \cdot 10^8$ cells/mL with 7.5 μ M PS for 5 minutes; ^b estimated by use of a calibration curve of the PS in PBS containing soluble lysed cell material; n.d. = none detected.

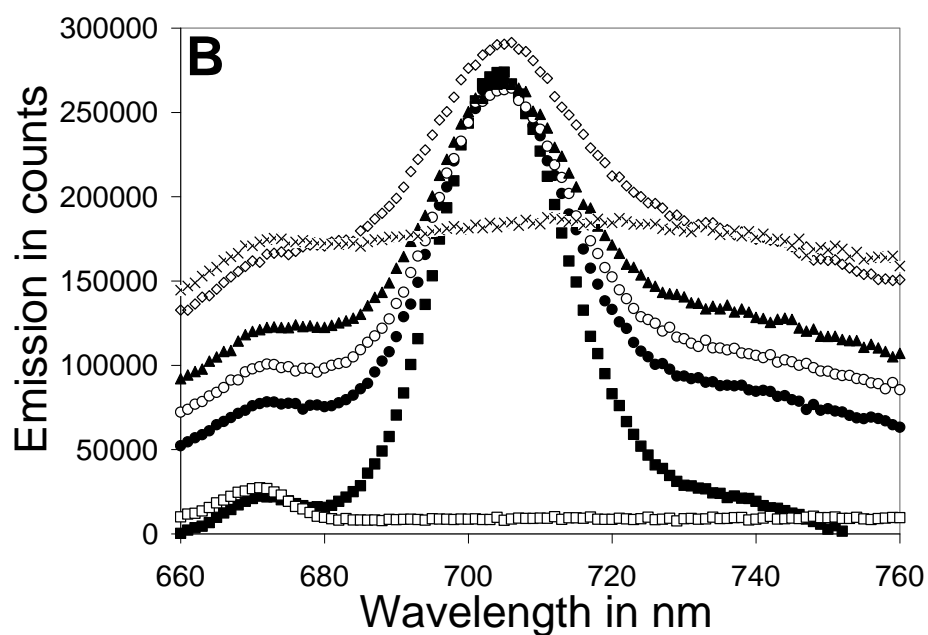
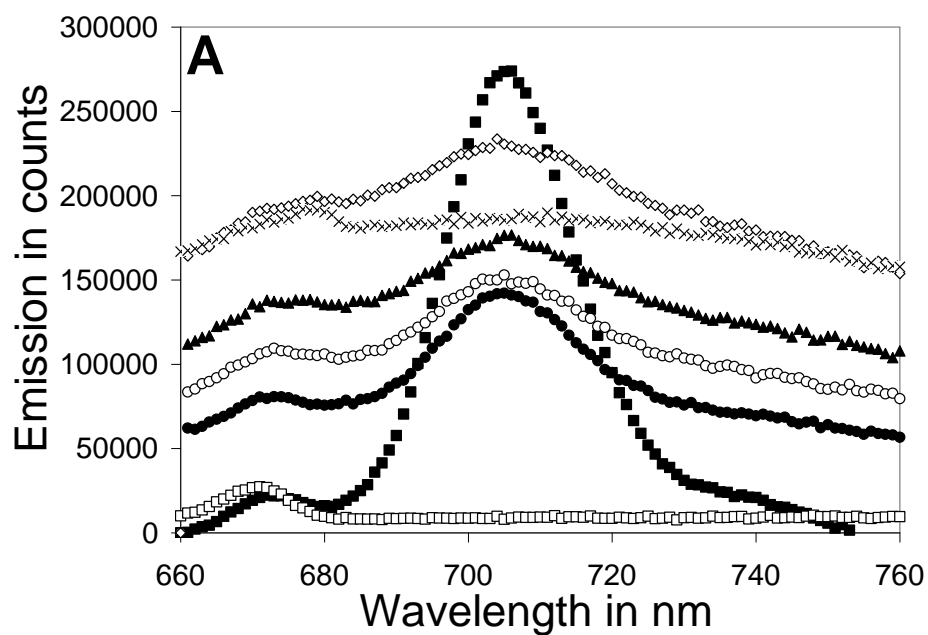
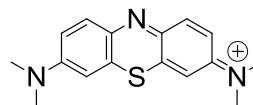
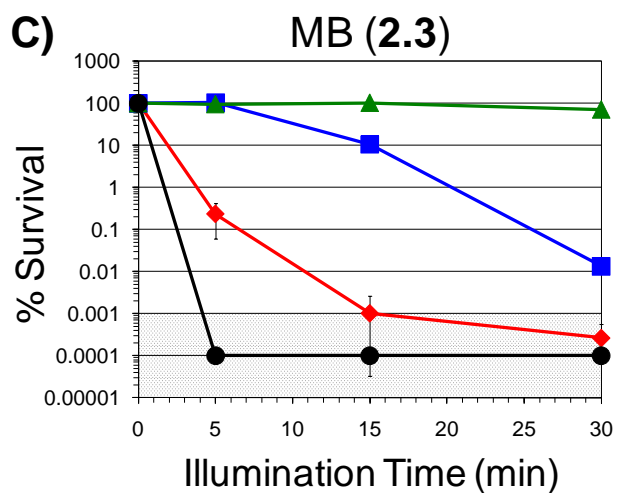
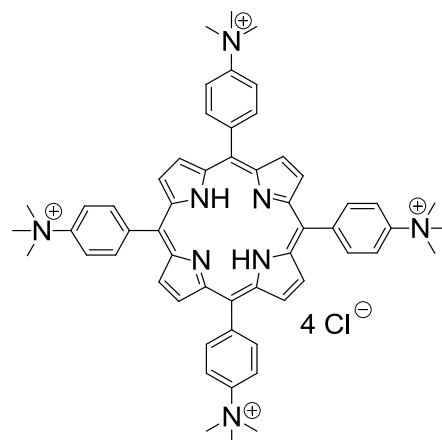
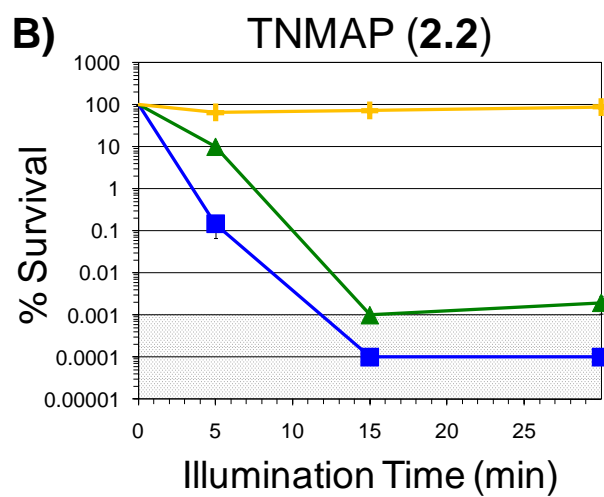
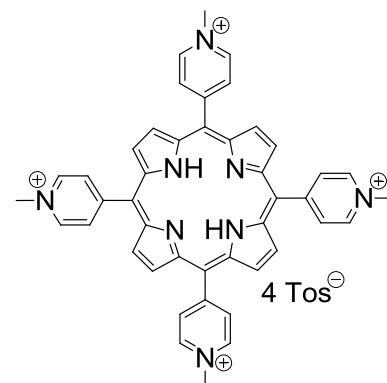
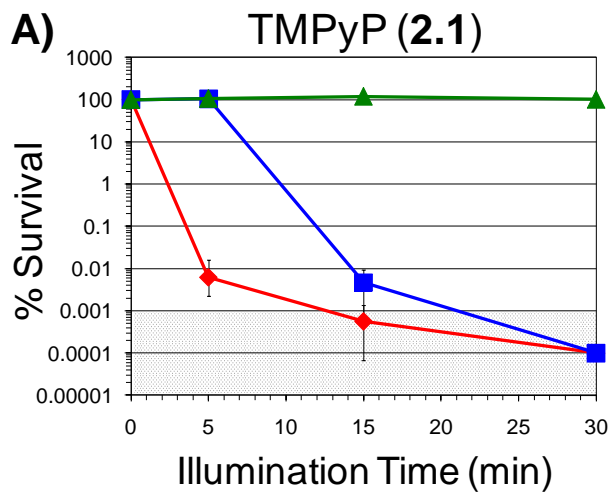


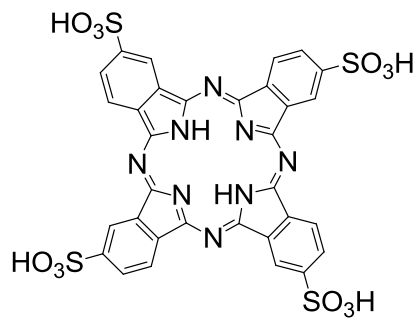
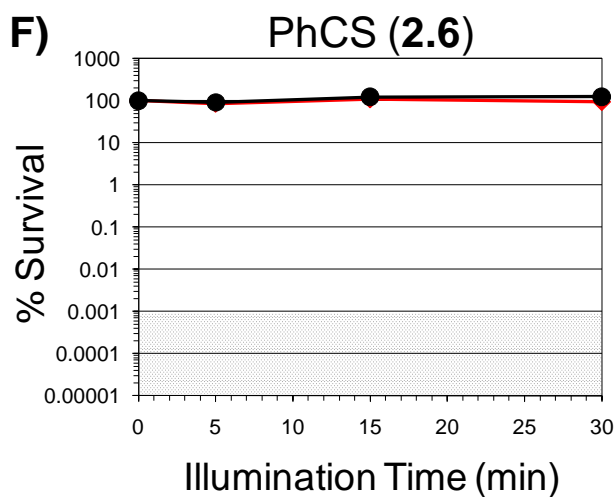
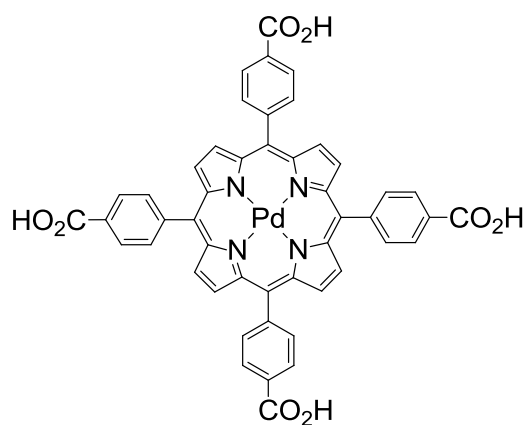
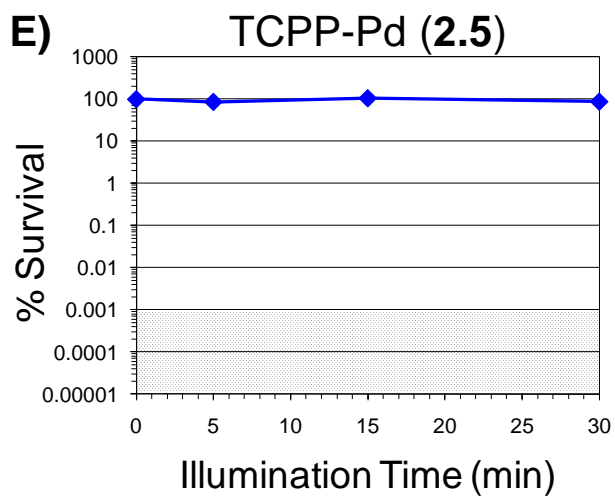
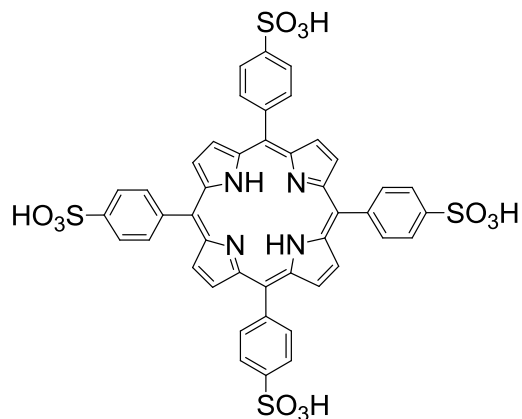
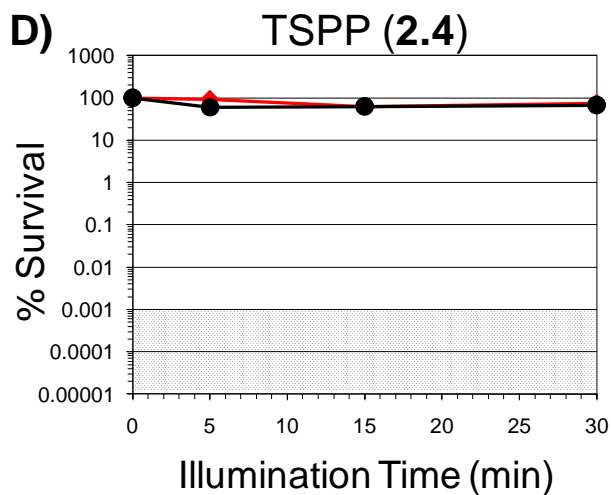
Figure 2.3: Fluorescence spectra of 5 μM PhCS (**2.6**) in different ratios of PBS buffer (0.05% Tween) and cell lysate from 10^8 CFU/mL bacterial cell suspension; excitation 602 nm; band width 4 nm; integration 0.5 s: A) *M. smegmatis* B) *E. coli*; PBS with 0.05% Tween 80 (\square), 5 μM **2.6** in PBS-Tween (\blacksquare), 5 μM **2.6** in PBS-Tween : cell lysate 2:1 (\bullet); 5 μM **2.6** in PBS-Tween : cell lysate 1:1 (\circ); 5 μM **2.6** in PBS-Tween : cell lysate 1:2 (\blacktriangle); 5 μM **2.6** in cell lysate (\diamond); cell lysate (x) (Reprinted from Ref [20] with permission from Oxford University Press. Copyright 2009).

Reference Studies with Escherichia coli. To validate our procedure and methods, a set of experiments was conducted using *E. coli*. Dark controls, i.e. incubation of the cells with the photosensitizer present in the dark, were used to evaluate the toxicity of the photosensitizers. The photosensitizers **2.2** and **2.5** displayed dark toxicity against *E. coli* at 7.5 μM and 75 μM , but PS **2.1**, **2.3**, **2.4** and **2.6** did not show any reduction at 75 μM even after 1 hour incubation in the dark. Light controls (illumination of cell suspensions without PS present) did not have any adverse effect on the survival of *E. coli*.

As suggested in the literature, *E. coli* can be inactivated with positively charged PSs **2.1-3** (Figure 2.4 A-C), but is resistant to negatively charged ones (**2.4-6**, Figure 2.4 D-F).¹⁰,¹⁸ TMPyP (**2.1**) resulted in 4 log and 5 log reductions in CFU after 5 or 15 minutes of illumination, respectively, at 750 nM. Lower concentrations did not afford any loss in viable cells. TNMAP (**2.2**) appears to be the most efficient photosensitizer, as the cell viability was reduced below the detection limit within 15 minutes of illumination at PS concentrations as low as 150 nM. MB (**2.3**) was found to be an efficient photosensitizer for *E. coli* as well.

Figure 2.4: Photodynamic inactivation of *E. coli* using photosensitizers **2.1-2.6**. The illumination time was varied over 5, 15, and 30 min, corresponding to total fluences of 18, 54, and 108 J/cm², respectively, at 60 mW/cm². PS concentrations are as follows: 75 μM (●), 7.5 μM (◆), 750 nM (■), 150 nM (▲), 100 nM (+). Variations in the bacterial concentration of the starter cultures (1-4×10⁸ CFU/mL) resulted in a variation of the detection limit spanning the region of 0.001-0.0001% survival (shaded). As the plating technique employed did not allow for detection of survival rates of < 0.0001%, data points below the detection limit are set to 0.0001% survival for graphing purposes.





The ability of *E. coli* to be inactivated photodynamically has been demonstrated numerous times, and several examples are cited in Table 2.3. Detailed direct comparison of PDI efficacies from different studies is difficult, because loss in viable cells is highly dependent on the illumination parameters (such as the type of light source, wavelength, illumination time and fluence rate). However, it is apparent that our results reflect the trends shown in previously published studies.^{3, 18, 19, 25}

Table 2.3: Photodynamic inactivation of *E. coli* by TMPyP (2.1) and TNMAP (2.2)

Photosensitizer	Concentration (μM)	Viable cell reduction from CFU count	Illumination conditions	Reference
TMPyP (2.1)	7.3	5 log	400-700 nm, 18 J/cm ²	this work
	0.73	4.5 log	400-700 nm, 54 J/cm ²	this work
	7.3	1 log	407 nm, 2.5 J/cm ²	19
	8.4	2 log	250 W tungsten lamp, 11 J/cm ²	3
	5	2 log	600-700 nm, 2.4 J/cm ²	25
	5	3 log	600-700 nm, 12 J/cm ²	25
	5	4.5 log	600-700 nm, 24 J/cm ²	25
	7	4 log	250 W tungsten lamp, 1.1 J/cm ²	18
TNMAP (2.2)	0.73	5-6 log	400-700 nm, 108 J/cm ²	this work
	0.150	4.5 log	400-700 nm, 108 J/cm ²	this work
	7.4	5 log	250 W tungsten lamp, 1.1 J/cm ²	18

Discussion

Overall, our results demonstrate that cationic PS can be potent photodynamic inactivators of mycobacteria, whereas anionic PS exhibit little effect. Comparison of the photophysical properties of the PS (Table 2.4) alone, however, cannot be used to rationalize the observed differences in the extent of PDI mediated by each, as such properties may be significantly different within the mycobacterial cytoplasm, or at the cell surface where the PS may bind. For example, PS **2.1** exhibits very favorable photophysical properties, with a triplet state quantum yield of 0.73²⁶ and a quantum yield of singlet oxygen production (Φ_{Δ}) of 0.74 (Table 2.4). PS **2.2** and **2.3** both exhibit Φ_{Δ} of ~0.5, whereas our study shows that **2.2** appears to be significantly more effective against *M. smegmatis*. Among the anionic PS, TSPP (**2.4**) also shows a favorable Φ_{Δ} of 0.75, yet efficient inactivation of *M. smegmatis* was not observed with any anionic PS (**2.4-6**).

Table 2.4: Published Values for Photophysical Properties of employed Photosensitizers (Reprinted from Ref [20] with permission from Oxford Univeristy Press. Copyright 2009).

PS	Φ_{Δ}	Medium	Method	Reference
TMPyP (2.1)	0.74	PBS	O ₂ consumption	27
TNMAP (2.2)	0.48	PBS	¹ O ₂ luminescence	28
MB (2.3)	~0.5	H ₂ O	Substrate consumption	27
TSSP (2.4)	0.75	PBS	¹ O ₂ luminescence	28
PhCS (2.5)	0.14	H ₂ O	Product appearance	27

Looking beyond photophysical properties as the primary explanation for the observed mycobactericidal PDI effects, we hypothesize that PS binding may be the critical factor. Interestingly, cationic PS have been reported to bind efficiently to both Gram positive as well

as Gram negative bacteria,²⁹ whereas anionic PS are known to only bind and photoinactivate the former.³⁰ Although *M. smegmatis* is categorized as Gram positive, our data unequivocally shows that it behaves in a similar fashion as a Gram negative bacterium: cationic PS were effective in mediating the photodynamic inactivation of *M. smegmatis*, anionic ones were clearly unable to do so. Although the extent of PS localization, aggregation, penetration across the mycobacterial membrane, and retention (as well as the kinetics of such processes) are beyond the scope of this current study, our photosensitizer binding study strongly suggests that the localization and/or binding affinity of the photosensitizer to the mycobacterial cell is crucial for the efficacy of the PDI process, and suggests that rapid fluorescence binding assays may be used as an initial screening tool for future PS development.

Recently, O’Riordan et al. investigated the *in vivo* susceptibility of localized *M. bovis* BCG-induced granulomatous infections in murine models towards photodynamic inactivation.^{31, 32} Their results showed promise, with 1-2 log units reduction in viable cells. However, the PS employed in that study, verteporfin (an anionic porphyrin) and two phenothiazine derivatives (weakly cationic and similar to MB, **2.3**), would be predicted by our present study as being non-ideal candidates for mediating PDI inactivation of mycobacteria due to their poor ability to associate with the negatively charged cell surface of the mycobacterium. Thus, we conclude that future *in vivo* studies on utilizing PDI to clear mycobacterial infections should focus on the use of highly cationic photosensitizers, with the caveat that other factors such as compound lipophilicity, aggregation, or localization need also to be considered.

The results reported herein detail the first fundamental *in vitro* survey of mycobacterial photodynamic inactivation using a range of photosensitizer types, concentrations and light doses, and provide the foundation to help direct future *in vivo* studies. We have observed the greatest extent of mycobacterial cell inactivation (up to 6 log units) reported to date, while maintaining excellent photodynamic conditions of short illumination times and extremely low (nM) PS concentrations. Our data also indicates that highly charged cationic PS should be employed against Gram positive mycobacteria, as association with the mycobacterial cell appears to be the primary factor in cell inactivation, albeit moderate to good photophysical properties play a contributing role. One of the challenges which we are actively pursuing is the development of photosensitizers which selectively target mycobacteria, thereby increasing localization of the PS in the bacterium over the host tissue. With the ongoing development of fiber-optic based PDT to treat lung tumors and small-cell carcinomas,³³⁻³⁵ photodynamic inactivation of adult pulmonary tuberculosis might be an attractive alternative treatment option, particularly for MDR-TB where cost efficient antibiotics are ineffective, or when rapid reduction in bacterial load is required.

Experimental Methods

Materials and Instrumentation. Buffer salts were purchased from Fisher Scientific, Middlebrook 7H9 Agar and 7H10 Broth from BD Difco, and LB broth Miller from EMD Chemicals. Unless otherwise specified, all other chemicals were obtained from commercial sources in the highest purity available. Ultra pure water used for all media and buffers was

provided by an Easypure II system (Barnstead). Optical density measurements were performed on a Genesys 10 uv scanning UV-vis Instrument from Thermo Electron Corp. Fluorescence spectra were recorded on a spectrometer from Photon Technology International. All procedures were carried out under commonly practiced sterile techniques.

Photosensitizers. The photosensitizers 5,10,15,20-tetrakis(1-methyl-4-pyridinyl)porphyrin tetratosylate **2.1**, 5,10,15,20-tetrakis(4-N,N,N-trimethylanilinium)porphyrin tetrachloride **2.2**, 5,10,15,20-tetrakis(4-sulfonatophenyl)porphyrin **2.4**, 5,10,15,20-tetrakis(4-carboxyphenyl)porphyrin-Pd(II) **2.5**, and phthalocyanine tetrasulfonic acid **2.6** were obtained from Frontier Scientific (USA), and methylene blue **2.3** was purchased from Fisher Scientific (USA). They were used without further purification. Stock solutions of each photosensitizer at a concentration of 0.75 mmol/L in ultrapure water were prepared and stored in the dark at 4 °C.

Bacterial strains and growth conditions. The bacterial strains *Mycobacterium smegmatis* mc² 155, kindly donated by Prof. William Jacobs (Albert Einstein College of Medicine, USA), and *Escherichia coli* BL21(Dε3)pLysS (Stratagene, USA) were used in this study. *M. smegmatis* was grown in 5 ml cultures in Middlebrook 7H9 media with ADS and with 100 µg/mL cycloheximide as the antibiotic.³⁶ *E. coli* was cultured in LB Broth Miller with 50 µg/mL chloramphenicol as well as 100 µg/mL ampicillin. The cells were incubated at 37 °C on an orbital shaker (400 rpm for *M. smegmatis*; 500 rpm for *E. coli*) until an optical density (OD₆₀₀) of 0.65-0.70 (*M. smegmatis*) or 0.33-0.40 (*E. coli*) at 600 nm corresponding to a concentration of 10⁸ CFU/mL was reached.

Incubation of cells with photosensitizer. The 5 mL culture with a concentration of 10⁸ CFU/mL was pelleted by centrifugation (10 min, 3716 x g) at room temperature, the

supernatant discarded, and the cells were resuspended in a total volume of 5 mL PBS (170 mM NaCl, 3.4 mM KCl, 10.0 mM Na₂HPO₄, 1.8 mM KH₂PO₄, pH 7.2 with additional 0.05 % Tween 80 for *M. smegmatis*) and the appropriate volume of the photosensitizer stock solution. The cells were incubated for 5 minutes in the dark at 37 °C under agitation.

Illumination of cells. All photosensitization experiments were performed using a noncoherent light source, PDT light model LC122 (LumaCare, USA), and the fluence rate was measured with an Orion power meter (Orphir Optronics Ltd., Israel). 1 mL aliquots of the cell suspension in PBS were added to a sterile 24 well plate (BD Falcon, flat bottom) and illuminated with visible light (400-700 nm) with a fluence rate of 60 mW/cm² for the duration of 1, 5, 15 or 30 minutes (corresponding to fluences of 3.6, 18, 54, 108 J/cm²) while magnetically stirred. After illumination an aliquot was used for viability assays. All experiments were conducted in triplicate at a minimum.

Cell survival assay. 100 µL from the illuminated cell suspension was 1:10 serially diluted six times and plated on square plates (Middlebrook 7H10-ADS solid media for *M. smegmatis* and LB-Miller, Agar plates for *E. coli*) as described by Jett and coworkers.³⁷ The plates were incubated at 37 °C in the dark for 48-60 h (*M. smegmatis*) or overnight (*E. coli*). The survival rate was determined from the ratio of CFU/mL of the illuminated solution and the dark control. Due to the plating technique employed, a maximum of a 5 log unit change in CFU corresponding to ≥ 1000 CFU/mL survival could be detected for an initial concentration of $1 \cdot 10^8$ CFU/mL. Unavoidable variations in the bacterial concentration of individual samples from starter cultures ($1 \cdot 8 \cdot 10^8$ CFU/mL for *E. coli*, $1 \cdot 4 \cdot 10^8$ CFU/mL for *M. smegmatis*) resulted in a variation of the detection limit spanning the region of 0.001-0.0001% survival (Figures 2.2 and 2.4, shaded areas). Survival rates of $< 0.0001\%$ could not

be detected. Samples with photosensitizer present but kept in the dark (dark control) and illuminated samples without photosensitizer present (light control) served as controls. Statistical significance was assessed via a two-tailed, unpaired Student's t-test.

PS Binding Assay. The binding/uptake of the PS by *M. smegmatis* was estimated using fluorescence spectroscopy. *M. smegmatis* was grown to an OD₆₀₀ of 0.6 in 5 ml cultures and treated with the PS as described above. The cells were pelleted by centrifugation and washed in PBS Tween 80 containing buffer (5 mL). The cells were then lysed with 4x1 minute bursts of a Branson 450 sonicator. The number of washing/centrifugation steps before cell lysis was varied from 1-3. After centrifugation the amount of extracted PS in the supernatant was determined by fluorescence spectroscopy. The concentration of recovered PS was estimated by comparison to a calibration curve of known concentrations of the PS in the same buffer (PBS Tween) containing water soluble cell material of *M. smegmatis* at a comparable concentration to the samples. Each data point is the average of 6-9 individual samples. The data was analyzed by Soft CRM 1.2.2 to test for possible outliers.

Fluorescence experiments with PhCS (2.6). *M. smegmatis* was grown as described to a concentration of 10⁸ CFU/mL. As a comparison *E. coli* was grown in LB media with ampicillin (100 µg/ml) and chloramphenicol (50 µg/ml) as antibiotics to 10⁸ CFU/mL. The cells were pelleted and resuspended in PBS buffer containing 0.05% Tween 80. The cells were lysed by 4 x 1 minute bursts with a Branson 450 sonicator. The suspension was centrifuged (30 min, 3716 x g) and the supernatant was used for fluorescence measurements. Fluorescence spectra of 5 µM solutions of **2.6** were recorded employing different ratios (Figure 2.3 caption for details) of PBS containing 0.05% Tween 80 and the lysed cell solutions. The combination of decreased fluorophore and high background emission made it

difficult to accurately quantify concentrations of PS **2.6** in the presence of *M. smegmatis* or *E. coli* cell lysate.

REFERENCES

1. World Health Organization, *Anti-Tuberculosis Drug Resistance in the World Report No. 4*. The WHO/IUALTD Global project on anti-tuberculosis drug resistance surveillance: Geneva, 2008.
2. Koch, R., Aetiologie der Tuberculose. *Berliner klinische Wochenschrift* **1882**, 19, (15), 221.
3. Stables, G. I.; Ash, D. V., Photodynamic therapy. *Cancer Treatment Reviews* **1995**, 21, (4), 311.
4. Ochsner, M., Photophysical and photobiological processes in the photodynamic therapy of tumours. *Journal of Photochemistry and Photobiology B: Biology* **1997**, 39, (1), 1.
5. Hamblin, M. R.; Hasan, T., Photodynamic therapy: a new antimicrobial approach to infectious disease? *Photochemical & Photobiological Sciences* **2004**, 3, (5), 436.
6. Jori, G.; Brown, S. B., Photosensitized inactivation of microorganisms. *Photochemical & Photobiological Sciences* **2004**, 3, (5), 403.
7. O'Riordan, K.; Akilov, O. E.; Hasan, T., The potential for photodynamic therapy in the treatment of localized infections. *Photodiagnosis and Photodynamic Therapy* **2005**, 2, (4), 247.
8. Wainwright, M., Photodynamic antimicrobial chemotherapy (PACT). *Journal of Antimicrobial Chemotherapy* **1998**, 42, (1), 13.
9. Maisch, T., Anti-microbial photodynamic therapy: useful in the future? *Lasers in Medical Science* **2007**, 22, (2), 83.
10. Maisch, T.; Szeimies, R.-M.; Jori, G.; Abels, C., Antibacterial photodynamic therapy in dermatology. *Photochemical & Photobiological Sciences* **2004**, 3, (10), 907.
11. Jori, G., Inactivation of Pathogenic Microorganisms by Photodynamic Techniques: Mechanistic Aspects and Perspective Applications. *Anti-Infective Agents in Medicinal Chemistry* **2007**, 6, (2), 119.
12. Macdonald, I. J.; Dougherty, T. J., Basic principles of photodynamic therapy. *Journal of Porphyrins and Phthalocyanines* **2001**, 5, 105.
13. Macdonald, I. J. D. T. J., Basic principles of photodynamic therapy. *Journal of Porphyrins and Phthalocyanines* **2001**, 5, 105.

14. Maisch, T., Revitalizes Strategies Against Multidrug-Resistant bacteria: Anti-microbial Photodynamic Therapy and Bacteriophage Therapy. *Anti-Infective Agents in Medicinal Chemistry* **2007**, 6, (2), 145.
15. Chaturvedi, V.; Dwivedi, N.; Tripathi, R. P.; Sinha, S., Evaluation of Mycobacterium smegmatis as a possible surrogate screen for selecting molecules active against multi-drug resistant Mycobacterium tuberculosis. *The Journal of General and Applied Microbiology* **2007**, 53, (6), 333.
16. Jabocs, W. R., Jr.; Hatfull, G. F., *Mycobacterium tuberculosis; a Once Genetically Intractable Organism*. ASM Press, Washington DC, 2000; p 1.
17. Merchat, M.; Bertolini, G.; Giacomini, P.; Villaneuva, A.; Jori, G., Meso-substituted cationic porphyrins as efficient photosensitizers of gram-positive and gram-negative bacteria. *Journal of Photochemistry and Photobiology B: Biology* **1996**, 32, (3), 153.
18. Merchat, M.; Spikes, J. D.; Bertoloni, G.; Jori, G., Studies on the mechanism of bacteria photosensitization by meso-substituted cationic porphyrins. *Journal of Photochemistry and Photobiology B: Biology* **1996**, 35, (3), 149.
19. Salmon-Divon, M.; Nitzan, Y.; Malik, Z., Mechanistic aspects of Escherichia coli photodynamic inactivation by cationic tetra-meso(N-methylpyridyl)porphine. *Photochemical & Photobiological Sciences* **2004**, 3, (5), 423.
20. Feese, E.; Ghiladi, R. A., Highly efficient in vitro photodynamic inactivation of Mycobacterium smegmatis. *Journal of Antimicrobial Chemotherapy* **2009**, 64, (4), 782.
21. O'Riordan, K.; Sharlin, D. S.; Gross, J.; Chang, S.; Errabelli, D.; Akilov, O. E.; Kosaka, S.; Nau, G. J.; Hasan, T., Photoinactivation of Mycobacteria In Vitro and in a New Murine Model of Localized Mycobacterium bovis BCG-Induced Granulomatous Infection. *Antimicrobial Agents and Chemotherapy* **2006**, 50, (5), 1828.
22. Maisch, T.; Bosl, C.; Szeimies, R. M.; Lehn, N.; Abels, C., Photodynamic Effects of Novel XF Porphyrin Derivatives on Prokaryotic and Eukaryotic Cells. *Antimicrobial Agents and Chemotherapy* **2005**, 49, (4), 1542.
23. Maisch, T.; Baier, J.; Franz, B.; Maier, M.; Landthaler, M.; Szeimies, R.-M.; Baeumler, W., The role of singlet oxygen and oxygen concentration in photodynamic inactivation of bacteria. *Proceedings of the National Academy of Sciences* **2007**, 104, (17), 7223.
24. Kalyanasundaram, K.; Neumann-Spallart, M., Photophysical and redox properties of water-soluble porphyrins in aqueous media. *The Journal of Physical Chemistry* **1982**, 86, (26), 5163.
25. Jori, G.; Coppellotti, O., Inactivation of Pathogenic Microorganisms by Photodynamic Techniques: Mechanistic Aspects and Perspective Applications. *Anti-Infective Agents in Medicinal Chemistry* **2007**, 6, 119.

26. Reddi, E.; Ceccon, M.; Valduga, G.; Jori, G.; Bommer, J. C.; Elisei, F.; Latterini, L.; Mazzucato, U., Photophysical Properties and Antibacterial Activity of Meso-substituted Cationic Porphyrins. *Photochemistry and Photobiology* **2002**, 75, (5), 462.
27. Wilkinson, F.; Helman, W. P.; Ross, A. B., Quantum yields of photosensitized formation of the lowest electronically excited singlet state of molecular oxygen in solution. *Journal of Physical and Chemical Reference Data* **1993**, 22, (1), 113.
28. Lambert C. R.; Reddi E. J.; Spikes J. D.; Rodgers M. A. J.; G., J., The effects of porphyrin structure and aggregation state on photosensitized process in aqueous and micellar media. *Photochemistry and Photobiology* **1986**, 44, (5), 595.
29. Weidenmaier, C.; Peschel, A., Teichoic acids and related cell-wall glycopolymers in Gram-positive physiology and host interactions. *Nature Reviews Microbiology* **2008**, 6, (4), 276.
30. Malik, Z.; Ladan, H.; Nitzan, Y., Photodynamic inactivation of Gram-negative bacteria: Problems and possible solutions. *Journal of Photochemistry and Photobiology B: Biology* **1992**, 14, (3), 262.
31. O'Riordan, K.; Sharlin, D. S.; Gross, J.; Chang, S.; Errabelli, D.; Akilov, O. E.; Kosaka, S.; Nau, G. J.; Hasan, T., Photoinactivation of Mycobacteria In Vitro and in a New Murine Model of Localized Mycobacterium bovis BCG-Induced Granulomatous Infection. *Antimicrobial Agents and Chemotherapy* **2006**, 50, (5), 1828.
32. O'Riordan, K.; Akilov, O. E.; Chang, S. K.; Foley, J. W.; Hasan, T., Real-time fluorescence monitoring of phenothiazinium photosensitizers and their anti-mycobacterial photodynamic activity against Mycobacterium bovis BCG in in vitro and in vivo models of localized infection. *Photochemical & Photobiological Sciences* **2007**, 6, (10), 1117.
33. Usuda, J.; Kato, H.; Okunaka, T.; Furukawa, K.; Tsutsui, H.; Yamada, K.; Suga, Y.; Honda, H.; Nagatsuka, Y.; Ohira, T.; Tsuboi, M.; Hirano, T., Photodynamic therapy (PDT) for lung cancers. *Journal of Thoracic Oncology* **2006**, 1, (5), 489.
34. Freitag, L., PDT in early central lung cancer. *Thorax* **2007**, 62, (5), 374.
35. Okunaka, T.; Kato, H.; Tsutsui, H.; Ishizumi, T.; Ichinose, S.; Kuroiwa, Y., Photodynamic therapy for peripheral lung cancer. *Lung Cancer* **2004**, 43, (1), 77.
36. Larsen, M., Some Common Methods in Mycobacterial Genetics. In *Molecular Genetics of Mycobacteria*, Hatfull, G. F., Ed. ASM Press: Washington DC, 2000; pp 313.
37. Bradley D. Jett, K. L. H., Mark M. Huycke, and Michael S. Gilmore, Simplified Agar Plate Method for Quantifying Viable Bacteria. *BioTechniques* **1997**, 23, (4), 648.

CHAPTER 3

Towards Microbe-Targeted Photosensitizers: Synthesis, Characterization and Photodynamic Activity of Porphyrin-Peptide Conjugates

Abstract

Porphyrin-peptide conjugates have a breadth of potential applications, including in photodynamic therapy, boron neutron capture therapy, as fluorescence imaging tags for tracking sub-cellular localization, as magnetic resonance imaging (MRI) positive-contrast reagents and as biomimetic catalysts. Here, we have developed two general routes to porphyrin-peptide conjugates using the Cu(I)-catalyzed Click reaction. Specifically, porphyrin-peptide conjugates (PPCs) containing a cationic porphyrin and peptides mimicking antimicrobial peptides were synthesized towards our goal of investigating targeted photosensitizers for use in the photodynamic inactivation of bacteria. Difficulties that needed to be overcome for efficient synthesis of PPCs were limited solubility of the quaternized pyridyl porphyrin in common solvents, undesired (de)metallation and transmetallation, as well as chromatographic purification. Photodynamic inactivation studies of a small library of PPCs against *M. smegmatis* confirmed our hypothesis that the porphyrin-based photosensitizer maintains its ability to efficiently inactivate bacteria when conjugated to a small peptide. Further, hemolysis assays revealed the lack of toxicity of the PPCs against sheep blood at concentrations employed for *in vitro* photodynamic inactivation.

Introduction

In the age of rising bacterial drug resistance against currently marketed antibiotics, new treatment regimens are desperately needed. Significant advances made in the past decade in treating several forms of cancer with photodynamic therapy^{1, 2} suggest that photodynamic inactivation (PDI) of localized bacterial infections might allow for the development of a valuable alternative or supplemental option to the current antibiotic-based treatments.³⁻⁶ PDI employs a localized, light-activated photosensitizer (PS) that generates cytotoxic species, particularly singlet oxygen, upon illumination with visible light.^{7, 8} Development of bacterial resistance against PDI is believed to be unlikely due to the unspecific damage caused by singlet oxygen.⁹

Our particular focus has been on the application of PDI against mycobacteria, the most prominent of which is *M. tuberculosis*, the causative agent of tuberculosis (TB) disease. TB is a significant health threat in the world today, with approximately one third of the world's population currently infected, resulting in 9.2 million new infections and 1.7 million deaths reported for 2006 alone.¹⁰ As described in Chapter 2, we have shown that mycobacteria, specifically *M. smegmatis* (a non-pathogenic surrogate for *M. tuberculosis*) can efficiently be inactivated (5-6 log units reduction in viable cell count) *in vitro* using basic commercially available dyes at nanomolar concentrations (≥ 150 nM) with short illumination times (15-30 minutes) using PDI.¹¹

However, in order for PDI to be clinically applicable, damage to the host tissue during the illumination period due to adventitiously bound photosensitizer must be minimized, necessitating research into microbe-targeted PS. Targeting of PS to cancerous

cells for photodynamic therapy has been investigated in some detail.^{12, 13} Explored targeting technologies include PS-antibody conjugates for recognition of tumor associated antigens,¹⁴⁻¹⁷ PS-polymer conjugates for improved pharmacokinetics and biodistribution,^{18, 19} a variety of PS-ligand conjugates for ligand recognition by over-expressed receptors on the cancer cells (lipoprotein,²⁰ estradiol,^{21, 22} epidermal growth factor,²³ insulin,²⁴⁻²⁷ transferrin cycle,^{28, 29} saccharides³⁰), and PS-scavenger conjugates for specific recognition by macrophages.³¹ Comparatively fewer strategies for microbe-targeted photosensitizers can be found in the literature. Such approaches include bacteriophage delivery,³² antibody^{15, 33-35} and polylysine^{34, 36-40} conjugation, appendage of cell penetrating peptides,⁴¹ and exploitation of specific drug-resistance mechanisms.⁴² In the past decade, Hamblin and co-workers have been at the forefront of bacteria-targeted photosensitizer research. They developed the hypothesis⁴³ that polylysine-containing PS should allow temporal selectivity of PS binding/uptake by bacteria due to the high positive charge density on the PS in comparison to mammalian cells (with their comparatively slower endocytosis uptake mechanism). Hamblin and co-workers demonstrated selective inactivation of *Actinomyces viscosus* (Gram-positive) and *Porphyromonas gingivalis* (Gram-negative), both oral pathogens, with a chlorin e₆-polylysine conjugate (20 lysine units), while sparing epithelial cells.⁴³ More recently, they investigated the influence of the polylysine chain length on the inactivation efficiency,³⁹ and the use of polylysine-chlorin conjugates in infected wounds of mouse models.⁴⁴⁻⁴⁶ Jori and co-workers demonstrated that porphycene- and cationic porphyrin-polylysine conjugates were able to inactivate *E. coli* and *S. aureus*.^{37, 47} While our work was in progress, Bourre et al. presented a study employing a tetraphenylporphyrin-cell penetrating peptide conjugate.⁴¹

They used a peptide sequence (GRKKRRGRRRGYKC) derived from the HIV-1 Tat protein, which has mammalian cell penetrating properties, and demonstrated inactivation of Gram-positive and Gram-negative bacteria. However, binding/uptake rates of the PPC by bacteria in comparison to mammalian cells were not reported.

We set out to contribute to and expand the limited repertoire of methodologies for targeting bacteria, particularly keeping applicability towards different bacterial genera in mind and using mycobacteria as a specific example. Our targeting strategy is based upon the ability of antimicrobial peptides (AMP) to disturb or penetrate the Gram-negative bacterial cell envelope. Antimicrobial peptides are low-molecular-weight peptides (12-50 amino acids) which have recently gathered significant attention in light of the search for new mechanisms in order to combat bacterial infections.⁴⁸⁻⁵⁰ AMPs are part of the human innate immune system, but are also found throughout the animal and plant kingdoms.⁵¹ AMPs were first discovered in the skin of frogs in the 1980s,^{52, 53} and today over 900 naturally occurring defense peptides have been identified.⁵⁴ Besides their typical broad-spectrum antibacterial properties, AMPs have been found to also possess antiviral,⁵⁵ antifungal,^{56, 57} antitumor⁵⁸ and immunomodulatory^{59, 60} properties. AMPs are generally amphiphatic with positively charged and hydrophobic regions.⁶¹ QSAR analysis of small synthetic peptides shows that the amino acid composition, rather than the specific sequence, is correlated to the degree of antimicrobial activity.^{62, 63} Generally, AMPs have a net positive charge [high degrees of arginine (R), lysine (K) or histidine (H)], while hydrophobic amino acids [tryptophan (W), phenylalanine (F), tyrosine (Y) or leucine (L)] have been shown to also correlate with antibacterial activity.⁶⁴ Interestingly, a multitude of highly active AMPs contain an arginine-

tryptophan rich motif, and its role has been investigated intensively.^{62, 65, 66} Amongst many interactions in the AMP-membrane binding process, the cationic side chains electrostatically bind to the phosphate groups of the phospholipids, whereas the hydrophobic groups anchor into the hydrophobic portions of the membrane.⁶⁶ Bacterial cell death is thought to be induced by the carpet or barrel-stave mechanism discussed in Chapter 1.⁶⁷ Preferential attack of bacterial cells by AMPs is driven by electrostatic interactions between the cationic AMP and the anionic bacterial cell surface, and is therefore not prevalent for zwitterionic mammalian cell surfaces.^{68, 69} Screening of a large number of small synthetic peptides for their antimicrobial properties showed that even very short peptide sequences (2-7 amino acids) can display high broad-spectrum antimicrobial activities.^{62, 70-75} For example, Kallenbach and co-workers recently investigated a series of (RW)_n (n = 1-5) peptides and found good bactericidal activity in the micromolar concentration range against *S. aureus* and *E. coli*.⁶⁵

Based on the cell membrane-binding properties of AMPs discussed above, we propose that antimicrobial peptide mimics might be suitable targeting tools for the design of novel microbe-targeted photosensitizers. Therefore, the porphyrin-peptide conjugates synthesized and investigated in this chapter were designed based upon the ability of the porphyrin macrocycle to produce singlet oxygen, and the capability of antimicrobial peptides to efficiently and preferentially bind to a bacterial cell surface for cell-specific targeting in the photodynamic inactivation of bacteria.

Additionally, the synthesis of porphyrin-peptide conjugates is of broad interest given the range of potential applications of such molecules. Photodynamic therapy and boron

neutron capture therapy represent two areas within the realm of (photo)medicine in which porphyrin-peptide conjugates could be exploited as selective targeting agents for anti-cancer, anti-bacterial or anti-viral therapeutics. PPCs might also have utility as fluorescence imaging tags for tracking sub-cellular localization, or when metallated with gadolinium, manganese or iron, have applicability as T1 relaxation agents (radiosensitizers) for use as magnetic resonance imaging positive-contrast reagents. As biomimetic catalysts, porphyrin-peptide conjugates may possess far greater functionality than traditional metalloporphyrins. By incorporating redox active and/or hydrogen bond donor/acceptor side chains that are intrinsic to the peptide, PPCs may access high-valent oxidation states not normally observed or stabilized in the parent porphyrin, provide a firm chemical or spectroscopic basis upon which to propose catalytic intermediates, aid in the interpretation of biochemical-biophysical data, and can serve as the next generation of hemoprotein active site model complexes.

Our synthetic strategy towards PPCs was derived from consideration of the following framework. Based upon the success of photodynamic inactivation with the water-soluble compound 5,10,15,20-tetrakis(1-methyl-4-pyridinyl)porphyrin tetratosylate (**2.1**) as described in Chapter 2, the porphyrin core unit in our PPCs was selected to be a cationic quaternized A₃B-pyridyl porphyrin. For the conjugation strategy, we were aiming for an approach that has the potential to tolerate reaction with small (up to 10 amino acids, prepared by solid phase synthesis) and larger peptides (10-50 amino acids, produced by recombinant protein expression). A number of conjugation methods have been successfully employed to append porphyrins and macrocycles to peptides and proteins. Examples include N-hydroxysuccinimide ester,⁴⁷ thiol-iodoacetamide,^{76, 77} thiol-maleimide,^{41, 78} cross-

metathesis,⁷⁹ Click chemistry,⁸⁰ and amide bond formation^{43, 81-83} based coupling strategies. Among these, the copper-catalyzed Huisgen 1,3-dipolar cycloaddition of azides and terminal alkynes forming 1,2,3-triazoles has attracted much attention in the past years, and appears particularly suitable for chemoselective bio-conjugation reactions. Several reports highlight its application by formation of bio-conjugates such as DNA-glycoconjugates,^{84, 85} peptide-protein conjugates,⁸⁶ protein modification⁸⁰ and protein microarray fabrication.⁸⁷ The reaction was first reported by Huisgen⁸⁸ and later reinvestigated by Sharpless⁸⁹ and Meldal⁹⁰ independently. The attractiveness of the reaction stems from the wide scope of application, ease of installation of azides or alkynes on chemical building blocks, lack of need for protecting groups, the use of benign solvents such as water, orthogonality to most other functional groups, high stability and regioselective formation of the 1,2,3-triazole product and avoidance of chromatography.⁹¹⁻⁹³ However, only few accounts of the use of 1,3-dipolar cycloaddition including porphyrins can be found in the literature.⁹⁴⁻¹⁰⁰

With this work, we have explored several possibilities for porphyrin-peptide conjugate formation using popular Click chemistry, including peptides with antimicrobial character, for use in targeted photodynamic inactivation. Conjugate formation was successful using protected peptides in solution. We report here the synthesis of a small library of porphyrin-peptide conjugates, all of which were purified by RP-HPLC and characterized extensively by various 2-dimensional NMR techniques (COSY, TOCSY, HSQC, HMBC). An initial study analyzing the ability of these PPCs to photoinactivate bacteria was conducted against *M. smegmatis*, and demonstrates the applicability of our approach.

Results

Synthesis of the parent ethynylphenyl porphyrin 3.1. The porphyrin **3.1** was synthesized in four steps (Figure 3.1). The porphyrin macrocycle was synthesized by the statistical condensation of pyrrole with 4-pyridinecarboxaldehyde and 4-[(trimethylsilyl)ethynyl]benzaldehyde under mildly acidic catalysis in refluxing fresh xylenes. The synthesis was adapted from a protocol by Liu et al.¹⁰¹ Recently developed alternative routes to pyridyl-containing porphyrins by Dogutan et al. promising improved yields were also briefly investigated, but proved to be more labor intensive.¹⁰² Porphyrin **3.2** was isolated from the mixture of porphyrins by column chromatography (2-3 successive purifications were necessary) yielding 8% of the desired product. Of note, undesired A₃B porphyrins formed from methylbenzaldehyde contaminants in aged xylenes solvent were also observed, and were inseparable from porphyrin **3.1**. Therefore, it was necessary to ensure the quality of the xylenes solvent used in the porphyrin condensation reaction. Following isolation of **3.2**, the deprotection of the ethyne group affording **3.3** was completed in a methanol/THF (1:4) solution in the presence of 1 equivalent potassium carbonate. The reaction progress was easily monitored by MALDI-TOF MS, and the deprotected porphyrin **3.3** was isolated in excellent yields after aqueous workup and recrystallization. In order to prevent undesired metallation with copper during later Click reactions, zinc was inserted into the porphyrin macrocycle by treatment of **3.3** with zinc acetate in THF/MeOH, yielding **3.4** in nearly quantitative yields after recrystallization. In order to impart water solubility, **3.4** was treated with iodomethane in DMF at elevated temperature. The color of the dissolved porphyrin changed from dark purple to green within 30 minutes. Completion of the reaction was

monitored by HPLC. The desired water-soluble ethynylphenyl porphyrin **3.1** was obtained in 97% yield after recrystallization from methanol and without the need for chromatographic purification.

Compounds **3.1-3.4** were characterized by NMR (^1H - and ^{13}C -) and UV-visible spectroscopies, as well as with MALDI-TOF or HR mass spectrometry. In addition, vapor diffusion of chloroform into a solution of **3.1** dissolved in methanol allowed growth of a single crystal, and the corresponding structure was solved by X-ray crystallography (Figure 3.2, Table 3.1). Atom connectivity for the porphyrin cation matches the structure deduced from NMR spectroscopy, and relevant bond distances are presented in Table 3.2. Some solvent, counterion and pyridinium disorder was observed, and is further discussed in the Appendix.

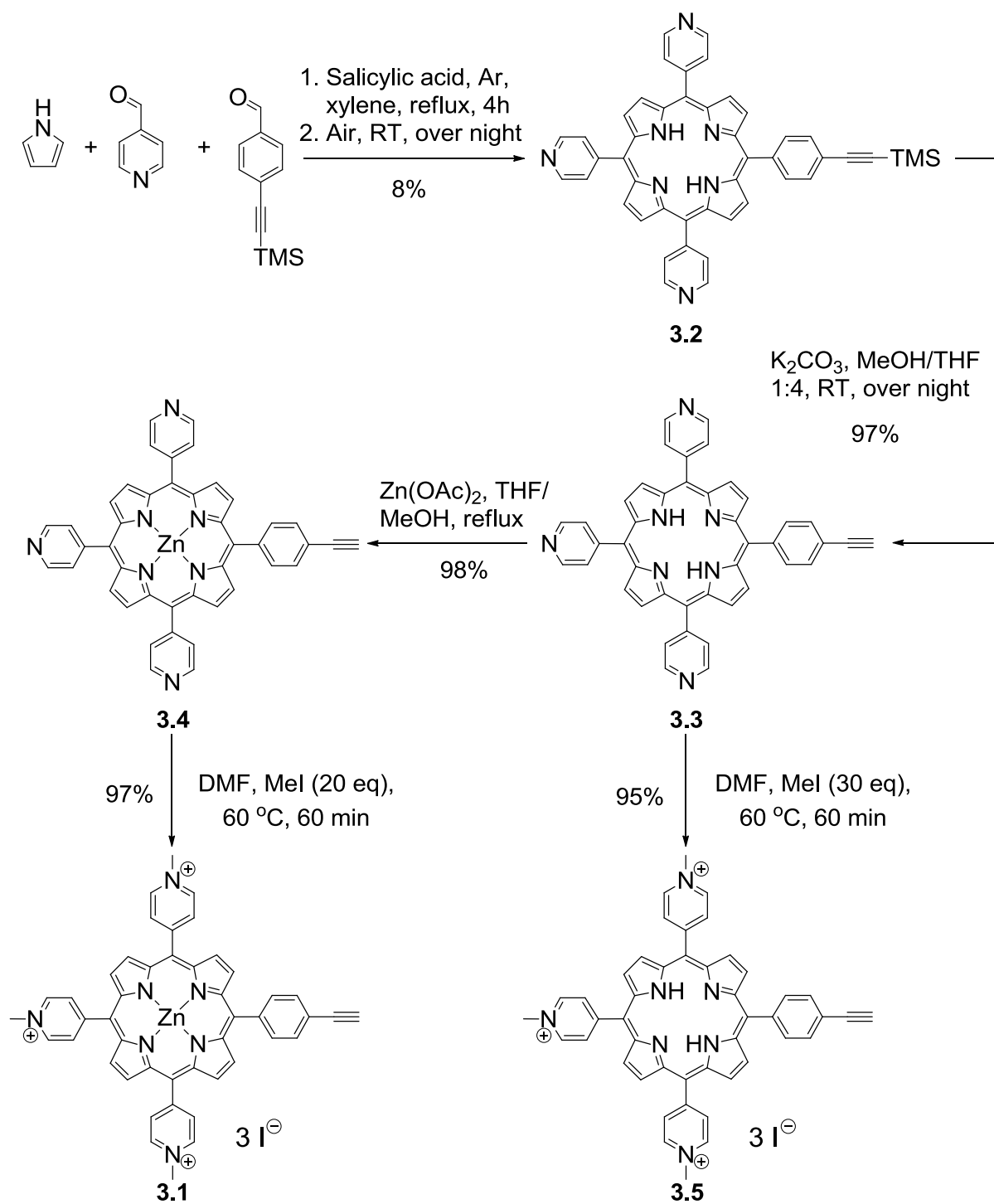


Figure 3.1: Synthesis of the ethynylphenyl porphyrins **3.1** and **3.5**.

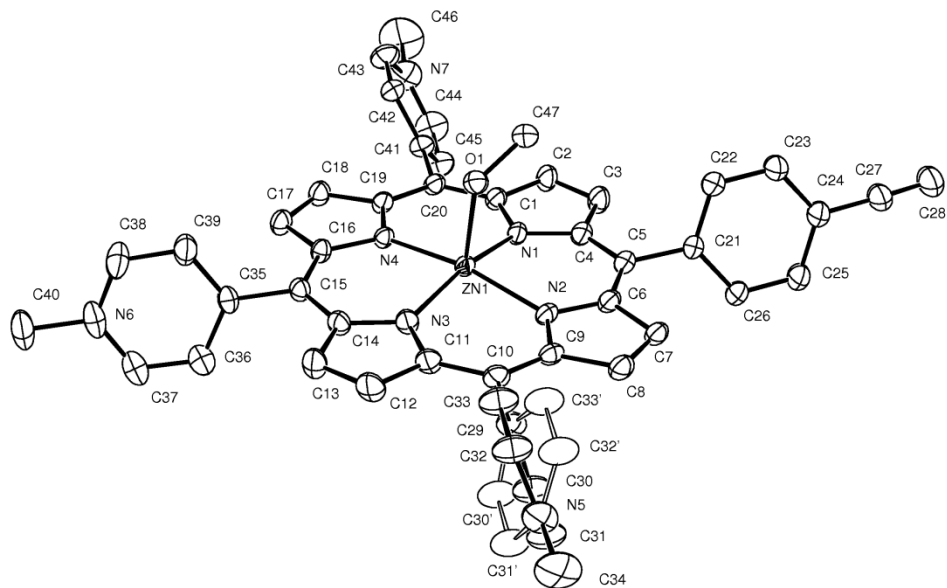


Figure 3.2: ORTEP drawing of the **3.1** cation. Ellipsoids are at the 50% probability level and hydrogen atoms were omitted for clarity. The minor component of the disordered atoms sites are depicted as “hollow” atoms.

Table 3.1: Summary of Crystal Data for **3.1**.

Formula	$C_{50.58}H_{43.34}Cl_9I_3N_7O_{1.58}Zn$
Formula Weight (g/mol)	1539.77
Crystal Dimensions (mm)	$0.52 \times 0.42 \times 0.03$
Crystal Color and Habit	red plate
Crystal System	triclinic
Space Group	P -1
Temperature, K	110
a , Å	13.3015(4)
b , Å	14.2060(4)
c , Å	16.2641(4)
α , °	98.0939(15)

Table 3.1: Continued

$\beta, ^\circ$	94.0276(14)
$\gamma, ^\circ$	96.4599(14)
$V, \text{\AA}^3$	3011.75(14)
Number of reflections to determine final unit cell	9876
Min and Max 2θ for cell determination, $^\circ$	5.08, 63.4
Z	2
F(000)	1501
ρ (g/cm ³)	1.698
$\lambda, \text{\AA}, (\text{MoK}\alpha)$	0.71073
$\mu, (\text{cm}^{-1})$	2.387
Diffractometer Type	Bruker-Nonius Kappa Axis X8 Apex2
Scan Type(s)	omega and phi scans
Max 2θ for data collection, $^\circ$	78.48
Measured fraction of data	0.984
Number of reflections measured	192713
Unique reflections measured	30608
R_{merge}	0.0359
Number of reflections included in refinement	30608
Cut off Threshold Expression	>2sigma(I)
Structure refined using	full matrix least-squares using F ²
Weighting Scheme	calc $w=1/[\text{sigma}^2(\text{Fo}^2)+(0.1309\text{P})^2+11.19$ 55P] where $\text{P}=(\text{Fo}^2+2\text{Fc}^2)/3$
Number of parameters in least-squares	745
R_1	0.0789
wR_2	0.2062
R_1 (all data)	0.1647
wR_2 (all data)	0.2712
GOF	1.023
Maximum shift/error	0.003
Min & Max peak heights on final ΔF Map ($e/\text{\AA}$)	-2.901, 3.086
Where:	
$R_1 = \sum (F_o - F_c) / \sum F_o$	
$wR_2 = [\sum w(F_o^2 - F_c^2)^2 / \sum (w F_o^4)]^{1/2}$	
$\text{GOF} = [\sum w(F_o^2 - F_c^2)^2 / (\text{No. of reflns.} - \text{No. of params.})]^{1/2}$	

Table 3.2: Selected bond length for **3.1** in Å.

Zn1-N1	2.054(4)
Zn1-N3	2.055(4)
Zn1-N4	2.061(3)
Zn1-N2	2.066(3)
Zn1-O1	2.128(3)
C27-C28	1.216(8)
C24-C27	1.419(7)
C28-H28	0.9500
N5-C34	1.471(6)
N6-C40	1.473(7)
N7-C46	1.480(8)
C5-C21	1.497(6)
C10-C29	1.489(6)
C15-C35	1.486(6)
C20-C41	1.490(6)
N1-4 plane-Zn1	0.256(2)

Initial survey of reaction conditions for the Click reaction. Conditions for the Click reaction were initially investigated using compound **3.4** and (azidomethyl)benzene as a model reaction affording **3.6**, which allowed monitoring of the reaction progress by MALDI-TOF MS (Figure 3.3 and Table 3.3). In order to find a starting point for the Click reaction conditions for the synthesis of porphyrin-peptide conjugates, different catalyst- and solvent systems were investigated. Further, the influences of an added base and temperature were also examined. The major issue for all entries that exhibited sluggish reaction progress was the precipitation of unreacted **3.4**, or alternatively the ascorbate co-reagent, from the reaction mixture. The zinc porphyrin **3.4** showed the highest solubility of 0.5 mg/mL in DMF. Complete conversion of the porphyrin starting material was observed with [Cu(OTf)]₂·tol, a Cu(I) catalyst (entries 4 and 5). Addition of diisopropylethylamine (DIEA) as a base

appeared to accelerate the reaction.^{89, 103} Conditions listed under entry 4 were therefore used for further refinement.

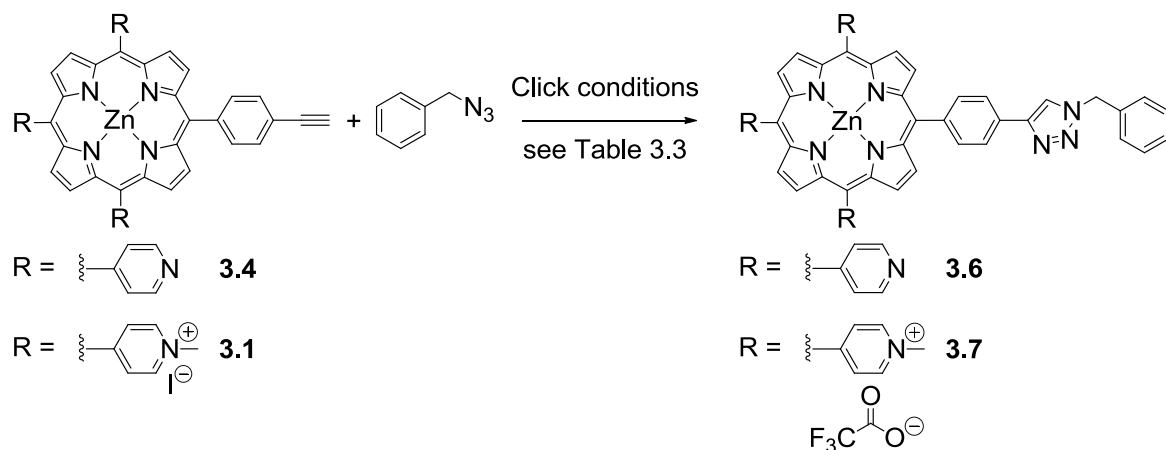


Figure 3.3: Initial survey of reaction conditions for the Click reaction of **3.1** or **3.4** with (azidomethyl)benzene.

Table 3.3: Initial survey of conditions for Click reaction of **3.4** (Figure 3.3).

Entry	Cu reagent	Base	Solvent	Temp °C	Time hours	Reaction progress
1	CuSO ₄ /ascorbate	DIEA (2eq)	THF/H ₂ O 1:1	45	48	No reaction
2	[Cu(OTf)] ₂ ·tol	DIEA (2eq)	THF	45	48	Very sluggish
3	[Cu(OTf)] ₂ ·tol/ ascorbate	DIEA (2eq)	THF/H ₂ O 10:1	45	48	No reaction
4	[Cu(OTf)] ₂ ·tol	DIEA (4 eq)	DMF	65	36	Complete
5	[Cu(OTf)] ₂ ·tol	None	DMF	65	48	Complete
6	CuSO ₄ /ascorbate	2,6-Lutidine (4 eq)	DMF/H ₂ O	65	48	Sluggish
7	CuSO ₄ /ascorbate	None	DMF	65	48	Very sluggish

The Click reaction between the water soluble, quaternized porphyrin **3.1** and (azidomethyl)benzene affording **3.7** was also successful using the conditions listed for entry 4 (Figure 3.3, Table 3.3). The resulting product was isolated by RP-HPLC on a semipreparative column (YMC Pack ODS-AQ column: 250 x 10 mm i.d. or 3 mm i.d., S-5 μm , 12 nm). Compound **3.7** was characterized by HRMS as well as $^1\text{H-NMR}$ and UV-visible spectroscopies.

Attempted porphyrin-peptide conjugate synthesis on Wang resin. With the establishment of the initial reaction conditions for the Click reaction employing **3.1** and **3.4** on hand, we attempted to react porphyrin **3.1** with peptides attached to a solid phase. This approach was anticipated to allow for convenient removal of reagents and excess starting materials. Three short peptides containing arginine or lysine as cationic amino acids along with *p*-azidophenylalanine were synthesized on a Wang resin and subjected to Click conditions for three days at 50 °C under agitation (Figure 3.4). After washing the resin with DMF and DCM, the products were cleaved off the resin using standard conditions.¹⁰⁴ The isolated porphyrin products were analyzed by HPLC, and products were identified by HRMS (LC-ESI, see experimental section). For compounds **3.8** and **3.10**, approximately equal quantities of free base porphyrin and the copper-complexed analog were identified in the UV-visible absorption chromatogram obtained by HPLC analysis (data not shown). In the case of **3.9**, only copper-complexed porphyrin **3.9-Cu** was found. Further, only very minor yields (estimated < 5 %) were obtained while significant amounts of unreacted peptide were identified by HPLC. Because of the low yields obtained, the compounds were not further purified by chromatography. In addition to the low yields, difficulties separating the copper-

complexed analog from the free base porphyrin led us to the conclusion to not further develop this approach.

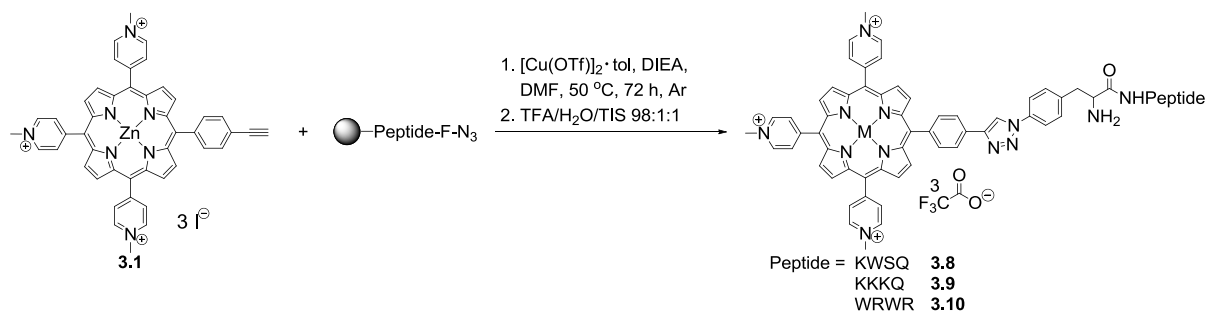


Figure 3.4: Porphyrin-peptide synthesis on the solid support.

Synthesis of PPCs via a solution approach. To circumvent the limitations observed in the solid support based approach, we investigated several routes towards the synthesis of PPCs by conducting the key Click reaction in solution. Our examined synthetic strategies are summarized in Figure 3.5. In Route A, peptides with incorporated, commercially available *p*-azidophenylalanine were employed and reacted with the ethyne moiety of the porphyrin yielding a porphyrin-peptide conjugate. The biotechnological techniques developed by Schultz and co-workers allow incorporation of *p*-azidophenylalanine into larger peptides (10-50 amino acids) by recombinant protein expression.¹⁰⁵ Therefore, we believe that Route A has the potential to provide access to porphyrin-peptide conjugates with larger peptides. Alternatively, we investigated the option of employing a 6-azidohexanoic acid linking fragment providing more structural flexibility to the conjugates. The azide-containing linker was installed in the last step of the solid phase peptide synthesis, as depicted in Route B.

Lastly, the use of a smaller amine-containing linker was briefly investigated as Route C. In this case, the linker was first coupled to the porphyrin, followed by amide bond formation to join the porphyrin with a side-chain protected peptide. The protecting groups were removed after the coupling reaction was complete.

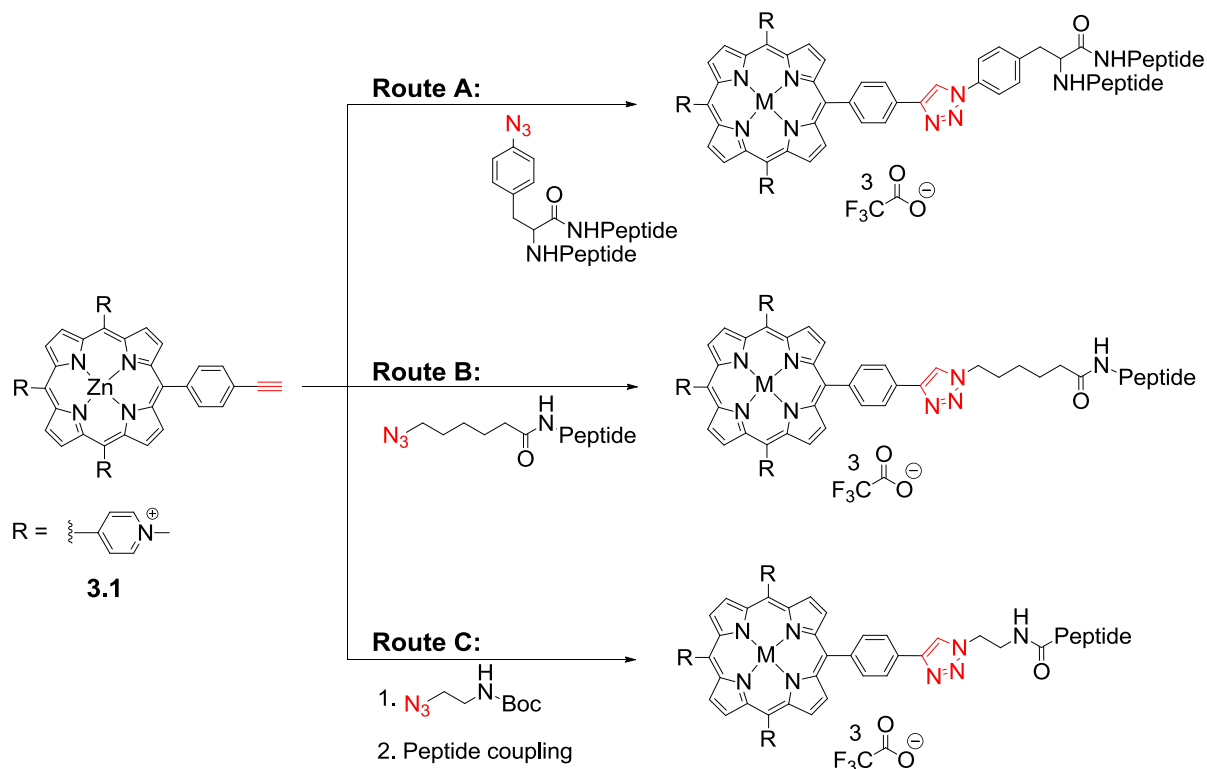


Figure 3.5: Overview of synthetic routes to porphyrin-peptide conjugates.

Route A. The ability of parent porphyrin **3.1** to react with an azide-containing amino acid was investigated using Fmoc protected *p*-azidophenylalanine (Figure 3.6). The previously determined Click reaction conditions were only modified slightly by adding a

small amount (1-2 mg) of Cu(0) powder to assist regeneration of the catalytic Cu(I) species. Although reactivity was observed at room temperature, the reaction time could be significantly reduced to 9-12 hours when the reaction was conducted at elevated temperature (65 °C). The crude product **Fmoc-3.11** was then treated with 20% piperidine in DMF (typical Fmoc deprotection conditions)¹⁰⁴ to yield the unprotected porphyrin-amino acid conjugate **3.11** in good yield. Purification was achieved by RP-HPLC. No transmetallation was observed for the final product **3.11**.

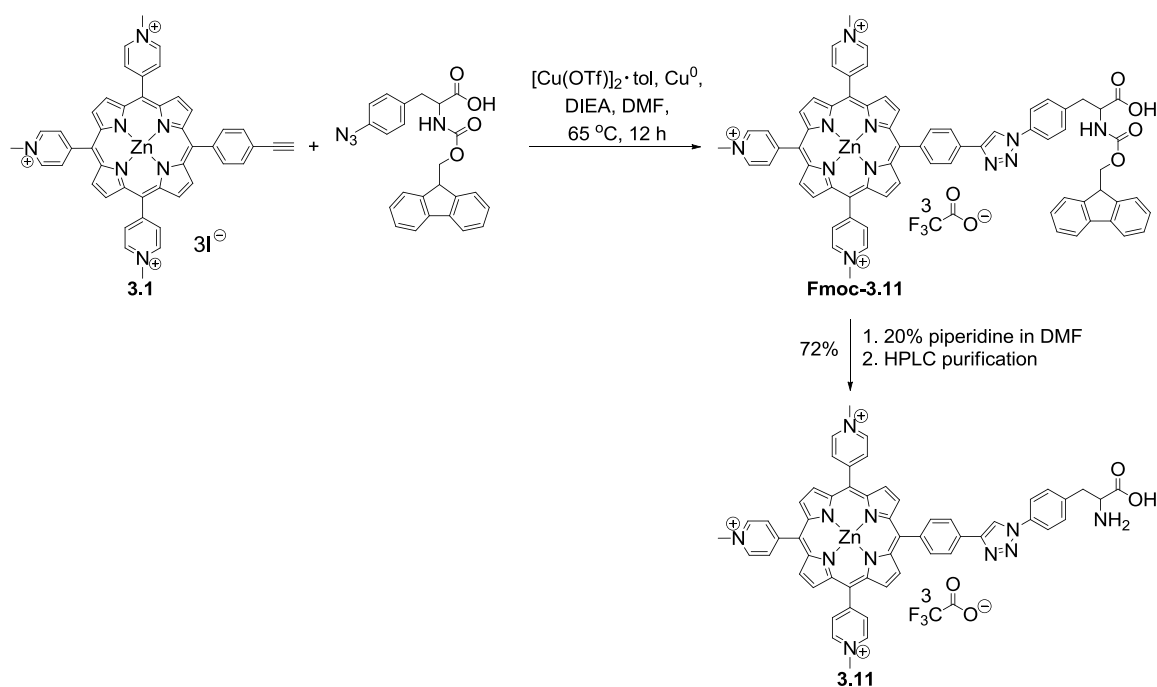


Figure 3.6: Formation of porphyrin-amino acid conjugate **3.11**.

As the next step, the reactivity of **3.1** with a tri-peptide (sequence $\text{N}_3\text{-FWR-OH}$) was investigated. No reaction was observed for attempts to react the peptide with unprotected side

chains. We assume that the multitude of functional groups present on the peptide complexed the catalytic copper(I) ions and therefore interfered with the Click reaction. Therefore, the peptide was synthesized on a highly acid sensitive 2-chlorotrityl resin, which allowed isolation of the side chain protected peptide upon cleavage with 1% TFA in dichloromethane. The crude peptide product was reacted using the established Click conditions with **3.1** (Figure 3.7). The resulting side chain protected PPC **3.12-Zn-prot.** was purified by RP-HPLC before deprotection with TFA/H₂O/TIS. Particular sensitivity towards ambient light was observed for **3.12**. Deprotection was therefore carried out in the dark and under argon using argon-degassed solutions. The final, deprotected PPC **3.12** was characterized in detail by NMR spectroscopies. Various 2D-NMR techniques (COSY, TOCSY, HSQC and HBMC) were used to assign all ¹H and ¹³C-NMR signals (Figure 3.8).

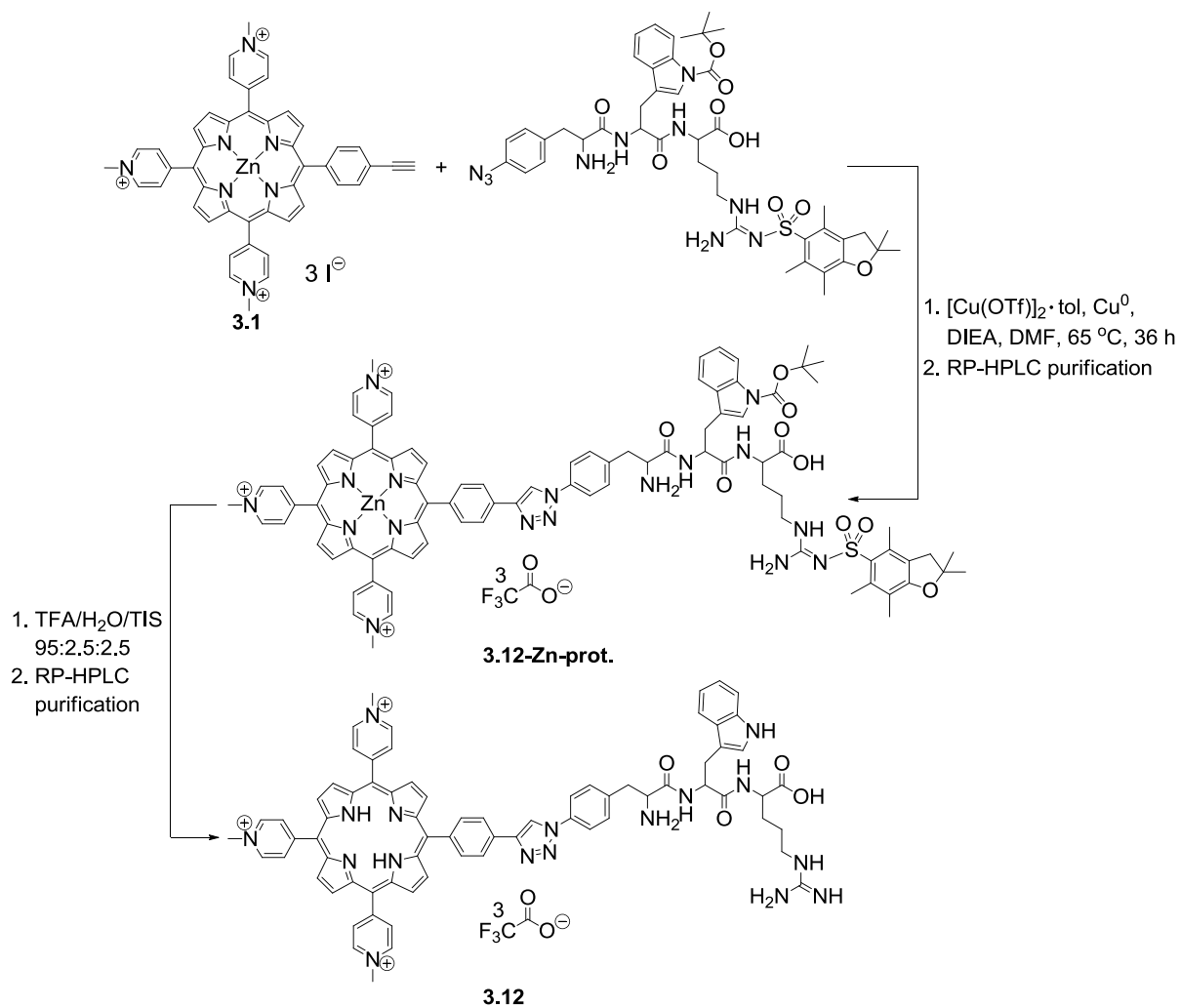


Figure 3.7: Synthesis of porphyrin-peptide conjugate **3.12**.

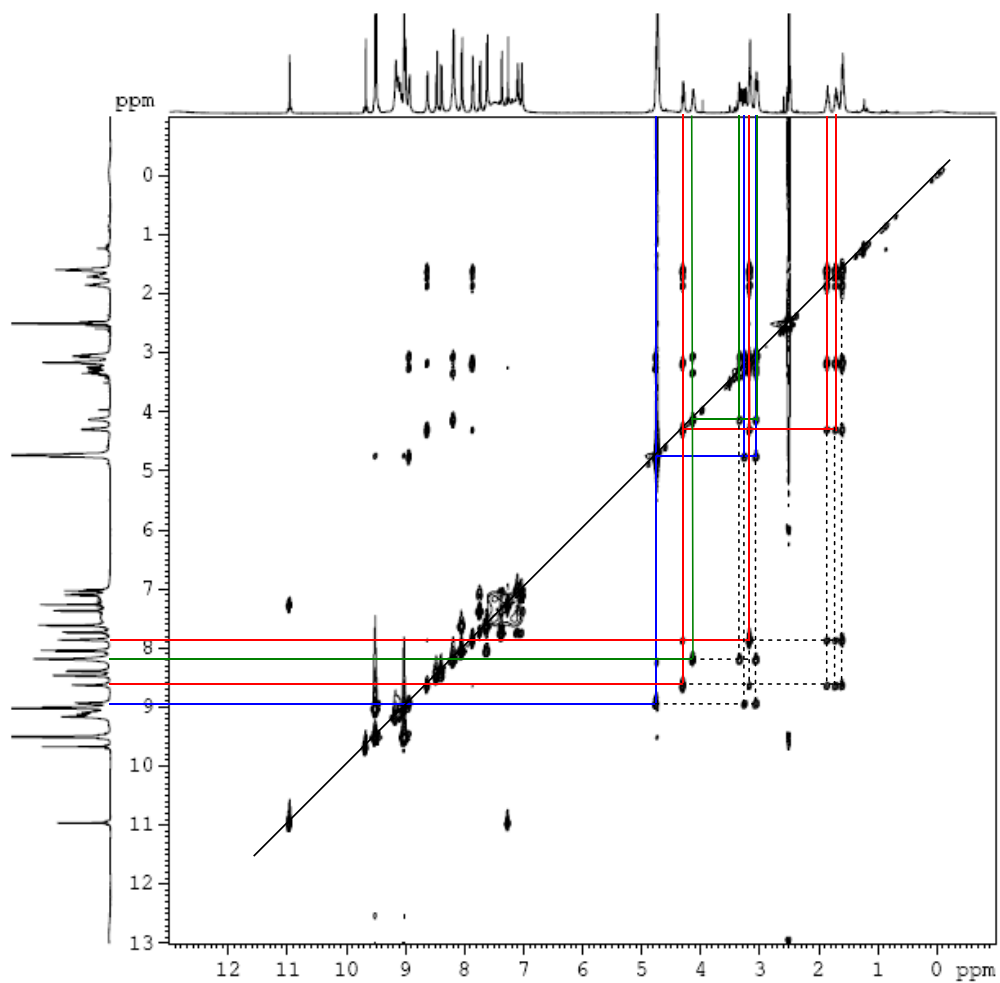
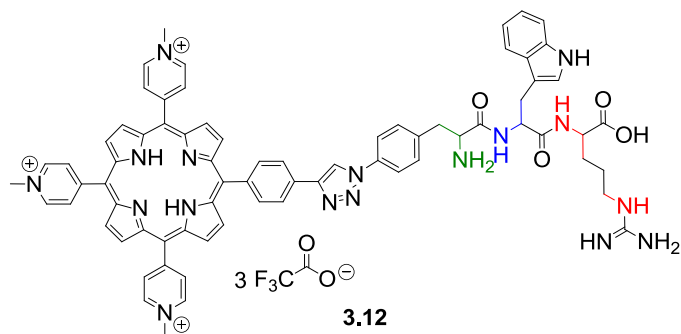


Figure 3.8: Total correlation (TOCSY) NMR spectrum of PPC **3.12**.

Route B. We hypothesized that in addition to the known light sensitivity of tryptophan,^{106, 107} the light sensitivity observed for **3.12** could also be exacerbated by the close proximity of the peptide moiety to the porphyrin. We therefore investigated the synthesis of a small number of porphyrin-peptide conjugates (N-terminal connection of the peptide) joined via a six carbon linker unit (Figure 3.9).

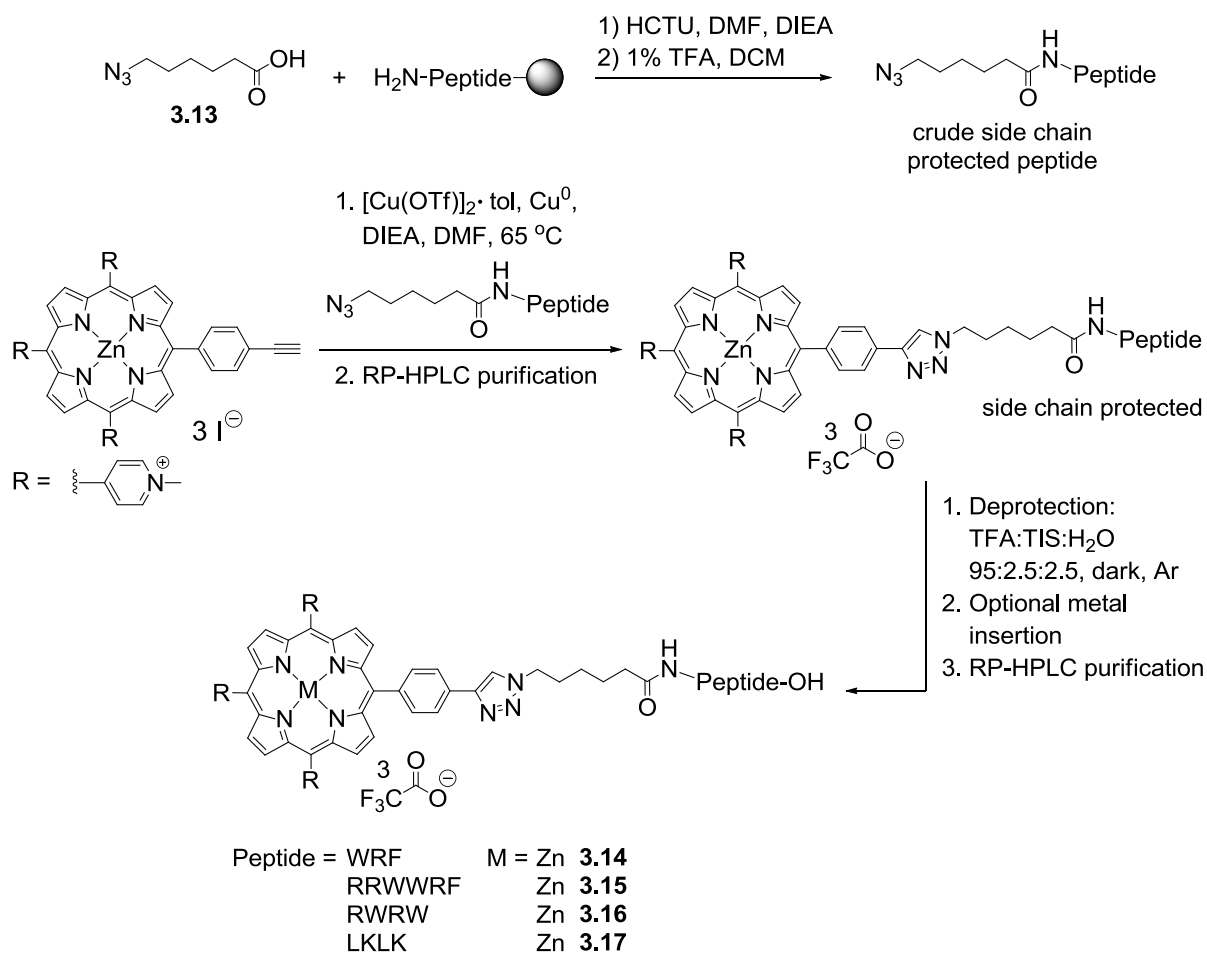


Figure 3.9: Synthesis of PPCs **3.14-3.17** via Route B.

The peptides were synthesized on a 2-chlorotrityl resin. In the last step, the linker, 6-azidohexanoic acid, which had been synthesized by nucleophilic displacement from the corresponding 6-bromohexanoic acid,¹⁰⁸ was coupled to the peptide by amide bond formation. The crude peptide isolated after treatment with 1% TFA was consequently reacted with porphyrin **3.1** under our previously established Click conditions (with only minor modification). Reactions were typically complete after 12 hours, and reaction progress was easily monitored by HPLC. The peptide side chain protected PPC was isolated by precipitation from the reaction mixture, and purified by RP-HPLC. Deprotection was conducted with 95% TFA in the dark under argon. The precipitated and washed crude PPC was then dissolved in methanol and treated with 1.5 equivalents of zinc acetate to reinsert the zinc ion lost during the deprotection procedure. A second chromatographic step was necessary to obtain pure products **3.14-3.17**. These PPCs were characterized by various 2D-NMR techniques as well as mass spectrometry and later tested in PDI experiments against *M. smegmatis* (*vide infra*).

Route C. A second route producing terminally (through C-terminus) appended PPCs was only briefly investigated (Figure 3.10). *tert*-Butyl-(2-azidoethyl)carbamate was first conjugated to porphyrin **3.1** using the Click reaction methods described earlier. Removal of the Boc protecting group was successful with a 3:1 mixture of TFA and DCM. The complexed zinc was removed from the porphyrin macrocycle under these conditions, but can easily be reinserted later in the reaction sequence if desired. Some copper insertion was observed after deprotection of the amine group, but **3.18-Cu** could be removed by chromatography. Porphyrin **3.18** was isolated by HPLC and characterized. Generation of a

PPC can be achieved by amide bond formation between **3.18** and a peptide. For proof of principle, this was only tested using Fmoc-protected-*p*-azidophenylalanine and not a peptide itself. Product formation was observed by RP-HPLC (data not shown). However, the compound was not further isolated or characterized.

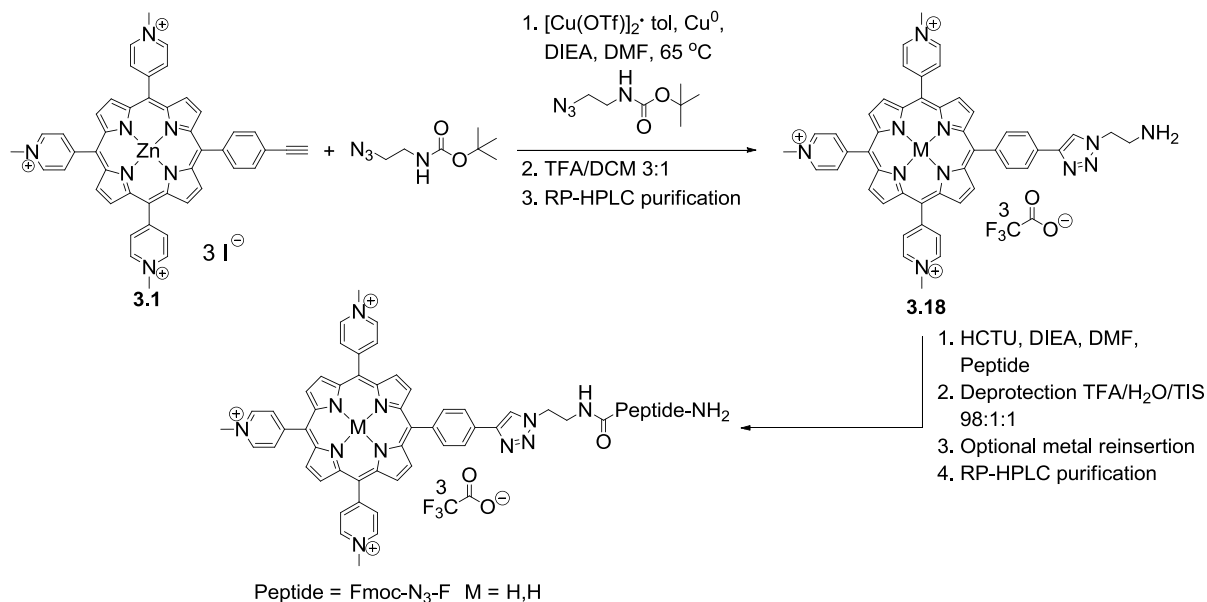


Figure 3.10: Route C for porphyrin-peptide conjugates attached via the C-terminus.

Porphyrin-anthracene conjugate. 9-Azidomethylantracene was kindly donated to us by Dr. Hasan Sadeghifar. Porphyrin **3.1** was also successfully reacted with 9-azidomethylantracene under the previously described Click conditions forming an porphyrin-anthracene conjugate **3.19** (Figure 3.11). This compound was also investigated in terms of its ability to inactivate *M. smegmatis* (*vide infra*).

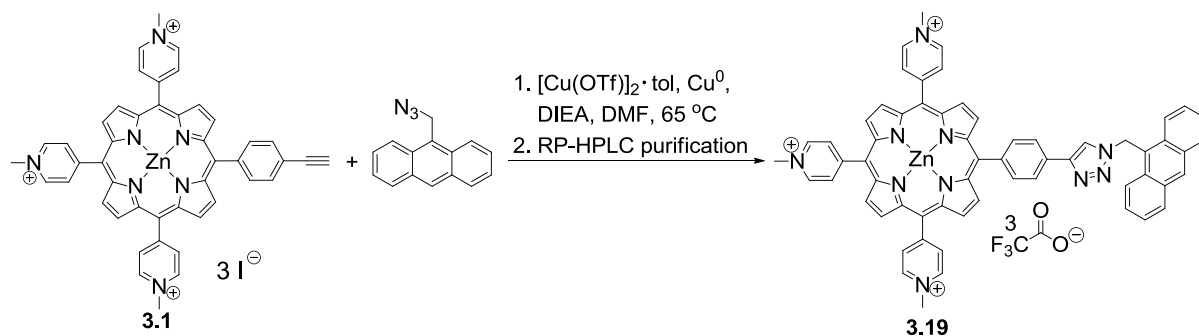


Figure 3.11: Synthesis of porphyrin **3.19**.

Challenges in Chromatography. Particular challenges were posed by the chromatographic purification of the synthesized PPCs. RP-HPLC was the method of choice for purification of compounds **3.7-3.19**, whereas benchtop size exclusion and ion exchange chromatographies were not successful. The particularly strong interaction of cationic porphyrins even with reverse phase solid phase materials has been recorded in the literature.¹⁰⁹ However, chromatographic separation was successful using a YMC Pack ODS-AQ RP-HPLC column (250·10 mm i.d. or 3 mm i.d., S-5 μm , 12 nm) containing a silanol-endcapped C_{18} -stationary phase in order to minimize strong or irreversible binding of cationic porphyrins. Additionally, the need for a low acid content in the eluent mixture was one of the constraints to be overcome in order to prevent demetallation of the final desired metallated porphyrin product during the purification step. The endcapped YMC Pack column produced good separation results even with a maximum acid content of 0.01% TFA in the aqueous mobile phase, while circumventing demetallation to a degree observable by ^1H -NMR spectroscopy.^{81, 109}

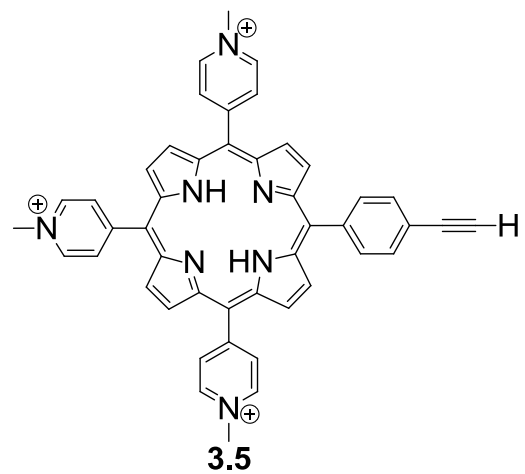
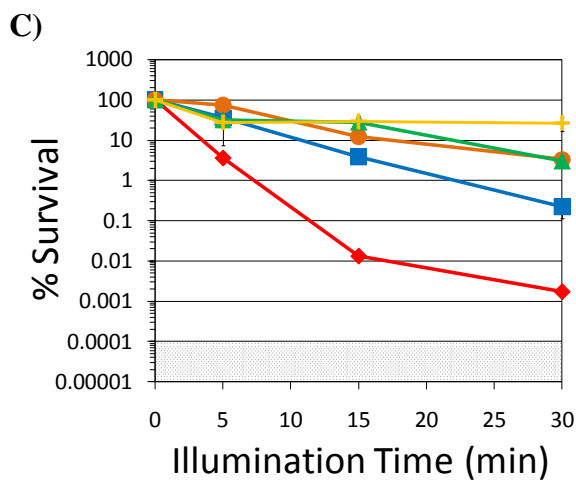
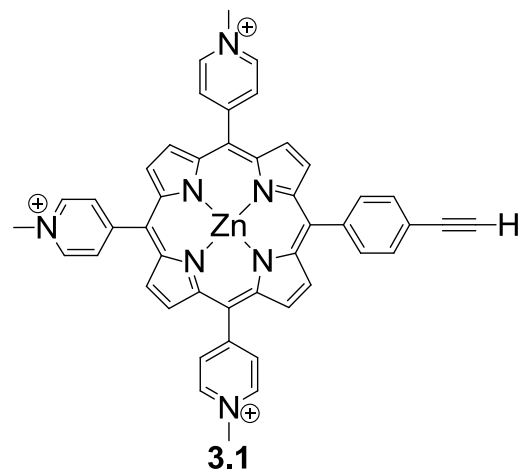
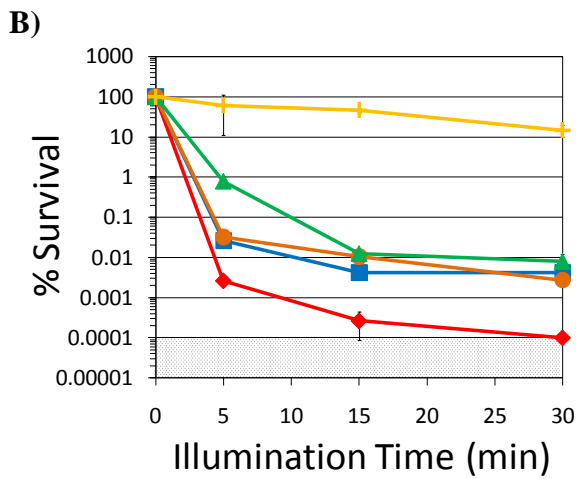
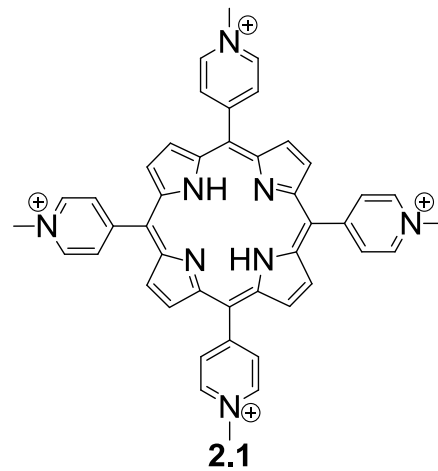
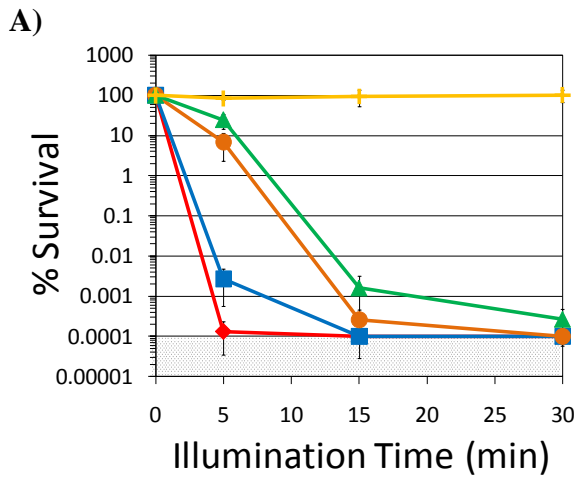
Two chromatographic steps were necessary for reaction sequences producing peptide side chain unprotected PPCs. The direct deprotection of the crude side chain protected PPCs resulted in decreased yields due to some copper-complexation by the porphyrin macrocycle. Cu-complexed PPCs were difficult, albeit possible, to separate from the desired free base porphyrin. Attempts to precipitate residual copper from the catalyst system before deprotection as the hydroxide or sulfide salts were not successful from H₂O/MeOH or H₂O/MeCN solvent systems. Therefore, optimal yields and purity of the product were only achievable with two chromatographic steps: a) directly following the Click reaction on the side chain protected PPC, and b) after deprotection of the peptide side chains of the purified PPCs (Figure 3.10).

Additional challenges regarding the purification and handling of the PPCs were posed by the limited solubility of the PPCs with protected peptide side chains (particularly with increasing number of protecting groups present) in H₂O/MeOH mixtures with H₂O contents of greater than 50%, whereas better solubility was observed in H₂O/MeCN mixtures (> 50% H₂O content). The best results were achieved by using acetonitrile as the organic mobile phase and by circumventing the instrumental auto-injection process. By injecting up to 2 mL of crude PPC solution directly onto the 10 mm RP-HPLC column using a 2 mL loop, which was directly connected to the column for sample injection but removed prior to the elution step, maximum loadings of the PPCs onto the RP-HPLC column could be achieved.

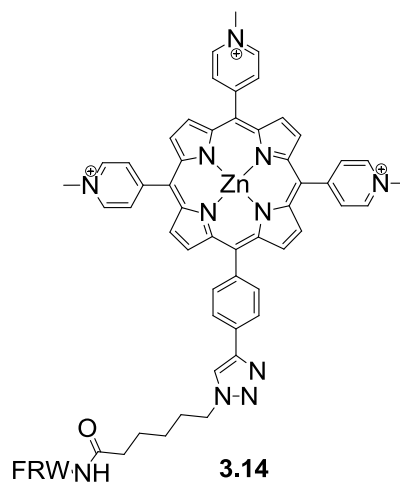
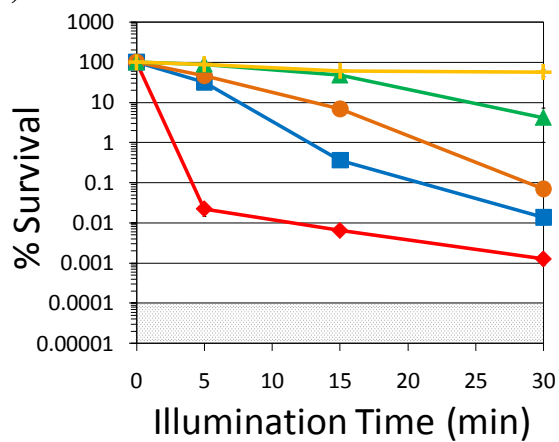
Photodynamic inactivation studies. The ability of PPCs **3.14-3.18** to inactivate *M. smegmatis* was compared to the non-peptide containing compounds **2.1**, **3.1**, **3.5** and **3.19**. The bacteria were grown to a concentration of $\sim 10^8$ colony forming units per mL (CFU/mL),

re-suspended in PBS-0.05% Tween-80 containing buffer, incubated with the photosensitizer in the dark for 5 minutes and subsequently illuminated with white light (400-700 nm) with a fluence rate of 60 mW/cm² for 5, 15 or 30 min (equivalent to a fluence of 18, 54 or 108 J/cm²). The percentage of survival was determined by the ratio of the colony count from illuminated and non-illuminated control cell suspensions. Results discussed in this section were all statistically significant with $P < 0.0001$ unless otherwise stated (Figure 3.12 A-H).

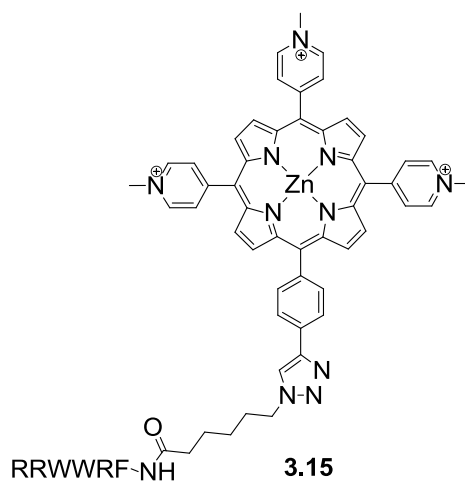
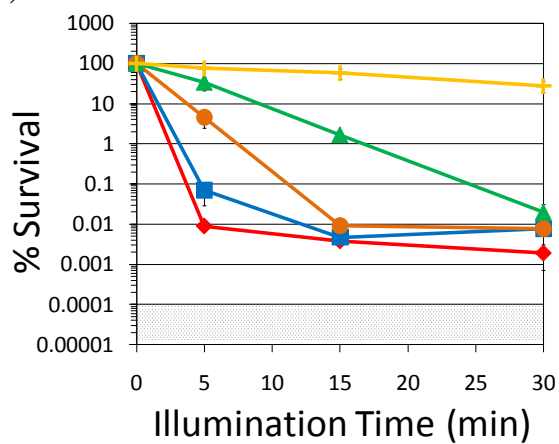
Figure 3.12: Photodynamic inactivation of *M. smegmatis* using photosensitizers **2.1, 3.1, 3.5, 3.14-3.17, 3.19**. The illumination time was varied over 5, 15, and 30 min, corresponding to total fluences of 18, 54, and 108 J/cm², respectively, at 60 mW/cm². PS concentrations are as follows: 5 μM (◆), 1 μM (■), 0.5 μM (●), 0.25 μM (▲), 0.1 μM (+). As the plating technique employed to determine % survival did not allow for detection of survival rates of <0.0001%, data points below the detection limit are set to 0.0001% survival for graphing purposes. The shaded areas correspond to undetectable cell survival with the assay employed.



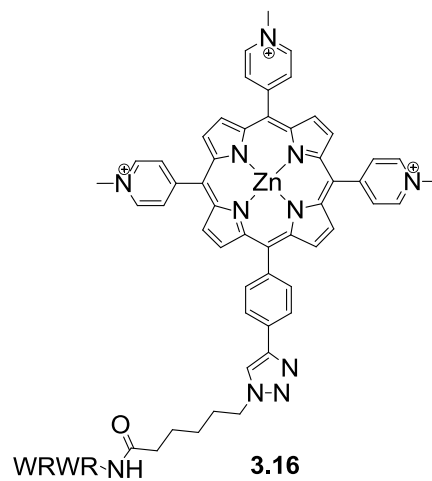
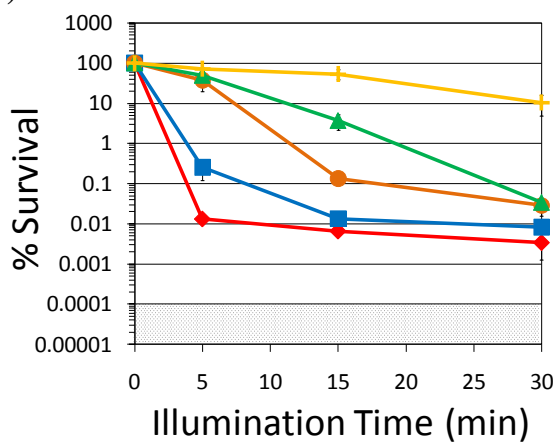
D)



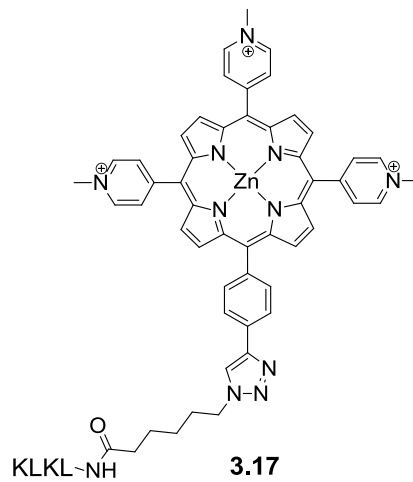
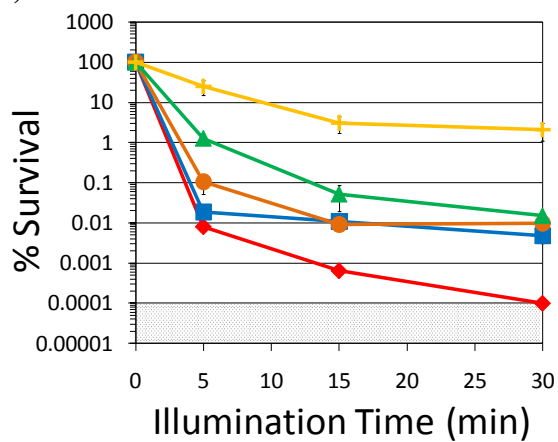
E)



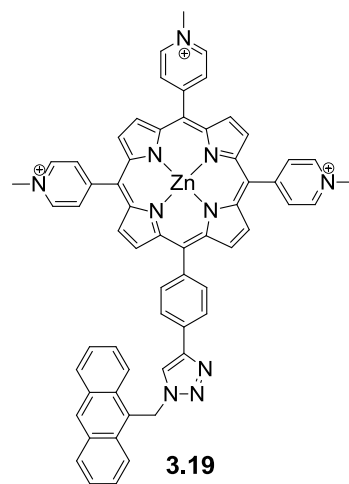
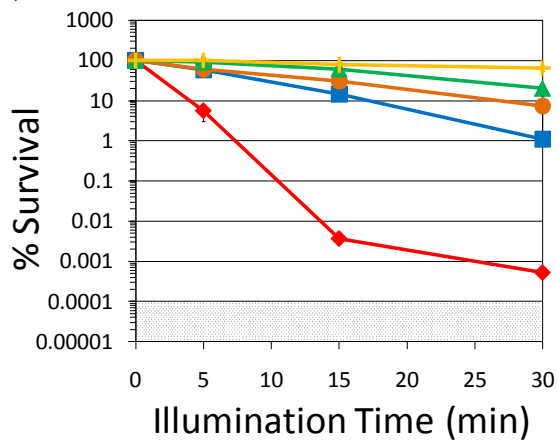
F)



G)



H)



The light- and PS-dose response curves for PS **2.1** and **3.1** against *M. smegmatis* appear similar, although **2.1** showed overall ~1-1.5 log units more reduction in viable cells than **3.1** (Figure 3.12 A and B). However, with 4-4.5 log units reduction in cell viability for concentrations as low as 0.25 μ M and illumination times of at least 15 minutes, **3.1** can be regarded as an excellent photosensitizer against *M. smegmatis*. It appeared that doubling the illumination time (30 minutes) in this concentration range did not improve the degree of viable cell loss. When the zinc ion was removed from the porphyrin macrocycle producing porphyrin **3.5**, a loss in photodynamic inactivation efficiency was observed (Figure 3.12 C). Specifically, a 5 log unit reduction in viable cells could only be achieved using **3.5** at 5 μ M concentration and 30 minutes illumination. For concentrations of 1 μ M or 0.25 μ M, survival rates of ~0.5-5% were observed. Shown in Figure 3.12 D-G are the PDI profiles for PPCs **3.14-3.17**. Amongst those, **3.14-3.16** contained high amounts of arginine and tryptophan, whereas **3.17** was comprised of lysine as the cationic amino acid and leucine as the hydrophobic component. We were pleased to find that all PPCs exhibited good PDI efficacy, albeit no significant improvements in the degree of viable cell loss when compared to **2.1** and **3.1** that would be directly attributable to improved binding properties of these novel compounds was observed. Compound **3.14**, which possesses the shortest peptide (3 amino acids) of the PPCs examined, exhibited inactivation of > 4 log units only at 5 μ M concentration and 15 or 30 minutes illumination time (Figure 3.12 D). PPC **3.15** contained the peptide FRWWRR which is similar to Combi 1, a synthetic antimicrobial peptide (FRWWRR, N-acetylated and C-amidated termini) that has been identified as a potent antimicrobial peptide with IC₅₀ values ranging from 5-39 μ g/mL (activity similar to natural

AMPs) against a variety of organisms from a synthetic library screen.^{110, 111} Compared to **3.16**, elongation of the peptide appeared to improve PDI slightly at submicromolar concentrations (> 4 log unit reduction for 0.25 μ M at 15 minutes; Figure 3.12 E and F). However, for higher concentrations (1 and 5 μ M), survival rates did not improve further and a minimum of 0.002% survival was observed which is about 1 log unit higher when compared to the minimal survival for porphyrin **3.1** (5 μ M, 30 min illumination). For **3.16**, which contains an RWRW sequence, > 4 log units reduction in viable cells could be achieved with a 5-fold lower concentration (1 μ M) and 15 minutes illumination time compared to **3.14** (Figure 3.12 F). Submicromolar concentrations of **3.16** produced survival rates of about 0.1% for 15 minutes (0.25 μ M) and 30 minutes illumination time (0.5 and 0.25 μ M). At 0.1 μ M concentration of **3.15**, **3.16** and **3.1**, a slight loss in viable cells (1 log unit) was observed after 30 minutes illumination. The PDI profile of **3.17** (LCLK sequence) looked remarkably similar to the one of **3.1** except for the lowest concentration tested, where 0.1 μ M of **3.17** was able to cause cell death for up to 97% of *M. smegmatis* cells at illumination times as short as 15 minutes (Figure 3.12 G). At 0.25 and 0.5 μ M concentrations, survival rates between 0.05-0.01% were observed. Interestingly, in the concentration range of 1-0.5 μ M for PSs **3.1**, **3.15**-**3.17**, an increase in the illumination time did not seem to improve the incidence of bacterial cell death, possibly hinting to photodegradation of these compounds.

Finally, of all the PSs examined herein, conjugate **3.19**, which contains an anthracene moiety as a hydrophobic substituent, was the least able to inactivate *M. smegmatis* (Figure 3.12 H). Although a 5 log unit reduction in viable cells was observed at 5 μ M concentration

for 30 minutes illumination, submicromolar concentrations only yielded a 1 log unit loss of cells for the same illumination time.

Compounds **3.11** and **3.12** (synthesized by Route A) were also briefly investigated (Table 3.4). **3.11** synthesized from porphyrin **3.1** and *p*-azidophenylalanine showed about 99.5% inactivation of viable cells after 15 minutes, and 99.999% after 30 minutes at 1 μ M concentration. At 0.1 μ M, only a modest 1 log unit reduction in viable cells was observed, resembling **3.1** (Figure 3.12 B, Table 3.4). By contrast, **3.12** was found to be a comparatively poor photosensitizer for the inactivation of *M. smegmatis* at concentrations of ≤ 10 μ M. However, 3 and > 4 log units reduction in viable cells were observed for 10 μ M of **3.12** for 15 and 30 minutes illumination, respectively. At 1 μ M, **3.12** only inactivated 1 log unit of viable cells.

Table 3.4: Photodynamic inactivation with **3.11** and **3.12** against *M. smegmatis*, 60 mW/cm².

Compound	Peptide sequence	PS concentration μ M	Illumination time	
			15 min	30 min
3.11	F	1	0.46 \pm 0.04	0.001 \pm 0.0001
		0.1	73.8 \pm 1.9	12.6 \pm 0.3
3.12	FWR	10	0.17 \pm 0.05	0.003 \pm 0.001
		1	72.1 \pm 0.9	29.7 \pm 0.4
		0.1	162.1 \pm 24.4	114.6 \pm 11.8

Photostability. Compounds **2.1**, **3.1**, **3.5**, **3.14-3.17** and **3.19** were investigated for their stability under the illumination conditions used in the photodynamic inactivation experiments. 1 mL samples of the photosensitizer (5 μ M) in PBS-Tween buffer were

illuminated at 60 mW/cm² and aliquots were taken at 5, 15 and 30 minutes illumination time for UV-visible spectroscopic analysis. Table 3.5 displays the % decrease in the Soret absorption band upon illumination relative to a dark control. From the data it is clear that PSs without peptides were more stable. **2.1** exhibited the highest stability of all PSs tested with a loss in the Soret band of less than 5% throughout the experiment, whereas the Soret band intensities for **3.1** and **3.5** were reduced by about 40% and 25%, respectively, after illumination for 30 minutes. Amongst the peptide containing PPCs, **3.17** containing a LKLLK sequence was the most stable, and showed a similar stability profile compared to its parent compound **3.1**. As observed during the development of the synthesis of these PPCs, **3.12** was found to be the most light sensitive compound, losing close to 40% of the intensity of the Soret band after the first 5 minutes of illumination. Generally, the Soret band was reduced to 50-60% of its original intensity for all R/W rich PPCs and **3.19** after 30 minutes of illumination. From the data shown in Table 3.5, it appears that the stability of the PS decreases in the presence of 1) a peptide or amino acid, and/or 2) light sensitive substituents such as W, R and anthracene. However, 1:1 molar mixtures of **2.1**, **3.1** and **3.5** with the N-acetylated and C-amidated peptide RWRW did not significantly alter the photostability of these porphyrins (data not shown).

Table 3.5: Light sensitivity of selected porphyrin compounds. The % decrease of Soret absorption band is displayed as a function of varying illumination times (60 mW/cm²). A concentration of 5 μM porphyrin in PBS-Tween buffer was employed.

Compound	Substituent	Illumination time		
		5 min	15 min	30 min
2.1	Pyridyl	96.1±0.1	96.6±0.5	96.8±0.1
3.1	Ethyne	80.1±2.4	74.5±0.3	61.3±0.3
3.5	Ethyne	84.9±0.9	82.3±2.6	76.5±1.9
3.11	F	71.4±3.1	63.3±3.2	52.5±3.5
3.12	FWR	62.6±0.1	57.0±0.7	50.6±6.2
3.14	hexWRF	69.3±1.1	61.7±2.0	53.5±3.1
3.15	hexFRWWR	72.9±0.3	62.4±0.3	55.3±0.3
3.16	hexRWRW	70.8±1.9	60.7±0.6	57.4±2.7
3.17	hexLCLK	85.5±0.5	78.0±1.4	67.7±1.5
3.19	anthracene	74.7±0.7	64.0±1.9	53.6±1.4

Hemolysis Assays. Photosensitizer toxicity was evaluated using hemolysis assays. 10% defibrinated sheep blood was treated with the PS at varying concentrations for one hour at 37 °C under agitation, and the % red blood cell lysis was determined by UV-visible spectroscopic analysis of the supernatant (Table 3.6). At concentrations below 10 μM (the range important for PDI experiments), none of the PSs listed in Table 3.6 exhibited significant (> 10%) hemolytic activity towards red blood cells. An increase in the degree of red blood cell lysis was observed starting at 50 μM for **3.19**, whereas significant lysis for **3.1** and **3.5** did not occur until 500 μM concentration. For PPCs **3.14-3.17** and PS **3.19**, irreversible aggregation or clumping of the red blood cells was observed, therefore HD₅₀ values could not be determined. For comparison to **3.15**, a commercially obtained, N-terminal acetylated peptide with the sequence Ac-RRWWRW-NH₂ was also investigated. No

significant lysis or aggregation of red blood cells was observed for this antimicrobial peptide up to 500 μM . As a further control, TFA/NaOH (1:1) mixtures of up to 2 mM did not show any red blood cell lysis (data not shown).

Table 3.6: Hemolysis assay with 10% defibrinated sheep blood. % hemolysis at varying concentrations of the photosensitizer is listed.

	Concentration of PS in μM								
	0.5	1	5	10	50	100	200	300	500
2.1	<1	<1	<1	<1	<1	<1	1(1)	1(1)	3(1)
3.1	<1	<1	<1	8(1)	3(1)	3(1)	5(1)	8(1)	39(1)
3.5	<1	<1	8(4)	<1	2(1)	4(1)	4(1)	7(1)	31(3)
3.14	<1	<1	<1	<1	<1	7(6) ^a	26(5) ^a	27(4) ^a	27(12) ^a
3.15	2(1)	2(1)	5(1)	11(1)	9(1)	36(3)	68(1) ^a	85(2) ^a	88(1) ^a
3.16	2(2)	<1	1(1)	4(3)	4(1)	10(1)	25(2) ^a	21(1) ^a	21(1) ^a
3.17	<1	2(1)	3(1)	6(1)	9(1)	8(1) ^a	13(4) ^a	24(1) ^a	51(4) ^a
3.19	<1	<1	3(1)	8(1)	21(6) ^a	14(5) ^a	11(2) ^a	13(2) ^a	15(8) ^a
RRWRF	<1	<1	9(1)	3(2)	3(1)	4(1)	4(1)	7(1)	7(1)

^a aggregation/clumping of the red blood cells was observed.

Minimum Inhibitory Concentration (MIC) Assays. Dark toxicity of the synthesized porphyrins in comparison to selected antimicrobial peptides was assessed by determination of MIC values by broth microdilutions. $5 \cdot 10^5$ CFU/mL of *M. smegmatis* was incubated in Mueller-Hinton broth in the presence of different concentrations of either the porphyrin or peptide in question (256 $\mu\text{g/mL}$ max. concentration, MIC values are expressed in $\mu\text{g/mL}$ according to convention)¹¹² for three days. Dark toxicity of PPCs was low towards *M.*

smegmatis (100-fold higher compared to the concentration range used for PDI), but growth was inhibited by the parent porphyrins **3.1** and **3.5** at 128 μg (113 μM) and 64 μg (60 μM), respectively. Of the antimicrobial peptides surveyed (**AMP1-AMP6**), only **AMP3** and **AMP4** were able to inhibit bacterial growth at concentrations $< 256 \mu\text{g/mL}$. The peptide sequence of **AMP4** corresponds to the peptide in PPC **3.15**, but interestingly the antimicrobial activity of **AMP4** was not reflected in PPC **3.15**.

Table 3.7: Minimum Inhibitory Concentrations for porphyrins and selected antimicrobial peptides against *M. smegmatis* as determined by broth microdilution. Assay was conducted in Mueller-Hinton broth with 256 $\mu\text{g/mL}$ as the highest concentration tested.

	Peptide	MIC value $\mu\text{g/mL}$ (μM)
2.1	none	64 (47)
3.1	none	128 (113)
3.5	none	64 (60)
3.11	F	> 256 (200)
3.12	FWR	> 256 (163)
3.14	WRF	> 256 (148)
3.15	FRWWRR	> 256 (115)
3.16	RWRW	> 256 (133)
3.17	LKLK	128 (74)
3.19	None	> 256 (194)
AMP1	Ac-WRF-NH ₂	> 256 (466)
AMP2	Ac-RWRW-NH ₂	> 256 (344)
AMP3	Ac-RWRWRWRW-NH ₂	8 (6)
AMP4	Ac-FRWWRR-NH ₂	16 (15)
AMP5	Ac-LKLK-NH ₂	> 256 (471)
AMP6	Ac-KLKL ₅ KLK-NH ₂	> 128 (94)

Discussion

Work presented in this Chapter represents the initial phase of our research program devoted to the theme of microbe-targeted photodynamic inactivation, with the ultimate goal of providing an alternative or supplemental treatment option for localized bacterial infections. Although PDI has been investigated by many groups for decades, there exists only a limited number of studies exploring targeted PSs that discriminate between bacterial and mammalian cells.^{32, 33, 41-43} In particular, studies towards the inactivation of mycobacteria are lacking.^{11, 113, 114} Therefore, our specific goals for the initial phase of this research project were to develop the means to synthesize and evaluate the photodynamic inactivation potential of water-soluble porphyrin-peptide conjugates as possible microbe-targeted photosensitizers. The peptide moiety incorporated is hypothesized to serve as the targeting entity by anchoring the photosensitizer in the bacterial cell membrane according to the suggested mode of action by antimicrobial peptides.⁶⁷

Huisgen's Cu(I)-catalyzed 1,3-dipolar cycloaddition of an alkyne and azide was used as the linking strategy because of its known stability and regioselective formation of products, possibility for bio-conjugation in water with larger peptides, orthogonality to most functional groups and high yields.^{80, 88-90} The alkyne-containing parent porphyrin **3.1** was designed based on the remarkable ability of 5,10,15,20-tetrakis(1-methyl-4-pyridinyl)-porphyrin tetratosylate **2.1** to inactivate *M. smegmatis*. The ethyne functionalized porphyrins **3.1** and **3.5** were synthesized in four and three steps, respectively, and characterized (Figures 3.1 and 3.2). The needed azide functional group was incorporated according to the three routes demonstrated in Figure 3.5. In Route A, the commercially available *p*-

azidophenylalanine was incorporated into the peptide sequence. The advantage of this strategy is the possibility to place the unnatural amino acid at any position in the sequence. The biotechnological tools for the incorporation of *p*-azidophenylalanine into larger peptides and proteins have been developed by Schultz and co-workers¹⁰⁵, among others, and therefore Route A presents the potential for spatially-controlled bio-conjugation of porphyrins to larger peptides and proteins produced by recombinant expression. Nonetheless, for our proof-of-principle we initially focused on the conjugation with smaller peptides synthesized on the solid phase. Porphyrins **3.11** and **3.12** were successfully synthesized by Route A. However, especially for **3.12**, light sensitivity under ambient light conditions was observed, and was attributed to either the light sensitive amino acid tryptophan, or the specific molecular arrangement with the close proximity of the peptide to the porphyrin. Improved light stability under ambient light conditions was observed for PPCs synthesized by Route B. In this case, the azide moiety was introduced by attachment of 6-azidohexanoic acid to the N-terminus during the solid phase peptide synthesis by standard amide bond formation. The Click reaction between **3.1** and 6-azidohexanoic acid substituted peptides produced PPCs in higher yields and shorter reaction times versus conjugates prepared by Route A. However, this route only allowed for the attachment of the peptide through the N-terminus. Appendage of the peptide through the C-terminus can in principal be achieved by Route C. The established Click conditions included [Cu(OTf)₂·tol and Cu(0) powder as the catalyst system, degassed DMF as the solvent, 4 equivalents of DIEA and mildly elevated temperatures. Under these conditions, porphyrin-to-peptide conjugation was only successful with side chain protected peptides. We hypothesize that when unprotected, the peptides possess enough coordination

sites for sequestering the copper catalyst, thereby rendering the copper unavailable for catalytic turnover. However, recent investigations by Finn and co-workers described bio-conjugation using CuSO_4 /ascorbate as the catalyst while employing the protein BSA as a substrate and tris(3-hydroxypropyltriazolylmethyl)amine as a ligand in 95% aqueous buffer.⁸⁰ Extrapolation of their findings to our systems might allow extension to aqueous conditions and unprotected peptides in the future. The progress of the Click reaction was conveniently monitored by HPLC. It was observed that starting materials converted cleanly and completely to products with estimated yields from the UV-visible absorption trace (HPLC) between 80-95%. Losses resulting in overall lower yields after isolation occurred in the chromatographic purification process, although yields of 65-85% of pure PPCs were still achieved. Particular technical challenges were posed by limited solubility of the crude side chain protected PPC mixtures in $\text{H}_2\text{O}/\text{MeCN}$ and complexation of residual copper by the free base porphyrin macrocycle. Therefore, it was necessary to perform chromatography in two steps: first on the PPC with protected side chains, followed by a second chromatographic step after acidic removal of the protecting groups in order to minimize copper insertion into the macrocycle during the deprotection step. Copper-complexed PPCs were tedious to remove from the product mixture.

By utilizing Route B, a small library of PPCs was successfully synthesized and characterized. The following peptides were chosen for initial investigation of our synthetic approach: WRF, RWRW, FRWWRR and LKLK. These peptides were selected partially based on their reported antimicrobial activity (and derivatives thereof, usually N-acetylated and C-amidated termini). Because of their superior antimicrobial activity, several peptides

with W/R rich motifs were selected. The ability of simple peptides with the repeat sequence $(RW)_n$ to kill bacteria has been discussed by Kallenbach and co-workers.⁶⁵ They reported that antimicrobial potency as well as the hemolytic activity rises with increased chain length (n). As an example, an IC_{50} value of 730 μM against *E. coli* was reported for Ac-RWRW-NH₂.⁶⁵ The peptide Ac-FRWWRR-NH₂ was identified from a combinatorial library screen as a potent antimicrobial peptide.^{110, 111} Its sequence is remarkably similar to an active fragment of bovine lactoferrin (amino acids 4-9, RRWQWR), a natural antimicrobial peptide.⁶⁶ This peptide has been reported to adopt an amphipathic structure in the presence of SDS micelles, and be able to penetrate into bacterial cells by crossing the cell membrane.¹¹⁰ Finally, a lysine containing peptide with the sequence LKLK was also employed. This peptide was derived from the synthetic antimicrobial peptide KLKL₅KLK.¹¹⁵⁻¹¹⁷

Photodynamic inactivation experiments were performed to survey the ability of the synthesized porphyrins to inactivate *M. smegmatis*. The parent porphyrin **3.1** showed excellent inactivation (≥ 4 log units) at concentrations as low as 0.25 μM , whereas the free base analog **3.5** only yielded good inactivation (> 3 log units) at 5 μM . All PPCs **3.14-3.17** exhibited similar dose-response curves with rather subtle differences: Generally, 3-4 log units inactivation was observed at 0.5 μM concentration and 15 minutes illumination. Comparison of the W/R rich PPCs **3.14-3.16** shows an overall 1-2 log unit improvement with elongation of the peptide. The PPC containing the positively charged lysine residues was also very effective in inactivating *M. smegmatis*. Noteworthy is the statistically significant ($P < 0.0001$) 2 log unit reduction in the bacterial count with this PS even at 0.1 μM concentration (30 minutes illumination). This result might point to improved binding of the PS to the

bacterium and calls for further investigation to support this hypothesis. The lack of improved reduction in the viable cell count for all PPC in the 1-0.5 μM concentration range upon doubling the illumination time from 15 to 30 minutes was most likely caused by a significant reduction in porphyrin concentration by photodegradation. Data from photostability assays (Table 3.5) support this notion. The photostability of all compounds synthesized for this work was determined to be significantly lower when compared to the commercially available 5,10,15,20-tetrakis(1-methyl-4-pyridinyl)porphyrin tetratosylate **2.1**, limiting application of the novel compounds to short illumination times (up to 15 minutes). Conjugate **3.17**, which does not contain amino acids that are prone to photooxidation (i.e., tryptophan), was found to be the most stable PPC.

Toxicity of the PPCs was surveyed by hemolysis and minimum inhibitory concentration assays. PPCs did not lyse red blood cells in the concentration range relevant for PDI experiments. However, for concentrations $> 100 \mu\text{M}$, irreversible aggregation of the cells was observed. None of the PPCs showed any antibiotic-type toxicity when incubated in the dark with *M. smegmatis*. **AMP3** [(RW)₄] and **AMP4** (FRWWRR) were identified to have good antimicrobial activity against *M. smegmatis*. Interestingly, the antimicrobial activity of **AMP4** is not reflected in PPC **3.15** which contains the same peptide sequence. The antimicrobial activity of **AMP4** may stem from its ability to cross bacterial membranes followed by lethal interaction with intracellular targets rather than permeabilization of the lipid bilayer.¹¹⁰ The impairment of this mode of action due to the conjugation to a porphyrin such as in PPC **3.15** might explain the difference in MIC values.

In summary, we have investigated a series of water soluble porphyrin peptide conjugates as potential microbe-targeted photosensitizers. Three routes to PPCs were investigated employing Cu(I)-catalyzed Click chemistry. All PPCs were synthesized in good yields and were characterized in detail by 2D-NMR spectroscopic techniques. Although no obvious improvements in the dose response curves of the PPCs **3.14-3.17** (when compared to **3.1** and **2.1**) that would be directly attributable to the improved binding of the PPCs to the bacteria were apparent (with the exception of **3.17** at 0.1 μM), all PPCs can be classified as excellent PSs (inactivation of 3-4 log units) for concentrations as low as 0.25 (**3.15**, **3.17**) or 0.5 μM (**3.14**, **3.16**). The lack of hemolytic activity in the concentration range for PDI further highlights the potential of these compounds.

Outlook

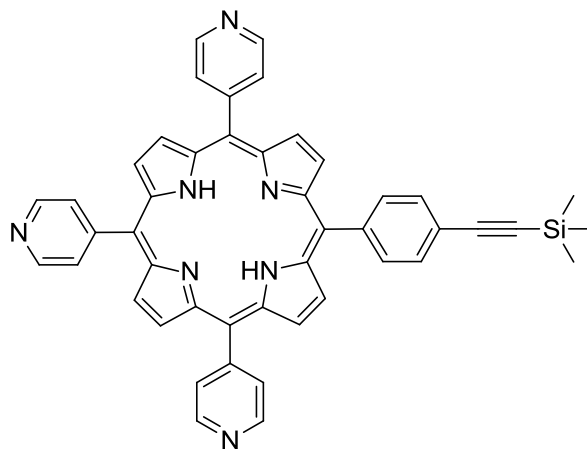
With these initial results at hand, we are now preparing for the next phase of this research project. Beyond expanding the scope to a larger library of PPCs and other bacteria, such as *Escherichia coli* and *Staphylococcus aureus*, we are particularly interested in further investigating the mode of action and the potential of PPCs in targeting bacteria. To further understand and interpret the rather subtle differences amongst PPCs observed in the PDI experiments, we are planning on investigating their photophysical properties, such as the relative singlet oxygen production of these compounds.^{118, 119} In addition, we are interested in more detailed information about the binding properties of the PPCs, or more generally, the mode of interaction between the PS and the bacterial cell surface. Fluorescence binding

assays (performed in Chapter 2) will yield information regarding possible improved binding of these novel compounds. In addition, calcein leakage assays¹²⁰ from micelles might allow us to draw further conclusions regarding the mode of attack of PPCs on model bacterial membranes. However, the main focus of future investigations will be the comparison of the interaction of PPCs with mammalian versus bacterial cells in order to establish if the conjugation of porphyrins with antimicrobial peptides could be a useful tool towards bacterial-targeted photosensitizers.

Experimental Methods - Synthesis

Materials and Methods. Reagents and solvents were purchased from commercial sources and were of reagent grade quality unless otherwise stated. Dry DMF was used as received. Reagents used in the peptide synthesis were dried and stored over activated 3 Å molecular sieves. *p*-Azidophenylalanine was obtained from Bachem. Copper(I) triflate toluene complex was purchased from Sigma Aldrich. Other amino acids and resins for peptide synthesis were purchased from Peptide International, NovaBiochem or AAPPTec. Preparation and handling of air-sensitive materials was carried out under an argon atmosphere using standard Schlenk techniques. Solvents and solutions were deoxygenated by bubbling argon (10-20 min) directly through the solution. Silica gel 170-400 mesh 60 Å (JT Baker) was used for flash column chromatography. Ultrapure water was provided by an Easypure II system (Barnstead).

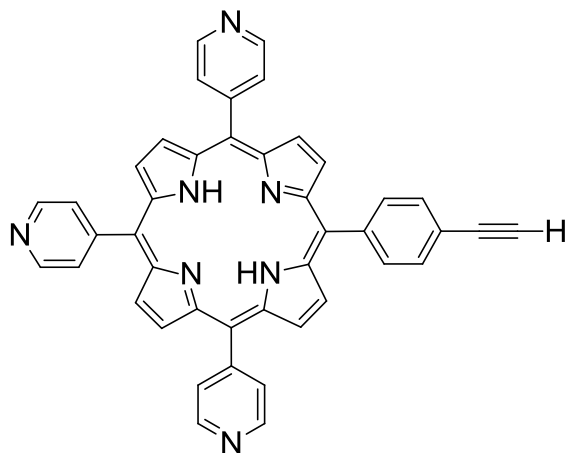
Instrumentation. NMR spectra were measured on a Varian Mercury (300 and 400 MHz) or Bruker Avance (500 or 700 MHz) NMR instrument. All spectra were recorded in 5-mm-o.d. NMR tubes, and chemical shifts were reported as δ (ppm) values using the solvent DMSO (2.50 ppm for ^1H - and 39.51 ppm for ^{13}C -NMR) or CDCl_3 (7.26 ppm for ^1H - and 77.23 ppm for ^{13}C -NMR) as references. Hexafluorobenzene (δ -163 ppm) was used as an external reference for ^{19}F -NMR spectra. High-resolution mass spectra (HRMS) spectra were recorded on an Agilent Technologies 6210 LC-TOF ESI spectrometer with a mass range of 50 - 12,000 m/z, resolution of $> 13,000$ FWHM (2,722 m/z), and a mass accuracy of < 2 ppm. Matrix assisted laser desorption ionization time of flight (MALDI-TOF MS) mass spectra were recorded on a Bruker Daltonics Omnix MALDI-TOF MS spectrometer with a mass range of 0 ~ 200,000 m/z and a resolution of $> 10,000$ FWHM (3,147 m/z). MALDI TOF-MS spectra were calibrated externally, and popop [1,4-bis(5-phenyloxazol-2-yl) benzene] was used as matrix. UV-visible spectra were recorded on a Cary 50 UV-vis spectrometer. Molar absorption coefficients (ϵ) are reported in $10^3 \text{ M}^{-1}\text{cm}^{-1}$. HPLC analyses and purifications were performed on a Waters 2796 Bioseparations module connected to a Waters 2996 photodiode array detector. A YMC Pack ODS-AQ column (250 x 10 mm i.d. or 3 mm i.d., S-5 μm , 12 nm) served as the stationary phase. Ultrapure water with 0.01% TFA and acetonitrile or methanol were used as mobile phases.



5-[4-(Trimethylsilylethynyl)phenyl]-10,15,20-tris-(4-pyridinyl)porphyrin 3.2.

5.0 g (47 mmol) 4-pyridinecarboxaldehyde, 2.4 g (12 mmol) 4-[(trimethylsilyl)ethynyl]benzaldehyde and 4.0 g (29 mmol) salicylic acid were dissolved and heated to reflux in 500 mL fresh xylenes in a 1 L-3 neck flask equipped with a reflux condenser under an argon atmosphere. 4.1 mL (60 mmol) of freshly distilled pyrrole was added dropwise over 10 minutes in the dark. The solution turned black within a few minutes after the addition of the pyrrole was completed. The mixture was heated to reflux for 4 hours, then allowed to cool to room temperature. Oxidation was afforded by stirring the mixture open to air over night at room temperature. 4.0 mL (29 mmol) triethylamine was added before the solvent was removed by rotary evaporation. The crude product mixture was filtered twice through a short silica plug in a filter frit, eluting with DCM:EtOH 100:1 and increasing polarity to DCM:EtOH:NEt₃ 100:2:0.2. Porphyrin fractions containing the desired product (identified by TLC) were combined and the solvent was removed by rotary evaporation. The porphyrin was recrystallized from dichloromethane/methanol, and the crystalline product was washed repeatedly with MeOH until the supernatant was only slightly colored. The porphyrin was

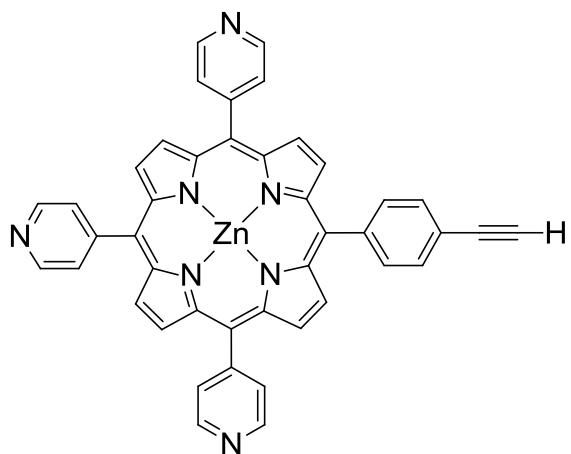
further purified by flash column chromatography on silica gel eluting with DCM:EtOH:NEt₃ 100:2:0.2 increasing polarity to 100:3.0.3. After recrystallization, flash column chromatography was repeated under identical conditions. A final recrystallization afforded 870 mg (8%) of purple crystals. ¹H-NMR (300 MHz, CDCl₃) δ 9.06 (d, 6H, *J*³ = 5.4 Hz, pyridyl), 8.91-8.82 (m, 8H, β-pyrrole), 8.17-8.14 (m, 8H, pyridyl and phenyl), 7.90 (d, 2H, *J*³ = 8.4 Hz, phenyl), 0.39 (s, 9H, TMS), -2.89 ppm (s, 2H, NH); ¹³C-NMR (100 MHz, CDCl₃) δ 150.0 (quart. C, pyridyl), 148.5 (pyridyl), 141.8 (quart. C, phenyl), 134.5 (phenyl), 133-130 (br, β-C porphyrin), ¹²¹ 130.6 (phenyl), 129.5 (pyridyl), 123.2 (quart. C, phenyl), 120.8 (quart. C, meso porphyrin), 117.7 (quart. C, meso porphyrin), 117.4 (quart. C, meso porphyrin), 104.8 (quart. C, ethyne), 96.2 ppm (quart. C, ethyne), 0.2 ppm (CH₃, TMS group), peaks for α-C are broadened due to NH tautomerism and were not observed; ¹²¹ UV-vis (CHCl₃, ε) λ_{abs} 306 (18.9), 419 (470.2 Soret), 514 (21.2), 548 (7.5), 589 (6.4), 644 (3.0) nm; IR (KBr) ν 2156 cm⁻¹ (ethyne stretch); HRMS (ESI) obsd. 714.2791, calcd. 714.2796 (C₄₆H₃₆N₇Si, [M+H]⁺); R_f (silica, CH₂Cl₂:MeOH:NEt₃ 100:2:0.2) 0.4.



5-(4-Ethynylphenyl)-10,15,20-tris-(4-pyridinyl)porphyrin 3.3.

400 mg (0.56 mmol) 5-[4-(trimethylsilylethynyl)phenyl]-10,15,20-tris-(4-pyridinyl)-porphyrin was dissolved in 60-80 mL THF/MeOH (4:1). After the addition of 80 mg (0.56 mmol) K_2CO_3 , the reaction was stirred at room temperature over night. After filtration, the solvent was evaporated to dryness. The crude product was redissolved in DCM and extracted with brine three times. The combined organic phases were dried over Na_2SO_4 and filtered. The product was recrystallized from DCM/methanol to afford 350 mg (0.54 mmol, 97%) as purple crystals. 1H -NMR (300 MHz, $CDCl_3$) δ 9.03 (m, 6H, pyridyl), 8.91-8.83 (m, 8H, β -pyrrole), 8.17-8.13 (m, 8H, pyridyl and phenyl), 7.89 (d, 2H, $J^3 = 8.4$ Hz, phenyl), 3.33 (s, 1H, ethyne), -2.89 ppm (br s, 2H, NH); ^{13}C -NMR (100 MHz, $CDCl_3$) δ 150.1 (quart. C, pyridyl), 148.6 (pyridyl), 142.2 (quart. C, phenyl), 134.6 (phenyl), 130-133 (br, β -C porphyrin, signal broad due to NH tautomerism of porphyrin),¹²¹ 130.9 (phenyl), 129.5 (pyridyl), 122.3 (quart. C, phenyl), 120.7 (quart. C, meso porphyrin), 117.8 (quart. C, meso porphyrin), 117.5 (quart. C, meso porphyrin), 83.6 (ethyne), 78.9 ppm (quart. C, ethyne), peaks for α -C are broadened due to NH tautomerism and were not observed;¹²¹ UV-vis

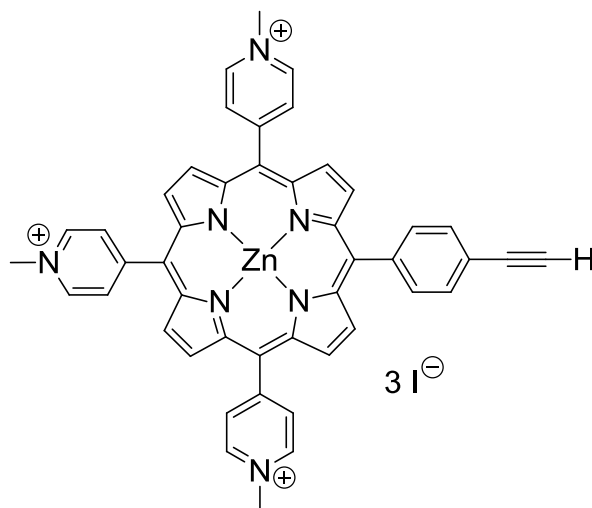
(CHCl₃, ε) λ_{abs} 307 (15.2), 419 (344.3, Soret), 514 (17.3), 548 (6.4), 589 (5.4), 647 nm (3.3); MALDI-TOF-MS obsd. 641.3, calcd. 641.2 (C₄₃H₂₇N₇, [M]⁺); R_f (alumina, CH₂Cl₂:MeOH 5:0.1) 0.5.



5-(4-Ethynylphenyl)-10,15,20-tris-(4-pyridinyl)porphyrin zinc(II) 3.4.

500 mg (0.78 mmol) of 5-(4-ethynylphenyl)-10,15,20-tris-(4-pyridinyl)porphyrin was dissolved in 250 mL THF in a 3 neck flask equipped with a reflux condenser. 716 mg (3.9 mmol) zinc (II) acetate was dissolved in methanol and added to the porphyrin solution. The mixture was then heated to reflux for 2 hours. Reaction progress was monitored by MALDI-TOF MS. After cooling to room temperature, the solution was reduced to a volume of 50 mL. MeOH was added until the porphyrin started to precipitate, after which the solution was kept in the freezer overnight. The by centrifugation collected porphyrin was recrystallized from THF/MeOH and washed with MeOH ten times. 540 mg (0.76 mmol, 98%) of 5-(4-ethynylphenyl)-10,15,20-tris-(4-pyridinyl)porphyrin zinc(II) was obtained as dark purple crystals. ¹H-NMR (300 MHz, DMSO) δ 9.00 (m, 6H, pyridyl H), 8.85-8.80 (m, 8H, β-

pyrrole), 8.21 (d, 6H, $J^3 = 6.0$ Hz, pyridyl), 8.19 (d, 6H, $J^3 = 8.0$ Hz, phenyl), 7.91 (d, 2H, $J^3 = 8.0$ Hz, phenyl), 4.46 ppm (s, 1H, ethyne); ^{13}C -NMR (100 MHz, DMSO) δ 150.3 (quart. C, pyridyl), 149.3 (α -C, porphyrin), 148.62 (α -C, porphyrin), 148.59 (α -C, porphyrin), 148.52 (α -C, porphyrin), 148.0 (pyridyl), 143.0 (quart. C, phenyl), 134.4 (phenyl), 132.3 (β -C, porphyrin), 131.9 (β -C, porphyrin), 131.7 (β -C, porphyrin), 130.1 (phenyl), 129.3 (pyridyl), 121.2 (quart. C, phenyl), 120.4 (quart. C, meso porphyrin), 118.0 (quart. C, meso porphyrin), 117.7 (quart. C, meso porphyrin), 83.8 (ethyne), 81.9 ppm (quart. C, ethyne); UV-vis (THF, ϵ) λ_{abs} 316 (17.4), 424 (466.9 Soret), 556 (17.6), 595 nm (4.3); HRMS (ESI) obsd. 704.1531, calcd. 704.1536 ($\text{C}_{43}\text{H}_{26}\text{N}_7\text{Zn}$, $[\text{M}+\text{H}]^+$); R_f (alumina, CH_2Cl_2 :MeOH 5:0.1) 0.1.



5-(4-Ethynylphenyl)-10,15,20-tris-(4-methylpyridin-4-ium-1-yl)porphyrin zinc(II) tri iodide
3.1.

500 mg (0.71 mmol) of 5-(4-ethynylphenyl)-10,15,20-tris-(4-pyridinyl)porphyrin zinc(II) was suspended in 75 mL dry DMF under argon atmosphere. After the addition of 440 μL (7.1 mmol) iodomethane, the mixture was heated to 60 $^{\circ}\text{C}$ for 60 minutes. Another 10

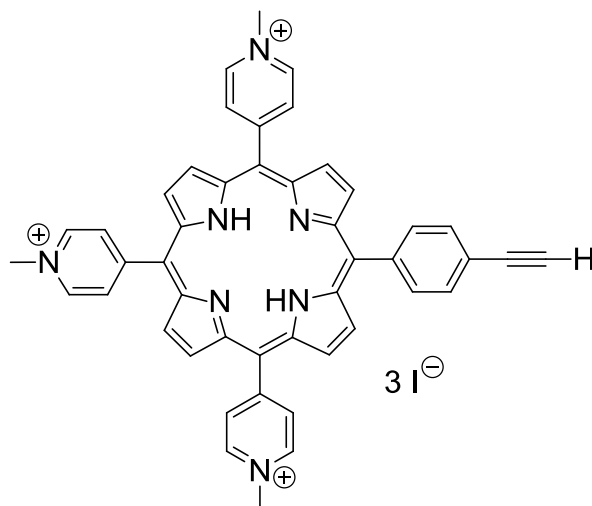
equivalents of iodomethane was added after 30 min. The solution turned from purple to green within 30 min. Completion of the reaction was verified by reverse phase HPLC. The porphyrin was precipitated by addition of diethyl ether and collected by centrifugation. The product was recrystallized from MeOH to afford 780 mg (0.69 mmol, 97%) of the quaternized porphyrin as dark purple crystals. HPLC conditions: Solvent A (water with 0.01% TFA), solvent B (MeCN), flow 4 mL/min, retention time: 12.4 minutes.

Table 3.8: RP-HPLC conditions for **3.1**.

Time (min)	% A	% B
0	95	5
3	95	5
20	5	95
25	5	95

¹H-NMR (300 MHz, CDCl₃) δ 9.44 (d, 6H, $J^3 = 6.4$ Hz, pyridyl), 9.07 (m, 4H, β-pyrrole), 9.00-8.9 (m, 10H, β-pyrrole and pyridyl), 8.20 (d, 2H, $J^3 = 7.8$ Hz, phenyl), 7.96 (d, 2H, $J^3 = 7.8$ Hz, phenyl), 4.71 (s, 9H, CH₃ porphyrin), 4.53 (s, 1H, ethyne); ¹³C-NMR (100 MHz, CDCl₃) δ 158.8 (quart. C, pyridyl), 150.6 (α-C, porphyrin), 149.1 (α-C, porphyrin), 148.9 (α-C, porphyrin), 148.7 (α-C, porphyrin), 144.4 (pyridyl), 143.0 (quart. C, phenyl), 135.1 (phenyl), 134.0 (β-C, porphyrin), 133.4 (β-C, porphyrin), 133.1 (β-C, porphyrin), 132.8 (pyridyl), 132.6 (β-C, porphyrin), 130.9 (phenyl), 123.0 (quart. C, phenyl), 122.2 (quart. C, meso porphyrin), 116.4 (quart. C, meso porphyrin), 115.8 (quart. C, meso porphyrin), 84.2 (ethyne), 82.4 (ethyne), 48.5 ppm (CH₃ porphyrin); UV-vis (H₂O, ε) λ_{abs} 225 (66.2), 320

(21.7), 435 (195.0, Soret), 536 (16.5), 608 nm (6.9); HRMS (ESI) obsd. 249.4052, calcd. 249.4050 (C₄₆H₃₁N₇Zn, [M]³⁺).



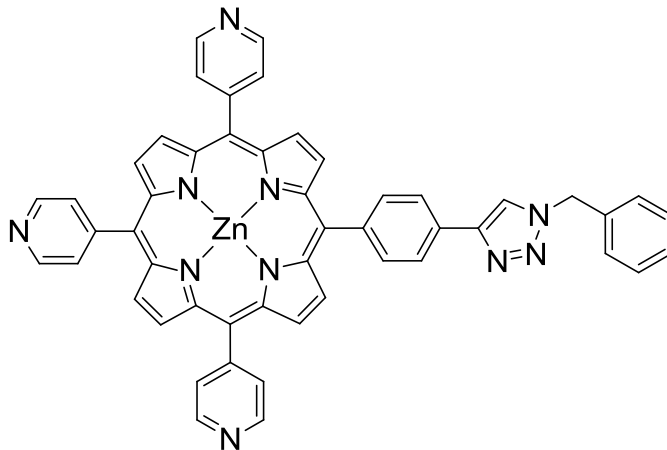
5-(4-Ethynylphenyl)-10,15,20-tris-(4-methylpyridin-4-ium-1-yl)porphyrin tri iodide 3.5.

50 mg (0.078 mmol) of 5-(4-ethynylphenyl)-10,15,20-tris-(4-pyridinyl)porphyrin was suspended in 5 mL dry DMF and heated to 60 °C. Three 50 μ L (0.78 mmol) portions of iodomethane were added over the time period of 1 h, and the reaction progress was monitored by HPLC. After completion, the porphyrin was precipitated by addition of diethylether. The collected product was recrystallized from MeOH to afford 80 mg (0.074 mmol, 95%) of the desired product. HPLC conditions: Solvent A (water with 0.01% TFA), solvent B (MeCN), flow 4 mL/min, retention time: 12.5 minutes.

Table 3.9: RP-HPLC conditions for **3.5**.

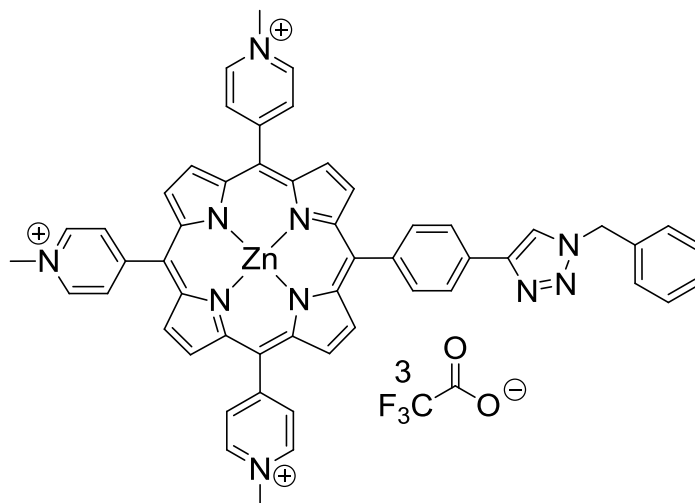
Time (min)	% A	% B
0	95	5
3	95	5
20	5	95
25	5	95

$^1\text{H-NMR}$ (400 MHz, DMSO) δ 9.48 (d, 6H, $J^3 = 5.6$ Hz pyridyl), 9.18 (m, 4H, β -pyrrole), 9.17-9.01 (m, 10H, β -pyrrole and pyridyl), 8.25 (d, 2H, $J^3 = 7.8$ Hz, phenyl), 7.99 (d, 2H, $J^3 = 7.8$ Hz, phenyl), 4.72 (s, 9H, methyl porphyrin), 4.55 (s, 1H, ethyne), -3.05 ppm (s, br, 2H, NH); $^{13}\text{C-NMR}$ (100 MHz, DMSO) δ 156.5 (quart. C, pyridyl), 144.2 (pyridyl), 140.9 (quart. C, phenyl), 134.50 (phenyl), 133.0-1.31.0 (br, β -C, porphyrin), 132.1 (pyridyl), 130.6 (phenyl), 122.1 (quart. C, phenyl), 121.8 (quart. C, meso porphyrin), 115.4 (quart. C, meso porphyrin), 114.8 (quart. C, meso porphyrin), 83.3 (ethyne), 82.9 ppm (quart. C, ethyne), peaks for α -C are broadened due to NH tautomerism and were not observed;¹²¹ UV-vis (H_2O with 0.01% TFA/MeCN) λ_{abs} 426, 521, 557, 591, 648 nm; HRMS (ESI) obsd. 228.7670, calcd. 228.7672 ($\text{C}_{46}\text{H}_{36}\text{N}_7$, $[\text{M}]^{3+}$).



5-(4-(4-(1-Benzyl)-1,2,3-triazolyl)phenyl)-10,15,20-tris-(4-pyridinyl)porphyrin zinc(II) 3.6.

Porphyrin **3.4** (1 eq) and (azidomethyl)benzene (2 eq) were reacted under varying conditions listed in Table 3.3. The reactions were monitored by MALDI-TOF MS. The products were not further isolated or purified. MALDI-TOF-MS obsd. 836 calcd. 836 ($C_{50}H_{32}N_{10}Zn$, $[M]^+$).



5-(4-(4-(1-Benzyl)-1,2,3-triazolyl)phenyl)-10,15,20-tris-(4-methylpyridin-4-ium-1-yl)porphyrin zinc(II) tris(trifluoroacetate) 3.7.

5 mg (6.6 μmol) of porphyrin **3.1** and 1.8 mg (13 μmol) of (azidomethyl)benzene were dissolved in 2 mL of dry DMF and degassed by bubbling argon through the solution for 10 minutes. A solution of the catalyst, $[\text{Cu}(\text{OTf})_2] \cdot \text{tol}$ (0.15 eq), in degassed DMF was added. The mixture was stirred at 65 $^\circ\text{C}$ for 24 hours and another 0.15 eq of the catalyst was added. After another 12 hours, the resulting product was isolated by addition of diethylether. The by centrifugation collected product was triturated with acetone, diethylether, methanol and dichloromethane before drying under vacuum. The product was obtained in 70% yield after HPLC purification. HPLC conditions: Solvent A (water with 0.01% TFA), solvent B (MeOH), flow 4 mL/min, retention time: 14.2 minutes.

Table 3.10: RP-HPLC conditions for **3.7**.

Time (min)	% A	% B
0	95	5
3	65	35
8	65	35
28	55	45
33	55	45

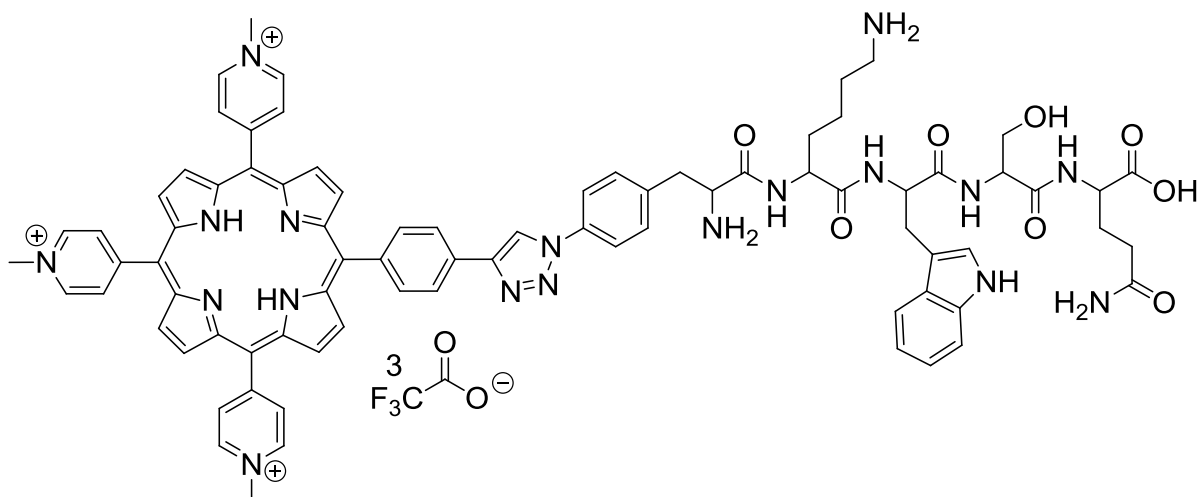
¹H-NMR (400 MHz, DMSO) δ 9.40 (m, 6H, pyridyl), 9.00 (m, 4H, β -pyrrole), 8.96 (m, 4H, β -pyrrole), 8.92-8.87 (several m overlapping, 7H, pyridyl, 1,2,3-triazole), 8.30 (d, 2H, $J^3 = 8.0$ Hz, phenyl porphyrin), 8.23 (d, 2H, $J^3 = 8.0$ Hz, phenyl porphyrin), 7.44 (m, 4H, phenyl), 5.78 (s, 2H, methylene), 4.70 and 4.69 ppm (s, 9H, methyl groups); UV-vis (H₂O with 0.01% TFA/MeOH 6:4) λ_{abs} 255, 320, 437, 564, 609 nm; HRMS (ESI) obsd. 293.75986, calcd. 293.7597 (C₅₃H₄₁N₁₀Zn, [M]³⁺).

Peptide synthesis

Peptides were synthesized by standard manual solid phase synthesis using Fmoc protecting group chemistry.^{122, 123} The Wang resin was employed for Click reactions on the resin and 2-chlorotriylchloride resin for side chain protected peptides. The later peptides were cleaved from the resin with DCM:TFA 99:1 according to standard procedure and precipitated by addition of water.¹²² Peptides were cleaved from the Wang resin with TFA:H₂O:triisopropylsilane (TIS) 95:2.5:2.5. The following protected amino acids were used: Fmoc-Arg(Pbf)-OH, Fmoc-Gln(Trt)-OH, Fmoc-Leu-OH, Fmoc-Lys(Boc)-OH, Fmoc-*p*-N₃Phe-OH, Fmoc-Phe-OH, Fmoc-Ser(^tBu)-OH, Fmoc-Trp(Boc)-OH.

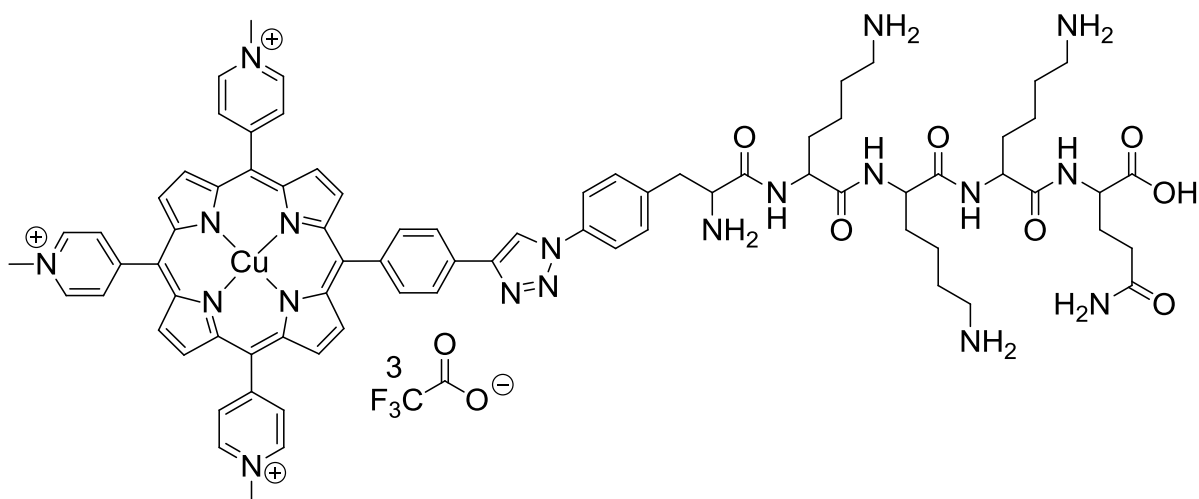
General procedure for the heterogenous Click reaction of 5-(4-ethynylphenyl)-10,15,20-tris-(4-methylpyridin-4-ium-1-yl)porphyrin zinc(II) tri iodide 3.1 employing side chain protected peptide bearing resins.

The resin carrying the respective peptide was suspended in 3 mL dry DMF and one equivalent of quaternized Zn porphyrin **3.1**, two equivalents of dry diisopropylethylamine (DIEA) and 0.15-0.5 equivalents of copper(I) triflate toluene complex [Cu(OTf)₂-tol] were added under argon atmosphere. The mixture was agitated at 50 °C on an orbital shaker for 72 hours. The resin turned greenish in color during that time. The resin was washed with DMF and DCM several times, after which the product was released from the resin by treatment with TFA:H₂O:TIS 98:1:1. The crude product mixture was analyzed by HPLC and HRMS. The yields were too small (estimated < 5%) to justify purification and isolation of the products.



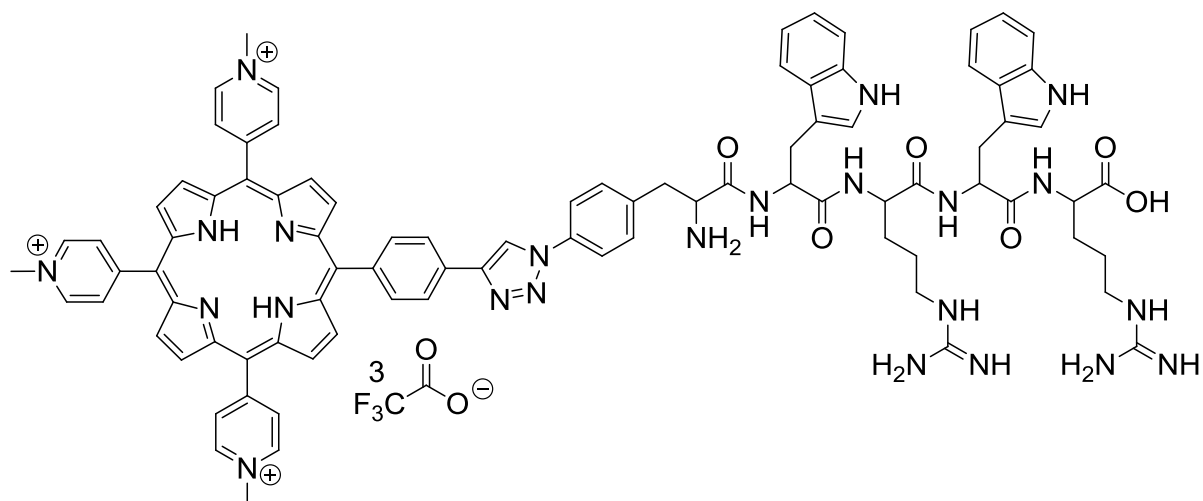
Conjugate (MePy)₃Por-(NH₂)-FKWSQ-OH 3.8.

HRMS (ESI) obsd. 473.8816, calcd. 473.8823 (C₈₀H₈₁N₁₈O₈, [M]³⁺); obsd. 355.6631, calcd. 355.6635 (C₈₀H₈₂N₁₈O₈, [M+H]⁴⁺); obsd. 710.3190, calcd. 710.3194 (C₈₀H₈₀N₁₈O₈, [M-H]²⁺).



Conjugate (MePy)₃PorCu-(NH₂)-FKKKQ-OH 3.9-Cu.

HRMS (ESI) obsd. 488.5454, calcd. 488.5465 (C₇₈H₈₈N₁₉O₇Cu, [M]³⁺); obsd. 366.6607, calcd. 366.6618 (C₇₈H₈₉N₁₉O₇Cu, [M+H]⁴⁺); obsd. 244.7761, calcd. 244.7768 (C₇₈H₉₁N₁₉O₇Cu, [M+3H]⁶⁺).

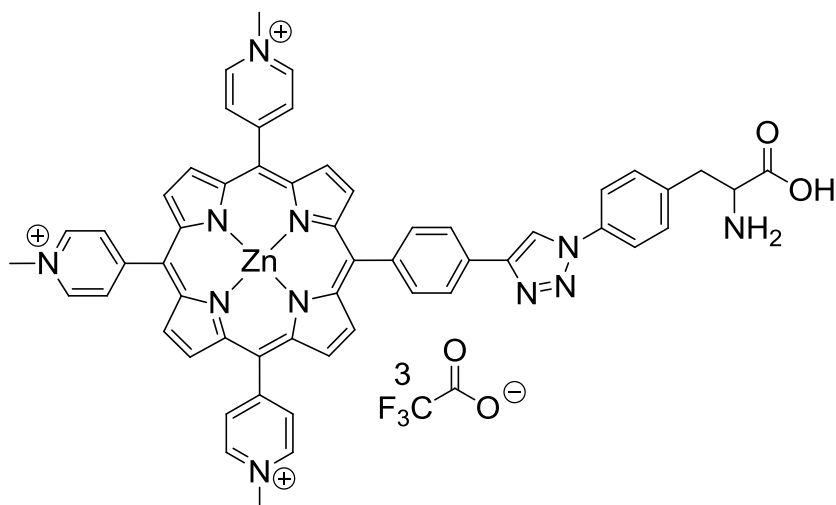


Conjugate (MePy)₃Por-(NH₂)-FWRWR-OH 3.10.

HRMS (ESI) obsd. 394.4365, calcd. 394.4375 (C₈₉H₉₁N₂₃O₆, [M+H]⁴⁺); obsd. 315.7506, calcd. 315.7515 (C₈₉H₉₃N₂₃O₆, [M+2H]⁵⁺); obsd. 263.2932, calcd. 263.2941 (C₈₉H₉₄N₂₃O₆, [M+3H]⁶⁺).

General procedure for Click reaction in solution using 5-(4-ethynylphenyl)-10,15,20-tris-(4-methylpyridin-4-ium-1-yl)porphyrin zinc(II) tri iodide 3.1.

5-(4-Ethynylphenyl)-10,15,20-tris-(4-methylpyridin-4-ium-1-yl)porphyrin zinc(II) tri iodide **3.1** (1 eq), the corresponding azide (1.2 eq), and dry DIEA (4 eq) were dissolved in dry, degassed DMF under argon atmosphere. 1-2 mg of Cu(0) powder and 0.15 mol% copper(I) triflate toluene complex [Cu(OTf)₂-tol] were added. The mixture was heated to 65 °C with stirring, typically overnight. The reaction progress was monitored by HPLC. The porphyrin products were precipitated from the reaction mixture by addition of diethyl ether and collected by centrifugation. Details on isolation and purification are listed for each compound below.



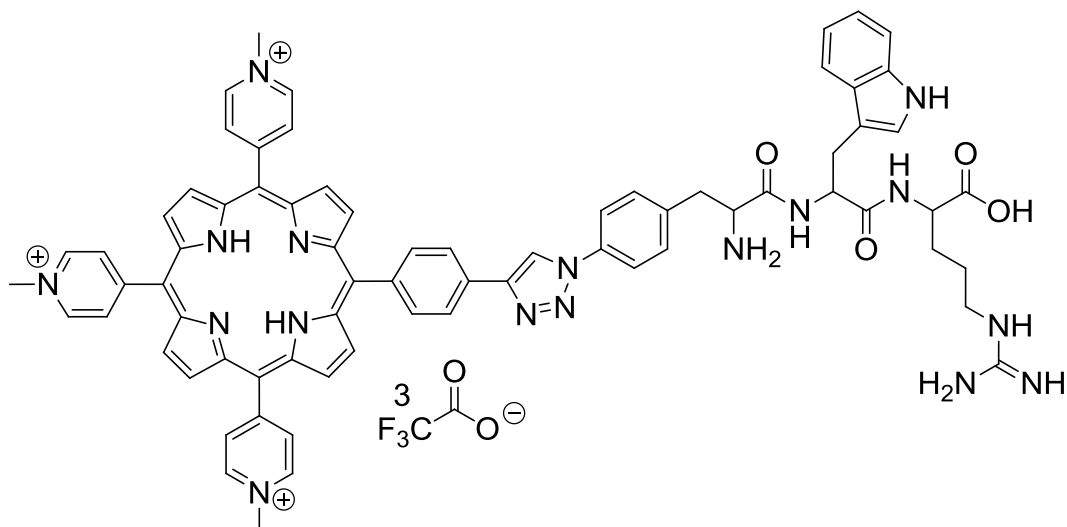
Conjugate (MePy)₃Por-(NH₂)-F-OH 3.11.

The reaction was complete after 12 h. The porphyrin was filtered through a syringe filter (0.2 μm) and precipitated by the addition of an equal volume of diethyl ether. The precipitate was washed with ether 3 times. Removal of the Fmoc protecting group was afforded by treatment of the porphyrin with 20% piperidine in DMF for 20 min. The porphyrin was then precipitated from the reaction mixture by addition of diethyl ether, washed with ether several times, then purified by HPLC. 72% of the desired product was isolated as the TFA salt. HPLC conditions: Solvent A (water with 0.01% TFA), solvent B (MeOH), flow 4 mL/min, retention time: 14.0 minutes (30.0 minutes for Fmoc protected analog).

Table 3.11: RP-HPLC conditions for **3.11**.

Time (min)	% A	% B
0	65	35
1	65	35
18	30	70
19	10	90
22	10	90

$^1\text{H-NMR}$ (500 MHz, DMSO) δ 12.90 (br s, COOH), 9.67 (s, 1H, triazole), 9.48 (d, 6H, $J^3 = 6.0$ Hz, pyridyl), 9.20-9.02 (m, 6H, β -pyrrole), 9.00 (d, 2H, $J^3 = 3.2$ Hz, β -pyrrole), 8.95 (d, 2H, $J^3 = 6.0$ Hz, pyridyl), 8.93 (d, 2H, $J^3 = 6.0$ Hz, pyridyl), 8.49 (br s, 3H, NH_2 Phe), 8.44 (d, 2H, $J^3 = 7.2$ Hz, phenyl porphyrin), 8.34 (d, 2H, $J^3 = 7.2$ Hz, phenyl porphyrin), 8.08 (d, 2H, $J^3 = 7.8$ Hz, phenyl Phe), 7.62 (d, 2H, $J^3 = 7.8$ Hz, phenyl Phe), 4.73 (s, 9H, CH_3 porphyrin), 4.34 (br m, 1H, α -C, Phe), 3.27 (m, 2H, β -C, Phe); $^{13}\text{C-NMR}$ (125 MHz, DMSO) δ 170.4 (C=O), 158.2 (pyridyl), 157.7 (q, $J^2 = 31$ Hz, C=O, TFA), 150.2 (α -C, porphyrin), 148.4 (α -C, porphyrin), 148.2 (α -C, porphyrin), 147.9 (α -C, porphyrin), 147.23 (quart. C, triazole), 143.79 (pyridyl), 141.66 (quart. C, phenyl), 135.93 (quart. C, phenyl Phe), 135.85 (quart. C, phenyl Phe), 134.85 (br, phenyl), 133.5 (β -C, porphyrin), 132.5 (β -C, porphyrin), 132.3 (β -C, porphyrin), 132.1 (pyridyl) 131.8 (β -C, porphyrin), 131.2 (phenyl Phe), 129.9 (quart. C, phenyl porphyrin), 123.9 (br, phenyl porphyrin), 122.9 (quart. C, meso porphyrin), 120.1 (phenyl Phe and triazole), 117.2 (q, $J^1 = 307$ Hz, CF_3 , TFA), 115.7 (quart. C, meso porphyrin), 115.0 (meso C, porphyrin), 53.1 (α -C, Phe), 47.7 (CH_3 porphyrin), 35.4 ppm (β -C, Phe); $^{19}\text{F-NMR}$ (376 MHz, DMSO) δ -73.62 ppm (TFA anion); UV-vis (H_2O) λ_{abs} 255, 318, 440, 567, 618 nm; HRMS (ESI) obsd. 318.0984, calcd. 318.0985 ($\text{C}_{55}\text{H}_{44}\text{N}_{11}\text{O}_2\text{Zn}$, $[\text{M}]^{3+}$).



Conjugate (MePy)₃P-(NH₂)-FWR-OH 3.12.

The reaction was complete after 36 h. The side chain protected product from the Click reaction was purified by HPLC. HPLC Purification: Solvent A (water with 0.01% TFA), solvent B (MeOH), flow 4 mL/min, retention time: 12 minutes.

Table 3.12: RP-HPLC conditions for **3.12-prot**.

Time (min)	% A	% B
0	65	35
1	65	35
13	30	70
14	10	90
17	10	90

The side chain protected porphyrin conjugate was carefully deprotected with TFA:H₂O:TIS 95:2.5:2.5 in the dark and under argon. The conjugate was precipitated by addition of cold diethyl ether, isolated by centrifugation, redissolved in degassed water, stirred in the dark for 2 h, and finally purified by HPLC. 71% of deprotected **3.12** were isolated as a red colored

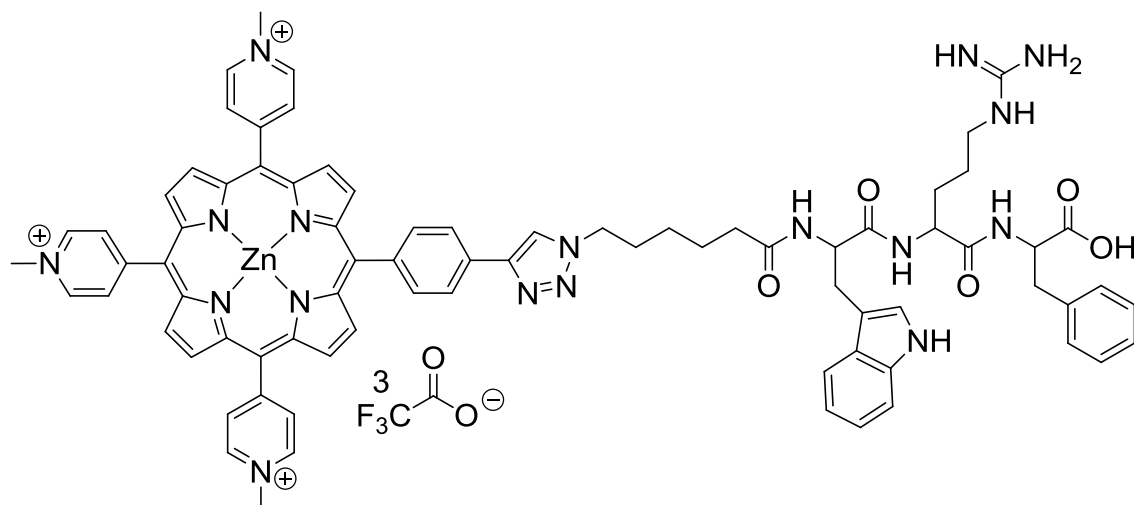
film. HPLC purification: Solvent A (water with 0.01% TFA), solvent B (MeOH), flow 4 mL/min, retention time: 16 minutes.

Table 3.13: RP-HPLC conditions for **3.12**.

Time (min)	% A	% B
0	95	5
2	95	5
4	70	30
17	61	39
19	20	80
21	20	80

$^1\text{H-NMR}$ (500 MHz, DMSO) δ 12.95 (br s, 1H, COOH, Arg), 10.96 (d, 1H, $J^3 = 2.0$ Hz, NH indole Trp), 9.67 (s, 1H, triazole), 9.51 (d, 6H, $J^3 = 6.6$ Hz, pyridyl), 9.20-9.05 (br m, 8H, β -pyrrole), 9.02 (d, 4H, $J^3 = 6.6$ Hz, pyridyl), 9.00 (d, 2H, $J^3 = 6.6$ Hz, pyridyl), 8.93 (d, 1H, $J^3 = 7.6$ Hz, NH backbone, Trp), 8.63 (d, 1H, $J^3 = 7.6$ Hz, NH backbone, Arg), 8.47 (d, 2H, $J^3 = 8.2$ Hz, phenyl porphyrin), 8.39 (d, 2H, $J^3 = 8.2$ Hz, phenyl porphyrin), 8.18 (br s, 2H, NH_2 Phe), 8.04 (d, 2H, $J^3 = 8.5$ Hz, phenyl Phe), 7.86 (t, 1H, $J^3 = 5.5$ Hz, NH side chain, Arg), 7.74 (d, 1H, $J^3 = 7.6$ Hz, Trp), 7.61 (s, 2H, $J^3 = 8.5$ Hz, phenyl Phe), 7.37 (d, 1H, $J^3 = 7.8$ Hz, Trp), 7.26 (d, 1H, $J^3 = 2.0$ Hz, indole Trp), 7.10 (t, 1H, $J^3 = 7.8$ Hz, Trp), 7.03 (t, 1H, $J^3 = 7.6$ Hz, Trp), 7.70-7.00 (very br, 3H, NH guanidine), 4.73 (m, 10H, CH_3 porphyrin and α -H Trp), 4.29 (dd, 1H, $J^3 = 8.1$ Hz, $J^3 = 13.5$ Hz, α -H, Arg), 4.13 (m, 1H, α -H, Phe), 3.33 (m, 1H, β -H, Phe), 3.24 (m, 1H, β -H, Trp), 3.16 (m, 2H, CH_2 side chain, Arg), 3.08-3.00 (m, 2H, β -H, Phe and β -H, Trp), 1.85 (m, 1H, β -H, Arg), 1.70 (m, 1H, β -H, Arg), 1.59 (q, 2H, CH_2 side chain, Arg), -2.99 ppm (s, 2H, NH porphyrin); $^{13}\text{C-NMR}$ (125 MHz, DMSO) δ 173.3 (C=O, Arg),

171.4 (C=O, Trp), 168.1 (C=O, Phe), 158.2 (q, $J^2 = 31.9$ Hz, C=O, TFA), 156.9 (quart. C, guanidine, Arg), 156.6 (quart. C, pyridyl), 156.5 (quart. C, pyridyl), 147.1 (quart. C, triazole), 144.3 (pyridyl), 140.2 (quart. C, phenyl porphyrin), 136.2 (quart. C, indole, Trp close to NH), 135.8 (quart. C, phenyl Phe), 135.1 (phenyl porphyrin), 132.2 (pyridyl), 131.3 (phenyl Phe), 134.0-131.0 (br, β -C)¹²¹ 130.5 (quart. C, phenyl porphyrin), 127.3 (quart. C, indole of Trp), 124.2 (phenyl porphyrin), 124.0 (indole, Trp), 122.4 (quart. C, meso porphyrin), 121.0 (Trp), 120.1 (CH triazole and phenyl Phe overlapping), 118.6 (Trp), 118.3 (Trp), 116.9 (q, $J^1 = 298.7$ Hz, CF₃, TFA), 115.4 (quart. C, meso porphyrin), 114.7 (quart. C, meso porphyrin), 111.4 (Trp), 109.6 (quart. C, side chain connection, Trp), 53.6 (α -C, Trp), 53.3 (α -C, Phe), 51.9 (α -C, Arg), 47.9 (CH₃, porphyrin), 40.4 (CH₂-N side chain, Arg), 36.6 (β -C, Phe), 28.2 (β -C, Arg), 28.0 (β -C, Trp), 25.3 ppm (CH₂ side chain, Arg), peaks for α -C are broadened due to NH tautomerism and were not observed;¹²¹ ¹⁹F-NMR (376 MHz, DMSO) δ -73.44 ppm (TFA anion); UV-vis (H₂O) λ_{abs} 258, 425, 521, 559, 585, 642 nm; HRMS (ESI) obsd. 411.5211, calcd. 411.5208 (C₇₂H₆₈N₁₇O₄, [M]³⁺).



Conjugate (MePy)₃PorZn-hexWRF-OH 3.14.

The Click reaction was complete after 12 h. The solution was filtered (syringe filter 0.2 μm) and the porphyrin was precipitated by addition of diethyl ether. The side chain protected product was purified by HPLC. HPLC purification: Solvent A (water with 0.01% TFA), solvent B (MeCN), flow 4 mL/min, retention time: 9.5 minutes.

Table 3.14: RP-HPLC conditions for **3.14-prot.**

Time (min)	% A	% B
0	70	30
1	65	35
12	57	43
13	10	90
15	10	90

The side chain protected porphyrin conjugate was carefully deprotected with TFA:H₂O:TIS 95:2.5:2.5 in the dark and under argon. The conjugate was precipitated by addition of cold diethyl ether. 1.5 eq Zn(OAc)₂ were added in MeOH, and the mixture was stirred at 50 °C for

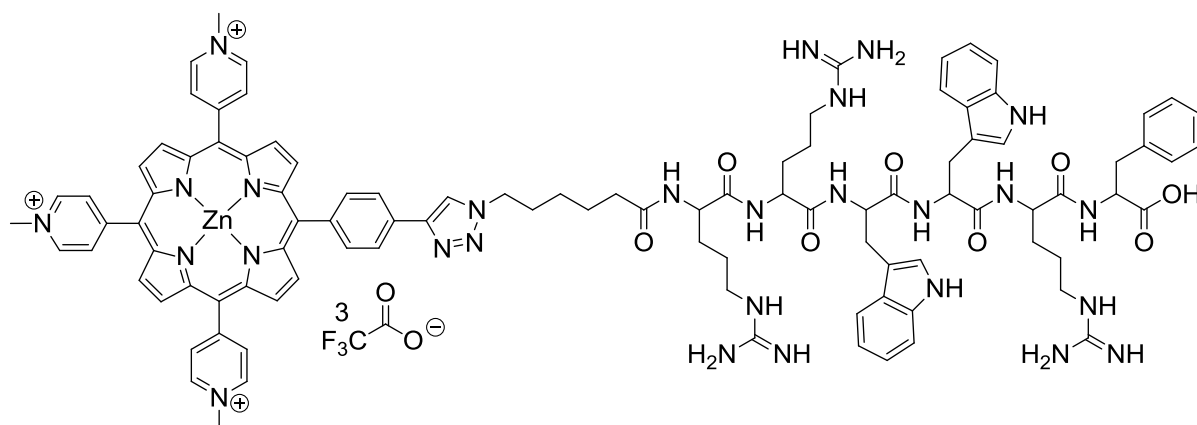
2 h. The solvent was removed and the crude porphyrin was dissolved in degassed water containing EDTA (1 mg/mL) and kept in the dark before being purified by HPLC. The porphyrin was isolated in overall 70% yield. HPLC purification: Solvent A (water with 0.01% TFA), solvent B (MeOH), flow 4 mL/min, retention time: 11.2 minutes.

Table 3.15: RP-HPLC conditions for **3.14**.

Time (min)	% A	% B
0	95	5
1	85	15
12	60	40
14	50	50
15	50	50

¹H-NMR (500 MHz, DMSO) δ 10.90 (s, 1H, NH indole, Trp), 9.46 (d, 6H, $J^3 = 6.00$ Hz, pyridyl), 9.07 (m, 4H, β -pyrrole, porphyrin), 9.04 (d, 2H, $J^3 = 4.75$ Hz, β -pyrrole, porphyrin), 8.99 (d, 2H, $J^3 = 4.75$ Hz, β -pyrrole, porphyrin), 8.95 (m, 6H, pyridyl), 8.87 (s, 1H, triazole), 8.33 (d, 2H, $J^3 = 8.25$ Hz, phenyl, porphyrin), 8.29 (d, 2H, $J^3 = 8.25$ Hz, phenyl, porphyrin), 8.22 (d, 1H, $J^3 = 8.0$ Hz, NH), 8.14 (d, 1H, $J^3 = 8.0$ Hz, NH), 8.09 (d, 1H, $J^3 = 8.0$ Hz, NH), 7.81 (m, 1H, NH side chain, Arg), 7.65 (d, 1H, $J^3 = 7.5$ Hz, Trp) 7.37 (d, 1H, $J^3 = 7.5$ Hz, Trp), 7.26 (m, 4H, Phe), 7.19 (m, 1H, Phe), 7.17 (m, 1H, Trp), 7.08 (t, 1H, $J^3 = 7.5$ Hz, Trp), 6.99 (t, 1H, $J^3 = 7.5$ Hz, Trp), 7.64-7.00 (very br, NH guanidine, Arg), 4.75 (s, 3H, CH₃, porphyrin), 4.74 (s, 6H, CH₃, porphyrin), 3.17-3.08 (several m overlapping, 4H, β -H Trp, CH₂ Arg side chain and β -H Phe), 2.98 (m, 1H, β -H, Arg), 2.94 (m, 1H, β -H, Trp), 2.12 (m, 2H, hexyl), 1.89 (m, 2H, hexyl), 1.72 (m, 1H, β -H, Arg), 1.51 (m, 1H, β -H, Arg), 1.50 (m,

4H, hexyl and CH₂ side chain, Arg), 1.20 ppm (m, 2H, hexyl); ¹³C-NMR (125 MHz, DMSO) δ 172.7 (C=O, Trp), 172.2 (C=O, hexyl), 171.9 (C=O, Arg), 171.3 (C=O, Phe), 158.2 (quart. C, pyridyl), 158.2 (q, $J^2 = 31.2$ Hz, C=O TFA), 156.9 (quart. C, guanidine, Arg), 150.2 (α -C, porphyrin), 148, 4 (α -C, porphyrin), 148.2 (α -C, porphyrin), 147.9 (α -C, porphyrin), 146.1 (quart. C, triazole), 143.7 (pyridyl), 141.2 (quart. C, phenyl porphyrin), 137.4 (quart. C, phenyl Phe), 136.1 (quart. C, indole, Trp), 134.8 (phenyl porphyrin), 133.5 (β -C, porphyrin), 132.5 (β -C, porphyrin), 132.3 (β -C, porphyrin), 132.1 (pyridyl), 131.8 (β -C, porphyrin), 129.1 (quart. C, phenyl, porphyrin), 129.1 (phenyl, Phe), 128.2 (phenyl, Phe), 127.4 (quart. C, indole, Trp), 126.5 (phenyl, Phe), 123.6 (phenyl porphyrin and indole Trp), 123.1 (quart. C, meso porphyrin), 121.7 (triazole), 120.8 (quart. C, phenyl and Trp), 118.6 (Trp), 118.2 (Trp), 117.2 (q, $J^1 = 298.7$ Hz, CF₃, TFA), 115.7 (quart. C, meso porphyrin), 114.9 (quart. C, meso porphyrin), 111.3 (Trp), 110.6 (quart. C, Trp), 55.5 (α -C, Phe), 53.4 (α -C, Trp), 52.0 (α -C, Arg), 49.6 (hexyl), 47.7 (CH₃, porphyrin), 40.4 (side chain, Arg), 36.7 (β -C, Phe), 35.0 (hexyl), 29.5 (hexyl), 29.4 (β -C, Trp), 25.4 (hexyl), 24.9 (side chain, Arg), 24.6 ppm (hexyl); UV-vis (H₂O) λ_{abs} 255, 321, 440, 565, 610 nm; HRMS (ESI) obsd. 464.8488, calcd. 464.8497(C₇₈H₇₆N₁₇O₅Zn, [M]³⁺).



Conjugate (MePy)₃PZn-hexRRWRF-OH 3.15.

The Click reaction was complete after 12 h. The solution was filtered (syringe filter 0.2 μm) and the porphyrin was precipitated by addition of diethyl ether. The side chain protected product was purified by HPLC. HPLC purification: Solvent A (water with 0.01% TFA), solvent B (MeCN), flow 4 mL/min, retention time: 10.4 minutes.

Table 3.16: RP-HPLC conditions for **3.15-prot.**

Time (min)	% A	% B
0	70	30
1	55	45
10	40	60
11	5	95
15	5	95
16	70	30

The side chain protected porphyrin conjugate was carefully deprotected with TFA:H₂O:TIS 95:2.5:2.5 in the dark and under argon. The conjugate was precipitated by addition of cold diethyl ether. 1.5 eq Zn(OAc)₂ were added in MeOH and the mixture was stirred at 50 °C for 2 h. The solvent was removed and the crude porphyrin was dissolved in degassed water

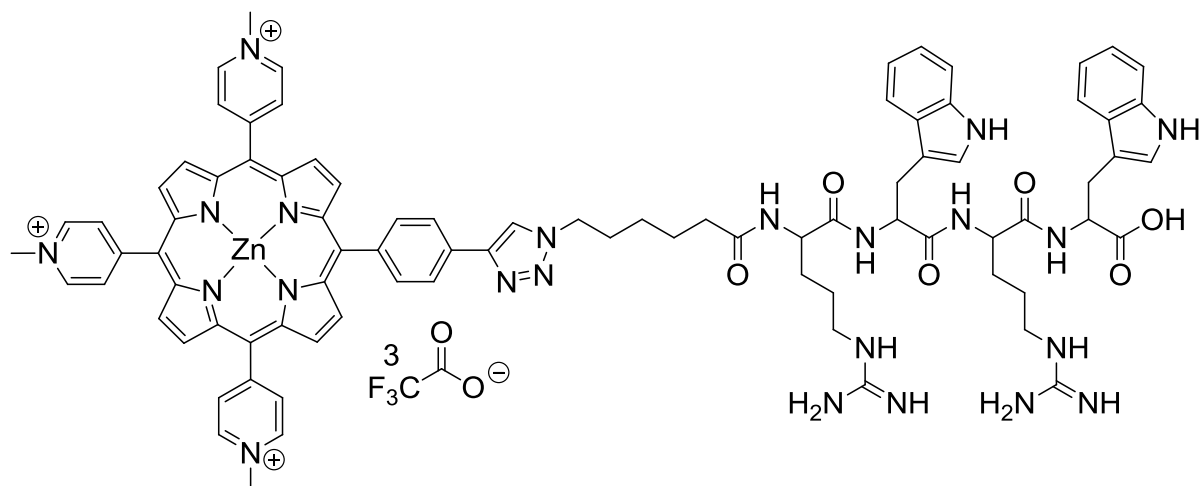
containing EDTA (10 mg/mL) and kept in the dark before being purified by HPLC. The porphyrin was isolated in overall 60% yield. HPLC purification: Solvent A (water with 0.01% TFA), solvent B (MeCN), flow 4 mL/min, retention time: 11.2 minutes.

Table 3.17: RP-HPLC conditions for **3.15**.

Time (min)	%A	%B
0	85	15
1	80	20
13	68	32
14	40	60
15	40	60
16	85	15

¹H-NMR (500 MHz, DMSO) δ 12.60 (br s, COOH, Phe), 10.81-10.79 (2 s, 2H, NH indole Trp), 9.44 (d, 6H, $J^3 = 5.5$ Hz, pyridyl), 9.06 (m, 4H, β -H, pyrrole porphyrin), 9.02 (d, 2H, $J^3 = 4.9$ Hz, β -H pyrrole porphyrin), 8.97 (d, 2H, $J^3 = 4.8$ Hz, β -H pyrrole porphyrin), 8.94 (m, 6H, pyridyl), 8.88 (s, 1H, triazole), 8.31 (d, 2H, $J^3 = 8.0$ Hz, phenyl porphyrin), 8.27 (d, 2H, $J^3 = 8.0$ Hz, phenyl porphyrin), 8.19 (br d, 1H, $J^3 = 7.5$ Hz, NH Phe), 8.14 (br s, 1H, NH Arg), 8.11-8.06 (m, 2H, NH Trp and NH Arg), 8.12 (br s, 1H, NH Arg), 7.78 (br d, 1H, NH Trp), 7.84 (br s, 1H, NH guanidine Arg), 7.74 (br s, 1H, NH guanidine Arg), 7.70 (br s, 1H, NH guanidine Arg), 7.56 (d, 1H, $J^3 = 7.75$ Hz, Trp), 7.54 (d, 1H, $J^3 = 7.75$ Hz, Trp), 7.33 (d, 4H, $J^3 = 7.75$ Hz, Trp), 7.24 (m, 4H, Phe), 7.17 (m, 1H, Phe), 7.12 (s, 4H, Trp), 7.05 (t, 2H, $J^3 = 7.75$ Hz, Trp), 7.45-7.00 (very br, 6H, NH guanidine Arg), 6.95 (t, 1H, $J^3 = 7.75$ Hz, Trp), 6.93 (t, 1H, $J^3 = 7.75$ Hz, Trp), 4.73 (s, 3H, CH₃ porphyrin), 4.72 (s, 6H, CH₃ porphyrin), 4.56 (m, 2H, α -C, Trp), 4.53-4.44 (m, 3H, hexyl and α -C, Trp), 4.33 (m, 1H, α -C,

Arg), 4.26 (br m, 2H, α -C, Arg), 3.14-3.00 (m, 9H, β -C, Trp and β -C, Phe and CH₂-N side chain Arg), 3.00-3.87 (m, 3H, β -C, Trp and β -C, Phe), 2.21 (m, 2H, hexyl), 1.97 (m, 2H, hexyl), 1.72-1.58 (m, 5H, β -C, Arg and hexyl), 1.57-1.40 (m, 9H, CH₂ side chain Arg and β -C, Arg), 1.35 (m, 2H, hexyl); ¹³C-NMR (125 MHz, DMSO) δ 172.7 (C=O, hexyl), 172.3-171.7 (6C, C=O, Trp, Arg, Phe), 158.3 (q, $J^2 = 36.2$ Hz, C=O TFA), 158.2 (quart. C, pyridyl), 156.9 (quart. C, guanidine Arg), 150.2 (α -C, porphyrin), 148.4 (α -C, porphyrin), 148.2 (α -C, porphyrin), 147.9 (α -C, porphyrin), 146.1 (quart. C, triazole), 143.7 (pyridyl), 141.1 (quart. C, phenyl porphyrin), 137.3 (quart. C, Phe), 136.0 (quart. C, Trp), 134.7 (phenyl porphyrin), 133.4 (β -C, porphyrin), 132.5 (α -C, porphyrin), 132.2 (α -C, porphyrin), 132.1 (pyridyl), 131.8 (α -C, porphyrin), 130.5 (quart. C, phenyl porphyrin), 129.3 (phenyl Phe), 128.2 (phenyl Phe), 127.3 (quart. C, Trp), 126.4 (phenyl Phe), 123.6 (phenyl porphyrin and Trp), 123.0 (quart. C, meso porphyrin), 121.8 (triazole), 120.8 (Trp), 118.4 (Trp), 118.2 (Trp), 117.2 (q, $J^1 = 300.0$ Hz, CF₃, TFA), 116.0 (quart. C, meso porphyrin), 114.9 (quart. C, meso porphyrin), 111.2 (Trp), 109.9 (quart. C, Trp), 53.5 and 53.4 (α -C, Trp and Phe), 52.1 (α -C, Arg), 49.6 (hexyl), 47.7 (CH₃, porphyrin), 40.5 (CH₂-NH, side chain Arg), 40.4 (CH₂-NH, side chain Arg), 36.7 (β -C, Phe), 35.0 (hexyl), 29.5 (hexyl), 29.3 (β -C, Arg), 29.2 (β -C, Arg), 28.8 (β -C, Arg), 27.6 (β -C, Trp), 25.6 (hexyl), 25.0 (CH₂, side chain Arg), 24.8 (CH₂, side chain Arg), 24.7 (hexyl); UV-vis (H₂O) λ_{abs} 258, 298, 321, 444, 568, 613 nm; HRMS (ESI) obsd. 630.9439, calcd. 630.9435 (C₁₀₁H₁₁₀N₂₇O₈Zn, [M]³⁺).



Conjugate (MePy)₃PZn-hexRWRW 3.16.

The Click reaction was complete after 12 h. The solution was filtered (syringe filter 0.2 μm) and the porphyrin was precipitated by addition of diethyl ether. The side chain protected product was purified by HPLC. HPLC purification: Solvent A (water with 0.01% TFA), solvent B (MeCN), flow 4 mL/min, retention time: 11.0 minutes.

Table 3.18: RP-HPLC conditions for **3.16-prot.**

Time (min)	% A	% B
0	70	30
1	55	45
10	40	60
11	5	95
15	5	95

The side chain protected porphyrin conjugate was carefully deprotected with TFA:H₂O:TIS 95:2.5:2.5 in the dark and under argon. The conjugate was precipitated by addition of cold diethyl ether. 1.5 eq Zn(OAc)₂ in MeOH were added and the mixture was stirred at 50 °C for

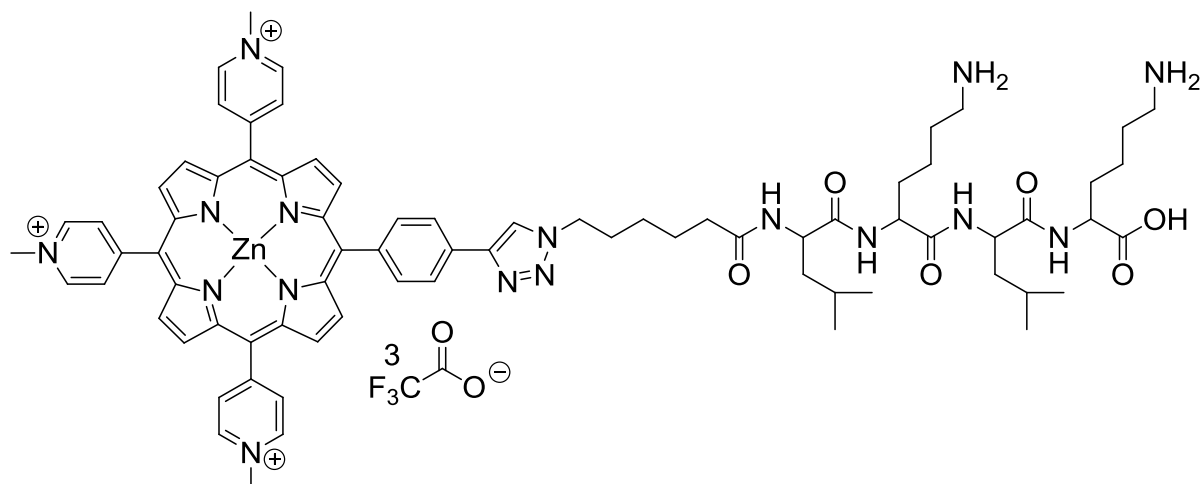
2 h. The solvent was removed and the crude porphyrin was dissolved in degassed water containing EDTA (10 mg/mL) and kept in the dark before being purified by HPLC. The porphyrin was isolated in overall 56 % yield. HPLC purification: Solvent A (water with 0.01% TFA), solvent B (MeCN), flow 4 mL/min, retention time: 7.7 minutes.

Table 3.19: RP-HPLC conditions for **3.16**.

Time (min)	% A	% B
0	85	15
1	80	20
11	70	30
13	20	80
15	40	60

¹H-NMR (500 MHz, DMSO) δ 10.91 (s, 1H, NH indole Trp), 10.86 (s, 1H, NH indole Trp), 9.65 (m, 6H, pyridyl), 9.07 (m, 4H, β -pyrrole porphyrin), 9.04 (d, 2H, $J^3 = 4.5$ Hz, β -pyrrole porphyrin), 8.98 (d, 2H, $J^3 = 4.5$ Hz, β -pyrrole porphyrin), 8.94 (m, 6H, pyridyl), 8.90 (s, 1H, triazole), 8.33 (d, 2H, $J^3 = 8.0$ Hz, phenyl porphyrin), 8.28 (d, 2H, $J^3 = 8.0$ Hz, phenyl porphyrin), 8.22 (d, 1H, $J^3 = 7.0$ Hz, NH Trp), 8.13 (d, 1H, $J^3 = 7.5$ Hz, NH Arg), 8.04 (d, 1H, $J^3 = 7.5$ Hz, NH Arg), 7.92 (d, 1H, $J^3 = 7.5$ Hz, NH Trp), 7.82 (br m, 1H, NH guanidine, Arg), 7.76 (br m, 1H, NH guanidine, Arg), 7.58 (d, 1H, $J^3 = 7.5$ Hz, Trp), 7.54 (d, 1H, $J^3 = 7.5$ Hz, Trp), 7.34 (d, 1H, $J^3 = 7.5$ Hz, Trp), 7.33 (d, 1H, $J^3 = 7.5$ Hz, Trp), 7.25 (s, 2H, Trp), 7.16 (s, 2H, Trp), 7.05 (m, 2H, Trp), 6.98 (t, 1H, $J^3 = 7.5$ Hz, Trp), 6.93 (t, 1H, $J^3 = 7.5$ Hz, Trp), 4.74 (s, 9H, CH₃ porphyrin), 4.60 (m, 1H, α -CH, Trp), 4.55-4.45 (m, 3H, α -CH, Trp and hexyl), 4.39 (m, 1H, α -C, Arg), 4.28 (m, 1H, α -C, Arg), 3.23-2.97 (m, 8H, β -CH, Trp

and CH₂-N side chain, Arg), 2.17 (m, 2H, hexyl), 1.98 (m, 2H, hexyl), 1.72 (m, 1H, β -CH, Arg), 1.66 (m, 1H, β -CH, Arg), 1.66-1.39 (8H, hexyl, CH₂ side chain and β -CH, Arg), 1.35 ppm (m, 2H, hexyl); ¹³C-NMR (176 MHz, DMSO) δ 173.1 (C=O, Trp), 172.5 (C=O, hexyl), 171.5 (C=O, Trp), 171.3 (C=O, Arg), 171.2 (C=O, Arg), 158.4 (q, $J^2 = 31.7$ Hz, C=O, TFA), 158.2 (quart. C, pyridyl), 156.93 (quart. C, guanidine Arg), 156.91 (quart. C, guanidine Arg), 150.2 (α -C, porphyrin), 148.4 (α -C, porphyrin), 148.2 (α -C, porphyrin), 147.9 (α -C, porphyrin), 146.1 (quart. C, triazole), 143.77 (pyridyl), 143.73 (pyridyl), 141.1 (quart. C, phenyl porphyrin), 136.09 (quart. C, Trp), 136.05 (quart. C, Trp), 134.8 (phenyl porphyrin), 133.5 (β -C, porphyrin), 132.5 (β -C, porphyrin), 132.3 (pyridyl), 131.8 (β -C, porphyrin), 130.6 (quart. C, phenyl porphyrin), 127.4 (quart. C, Trp), 127.3 (quart. C, Trp), 123.71 (Trp), 123.66 (Trp), 123.61 (phenyl porphyrin), 123.1 (quart. C, meso porphyrin), 121.9 (triazole), 120.9 (Trp), 120.8 (Trp), 118.5 (Trp), 118.4 (Trp), 118.20 (Trp), 118.18 (Trp), 117.1 (q, $J^1 = 298.7$ Hz, CF₃ TFA), 115.7 (quart. C, meso porphyrin), 114.9 (quart. C, meso porphyrin), 111.4 (Trp), 111.2 (Trp), 109.8 (quart. C, Trp), 109.5 (quart. C, Trp), 53.2 (α -C, Trp), 53.1 (α -C, Trp), 52.2 (α -C, Arg), 52.1 (α -C, Arg), 49.6 (hexyl), 47.7 (CH₃, porphyrin), 40.5 (CH₂-N, Arg), 40.4 (CH₂-N, Arg), 35.0 (hexyl), 29.6 (hexyl), 29.4 (β -C, Arg), 28.9 (β -C, Arg), 27.6 (β -C, Trp), 27.1 (β -C, Trp), 25.6 (hexyl), 25.1 (CH₂, side chain Arg), 24.9 (CH₂, side chain Arg), 24.7 (hexyl); UV-vis (H₂O) λ_{abs} 220, 258, 290, 319, 442, 568, 614 nm; HRMS (ESI) obsd. 529.8873, calcd. 529.8870 (C₈₆H₈₉N₂₂O₆Zn, [M]³⁺).



Conjugate (MePy)₃PZn-hexLKLK-OH 3.17.

The Click reaction was complete after 12 h. The solution was filtered (syringe filter 0.2 μm) and the porphyrin was precipitated by addition of diethyl ether. The side chain protected product was purified by HPLC. HPLC purification: Solvent A (water with 0.01% TFA), solvent B (MeCN), flow 4 mL/min, retention time: 9.7 minutes.

Table 3.20: RP-HPLC conditions for **3.17-prot.**

Time (min)	% A	% B
0	80	20
1	70	30
10	60	40
12	50	50
13	80	20

The side chain protected porphyrin conjugate was carefully deprotected with TFA:H₂O:TIS 95:2.5:2.5 in the dark and under argon. The conjugate was precipitated by addition of cold diethyl ether. 1.5 eq Zn(OAc)₂ in MeOH were added and the mixture was stirred at 60 °C for

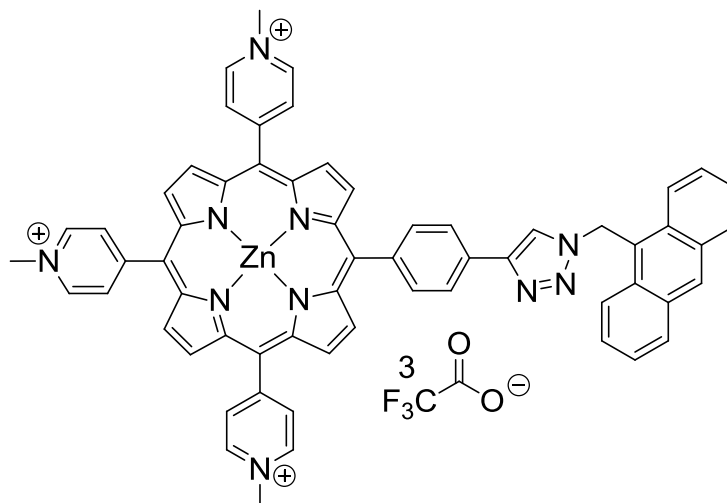
2 h. The solvent was removed and the crude porphyrin was dissolved in degassed water containing 1mg/mL EDTA and kept in the dark before being purified by HPLC. Porphyrin **3.17** was isolated in 74% overall yield. HPLC purification: Solvent A (water with 0.01% TFA), solvent B (MeCN), flow 4 mL/min, retention time: 11.6 minutes.

Table 3.21: RP-HPLC conditions for **3.17**.

Time (min)	% A	% B
0	95	5
1	85	15
12	70	30
14	50	50
15	50	50

¹H-NMR (500 MHz, DMSO) δ 9.47 (d, 6H, $J^3 = 6.5$ Hz, pyridyl), 9.08 (m, 4H, pyridyl), 9.03 (d, 2H, $J^3 = 4.5$ Hz, β -pyrrole), 9.00 (d, 2H, $J^3 = 4.5$ Hz, β -pyrrole), 8.95-8.91 (m, 7H, pyridyl and triazole), 8.33 (d, 2H, $J^3 = 8.3$ Hz, phenyl, porphyrin), 8.28 (d, 2H, $J^3 = 8.3$ Hz, phenyl, porphyrin), 8.14-8.06 (m, 3H, NH backbone, Lys, Leu, Lys), 7.92 (br s, NH₂, Lys), 7.87 (d, NH, $J^3 = 8.0$ Hz, Lys), 4.744 (s, 3H, CH₃, porphyrin), 4.735 (s, 6H, CH₃, porphyrin), 4.54 (hexyl), 4.32 (m, 2H, α -CH, Leu), 4.26 (m, 1H, α -CH, Lys), 4.16 (m, 2H, α -CH, Lys), 2.78 (m, 4H, CH₂-N, side chain, Lys), 2.21 (m, 2H, hexyl), 2.00 (m, 2H, hexyl), 1.7.9-1.4. (m, 18H, several signals overlapping; CH, Leu and β -CH, Lys and β -CH, Leu and 2x hexyl and CH₂ side chain, Lys), 1.36 (m, 6H, CH₂ side chain, Lys and hexyl), 0.90 ppm (m, 12H, CH₃, Leu); ¹³C-NMR (125 MHz, DMSO) δ 173.3 (C=O, Lys), 172.5 (C=O, Leu), 172.3 (C=O, hexyl), 172.0 (C=O, Leu), 171.2 (C=O, Lys), 158.2 (quart. C, pyridyl), 158.1 (q, $J^2 = 31.2$ Hz,

C=O, TFA), 150.2 (α -C, porphyrin), 148.4 (α -C, porphyrin), 148.2 (α -C, porphyrin), 147.9 (α -C, porphyrin), 146.1 (quart. C, triazole), 143.8 (pyridyl), 141.1 (quart. C, phenyl, porphyrin), 134.8 (phenyl, porphyrin), 133.4 (β -C, porphyrin), 132.5 (β -C, porphyrin), 132.3 (β -C, porphyrin), 132.1 (pyridyl), 131.8 (β -C, porphyrin), 130.6 (quart. C, phenyl porphyrin), 123.6 (phenyl, porphyrin), 123.1 (quart. C, meso, porphyrin), 121.9 (triazole), 117.2 (q, $J^I=$ 299.7 Hz, CH₃, TFA), 115.7 (quart. C, meso, porphyrin), 114.9 (quart. C, meso, porphyrin), 52.2 (α -C, Lys), 51.7 (α -C, Lys), 51.2 (α -C, Leu), 50.8 (α -C, Leu), 49.6 (hexyl), 47.7 (CH₃, porphyrin), 40.3 (β -C, Leu), 40.1 (β -C, Leu), 38.7 (CH₂-NH₂, Lys), 38.6 (CH₂-NH₂, Lys), 35.0 (hexyl), 30.9 (β -C, Lys), 30.4 (β -C, Lys), 26.6 (CH₂-CH₂-NH₂, Lys), 25.6 (hexyl), 24.8 (hexyl), 24.4 (CH, Leu), 24.0 (CH, Leu), 23.2 (CH₃, Leu), 23.1 (CH₃, Leu), 22.4 (side chain, Lys), 22.2 (side chain, Lys), 21.53 (CH₃, Leu), 21.52 ppm (CH₃, Leu); UV-vis (H₂O, ϵ) λ_{abs} 253, 320, 436, 563, 609 nm; HRMS (ESI) obsd. 462.5515, calcd. 432.5528. (C₇₆H₉₁N₁₆O₆Zn, [M]³⁺).



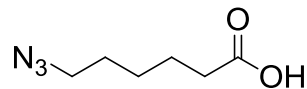
Conjugate (MePy)₃PZn-anthracene 3.19.

The 9-azidomethylantracene was synthesized according to literature procedure by Dr. H. Sadeghifar (Department of Forest Biomaterials).¹²⁴ The Click reaction was complete after 12 h. The solution was filtered (syringe filter 0.2 μm) and the porphyrin was precipitated by addition of diethyl ether. The product was purified by HPLC. The reaction yielded 86% of porphyrin **3.19**. HPLC purification: Solvent A (water with 0.01% TFA), solvent B (MeCN), flow 4 mL/min, retention time: 9.9 minutes.

Table 3.22: RP-HPLC conditions for **3.19**.

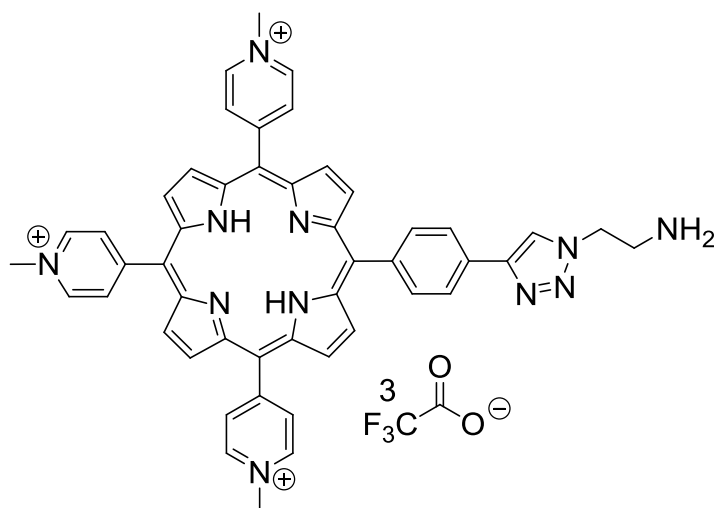
Time (min)	% A	% B
0	80	20
1	75	25
8	60	40
9	5	95
12	5	95

$^1\text{H-NMR}$ (700 MHz, DMSO) δ 9.45 (m, 6H, pyridyl), 9.04 (m, 4H, β -pyrrole), 8.95 (d, 2H, $J^3 = 4.2$ Hz, β -pyrrole) 8.93 (d, 2H, $J^3 = 4.2$ Hz, β -pyrrole), 8.90 (m, 6H, pyridyl), 8.30 (triazole), 8.74 (m, 3H, anthracene), 8.24 (m, 4H, phenyl, porphyrin and anthracene), 8.18 (d, 2H, $J^3 = 7.7$ Hz, phenyl, porphyrin), 7.75 (m, 2H, anthracene), 7.66 (m, 2H, anthracene), 6.85 (s, 2H, CH_2), 4.72 (s, 3H, CH_3 , porphyrin), 4.71 ppm (s, 3H, CH_3 , porphyrin); $^{13}\text{C-NMR}$ (176 MHz, DMSO) δ 157.7 (quat. C, pyridyl), 157.5 (q, $J^2 = 29.9$ Hz, C=O, TFA), 150.2 (α -C, porphyrin), 148.3 (α -C, porphyrin), 148.2 (α -C, porphyrin), 147.8 (α -C, porphyrin), 146.1 (quat. C, triazole), 143.71 (pyridyl), 143.67 (pyridyl), 141.1 (quat. C, phenyl porphyrin), 134.6 (phenyl porphyrin), 133.4 (β -C, porphyrin), 132.5 (β -C, porphyrin), 132.2 (β -C, porphyrin), 132.1 (β -C, porphyrin), 132.0 (pyridyl), 131.7 (β -C, porphyrin), 131.2 (quat. C, anthracene), 130.5 (quat. C, anthracene), 132.2 (quat. C, phenyl), 129.2 (triazole and anthracene), 127.2 (anthracene), 125.7 (quat. C, anthracene), 125.4 (anthracene), 124.1 (anthracene), 123.7 (phenyl, porphyrin), 123.0 (quat. C, meso porphyrin), 121.7 (anthracene), 115.5 (q, $J^1 = 299.3$ Hz, CF_3 , TFA) 115.6 (quat. C, meso porphyrin), 114.8 (quat. C, meso porphyrin), 47.7 (CH_3 , porphyrin), 46.0 ppm (CH_2); UV-vis (H_2O , ϵ) λ_{abs} 254, 323, 371, 393, 442, 567, 611 nm; HRMS (ESI) obsd. 327.1025, calcd. 327.1035 ($\text{C}_{61}\text{H}_{45}\text{N}_{10}\text{Zn}$, $[\text{M}]^{3+}$).



6-azidohexanoic acid **3.13**.

3.13 was synthesized according to literature procedure.¹⁰⁸ 1.8 g (9.2mmol) 6-bromohexanoic acid and 1.2 g (18.5 mmol) sodium azide were suspended in 15 mL dry DMF. The mixture was heated to 85 °C for 3 hours, then let cool to 40 °C. Stirring was continued over night. The reaction mixture was diluted with DCM and extracted with 0.1 M HCl. The organic phase was then washed with brine and dried over anhydrous sodium sulfate. The solvent was removed under reduced pressure. 1.4 mg (97%) of 6 azidohexanoic acid were obtained as a clear oil. ¹H-NMR (300 MHz, CDCl₃) δ 3.28 (t, 2H, $J^3 = 6.7$ Hz), 2.38 (t, 2H, $J^3 = 7.5$ Hz), 1.72-1.57 (m, 4H), 1.48-1.39 ppm (m, 2H).



5-(4-(4-(1-(2-Aminoethyl))-1,2,3-triazolyl)phenyl)-10,15,20-tris-(4-methylpyridin-4-ium-1-yl)porphyrin tris(trifluoroacetate) **3.18**.

3.1 and *tert*-butyl-(2-azidoethyl)carbamate were reacted under Click conditions as described in the general procedure. **Boc-3.18** was precipitated from the reaction mixture by addition of diethylether and dried under vacuum. The porphyrin was then deprotected by addition of TFA/DCM 3:1 for 3 hours. Reaction progress was monitored by HPLC. The crude product was precipitated and washed with diethylether. **3.18** was suspended in water containing 1 mg/mL EDTA and purified by HPLC. The product was isolated with 50% yield. HPLC purification: Solvent A (water with 0.01% TFA), solvent B (MeOH), flow 4 mL/min, retention time: 10.7 minutes.

Table 3.23: RP-HPLC conditions for **3.18**.

Time (min)	% A	% B
0	95	5
2	75	25
20	60	40
22	20	80
25	20	80

$^1\text{H-NMR}$ (700 MHz, DMSO) δ 9.51 (m, 6H, pyridyl), 9.17 (br s, 4H, β -pyrrole, porphyrin), 9.09 (br s, 4H, β -pyrrole, porphyrin), 9.02 (m, 6H, pyridyl), 8.99 (s, 1H, triazole), 8.36 (m, 4H, phenyl, porphyrin), 4.85 (m, 2H, $\text{CH}_2\text{-NH}_2$, linker), 4.75 (s, 3H, CH_3 , porphyrin), 4.74 ppm (s, 6H, CH_3 , porphyrin); $^{13}\text{C-NMR}$ (176 MHz, DMSO) δ 158.0 (q, $J^2 = 31.7$ Hz, C=O, TFA), 156.6 (quart. C, pyridyl), 156.5 (quart. C, pyridyl), 146.3 (quart. C, triazole), 144.2 (pyridyl), 139.8 (quart. C, phenyl, porphyrin), 135.0 (phenyl, porphyrin), 132.11 (pyridyl), 134.0-130.0 (very br, β -C, porphyrin), 130.9 (quart. C, phenyl, porphyrin), 124.0 (phenyl, porphyrin), 122.9 (triazole), 122.5 (quart. C, meso, porphyrin), 117.0 (q, $J^1 = 298.7$ Hz, CF_3 , TFA), 115.4 (quart. C, meso, porphyrin), 47.8 (CH_3 , porphyrin), 47.3 ($\text{CH}_2\text{-N}$, linker), 38.6 ppm (linker), peaks for α -C are broadened due to NH tautomerism; 121 UV-vis (H_2O) λ_{abs} 257, 424, 520, 556, 588, 643 nm; HRMS (ESI) obsd. 257.4535, calcd. 257.4536 ($\text{C}_{48}\text{H}_{42}\text{N}_{11}$, $[\text{M}]^{3+}$).

X-ray crystallography.

Single crystal growth conditions. 1 mg porphyrin were dissolved in 0.5 mL MeOH in a 1.7 mL glass vial placed inside a scintillation vial filled with chloroform. The chloroform was allowed to diffuse into the methanol solution for 3 weeks yielding plate like crystals.

Data Collection and Processing. A crystal of **3.1** was selected and mounted on a Mitegen polyimide micromount with a small amount of HO-125 fluorocarbon oil. All X-ray measurements were made on a Bruker-Nonius Kappa Axis X8 Apex2 diffractometer at a temperature of 110 K. The unit cell dimensions were determined from a symmetry constrained fit of 9876 reflections with $5.08^\circ < 2\theta < 63.4^\circ$. The data collection strategy was a number of ω and ϕ scans which collected data up to 78.48° (2θ). The frame integration was performed using SAINT (Bruker-Nonius, SAINT version 2009.9, 2009, Bruker-Nonius, Madison, WI 53711, USA). The resulting raw data was scaled and absorption corrected using a multi-scan averaging of symmetry equivalent data using SADABS (Bruker-Nonius, SADABS version 2009.9, 2009, Bruker-Nonius, Madison, WI 53711, USA).

Structure Solution and Refinement. The structure was solved by direct methods using the SIR92 program.¹²⁵ All non-hydrogen atoms were obtained from the initial solution. The hydrogen atoms were introduced at idealized positions and were allowed to ride on the parent atom. Several disorders were evident in the structure. These included the pyridinium ring bound to the C10 meso carbon, 2 of the 3 iodide anions were disordered, several chloroform molecules and a fractionally occupied methanol molecule all were disordered. See Appendix for more details. The structural model was fit to the data using full matrix least-squares based on F2. The calculated structure factors included corrections for anomalous dispersion from

the usual tabulation. The structure was refined using the XL program from SHELXTL (Bruker-AXS, XL version 2009.9, 2009, Bruker-AXS, Madison, WI 53711, USA), graphic plots were produced using the NRCVAX crystallographic program suite. Additional information and other relevant literature references can be found in the reference section of the Facility's Web page (<http://www.xray.ncsu.edu>).

Experimental Methods - Biology

Materials and Instrumentation. Buffer salts were purchased from Fisher Scientific, Middlebrook 7H9 Agar and 7H10 broth from BD Difco, and LB broth Miller from EMD Chemicals. Unless otherwise specified, all other chemicals were obtained from commercial sources in the highest purity available. Ultra pure water used for all media and buffers was provided by an Easypure II system (Barnstead). Optical density measurements were performed on a Genesys 10 uv scanning UV-vis Instrument from Thermo Electron Corp. All procedures were carried out under commonly practiced sterile techniques. The photosensitizer 5,10,15,20-tetrakis(1-methyl-4-pyridinyl)porphyrin tetratosylate **2.1**, was obtained from Frontier Scientific (USA) and used without further purification. Stock solutions of the photosensitizers at a concentration of 0.1 mmol/L in ultrapure water were prepared and stored in the dark at -80 °C.

Bacterial strains and growth conditions. The bacterial strain *Mycobacterium smegmatis* mc² 155, kindly donated by Prof. William Jacobs (Albert Einstein College of Medicine, USA), was used in this study. *M. smegmatis* was grown in 5 mL cultures in

Middlebrook 7H9 media with ADS and with 100 µg/mL cycloheximide as the antibiotic.¹²⁶ The cells were incubated at 37 °C on an orbital shaker (400 rpm) until an optical density (OD₆₀₀) of 0.65-0.70 at 600 nm corresponding to a concentration of 10⁸ CFU/mL was reached.

Incubation of cells with photosensitizer. The 5 mL culture with a concentration of 1-2·10⁸ CFU/mL was pelleted by centrifugation (10 min, 3716 x g) at room temperature, the supernatant discarded, and the cells were resuspended in a total volume of 5 mL PBS-Tween (170 mM NaCl, 3.4 mM KCl, 10.0 mM Na₂HPO₄, 1.8 mM KH₂PO₄, pH 7.2 with additional 0.05 % Tween 80) and the appropriate volume of the photosensitizer stock solution. The cells were incubated for 5 minutes in the dark at 37 °C under agitation.

Illumination of cells. All photosensitization experiments were performed using a noncoherent light source, PDT light model LC122 (LumaCare, USA), and the fluence rate was measured with an Orion power meter (Orphir Optronics Ltd., Israel). 1 mL aliquots of the cell suspension in PBS were added to a sterile 24 well plate (BD Falcon, flat bottom) and illuminated with visible light (400-700 nm) with a fluence rate of 60 mW/cm² for the duration of 5, 15 or 30 minutes (corresponding to fluences of 18, 54, 108 J/cm²) while magnetically stirred. After illumination an aliquot was used for viability assays. All experiments were conducted in triplicate at a minimum.

Cell survival assay. 100 µL from the illuminated cell suspension was 1:10 serially diluted six times and plated on square plates (Middlebrook 7H10-ADS solid media) as described by Jett and coworkers.¹²⁷ The plates were incubated at 37 °C in the dark for 48-60 hours. The survival rate was determined from the ratio of CFU/mL of the illuminated

solution and the dark control. Due to the plating technique employed, a maximum of a 6 log unit change in CFU corresponding to ≥ 100 CFU/mL survival could be detected for an initial concentration of $1 \cdot 10^8$ CFU/mL. Unavoidable variations in the bacterial concentration of individual samples from starter cultures ($1\text{-}3 \cdot 10^8$ CFU/mL) resulted in a variation of the detection limit spanning the region of 0.0001-0.00001% survival (Figures 3.13, shaded areas). Survival rates of $< 0.00001\%$ could not be detected. Samples with the photosensitizer present but kept in the dark (dark control) and illuminated samples without the photosensitizer present (light control) served as controls. Statistical significance was assessed via a two-tailed, unpaired Student's t-test.

Photostability assays. 1 mL samples of 5 μM solutions of the respective PS in PBS-Tween (0.05% Tween-80) buffer were illuminated with white light from a PDT light model LC122 (LumaCare, USA) [400-700 nm and 60 mW/cm^2] in a 24-well plate while magnetically stirred. After 5, 15 and 30 minutes, 80 μL aliquots were removed and analyzed by UV-visible spectroscopy. The % change in the Soret band absorption was determined from quotients of the illuminated sample and the dark control. Experiments were done in duplicate at a minimum.

Hemolysis assays. The hemolytic activity of the porphyrin compounds and select antimicrobial peptides was assayed using fresh, defibrinated sheep blood (Hemostat Laboratories, USA). The washed red blood cells were diluted 10-fold into PBS buffer (HyClone, Thermo Scientific, pH 7.2, 6.7 mM phosphate). Diluted blood samples were incubated with varying concentrations of porphyrins or antimicrobial peptides (250 or 500 μL total volume) for 1 hour at 37 $^\circ\text{C}$ under agitation, followed by centrifugation at 9600 x g

for 10 minutes. 100 μL of the supernatant of each sample was diluted into 700 μL of PBS buffer and the UV-visible absorbance was measured at 540 nm relative to a blank sample containing an equivalent concentration of the respective porphyrin. 0% hemolysis was determined by incubation of red blood cells with PBS buffer only, and 100% lysis was obtained by treatment with 1% Triton-X. Experiments were done in duplicate at a minimum.

Broth microdilution for MIC determination. *M. smegmatis* was grown overnight in Mueller-Hinton broth and diluted to a concentration of $5 \cdot 10^5$ CFU/mL. Triplicate samples containing bacteria in Mueller-Hinton broth and 256 $\mu\text{g/mL}$ of the porphyrin or AMP in question were prepared, and two wells of a 96-well microtiter plate were filled with 200 μL for each sample. The remaining rows of wells were filled with 100 μL of broth containing $5 \cdot 10^5$ CFU/mL *M. smegmatis*. With a multichannel pipettor, 100 μL was withdrawn from the first row of wells containing 256 $\mu\text{g/mL}$ of the compound to be tested and mixed 4 times with the broth in the second row. Such dilution steps (continued with dilution from the second row to the third row) were continued across the entire plate. The plate was covered and incubated in a plastic sealed container for 3 days at 37 $^{\circ}\text{C}$ in the dark, before the MIC values were determined from the wells that did not show any growth of bacteria. Controls did not contain porphyrin or AMPs.

Acknowledgements

We would like to thank Dr. Paul Boyle for solving the crystal structure of compound **3.1**. The authors also wish to thank the Department of Chemistry of North Carolina State

University and the State of North Carolina for funding the purchase of the Apex2 diffractometer. Mass spectra were obtained at the NCSU Department of Chemistry Mass Spectrometry Facility. Funding was obtained from the North Carolina Biotechnology Center and the NCSU Department of Chemistry.

REFERENCES

1. Stables, G. I.; Ash, D. V., Photodynamic therapy. *Cancer Treatment Reviews* **1995**, 21, (4), 311.
2. Ochsner, M., Photophysical and photobiological processes in the photodynamic therapy of tumours. *Journal of Photochemistry and Photobiology B: Biology* **1997**, 39, (1), 1.
3. Hamblin, M. R.; Hasan, T., Photodynamic therapy: a new antimicrobial approach to infectious disease? *Photochemical & Photobiological Sciences* **2004**, 3, (5), 436.
4. Jori, G.; Brown, S. B., Photosensitized inactivation of microorganisms. *Photochemical & Photobiological Sciences* **2004**, 3, (5), 403.
5. O'Riordan, K.; Akilov, O. E.; Hasan, T., The potential for photodynamic therapy in the treatment of localized infections. *Photodiagnosis and Photodynamic Therapy* **2005**, 2, (4), 247.
6. Wainwright, M., Photodynamic antimicrobial chemotherapy (PACT). *Journal of Antimicrobial Chemotherapy* **1998**, 42, (1), 13-28.
7. Jori, G., Inactivation of Pathogenic Microorganisms by Photodynamic Techniques: Mechanistic Aspects and Perspective Applications. *Anti-Infective Agents in Medicinal Chemistry* **2007**, 6, (2), 119.
8. Macdonald, I. J.; Dougherty, T. J., Basic principles of photodynamic therapy. *Journal of Porphyrins and Phthalocyanines* **2001**, 5, 105-129.
9. Maisch, T., Revitalizes Strategies Against Multidrug-Resistant bacteria: Anti-microbial Photodynamic Therapy and Bacteriophage Therapy. *Anti-Infective Agents in Medicinal Chemistry* **2007**, 6, (2), 145.
10. World Health Organization, *Anti-Tuberculosis Drug Resistance in the World Report No. 4*. The WHO/IUALTD Global project on anti-tuberculosis drug resistance surveillance: Geneva, 2008.
11. Feese, E.; Ghiladi, R. A., Highly efficient in vitro photodynamic inactivation of *Mycobacterium smegmatis*. *Journal of Antimicrobial Chemotherapy* **2009**, 64, (4), 782.
12. Hudson, R.; Boyle, R. W., Strategies for selective delivery of photodynamic sensitizers to biological targets. *Journal of Porphyrins and Phthalocyanines* **2004**, 8, 954.

13. Hamblin, M. R., Covalent photosensitizer conjugates for targeted photodynamic therapy. *Trends in Photochemistry & Photobiology* **2002**, 9, 1.
14. Yarmush, M. L.; Thorpe, W. P.; Strong, L.; Rakestraw, S. L.; Toner, M.; Tompkins, R. G., Antibody Targeted Photolysis. *Critical Reviews in Therapeutic Drug Carrier Systems* **1993**, 10, (3), 197.
15. Bhatti, M.; MacRobert, A.; Henderson, B.; Shepherd, P.; Cridland, J.; Wilson, M., Antibody-Targeted Lethal Photosensitization of *Porphyromonas gingivalis*. *Antimicrobial Agents and Chemotherapy* **2000**, 44, (10), 2615.
16. Hamblin, M. R.; Bamberg, M. P.; Miller, J. L.; Hasan, T., Cationic Photoimmunoconjugates Between Monoclonal Antibodies and Hematoporphyrin: Selective Photodestruction of Ovarian Cancer Cells. *Applied Optics* **1998**, 37, (31), 7184.
17. Hamblin, M. R.; Miller, J. L.; Hasan, T., Effect of Charge on the Interaction of Site-specific Photoimmunoconjugates with Human Ovarian Cancer Cells. *Cancer Research* **1996**, 56, (22), 5205.
18. Duncan, R.; Spreafico, F., Polymer Conjugates: Pharmacokinetic Considerations for Design and Development. *Clinical Pharmacokinetics* **1994**, 27, (4), 290.
19. Hamblin, M. R.; Miller, J. L.; Rizvi, I.; Ortel, B.; Maytin, E. V.; Hasan, T., Pegylation of a Chlorin e6 Polymer Conjugate Increases Tumor Targeting of Photosensitizer. *Cancer Research* **2001**, 61, (19), 7155.
20. Jori, G.; Reddi, E., The role of lipoproteins in the delivery of tumour-targeting photosensitizers. *International Journal of Biochemistry* **1993**, 25, (10), 1369.
21. James, D. A.; Swamy, N.; Paz, N.; Hanson, R. N.; Ray, R., Synthesis and estrogen receptor binding affinity of a porphyrin-estradiol conjugate for targeted photodynamic therapy of cancer. *Bioorganic & Medicinal Chemistry Letters* **1999**, 9, (16), 2379.
22. Swamy, N.; James, D. A.; Mohr, S. C.; Hanson, R. N.; Ray, R., An estradiol-Porphyrin conjugate selectively localizes into estrogen receptor-Positive breast cancer cells. *Bioorganic & Medicinal Chemistry* **2002**, 10, (10), 3237.
23. Gijssens, A.; Witte, P. D., Photocytotoxic action of EGF-PVA-Sn(IV)chlorin e6 and EGF-dextran-Sn(IV)chlorin e6 internalizable conjugates on A431 cells. *International Journal of Oncology* **1998**, 13, (6), 1171.
24. Hekrnreiter, M.; Kagan, J.; Chen, X.; Lau, K. Y.; D'Auria, M.; Vantaggi, A., Phototoxicity of (1*H*-indenyl)thiophenes. *Photochemistry and Photobiology* **1993**, 58, (1), 49.

25. Akhlynina, T. V.; Rosenkranz, A. A.; Jans, D. A.; Sobolev, A. S., Insulin-mediated Intracellular Targeting Enhances the Photodynamic Activity of Chlorin e6. *Cancer Research* **1995**, 55, (5), 1014.
26. Akhlynina, T. V.; Jans, D. A.; Rosenkranz, A. A.; Statsyuk, N. V.; Balashova, I. Y.; Toth, G.; Pavo, I.; Rubin, A. B.; Sobolev, A. S., Nuclear Targeting of Chlorin e6 Enhances Its Photosensitizing Activity. *Journal of Biological Chemistry* **1997**, 272, (33), 20328.
27. Akhlynina, T. V.; Jans, D. A.; Statsyuk, N. V.; Balashova, I. Y.; Toth, G.; Pavo, I.; Rosenkranz, A. A.; Naroditsky, B. S.; Sobolev, A. S., Adenoviruses synergize with nuclear localization signals to enhance nuclear delivery and photodynamic action of internalizable conjugates containing chlorin e6. *International Journal of Cancer* **1999**, 81, (5), 734.
28. Wellhoner, H. H.; Neville, D. M.; Srinivasachar, K.; Erdmann, G., Uptake and concentration of bioactive macromolecules by K562 cells via the transferrin cycle utilizing an acid-labile transferrin conjugate. *Journal of Biological Chemistry* **1991**, 266, (7), 4309.
29. Hamblin, M. R.; Newman, E. L., Photosensitizer targeting in photodynamic therapy I. Conjugates of haematoporphyrin with albumin and transferrin. *Journal of Photochemistry and Photobiology B: Biology* **1994**, 26, (1), 45.
30. Chen, X.; Hui, L.; Foster, D. A.; Drain, C. M., Efficient Synthesis and Photodynamic Activity of Porphyrin-Saccharide Conjugates: Targeting and Incapacitating Cancer Cells. *Biochemistry* **2004**, 43, (34), 10918.
31. Hamblin, M. R.; Miller, J. L.; Ortel, B., Scavenger-Receptor Targeted Photodynamic Therapy. *Photochemistry and Photobiology* **2000**, 72, (4), 533.
32. Embleton, M. L.; Nair, S. P.; Heywood, W.; Menon, D. C.; Cookson, B. D.; Wilson, M., Development of a Novel Targeting System for Lethal Photosensitization of Antibiotic-Resistant Strains of Staphylococcus aureus. *Antimicrobial Agents and Chemotherapy* **2005**, 49, (9), 3690
33. Berthiaume, F.; Reiken, S. R.; Toner, M.; Tompkins, R. G.; Yarmush, M. L., Antibody-targeted photolysis of bacteria in vivo. *Biotechnology (NY)* **1994**, 12, (7), 703.
34. Gross, S.; Brandis, A.; Chen, L.; Rosenbach-Belkin, V.; Roehrs, S.; Scherz, A.; Salomon, Y., Protein-A-mediated Targeting of Bacteriochlorophyll-IgG to Staphylococcus aureus: A Model for Enhanced Site-Specific Photocytotoxicity. *Photochemistry and Photobiology* **1997**, 66, (6), 872.
35. Embleton, M. L.; Nair, S. P.; Cookson, B. D.; Wilson, M., Selective lethal photosensitization of methicillin-resistant Staphylococcus aureus using an IgG-tin (IV) chlorin e6 conjugate. *Journal of Antimicrobial Chemotherapy* **2002**, 50, (6), 857.

36. Rovaldi, C. R.; Pievsky, A.; Sole, N. A.; Friden, P. M.; Rothstein, D. M.; Spacciapoli, P., Photoactive Porphyrin Derivative with Broad-Spectrum Activity against Oral Pathogens In Vitro. *Antimicrobial Agents and Chemotherapy* **2000**, 44, (12), 3364.
37. Polo, L.; Segalla, A.; Bertoloni, G.; Jori, G.; Schaffner, K.; Reddi, E., Polylysine-porphycene conjugates as efficient photosensitizers for the inactivation of microbial pathogens. *Journal of Photochemistry and Photobiology B: Biology* **2000**, 59, (1-3), 152.
38. Lauro, F. M.; Pretto, P.; Covolo, L.; Jori, G.; Bertoloni, G., Photoinactivation of bacterial strains involved in periodontal diseases sensitized by porphycene-polylysine conjugates. *Photochemical & Photobiological Sciences* **2002**, 1, (7), 468.
39. Hamblin, M. R.; O'Donnell, D. A.; Murthy, N.; Rajagopalan, K.; Michaud, N.; Sherwood, M. E.; Hasan, T., Polycationic photosensitizer conjugates: effects of chain length and Gram classification on the photodynamic inactivation of bacteria. *Journal of Antimicrobial Chemotherapy* **2002**, 49, (6), 941.
40. Gad, F.; Zahra, T.; Hasan, T.; Hamblin, M. R., Effects of Growth Phase and Extracellular Slime on Photodynamic Inactivation of Gram-Positive Pathogenic Bacteria. *Antimicrobial Agents and Chemotherapy* **2004**, 48, (6), 2173.
41. Bourre, L.; Giuntini, F.; Eggleston, I. M.; Mosse, C. A.; MacRobert, A. J.; Wilson, M., Effective photoinactivation of Gram-positive and Gram-negative bacterial strains using an HIV-1 Tat peptide-porphyrin conjugate. *Photochemical & Photobiological Sciences* **2010**, 9, (12), 1613.
42. Zheng, X.; Sallum, U.; Verma, S.; Athar, H.; Evans, C.; Hasan, T., Exploiting a Bacterial Drug-Resistance Mechanism: A Light-Activated Construct for the Destruction of MRSA. *Angewandte Chemie International Edition* **2009**, 48, (12), 2148.
43. Soukos, N. S.; Hamblin, M. R.; Hasan, T., The Effect of Charge on Cellular Uptake and Phototoxicity of Polylysine Chlorin(e6)-Conjugates. *Photochemistry and Photobiology* **1997**, 65, (4), 723.
44. Gad, F.; Zahra, T.; Francis, K. P.; Hasan, T.; Hamblin, M. R., Targeted photodynamic therapy of established soft-tissue infections in mice. *Photochemical & Photobiological Sciences* **2004**, 3, (5), 451.
45. Hamblin, M. R.; Zahra, T.; Contag, C. H.; McManus, A. T.; Hasan, T., Optical Monitoring and Treatment of Potentially Lethal Wound Infections In Vivo. *Journal of Infectious Diseases* **2003**, 187, (11), 1717.
46. Hamblin, M. R.; O'Donnell, D. A.; Murthy, N.; Contag, C. H.; Hasan, T., Rapid Control of Wound Infections by Targeted Photodynamic Therapy Monitored by In Vivo Bioluminescence Imaging. *Photochemistry and Photobiology* **2002**, 75, (1), 51.

47. Tome, J. P. C.; Neves, M. G. P. M. S.; Tome, A. C.; Cavaleiro, J. A. S.; Soncin, M.; Magaraggia, M.; Ferro, S.; Jori, G., Synthesis and Antibacterial Activity of New Poly-S-lysine-Porphyrin Conjugates. *Journal of Medicinal Chemistry* **2004**, 47, (26), 6649.
48. Wang, Z.; Wang, G., APD: the Antimicrobial Peptide Database. *Nucleic Acids Research* **2004**, 32, D590.
49. Wang, G., *Antimicrobial Peptides: Discovery, Design and Novel Therapeutic Strategies*. Wallingford: Oxfordshire, 2010.
50. Boman, H. G., Peptide Antibiotics and their Role in Innate Immunity. *Annual Review of Immunology* **1995**, 13, (1), 61.
51. Zasloff, M., Antimicrobial peptides of multicellular organisms. *Nature* **2002**, 415, (6870), 389.
52. Steiner, H.; Hultmark, D.; Engstrom, A.; Bennich, H.; Boman, H. G., Sequence and specificity of two antibacterial proteins involved in insect immunity. *Nature* **1981**, 292, (5820), 246.
53. Zasloff, M., Magainins, a class of antimicrobial peptides from *Xenopus* skin: isolation, characterization of two active forms, and partial cDNA sequence of a precursor. *Proceedings of the National Academy of Sciences of the United States of America* **1987**, 84, (15), 5449.
54. Tossi, A.; Mitaritonna, N.; Tarantino, C.; Giangaspero, A.; Sandri, L.; Winterstein, K., Antimicrobial Database; <http://www.bbcm.units.it/~tossi/pag1.htm>. In Universitaet Trieste.
55. Andersen, J. H.; Jenssen, H.; Sandvik, K.; Gutteberg, T. J., Anti-HSV activity of lactoferrin and lactoferricin is dependent on the presence of heparan sulphate at the cell surface. *Journal of Medical Virology* **2004**, 74, (2), 262.
56. De Lucca, A. J.; Walsh, T. J., Antifungal Peptides: Novel Therapeutic Compounds against Emerging Pathogens. *Antimicrobial Agents and Chemotherapy* **1999**, 43, (1), 1-11.
57. Theis, T.; Stahl, U., Antifungal proteins: targets, mechanisms and prospective applications. *Cellular and Molecular Life Sciences* **2004**, 61, (4), 437.
58. Papo, N.; Shai, Y., Host defense peptides as new weapons in cancer treatment. *Cellular and Molecular Life Sciences* **2005**, 62, (7), 784.
59. Jerala, R.; Porro, M., Endotoxin Neutralizing Peptides. *Current Topics in Medicinal Chemistry* **2004**, 4, 1173.

60. McPhee, J. B.; Scott, M. G.; Hancock, R. E. W., Design of Host Defence Peptides for Antimicrobial and Immunity Enhancing Activities. *Combinatorial Chemistry & High Throughput Screening* **2005**, 8, (3), 257.
61. Dathe, M.; Wieprecht, T., Structural features of helical antimicrobial peptides: their potential to modulate activity on model membranes and biological cells. *Biochimica et Biophysica Acta (BBA) - Biomembranes* **1999**, 1462, (1-2), 71.
62. Strøm, M. B.; Rekdal, Ø.; Svendsen, J. S., Antimicrobial activity of short arginine- and tryptophan-rich peptides. *Journal of Peptide Science* **2002**, 8, (8), 431.
63. Giuliani, A.; Pirri, G.; Nicoletto, S., Antimicrobial peptides: an overview of a promising class of therapeutics. *Central European Journal of Biology* **2007**, 2, (1), 1.
64. Chen, Y.; Guarnieri, M. T.; Vasil, A. I.; Vasil, M. L.; Mant, C. T.; Hodges, R. S., Role of Peptide Hydrophobicity in the Mechanism of Action of alpha-Helical Antimicrobial Peptides. *Antimicrobial Agents and Chemotherapy* **2007**, 51, (4), 1398.
65. Liu, Z.; Brady, A.; Young, A.; Rasimick, B.; Chen, K.; Zhou, C.; Kallenbach, N. R., Length Effects in Antimicrobial Peptides of the (RW)_n Series. *Antimicrobial Agents and Chemotherapy* **2007**, 51, (2), 597.
66. Chan, D. I.; Prenner, E. J.; Vogel, H. J., Tryptophan- and arginine-rich antimicrobial peptides: Structures and mechanisms of action. *Biochimica et Biophysica Acta (BBA) - Biomembranes* **2006**, 1758, (9), 1184.
67. Oren, Z.; Shai, Y., Mode of action of linear amphipathic alpha-helical antimicrobial peptides. *Peptide Science* **1998**, 47, (6), 451.
68. Epand, R. M.; Epand, R. F., Lipid domains in bacterial membranes and the action of antimicrobial agents. *Biochimica et Biophysica Acta (BBA) - Biomembranes* **2009**, 1788, (1), 289.
69. Hancock, R. E. W., Alterations in Outer Membrane Permeability. *Annual Review of Microbiology* **1984**, 38, (1), 237.
70. Mitra, R. N.; Shome, A.; Paul, P.; Das, P. K., Antimicrobial activity, biocompatibility and hydrogelation ability of dipeptide-based amphiphiles. *Organic & Biomolecular Chemistry* **2009**, 7, (1), 94.
71. Rathinakumar, R.; Walkenhorst, W. F.; Wimley, W. C., Broad-Spectrum Antimicrobial Peptides by Rational Combinatorial Design and High-Throughput Screening: The Importance of Interfacial Activity. *Journal of the American Chemical Society* **2009**, 131, (22), 7609.

72. Blondelle, S. E.; Perez-Paya, E.; Houghten, R. A., Synthetic combinatorial libraries: novel discovery strategy for identification of antimicrobial agents. *Antimicrobial Agents and Chemotherapy* **1996**, 40, (5), 1067.
73. Rathinakumar, R.; Wimley, W. C., Biomolecular Engineering by Combinatorial Design and High-Throughput Screening: Small, Soluble Peptides That Permeabilize Membranes. *Journal of the American Chemical Society* **2008**, 130, (30), 9849.
74. Chu, D. T. W.; Plattner, J. J.; Katz, L., New Directions in Antibacterial Research. *Journal of Medicinal Chemistry* **1996**, 39, (20), 3853.
75. Blondelle, S. E.; Houghten, R. A.; James, A. B., Chapter 17. Progress in Antimicrobial Peptides. In *Annual Reports in Medicinal Chemistry*, Academic Press: 1992; Vol. Volume 27, p 159.
76. Chaloin, L.; Bigey, P.; Loup, C.; Marin, M.; Galeotti, N.; Piechaczyk, M.; Heitz, F. d. r.; Meunier, B., Improvement of Porphyrin Cellular Delivery and Activity by Conjugation to a Carrier Peptide. *Bioconjugate Chemistry* **2001**, 12, (5), 691.
77. Brule, E.; de Miguel, Y. R., Supported metalloporphyrin catalysts for alkene epoxidation. *Organic & Biomolecular Chemistry* **2006**, 4, (4), 599.
78. Asayama, S.; Kawamura, E.; Nagaoka, S.; Kawakami, H., Design of Manganese Porphyrin Modified with Mitochondrial Signal Peptide for a New Antioxidant. *Molecular Pharmaceutics* **2006**, 3, (4), 468.
79. Sol, V.; Chaleix, V.; Granet, R.; Krausz, P., An efficient route to dimeric porphyrin-RGD peptide conjugates via olefin metathesis. *Tetrahedron* **2008**, 64, (2), 364.
80. Hong, V.; Presolski, S.; Ma, C.; Finn, M. G., Analysis and Optimization of Copper-Catalyzed Azide-Alkyne Cycloaddition for Bioconjugation. *Angewandte Chemie International Edition* **2009**, 48, (52), 9879.
81. Sibrian-Vazquez, M.; Jensen, T. J.; Hammer, R. P.; Vicente, M. G. H., Peptide-Mediated Cell Transport of Water Soluble Porphyrin Conjugates. *Journal of Medicinal Chemistry* **2006**, 49, (4), 1364.
82. Sibrian-Vazquez, M.; Jensen, T. J.; Fronczek, F. R.; Hammer, R. P.; Vicente, M. G. H., Synthesis and Characterization of Positively Charged Porphyrin-Peptide Conjugates. *Bioconjugate Chemistry* **2005**, 16, (4), 852.
83. Mihara, H.; Sakamoto, S.; Sakurai, S.; Ueno, A.; Haruta, Y.; Aoyagi, H., Supramolecular Assembly of alpha-Helix Peptide Conjugated with Porphyrins. *Peptides 1996; proceedings of the 24th European Peptide Symposium, September 8-13, 1996, Edinburgh, Scotland* **1998**, 24, 651.

84. Bouillon, C.; Meyer, A.; Vidal, S.; Jochum, A.; Chevolot, Y.; Cloarec, J. P.; Praly, J. P.; Vasseur, J. J.; Morvan, F., Microwave Assisted "Click" Chemistry for the Synthesis of Multiple Labeled-Carbohydrate Oligonucleotides on Solid Support. *The Journal of Organic Chemistry* **2006**, 71, (12), 4700.
85. Amblard, F.; Cho, J. H.; Schinazi, R. F., Cu(I)-Catalyzed Huisgen Azide-Alkyne 1,3-Dipolar Cycloaddition Reaction in Nucleoside, Nucleotide, and Oligonucleotide Chemistry. *Chemical Reviews* **2009**, 109, (9), 4207.
86. Meier, J. L.; Mercer, A. C.; Rivera, H.; Burkart, M. D., Synthesis and Evaluation of Bioorthogonal Pantetheine Analogues for in Vivo Protein Modification. *Journal of the American Chemical Society* **2006**, 128, (37), 12174.
87. Lin, P.-C.; Ueng, S.-H.; Tseng, M.-C.; Ko, J.-L.; Huang, K.-T.; Yu, S.-C.; Adak, A. K.; Chen, Y.-J.; Lin, C.-C., Site-Specific Protein Modification through Cu (I)-Catalyzed 1,2,3-Triazole Formation and Its Implementation in Protein Microarray Fabrication. *Angewandte Chemie International Edition* **2006**, 45, (26), 4286.
88. Huisgen, R.; Knorr, R.; Möbius, L.; Szeimies, G., 1.3-Dipolare Cycloadditionen, XXIII. Einige Beobachtungen zur Addition organischer Azide an CC-Dreifachbindungen. *Chemische Berichte* **1965**, 98, (12), 4014.
89. Rostovtsev, V. V.; Green, L. G.; Fokin, V. V.; Sharpless, K. B., A Stepwise Huisgen Cycloaddition Process: Copper(I)-Catalyzed Regioselective 'Ligation' of Azides and Terminal Alkynes. *Angewandte Chemie International Edition* **2002**, 41, (14), 2596.
90. Tornøe, C. W.; Christensen, C.; Meldal, M., Peptidotriazoles on Solid Phase: [1,2,3]-Triazoles by Regiospecific Copper(I)-Catalyzed 1,3-Dipolar Cycloadditions of Terminal Alkynes to Azides. *Journal of Organic Chemistry* **2002**, 67, (9), 3057.
91. Kolb, H. C.; Sharpless, K. B., The growing impact of click chemistry on drug discovery. *Drug Discovery Today* **2003**, 8, (24), 1128.
92. Lahann, J., *Click Chemistry for Biotechnology and Material Science*. Wiley: Chichester, West Sussex, 2009.
93. Meldal, M.; Tornøe, C. W., Cu-Catalyzed Azide-Alkyne Cycloaddition. *Chemical Reviews* **2008**, 108, (8), 2952.
94. Devaraj, N. K.; Decreau, R. A.; Ebina, W.; Collman, J. P.; Chidsey, C. E. D., Rate of Interfacial Electron Transfer through the 1,2,3-Triazole Linkage. *The Journal of Physical Chemistry B* **2006**, 110, (32), 15955.
95. Webb, J. E. A.; Maharaj, F.; Blake, I. M.; Crossley, M. J., A 'Click' Chemistry Route to 'Capped' Porphyrins. *Synlett* **2008**, 2008, (14), 2147,2149.

96. Megiatto, J. D.; Schuster, D. I.; Abwandner, S.; de Miguel, G.; Guldi, D. M., [2]Catenanes Decorated with Porphyrin and [60]Fullerene Groups: Design, Convergent Synthesis, and Photoinduced Processes. *Journal of the American Chemical Society* **132**, (11), 3847.
97. Takai, A.; Chkounda, M.; Eggenspieler, A.; Gros, C. P.; Lachkar, M.; Barbe, J.-M.; Fukuzumi, S., Efficient Photoinduced Electron Transfer in a Porphyrin Tripod-Fullerene Supramolecular Complex via pi-pi Interactions in Nonpolar Media. *Journal of the American Chemical Society* **132**, (12), 4477.
98. Ringot, C.; Sol, V.; Granet, R.; Krausz, P., Porphyrin-grafted cellulose fabric: New photobactericidal material obtained by "Click-Chemistry" reaction. *Materials Letters* **2009**, **63**, (21), 1889.
99. Elmer, S. L.; Man, S.; Zimmerman, S. C., Synthesis of polyglycerol, porphyrin-cored dendrimers using click chemistry. *European Journal Of Organic Chemistry* **2008**, (22), 3845.
100. Hasegawa, T.; Umeda, M.; Numata, M.; Li, C.; Bae, A.-H.; Fujisawa, T.; Haraguchi, S.; Sakurai, K.; Shinkai, S., 'Click chemistry' on polysaccharides: a convenient, general, and monitorable approach to develop (1->3)- β -D-glucans with various functional appendages. *Carbohydrate Research* **2006**, **341**, (1), 35.
101. Liu, Y.; Zhang, H.-J.; Cai, Y.-Q.; Wu, H.-H.; Liu, X.-L.; Lu, Y., Mild Oxidation of Styrene and Its Derivatives with Ionic Manganese Porphyrin Immobilized in the Similarly Structured Ionic Liquid. *Chemistry Letters* **2007**, **36**, (7), 848.
102. Dogutan, D. K.; Ptaszek, M.; Lindsey, J. S., Rational or statistical routes from 1-acyldipyrromethanes to meso-substituted porphyrins. Distinct patterns, multiple pyridyl substituents, and amphipathic architectures. *Journal Of Organic Chemistry* **2008**, **73**, (16), 6187.
103. Buckley, B. R.; Dann, S. E.; Heaney, H., Experimental Evidence for the Involvement of Dinuclear Alkynylcopper(I) Complexes in Alkyne-Azide Chemistry. *Chemistry – A European Journal* **2010**, **16**, (21), 6278.
104. Chan, W. C.; White, P. D., *Fmoc solid phase peptide synthesis: a practical approach*. Oxford University Press: Oxford; New York, 2000.
105. Chin, J. W.; Santoro, S. W.; Martin, A. B.; King, D. S.; Wang, L.; Schultz, P. G., Addition of p-Azido-l-phenylalanine to the Genetic Code of Escherichia coli. *Journal of the American Chemical Society* **2002**, **124**, (31), 9026.
106. Kerwin, B. A.; Remmele, R. L., Protect from light: Photodegradation and protein biologics. *Journal of Pharmaceutical Sciences* **2007**, **96**, (6), 1468.

107. Davies, M. J., Singlet oxygen-mediated damage to proteins and its consequences. *Biochemical and Biophysical Research Communications* **2003**, 305, (3), 761.
108. Grandjean, C.; Boutonnier, A.; Guerreiro, C.; Fournier, J.-M.; Mulard, L. A., On the Preparation of Carbohydrate-Protein Conjugates Using the Traceless Staudinger Ligation. *The Journal of Organic Chemistry* **2005**, 70, (18), 7123.
109. Kachadourian, R.; Menzeleev, R.; Agha, B.; Bocckino, S. B.; Day, B. J., High-performance liquid chromatography with spectrophotometric and electrochemical detection of a series of manganese(III) cationic porphyrins. *Journal of Chromatography B: Analytical Technologies in the Biomedical and Life Sciences* **2002**, 767, (1), 61.
110. Jing, W.; Hunter, H. N.; Hagel, J.; Vogel, H. J., The structure of the antimicrobial peptide Ac-RRWRF-NH₂ bound to micelles and its interactions with phospholipid bilayers. *Journal of Peptide Research* **2003**, 61, (5), 219.
111. Blondelle, S. E.; Houghten, R. A., Novel antimicrobial compounds identified using synthetic combinatorial library technology. *Trends in Biotechnology* **1996**, 14, (2), 60.
112. Wikler, M. A.; Cockerill, F. R.; Bush, K.; Dudley, M. N.; Eliopoulos, G. M.; Hardy, D. J.; Hecht, D. W.; Hindler, J. F.; Patel, J. B.; Powell, M.; Turnidge, J. D.; Weinstein, M. P.; Zimmer, B. L.; Ferraro, M. J.; Swenson, J. M., *Methods for Dilution Antimicrobial Susceptibility Test for Bacteria That Grow Aerobically; Approved Standard*. eighth ed.; Clinical and Laboratory Standards Institute: 2009; Vol. 29.
113. O'Riordan, K.; Sharlin, D. S.; Gross, J.; Chang, S.; Errabelli, D.; Akilov, O. E.; Kosaka, S.; Nau, G. J.; Hasan, T., Photoinactivation of Mycobacteria In Vitro and in a New Murine Model of Localized Mycobacterium bovis BCG-Induced Granulomatous Infection. *Antimicrobial Agents and Chemotherapy* **2006**, 50, (5), 1828.
114. O'Riordan, K.; Akilov, O. E.; Chang, S. K.; Foley, J. W.; Hasan, T., Real-time fluorescence monitoring of phenothiazinium photosensitizers and their anti-mycobacterial photodynamic activity against Mycobacterium bovis BCG in in vitro and in vivo models of localized infection. *Photochemical & Photobiological Sciences* **2007**, 6, (10), 1117.
115. Fritz, J. H.; Brunner, S.; Birnstiel, M. L.; Buschle, M.; Gabain, A. v.; Mattner, F.; Zauner, W., The artificial antimicrobial peptide KLKLLLLLKLK induces predominantly a TH2-type immune response to co-injected antigens. *Vaccine* **2004**, 22, (25-26), 3274.
116. Keun-Hyeung, L., Development of Short Antimicrobial Peptides Derived from Host Defense Peptides or by Combinatorial Libraries. *Current Pharmaceutical Design* **2002**, 8, (9), 795.

117. Nakajima, Y.; Alvarez-Bravo, J.; Cho, J.-h.; Homma, K.-i.; Kanegasaki, S.; Natori, S., Chemotherapeutic activity of synthetic antimicrobial peptides: correlation between chemotherapeutic activity and neutrophil-activating activity. *FEBS Letters* **1997**, 415, (1), 64.
118. Cincotta, L.; Foley, J. W.; Cincotta, A. H., Novel Red absorbing Benzo[a]phenoxazinium and Benzo[a]phenothiazinium Photosensitizers: *in vitro* evaluation. *Photochemistry and Photobiology* **1987**, 46, (5), 751.
119. Maisch, T.; Baier, J.; Franz, B.; Maier, M.; Landthaler, M.; Szeimies, R.-M.; Baeumler, W., The role of singlet oxygen and oxygen concentration in photodynamic inactivation of bacteria. *Proceedings of the National Academy of Sciences* **2007**, 104, (17), 7223.
120. Rezansoff, A. J.; Hunter, H. N.; Jing, W.; Park, I. Y.; Kim, S. C.; Vogel, H. J., Interactions of the antimicrobial peptide Ac-FRWWHR-NH₂ with model membrane systems and bacterial cells. *The Journal of Peptide Research* **2005**, 65, (5), 491.
121. Medfort, C. J., NMR Spectroscopy of Diamagnetic Porphyrins. In *The Porphyrin Handbook*, Kadish, K. M.; Smith, K. M.; Guillard, R., Eds. Academic Press: San Diego, CA, 2000; Vol. 10, pp 1.
122. Novabiochem, *2008/2009 Catalog*. EMD: 2008.
123. Chen, W. C.; White, P. D., *Fmoc solid phase peptide synthesis: a practical approach*. Oxford University Press: Oxford; New York, 2000.
124. Chang, K.-C.; Su, I.-H.; Senthilvelan, A.; Chung, W.-S., Triazole-Modified Calix[4]crown as a Novel Fluorescent On-Off Switchable Chemosensor. *Organic Letters* **2007**, 9, (17), 3363.
125. Altomare, A.; Cascarano, G.; Giacovazzo, C.; Guagliardi, A.; Burla, M. C.; Polidori, G.; Camalli, M., SIR92 – a program for automatic solution of crystal structures by direct methods. *Journal of Applied Crystallography* **1994**, 27, (3), 435.
126. Larsen, M., Some Common Methods in Mycobacterial Genetics. In *Molecular Genetics of Mycobacteria*, Hatfull, G. F., Ed. ASM Press: Washington DC, 2000; pp 313.
127. Bradley D. Jett, K. L. H., Mark M. Huycke, and Michael S. Gilmore, Simplified Agar Plate Method for Quantifying Viable Bacteria. *BioTechniques* **1997**, 23, (4), 648.

CHAPTER 4

Towards Photobactericidal Materials: Synthesis, Characterization and Photodynamic Activity of Porphyrin-Cellulose Nanocrystals

Abstract

Adherence and survival of pathogenic bacteria on surfaces leading to concomitant transmission to new hosts significantly contributes to the proliferation of pathogens, which in turn considerably increases the threat to human health especially by antibiotic resistant bacteria. Consequently, more research into effective surface disinfection and alternative materials (fabrics, plastics or coatings) with antimicrobial properties are needed. This chapter describes the synthesis and characterization of cellulose nanocrystals that were surface modified with a cationic porphyrin. The porphyrin was appended onto the cellulose surface by Huisgen 1,3-dipolar cycloaddition between azide groups on the cellulosic surface and porphyrinic alkynes. The resulting generally insoluble, crystalline material, CNC-Por (**4.4**), was characterized by infrared and diffusion $^1\text{H-NMR}$ spectroscopies, gel permeation chromatography and thermogravimetric analysis. Although only suspended in the aqueous system, compound **4.4** showed excellent efficacy in the photodynamic inactivation of *Mycobacterium smegmatis* and *Staphylococcus aureus*, albeit only slight activity against *Escherichia coli*. The synthesis, properties, and activity of CNC-Por (**4.4**) described in this

chapter serves as a benchmark towards our goal of developing photobactericidal materials useful for the health care and food preparation industries.

Introduction

Hospital acquired infections, in particular, highlight the issue of adherence and survival of bacteria on surfaces leading to an increase in the proliferation and transmission of bacteria. Specifically, antibiotic-resistant bacteria are a rising threat to human health. According to the Centers of Disease Control and Prevention, about 1.7 million healthcare associated infections cause upwards of 99,000 deaths annually in the United States.¹ 5-10% of all hospitalized patients are adversely affected, which in turn is adding about \$30-45 billion to health care costs every year.² Food processing/packaging-, food service- and waste water treatment industries, as well as personal households, are also areas of concern and can contribute to the spread of disease through contaminated or improperly disinfected surfaces. Consequently, more research into effective surface disinfection and alternative materials (fabrics, plastics or coatings) with antimicrobial properties is needed. In general terms, ideal antimicrobial surfaces necessitate a permanent or rechargeable antimicrobial character, harmlessness to the environment as well as efficient and user-independent inactivation of microbes. Several classes of antimicrobial agents are currently being investigated or are commercially available, amongst which are polymeric compounds containing quarternary ammonium,³⁻⁷ pyridinium^{8, 9} or phosphonium salts,^{5, 10} N-halamines,^{11, 12} biguanides,¹³ antibiotics,¹⁴ heavy metals such as Ag¹⁵⁻¹⁷ and phenol derivatives.¹⁵ Disadvantages of

currently available materials are the loss of antimicrobial activity by leaching of the biocide in non-covalent systems, consumption of the germicidal ability, environmentally hazardous agents or dependency on direct contact of the antimicrobial entity with the microorganism.

In the past few decades, photodynamic inactivation (PDI) has garnered the attention of many researchers as an alternative technique for eradicating microorganisms. In our laboratory we are interested in building a research program investigating several aspects of photodynamic inactivation of bacteria by a) the synthesis of novel photosensitizers (Chapter 3), and b) the exploration of possible applications of these principles towards materials with photobactericidal activity (this Chapter). We see great potential for photobactericidal materials to satisfy many of the desired characteristics mentioned above while overcoming some of the shortcomings of currently available antimicrobial materials. PDI employs light absorbing photosensitizers (PS), such as porphyrins, phthalocyanines or bacteriochlorins, that generate cytotoxic species, particularly singlet oxygen, upon illumination with visible light.¹⁸ Specifically, *in vitro* inactivation of bacteria in an aqueous system is achieved by uptake or binding of the PS to the bacteria, followed by illumination with low intensity visible light. The thereby-excited photosensitizer in its triplet state produces cytotoxic free radicals (type I mechanism) and singlet oxygen (type II mechanism), irreversibly damaging the bacteria, and ultimately leading to cell death.^{18, 19} The type II mechanism is thought to be the main pathway invoking cellular death.²⁰ Singlet oxygen, as opposed to some common disinfectants, can be regarded as an environmentally benign germicide. Specifically compared to chlorine and hypochlorite, singlet oxygen is short lived (lifetimes of 10^{-6} s in water²¹ and

0.1 s in air²² have been reported), and reverts back to harmless ground state oxygen if unreacted.

Interestingly, the success of photodynamic inactivation is not limited to direct contact and localization of the photosensitizer with the microbe. Singlet oxygen is known to be able to diffuse 100-200 nm (for comparison bacteria generally are several μm in length) in water and about 1 mm in air.²³ Bezman et al. were first to demonstrate this by photodynamic inactivation of *E. coli* with Rose Bengal immobilized on polystyrene beads.²⁴ Moreover, Dahl et al. demonstrated successful photodynamic inactivation of *Salmonella typhimurium* and *E. coli* by a flow of singlet oxygen through a 0.65 mm air gap between microbe and photosensitizer.²⁵ The feasibility of the concept 'photobactericidal surface' is further supported by studies showing that photosensitizers retain their ability to reduce a bacterial cell count when adsorbed, co-dissolved and casted as well as covalently bound to nanoparticles,^{26, 27} polymers,^{28, 29} films³⁰⁻³² or membranes.³³ Of particular interest for our work is a series of studies by Krausz and co-workers who have investigated the incorporation of select porphyrin photosensitizers into cellulose esterified plastic films and demonstrated the photobactericidal activity of such films.^{31, 32, 34}

Cellulose is Earth's most abundant natural biopolymer, and therefore, in our eyes, an excellent starting material for developing new, more sustainable materials from renewable resources.³⁵ Cellulose is a high molecular weight polymer of β -1,4-linked anhydro-*D*-glucose whose polymer chains assemble into microfibrils which are tightly cross-linked by an inter- and intrachain hydrogen bonding network.³⁶ Distortions in the chain packing causes amorphous regions within the otherwise crystalline microfibrils, which in turn can be

hydrolysed by acid treatment, resulting in rod-shaped cellulose nanocrystals [CNC (**4.1**), Figure 4.1].³⁷ These nanocrystals are interesting due to their intrinsic physical and chemical properties, such as their nanoscale size, high mechanical strength, ease of chemical modification, and ability to have molecular patterns etched on the crystal surface.^{36, 38}

Herein, we have focused on the surface modification of CNC (**4.1**) with the cationic porphyrin **3.1**, yielding the conjugate CNC-Por (**4.4**), which, to the best of our knowledge, represents the first attempt to covalently append cationic porphyrins to the surface of cellulose nanocrystals. The physical properties of CNC-Por (**4.4**) were investigated using a combination of spectroscopic and chemical analyses, thereby demonstrating the covalent linkage between the two moieties, while its photobactericidal characteristics were also examined. Photodynamic inactivation proved to be very efficient against *Staphylococcus aureus* as well as the very resilient *Mycobacterium smegmatis*, and mildly effective against *Escherichia coli* in aqueous suspension. Covalent attachment of **3.1** to **4.1** was achieved via the Huisgen's 1,3-dipolar addition (hereafter termed the 'Click reaction') between an azide on the CNC surface and an alkyne-containing porphyrin.^{39, 40} Click chemistry on the cellulose backbone has recently gained attention, particularly following the development of ionic liquids as solvents for crystalline cellulose.⁴¹⁻⁴³ Click chemistry allows access to hydrolytically stable, selectively functionalized products that are not accessible by standard cellulose esterification.^{44, 45} Further, the modular approach of the Click technology should enable attachment of a series of photosensitizers. We see potential for the incorporation of photosensitizer-modified-cellulose nanocrystals (PS-CNC) into paper, fabrics and plastics, thereby creating novel, biodegradable, photobactericidal materials from renewable sources.³⁶

The importance of cellulose containing fabrics is highlighted in the fact that *S. aureus* has been found to be able to survive for weeks under dry conditions on cotton fabrics used in the hospital environment.^{46, 47}

Results

Synthesis. The ethynylphenyl porphyrin **3.1** was synthesized in 4 steps as described in Chapter 3 (Figure 3.2), and characterized by UV-visible and NMR spectroscopies, high-resolution mass spectrometry and X-ray crystallography.

The nanocrystalline cellulose material employed in this study was obtained by acid hydrolysis of cotton fibers. Such treatment causes selective degradation of amorphous cellulosic regions producing defect-free, rod-like crystals with a length of 100-400 nm (Figure 4.1). Cellulose pulp from cotton filter paper (Whatman #1, 98% cellulose, 80% crystallinity) was treated with 2.5 M HBr and intermittent ultrasonication for optimized high yields of cellulose nanocrystals according to literature procedure.^{38, 48} The CNCs were isolated and purified by a series of centrifugation and washing steps.

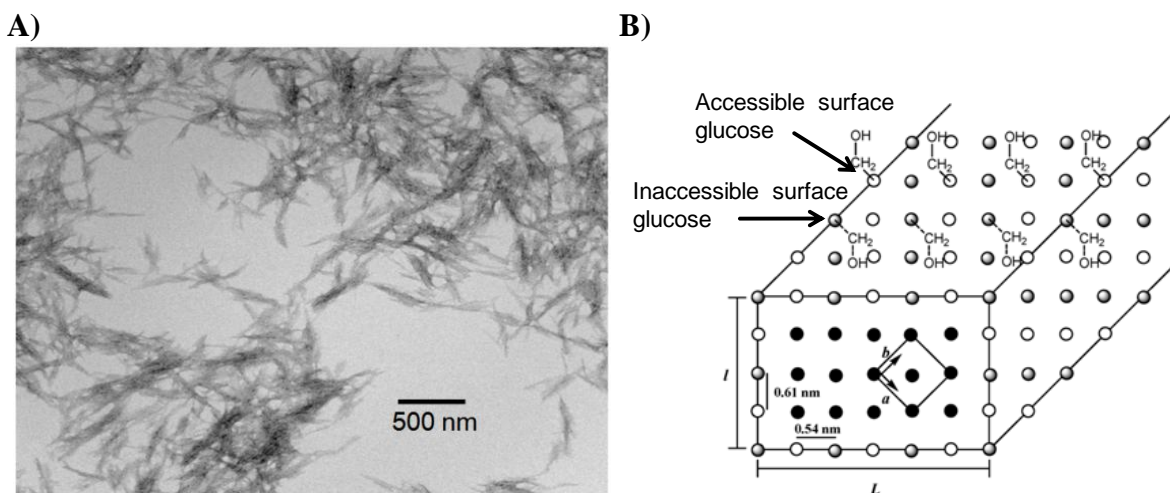


Figure 4.1: A) TEM image of CNC (**4.1**), B) Cross-sectional representation of the cellulose nanocrystal indicating the surface accessible reaction sites (Adapted with permission from Ref [36]. Copyright 2010 American Chemical Society).

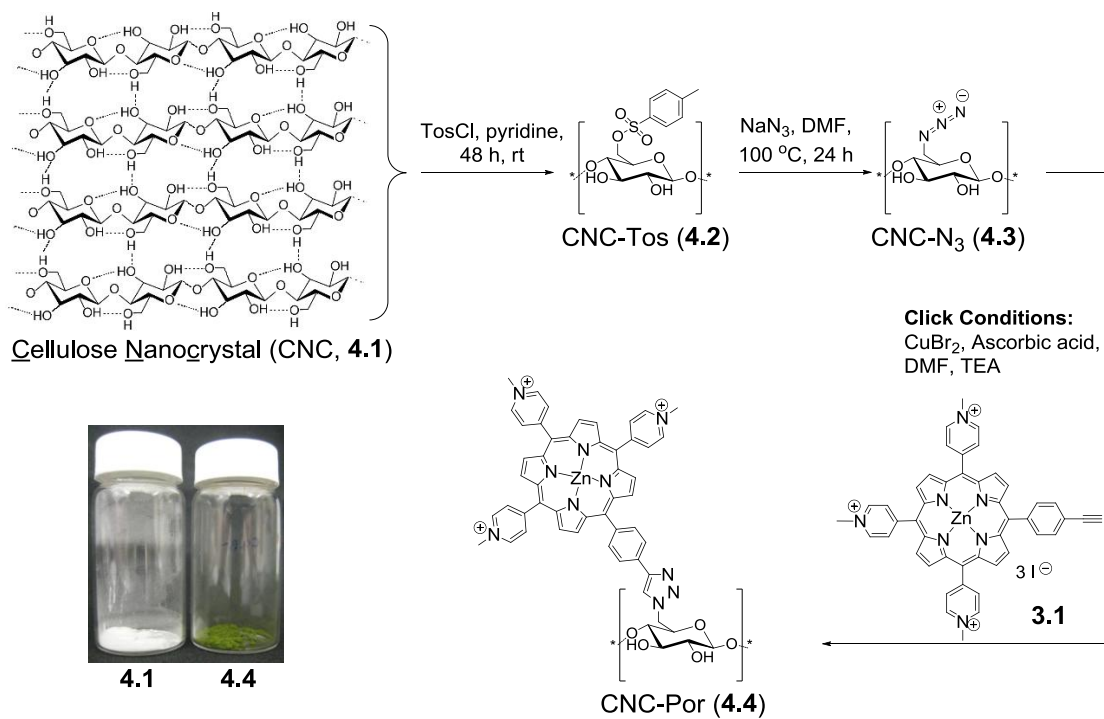


Figure 4.2: Synthesis of cellulose nanocrystal-porphyrin conjugate CNC-Por (**4.4**).

Modification of the primary hydroxyl groups of the CNCs for the installment of surface-azide groups was successful in two steps (Figure 4.2). First, the nanocrystals (**4.1**) were suspended in pyridine and treated with tosyl chloride, yielding the surface-tosylated cellulose analog **4.2**. FTIR spectroscopy revealed that in addition to the typical absorption bands of the cellulose backbone, new vibrational modes assigned to the aromatic ring (1596, 1495 and 815 cm^{-1}) and SO_2 [1363 (antisymmetric) and 1175 (symmetric) cm^{-1} , Figure 4.3] stretching modes appeared, verifying successful tosylate modification. The tosyl substituents were subsequently displaced by azide groups using sodium azide in a DMF suspension, yielding CNC- N_3 (**4.3**), which was characterized by FTIR spectroscopy (Figure 4.3). The azide-modified CNC (**4.3**) exhibited a new stretching band characteristic for the azide moiety at 2113 cm^{-1} , with concomitant loss of the vibrational modes associated with the tosylated precursor **4.2**. Elemental analysis of CNC- N_3 (**4.3**) revealed a nitrogen content of 3.75%. Taking the molecular weight of the anhydrous glucose unit of 162 g/mol and nitrogen (14 g/mol) into account, the degree of methylhydroxy substitution (DS) with surface azide groups was calculated as $\text{DS} = (0.0375 \cdot 162) / (3 \cdot 14) = 0.14$. The theoretical maximum of surface available primary hydroxyl groups can be determined from the following parameters: The average dimensions (8.6×7.7 nm) of the CNC rectangular rods have been determined by X-ray crystallography.⁴⁸ Thus, the amount of individual cellulose chains within a cotton crystallite can be calculated using the two lattice parameters of the cellulose I_β unit cell, $a = 0.61$ nm and $b = 0.54$ nm, respectively.^{49, 50} Based on this model, the planes corresponding to 0.61 nm are parallel to the long side ($C_1 = 8.6$ nm) of the rectangular whisker section whereas the 0.54 nm are parallel to the short side ($C_2 = 7.7$ nm).^{51, 52} Thus, within this average crystal,

there are $(8.6 \cdot 7.7) / (0.61 \cdot 0.54) = 201$ cellulose chains. At the surface, this corresponds to $2 \times (8.6 / 0.54) + 2 \cdot (7.7 / 0.61) = 57$ cellulose chains. The ratio of surface chains to the total number of chains within the crystals is therefore 0.29. Due to the two-fold screw axis of the glucose units within each chain, a maximum degree of primary hydroxyl groups on the surface of the CNC is about $0.29 / 2 = 0.145$ (Figure 4.1 B). Therefore, the two-step azide substitution was highly efficient, converting > 95% of the available surface methylhydroxy groups.

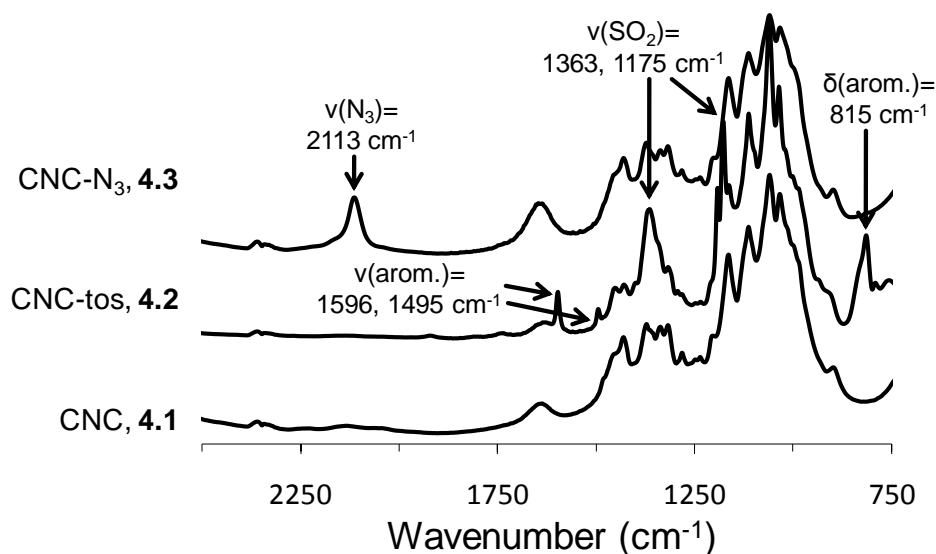


Figure 4.3: IR spectra of CNC (4.1), CNC-tos (4.2) and CNC-N₃ (4.3).

Appendage of the porphyrin onto the cellulose nanocrystalline surface was achieved by the Huisgen 1,3-dipolar cycloaddition (Click reaction).^{40, 44, 53-55} Several conditions including temperature (RT to 60 °C), solvents (EtOH, DMF) and Cu catalysts (CuI, CuBr₂/ascorbate, [Cu(OTf)]₂·tol) were surveyed, and CuBr₂ in combination with ascorbate in

DMF at elevated temperature in the presence of triethylamine proved to give the best results. The choice of DMF as the solvent was based upon the dissolution properties of the porphyrin **3.1**. Purification of the resulting product, an insoluble green crystalline material [(**4.4**), Figure 4.2], was achieved by careful washing and centrifuging.

IR characterization of 4.4. Clear evidence for the successful reaction of the ethyne functional group in **3.1** with the azide containing cellulose nanocrystals **4.3** was obtained from IR spectroscopic analysis (Figure 4.4). The IR spectrum of the azide surface-modified cellulose **4.3** (black trace) clearly exhibited an azide band at 2113 cm^{-1} , which is within the range of $2160\text{-}2080\text{ cm}^{-1}$ expected for the antisymmetric azide stretching motion.⁵⁶ Upon reaction with the ethyne containing porphyrin **3.1**, the azide band in the IR spectrum of the resulting product **4.4** was significantly diminished. Additionally, an intensity increase of the bands in the region around 1651 cm^{-1} indicated the presence of C=N double bonds arising from the porphyrin and triazole linkage. The broad band centered around 1647 cm^{-1} in the spectrum for the CNC-N₃ (**4.3**) is most likely due to the bending motion of adsorbed water and overlaps with the C=N stretching modes for CNC-Por (**4.4**).⁵⁷

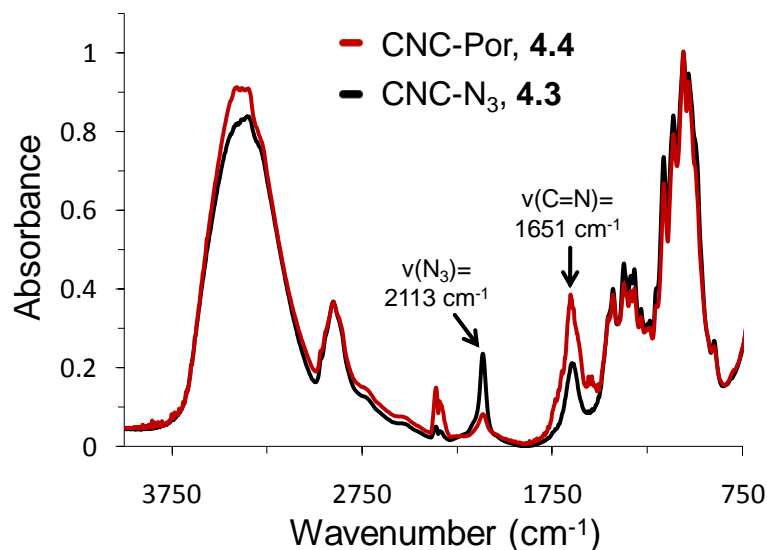


Figure 4.4: IR spectra of CNC-N₃ (**4.3**) and CNC-Por (**4.4**).

Molecular weight determination and porphyrin loading of 4.4. The molecular weight gain attributable to the appended porphyrins was assessed by gel permeation chromatography (GPC). Due to the insolubility of cellulosic samples in organic solvents, the hydroxyl groups were benzoylated prior to GPC analysis. Samples of **4.3** and **4.4** were dissolved in the ionic liquid, 1-allyl-3-methylimidazolium chloride, and treated with benzoyl chloride. The molecular weight distribution of **4.4** clearly shifted to higher molecular weights, with an average of 102,000 g/mol, compared to 69,000 g/mol for **4.3** (Figure 4.5, Table 4.1). This 48% increase in the average molecular weight further supports the notion of covalent appendage between the porphyrin **3.1** and the CNC-N₃ (**4.3**). Further, we have attributed the increase in polydispersity of the benzoylated CNC-Por sample (Table 4.1) when compared to the benzoylated CNC-N₃ material to a distribution of surface-bound porphyrins arising from the partial reaction of **3.1** with **4.3**. From the average mass increase between **4.3** and **4.4**, and

considering the average mass of the anhydrous glucose-N₃ unit of 166 g/mol, we were able to estimate the porphyrin loading of the CNCs as an average of one porphyrin molecule per 15 glucose molecules. Considering the degree of substitution of DS = 0.14 for the azide groups on the crystal surface, we estimate that approximately 50% of the azide groups were reacted with the cationic porphyrin, corresponding to an overall degree of substitution of DS = 0.07 for the porphyrin.

Alternatively, the porphyrin loading was determined indirectly by measuring the Zn-ion content by atomic absorption spectroscopy of a CNC-Por **4.4** sample in 1 M HCl using the standard addition method.⁵⁸ Under the assumption that one Zn-ion detected corresponds to one porphyrin molecule covalently attached to the cellulose nanocrystalline surface, a maximum loading of ~0.2 μmol porphyrin/mg CNC-Por was obtained. Using this method the porphyrin loading of extensively washed samples was determined as one porphyrin per roughly 20 glucose units.

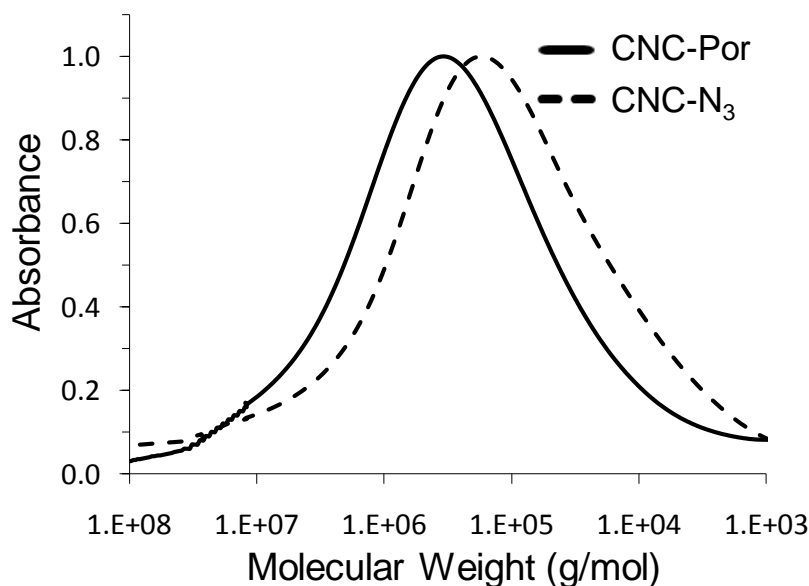


Figure 4.5: Gel permeation chromatography of benzyolated derivatives of CNC-N₃ (**4.3**) and CNC-Por (**4.4**) in THF.

Table 4.1: Molecular weight distributions of benzyolated derivatives of CNC-N₃ (**4.3**) and CNC-Por (**4.4**) in THF.

	Molecular Weight 10 ³ g/mol	Polydispersity
CNC-N ₃ (4.3), benzyolated	69	3.5
CNC-Por (4.4), benzyolated	102	5.8

Pulsed Field Gradient Spin Echo ¹H-NMR Spectroscopy. NMR characterization of CNC-Por (**4.4**) proved to be possible only upon acetylation due to the insolubility of this crystalline material in common solvents. Briefly, CNC-Por (**4.4**) was dissolved in 1-allyl-3-methylimidazolium chloride (AMIM-Cl) at 80 °C over 12 hours, and subsequently reacted with acetic anhydride. The resulting acetylated CNC-Por was rendered soluble in DMSO,

and therefore was amenable for characterization by NMR spectroscopy. The ^1H -NMR spectrum of acetylated **4.4** revealed the presence of proton resonances for cellulose alongside those of the porphyrin component. However, relative to the cellulose, the small concentration of the porphyrin (approximately 1 molecule/15-20 glucose units), which had only been appended to the surface of the cellulose nanocrystals, did not allow for any further conclusions regarding the covalent conjugation between the two entities. Therefore, pulsed field gradient spin echo ^1H -NMR experiments (PFGSE-LED pulse sequence) were performed.⁵⁹⁻⁶¹ PFGSE-NMR allows for the determination of diffusion coefficients even for mixtures of compounds.⁶² Diffusion NMR, with its ability to draw conclusions about molecular size, shape, aggregation or binding in complex solutions, has proven useful in a range of different fields such as bioanalytical, pharmaceutical, environmental and materials chemistry.⁶³⁻⁶⁸ In pulsed field gradient experiments, a magnetic gradient pulse whose strength varies throughout the sample is applied in addition to the static magnetic field. Thereby, it is possible to label the spins according to their translational position in the NMR tube. After this encoding pulse, the molecules are allowed to diffuse for a specified time period after which a decoding gradient pulse is applied. If diffusion to a different part of the sample has occurred, the decoding pulse will not completely reverse the phase change of the encoding pulse, and an attenuation of the NMR signal is observed. The change in resonance intensity for simple PFG pulse sequences is proportional to the diffusion coefficient (D) and square of the gradient pulse amplitude (G) as described in equation 4.1.:

(4.1)

in which I_0 denotes the signal intensity in the absence of a gradient pulse, δ the gradient duration, γ the magnetogyric ratio of the nucleus under investigation, and t_s the settling time. A plot of $\ln(I/I_0)$ over G^2 allows determination of D from the slope.⁶⁹

Figure 4.6 shows the results of the pulsed field gradient spin echo $^1\text{H-NMR}$ experiments with the acetylated compound **4.4**. The aromatic resonances of the porphyrin moiety can be found from 8.0-9.5 ppm, whereas the N-pyridyl-methyl groups show a signal at 4.7 ppm. The proton signals for the acetylated cellulose backbone appear ~ 2 ppm (acetyl groups) and between 3.5-5.2 ppm (cellulose backbone). A small attenuation of the signal intensity for the cellulose backbone of **4.4** was observed by increasing the gradient strength incrementally. Magnification of the aromatic porphyrin region around 8-9 ppm also exhibited an equally small change in signal intensity. This indicated that both the porphyrin and the acetylated cellulose diffused at the same rate (estimated diffusion coefficient $D = 2 \cdot 10^{-7}$ cm^2/s , Table 4.2), and therefore strongly suggests they are covalently connected. Figure 4.7 shows the results for the PFGSE- $^1\text{H-NMR}$ experiments of a mixture of the porphyrin **3.1** and acetylated CNC-N₃ (**4.3**). A faster loss in signal intensity for the porphyrin protons (i.e., δ 9.4 or 4.7 ppm as representative resonances) when compared to the methyl groups of the acetylated CNC-N₃ (**4.3**) (δ 2.0 ppm) was noted. The differences in relative proton signal intensity loss [$\ln(I/I_0)$] between the porphyrin **3.1**, acetylated CNC-N₃ and acetylated CNC-Por is also displayed as a function of gradient strength (G^2) in Figure 4.8. The respective diffusion coefficients determined from the NMR data differ by an order of magnitude with $2 \cdot 10^{-6}$ cm^2/s for the porphyrin **3.1** and $3 \cdot 10^{-7}$ cm^2/s for the acetylated CNC-N₃, whereas the diffusion rates for acetylated CNC-Por and CNC-N₃ are very similar (Table 4.2).

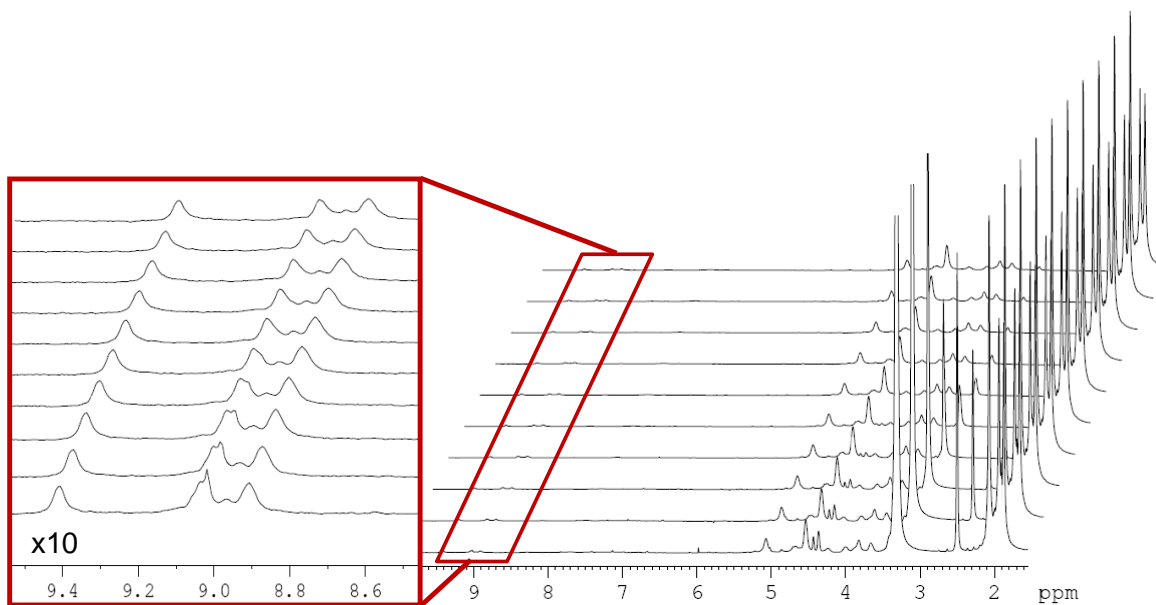


Figure 4.6: Pulsed field gradient spin echo ^1H -NMR spectra of acetylated CNC-Por.

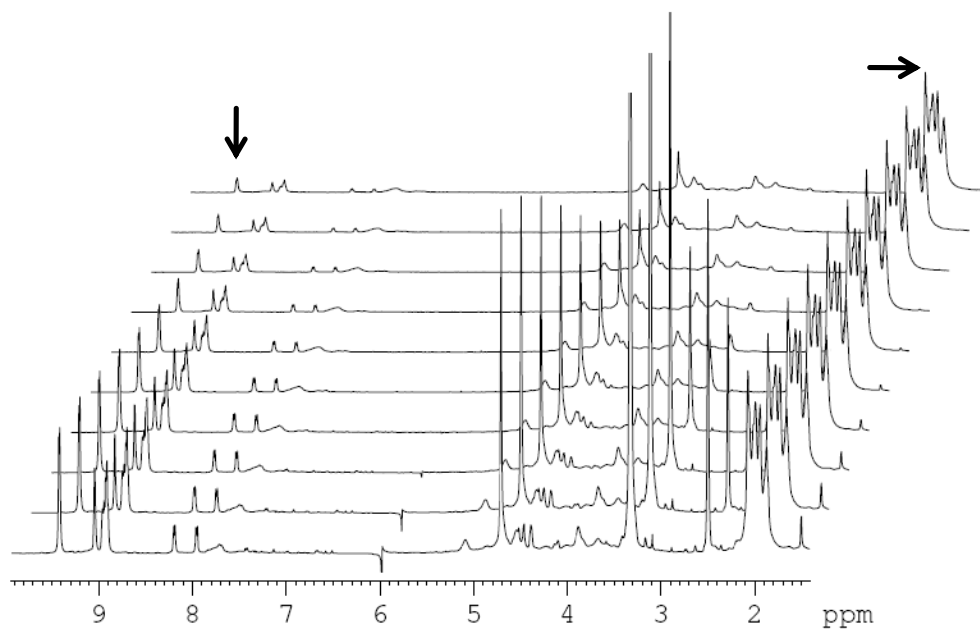


Figure 4.7: Pulsed field gradient spin echo ^1H -NMR control experiments of a mixture of porphyrin **3.1** and acetylated CNC- N_3 , marked signals were used for estimation of diffusion coefficients.

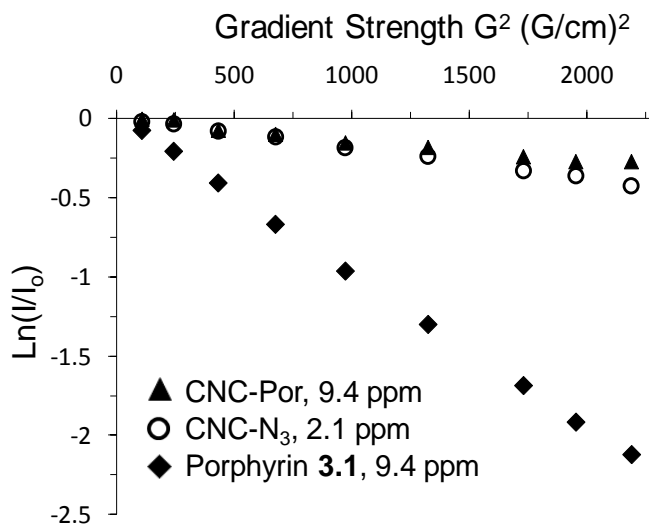


Figure 4.8: Graphical representation of the loss in proton signal intensity for PFGSE ¹H-NMR experiments comprised from data shown in Figures 4.6 and 4.7.

Table 4.2: Estimated diffusion coefficients D determined from PFGSE ¹H-NMR.

Compound	Fragment	δ ppm	D cm ² /s
CNC-Por (4.4 , acetylated)	Porphyrin	9.4	$2 \cdot 10^{-7}$
	Cellulose	2.1	$2 \cdot 10^{-7}$
CNC-N ₃ (4.3 , acetylated) mixture with porphyrin 3.1	Porphyrin	9.4	$2 \cdot 10^{-6}$
	Cellulose	2.1	$3 \cdot 10^{-7}$

Thermogravimetric analysis of CNC-Por 4.4. We also investigated the thermal behavior of the starting materials, porphyrin **3.1** and CNC-N₃ **4.3**, versus that of CNC-Por (**4.4**) by thermogravimetric analysis (Figure 4.9). 5% weight losses for both porphyrin **3.1** and CNC-N₃ (**4.3**) were observed at 235 °C and 285 °C, respectively. For the CNC-Por

conjugate a different thermal gravimetric behavior was apparent. Two degradation profiles were observed, with minor degradation commencing around 210 °C (weight loss of 20%) and major decomposition above 320 °C. This difference in thermal behavior further supports our claim that the CNC-N₃ (**4.3**) had been chemically modified upon Click reaction with the porphyrin **3.1**, producing a covalent linkage between the two.

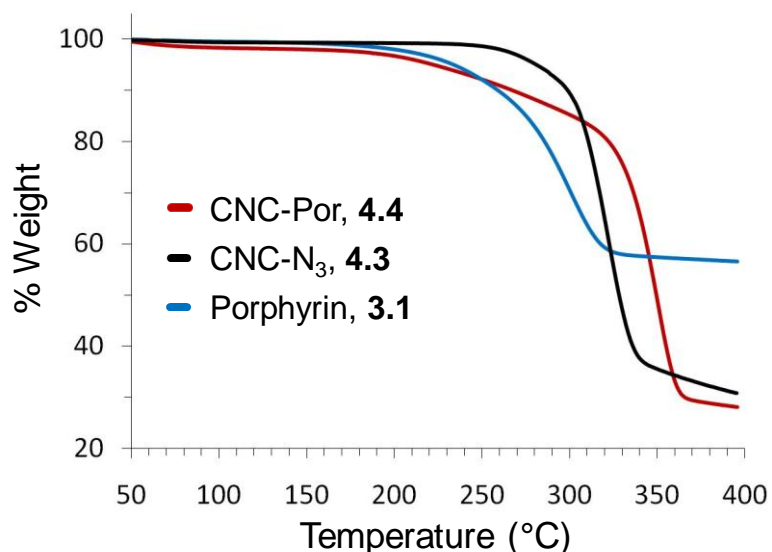


Figure 4.9: Thermal gravimetric analysis of CNC-Por (**4.4**).

Photodynamic Inactivation Studies with CNC-Por (4.4). The ability of CNC-Por (**4.4**) to inactivate *E. coli*, *M. smegmatis* and *S. aureus* was evaluated. The bacteria were grown to a concentration of $\sim 10^8$ colony forming units per mL (CFU/mL), re-suspended in PBS-0.05% Tween-80 containing buffer, incubated with the photosensitizer in the dark (incubation time was varied from 5-60 minutes) and subsequently illuminated with white light (400-700 nm) with a fluence rate of 60 mW/cm² for 15 or 30 min (equivalent to a fluence of 54 or 108

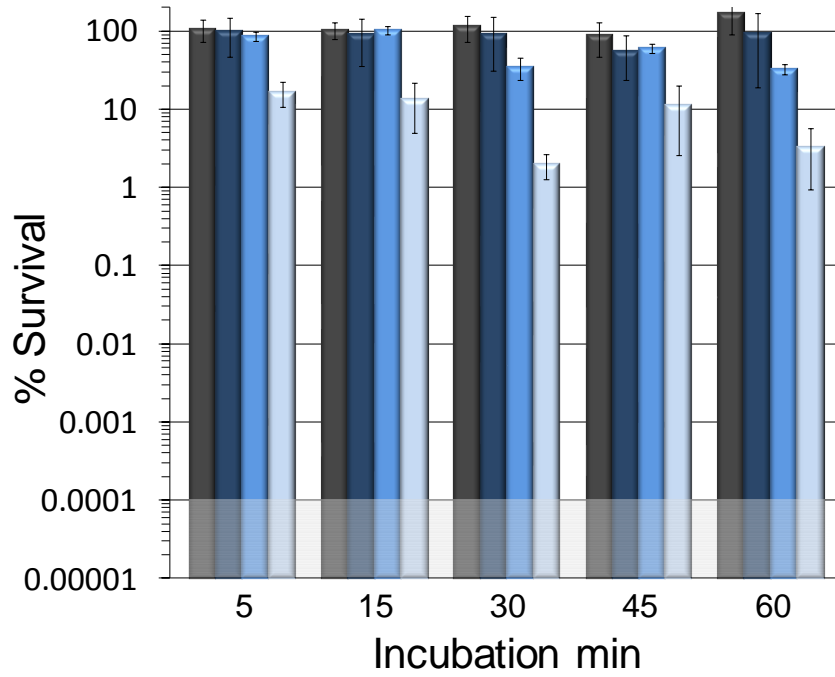
J/cm²). The stock solution for **4.4** was prepared based on the porphyrin loading determined by atomic absorption spectroscopy. Concentrations listed hereafter refer to the concentration of porphyrin on **4.4** present in the suspension. The percentage of survival was determined by the ratio of the colony count from illuminated and non-illuminated control cell suspensions. The results for light treated samples as well as dark controls are shown in panels A-C of Figure 4.10. *E. coli* appeared to be relatively resistant to photodynamic inactivation by CNC-Por (**4.4**) at 20 μ M based upon the porphyrin concentration (Figure 4.10 A). No statistically significant inactivation of *E. coli* was observed with 15 minutes illumination under all incubation periods tested ($P > 0.2$). With longer illumination times (30 minutes) a 1-2 log unit reduction in the cell count was observable ($P = 0.05$ for 45 and 60 minutes incubation time). The dark incubation time before the illumination step did not appear to play a significant role, although there was a slight improvement of ~ 0.5 log units in the inactivation of *E. coli* for incubation times of at least 30 minutes. Dark controls containing CNC-Por (**4.4**) showed no toxicity towards *E. coli*.

For PDI of *M. smegmatis*, no dark toxicity was apparent for the CNC-Por photosensitizer (Figure 4.10 B). For long dark incubation times (i.e., 60 minutes), a reduction of the cell count to about 30% was observed for both the bacteria-only and CNC-Por dark controls, which was most likely due to the lack of nutrients in the PBS buffered solutions. Upon illumination, *M. smegmatis* was found to be more susceptible to photodynamic inactivation by CNC-Por (**4.4**) than *E. coli*. Clear loss in viable cells was observed starting with 2 log units for 15 minutes incubation time, and increased to 3.5 log units after 60 minutes incubation for the same light dose (15 minutes, $P = 0.003$). When the illumination

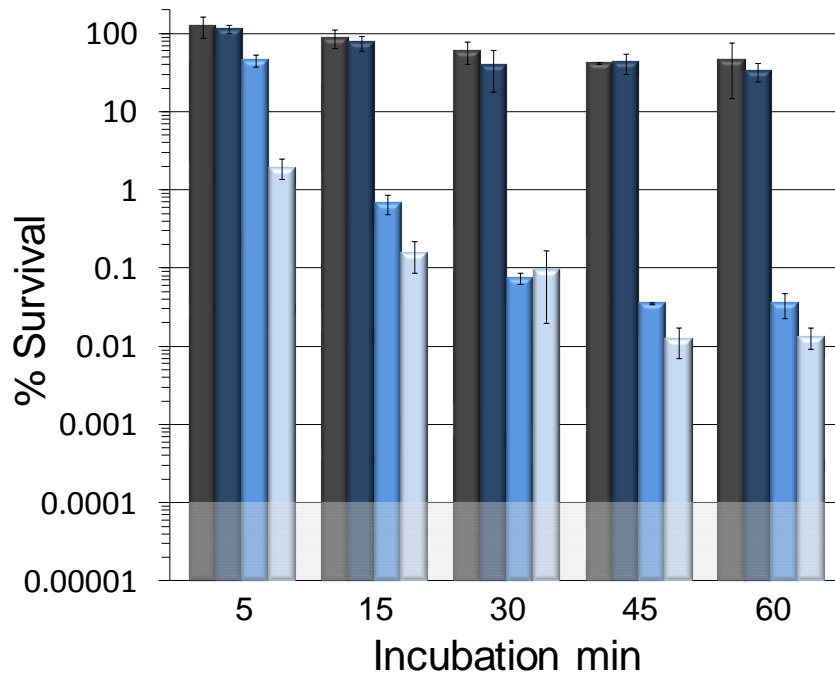
time was doubled to 30 minutes, only about 1% survival of *M. smegmatis* was observed even after 5 minutes incubation time ($P = 0.03$). For longer incubation times (≥ 45 minutes), doubling of the light dose resulted in slightly improved but statistically significant (0.5 log units, $P < 0.01$) lower survival rates.

Figure 4.10: Photodynamic inactivation of A) *E. coli*, B) *M. smegmatis* C) *S. aureus* using 20 μM CNC-Por (**4.4**) as the photosensitizer. The dark incubation time was varied over 5, 15, 30, 45 and 60 min. Displayed is the % survival in PBS buffered bacterial suspensions (■), CNC-Por dark control (■) and light treated samples after illumination times of 15 (■) or 30 (■) minutes (total fluences of 54, and 108 J/cm^2 , respectively, at 60 mW/cm^2). As the plating technique employed to determine % survival did not allow for detection of survival rates of $<0.0001\%$, data points below the detection limit are set to 0.0001% survival for graphing purposes. The shaded areas correspond to undetectable cell survival with the assay employed.

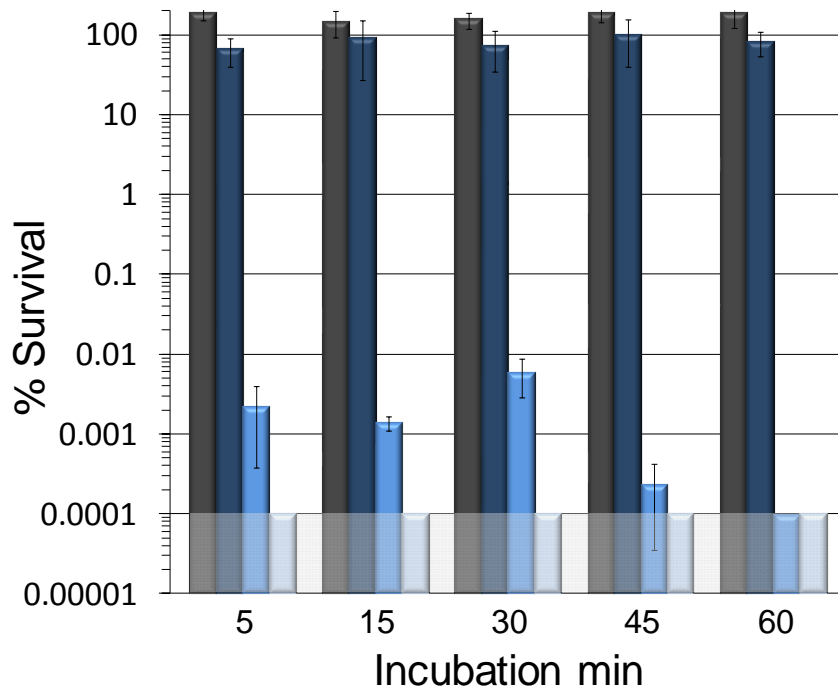
A) *E. coli*



B) *M. smegmatis*



C) *S. aureus*



For *M. smegmatis* a clear dependency of cell survival on the incubation time was apparent. This observation is unusual when compared to other studies with soluble photosensitizers. PS are thought to quickly bind to the bacterium, and therefore no differences in PDI for different incubation times are typically observed.^{18, 70-72}

Photodynamic inactivation of *S. aureus* using CNC-Por (**4.4**) was also found to be highly efficient (Figure 4.10 C). *S. aureus* is classified as a Gram-positive bacterium with an easily penetrated cell envelope lacking an outer cell membrane. Therefore, significant vulnerability to singlet oxygen and other reactive species produced in the photosensitizer mediated process was expected. *M. smegmatis* and *E. coli*, on the contrary, both contain an outer cell membrane for enhanced protection.⁷³⁻⁷⁵ At 20 μ M concentration of CNC-Por (**4.4**),

short incubation times of 5 to 15 minutes were sufficient for a viable cell reduction of an impressive 5 log units after 15 minutes illumination ($P = 0.003$). For all samples illuminated for 30 minutes, no CFUs were detected, and survival rates were therefore below the detection limit of $< 0.0001\%$.

Figure 4.11 describes the concentration dependence of the CNC-Por photosensitizer for *S. aureus* and *M. smegmatis* at fixed incubation (30 minutes) and illumination times (15 minutes). For *S. aureus*, a 5 log unit loss in viable cells was observed for concentrations as low as 10 μM ($P = 0.002$) of CNC-Por (**4.4**). At 5 μM of **4.4**, photodynamic inactivation dropped to a modest 90% reduction in viable cells ($P = 0.003$). For *M. smegmatis*, however, 20 μM of CNC-Por (**4.4**) appeared to be the necessary threshold concentration to obtain good inactivation under the illumination and incubation conditions examined. No killing of bacteria was observed for photosensitizer concentrations between 1-10 μM . No inactivation of *E. coli* was detected in the range of 1-10 μM of **4.4** under the conditions described (data not shown).

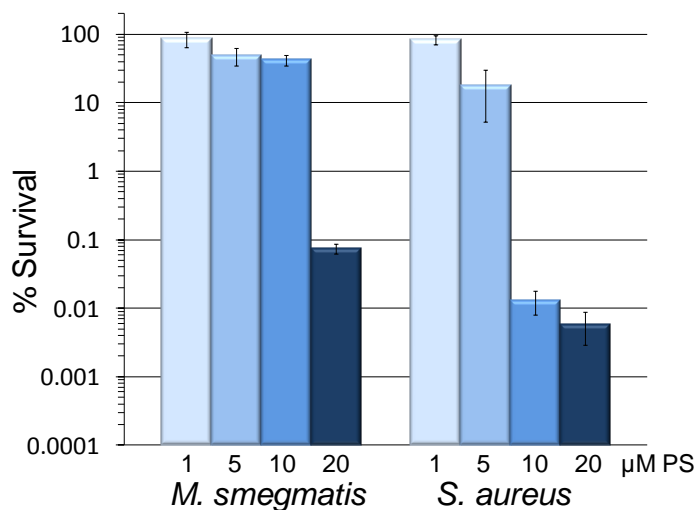


Figure 4.11: Concentration dependence of PDI for *M. smegmatis* and *S. aureus* using CNC-Por (4.4) at constant incubation (30 min) and illumination times (15 min).

Control experiments included monitoring of cell survival in PBS buffered solution in the dark (Figure 4.10 ■), PS treatment of the bacteria in the dark (Figure 4.10 ■), and light exposure of bacterial suspensions to azide surface-modified cellulose (Table 4.3).

Table 4.3: Light control experiments with azide surface-modified CNC-N₃ (4.3).^a

Bacterium	% Survival	
	15 min Illumination ^b	30 min Illumination ^b
<i>E. coli</i>	107.23 ± 13.29	80.75 ± 16.41
<i>M. smegmatis</i>	92.42 ± 11.50	100.53 ± 22.95
<i>S. aureus</i>	106.15 ± 26.03	74.25 ± 13.66

^a CNC concentration in control experiments was equivalent to 20 μM CNC-Por content for PDI experiments; ^b illumination with white light (400-700 nm, 60 mW/cm²).

As shown in Table 4.3 the presence of azide surface-modified cellulose nanocrystals **4.3** did not significantly affect the survival of any of the bacterial strains investigated after illumination for 15 or 30 minutes. Therefore, any loss in the viable cell count can be attributed to the photosensitizing action of the porphyrin incorporated into compound **4.4**, if the levels of unbound porphyrin impurity are negligible. The CNC-Por material used for photodynamic inactivation experiments presented in this chapter was carefully and extensively washed with DMF, 0.05 M acetic acid, ultrapure water and ethanol to remove any adventitiously bound ethynylphenyl porphyrin **3.1** from the cellulose-porphyrin conjugate (**4.4**). UV-visible spectroscopic analysis of the supernatant of the CNC-Por stock solution revealed the presence of dissolved porphyrin species of up to 88 nM based on a 20 μ M CNC-Por solution as used in PDI experiments. Table 4.4 lists the results of photodynamic inactivation of the water soluble ethynyl phenyl porphyrin **3.1** at 100 and 50 nM concentrations for comparison. Both *E. coli* and *S. aureus* are susceptible to significant photodynamic inactivation by **3.1** at 100 and 50 nM. *E. coli*, a Gram-negative bacterium, did display an impressive 3-4 log unit reduction in cell viability at 50 nM concentration of the PS after 30 minutes of illumination ($P < 0.001$). *S. aureus*, a Gram-positive bacterium with an easier to penetrate cell envelope compared to Gram-negative bacteria, displayed a 5 log unit reduction after 15 minutes, and a 6 log unit reduction after 30 minutes illumination at 50 nM concentration **3.1** ($P < 0.001$). Additionally, even at 10 nM **3.1** significant reduction in *S. aureus* was observed. However, *M. smegmatis* can only be inactivated by roughly 1 log unit at 100 nM concentration and 30 minutes illumination ($P < 0.001$). These data show that the

presence of unbound porphyrin in the CNC-Por stock solution needs to be carefully considered when evaluating the efficiency of CNC-Por (4.4) to inactivate bacteria.

Table 4.4: Results of PDI studies with the water soluble porphyrin 3.1 as a function of different bacteria, PS and light doses.

Bacterium	Concentration nM	% Survival ^{a, b}	
		15 min illumination	30 min illumination
<i>E. coli</i>	100	0.0021 ± 0.0015	0.0003 ± 0.0002
	50	24.65 ± 15.80	0.0644 ± 0.0582
<i>M. smegmatis</i>	100	46.64 ± 5.10	14.71 ± 4.72
<i>S. aureus</i>	100	0.0002 ± 0.0002	0.00009 ± 0.00009
	50	0.0006 ± 0.0003	0.00003 ± 0.00002
	10	0.14 ± 0.01	0.003 ± 0.001

^a Samples were incubated for 5 min in the dark before illumination; ^b illumination with white light (400-700 nm, 60 mW/cm²).

Discussion

Only a few examples of porphyrin-cellulose conjugates can be found in the literature. Most of these employed esterified cellulose as a backbone that can be cast into a plastic film with limited thermal stability.^{31, 32, 34, 76, 77} Krausz and coworkers have appended neutral, anionic and cationic porphyrins to cellulose esters as well as to cotton fabric, and were able to demonstrate photobactericidal activity of the materials.^{31, 32, 34, 78, 79} In our work, we chose crystalline nanocellulose as the polymeric backbone. Surface modification with porphyrins of crystalline cellulose has not yet been reported to the best of our knowledge. Cellulose

nanocrystals offer a particular degree of molecular control for precise functionalization due to their rigidity, defined surface structure and dimensions, all of which are not offered by cellulose esters. Further, cellulose nanocrystals are readily bio-degradable, and as a renewable resource provide an excellent starting material for the systematic investigation of cellulose-porphyrin conjugates and their interactions with microbes in order to develop new materials with photobactericidal activity.

Herein, we describe the successful synthesis, characterization and photodynamic inactivation study for the porphyrin-cellulose nanocrystalline conjugate **4.4** against three types of bacteria. We developed a synthetic strategy which produces cellulose nanocrystalline materials with covalently surface appended photosensitizers with potential use in papers or cotton fabrics for clothing, towels, lab coats, scrub suits or privacy drapes in hospitals. Specifically, the ethyne containing porphyrin **3.1** and azide surface modified cellulose **4.3** moieties were joined using the Cu(I)-catalyzed Huisgen's 1,3-dipolar cycloaddition. Using infrared and diffusion NMR spectroscopies, and supported by gel permeation chromatography and thermogravimetric analysis, the covalent linkage between the porphyrin and the cellulose was clearly demonstrated. The modular approach of the Click technology may enable appendage of an array of ethyne containing porphyrins to cellulose nanocrystals, and the resulting conjugates can consequently be screened for their ability to inactivate bacteria.

The porphyrin loading on the cellulose surface was determined from independent samples from the molecular mass increase measured by gel permeation chromatography of benzoyl-derivatized **4.4**, as well as by measurement of the zinc-ion content of **4.4** by atomic

absorption spectroscopy. The loading was found to be in the range of one porphyrin molecule per 15-20 glucose units. Consequently, the maximum degree of substitution with porphyrin based on the surface available hydroxyl groups was calculated as $DS = 0.07$. Based upon the azide surface modification of $DS = 0.14$, about 50% of all azide groups successfully reacted with the porphyrin **3.1**, explaining the residual azide band observed in the IR spectrum of **4.4** (Figure 4.4). Possible explanations for the partial substitution include CNC aggregation during the Click reaction, which would leave some sites inaccessible for reaction, or a steric argument where surface-crowding, exacerbated by the electrostatic repulsion between the positively charged porphyrin moieties, results in the incomplete reaction of the azide groups. Strategies for increased surface loading could involve spacer units, thereby imparting the conjugated molecules more spatial flexibility. The spacer could be incorporated in the porphyrin as a longer chain tether with terminal alkyne, or as a tether with a terminal azide linked to the cellulose surface. In a related system, Krausz and coworkers observed increased porphyrin loadings for porphyrin-cellulose-laurate esters if a spacer of 11 carbons instead of 4 were installed on the porphyrin (estimated as $DS = 0.19$, however not a surface reaction).³²

Our photodynamic inactivation experiments show potential of **4.4** as a photosensitizer on solid support. The degree of bacterial inactivation varied vastly over the conditions and the three different classes of bacteria [*E. coli* (Gram-negative), *S. aureus* (Gram-positive) and *M. smegmatis* (mycobacterium)] investigated. PS mediated inactivation was observed ranging from 2 log units reduction for *E. coli* (60 min incubation, 30 min illumination, 99% cell loss, $P = 0.05$) to 6 log units reduction for *S. aureus* (5 min incubation, 30 min illumination, 99.9999% cell loss, $P = 0.03$). Compared to using dissolved PS for

photodynamic inactivation experiments, a 100-500 fold increase in porphyrin concentration was needed in order to affect photodynamic inactivation with the insoluble compound **4.4** (also see Chapter 3).⁸⁰ Nevertheless, this supports the idea that direct binding and uptake of the photosensitizer are not necessary for photodynamic inactivation, and that the production of singlet oxygen in close proximity to the bacteria can also result in cellular death.²³⁻²⁵ *S. aureus* seemed to be the most susceptible bacterium for photodynamic inactivation, which is plausible considering the comparably permeable cell wall of Gram-positive bacteria.⁸¹ Even lowering of the concentration to 5 μM porphyrin on **4.4** still allowed ~ 1 log inactivation after incubation and illumination for 15 minutes each ($P = 0.003$). The highest viable cell loss observed for *E. coli*, for comparison, was only about 99% ($P = 0.05$). We suggest that the additional permeation barrier (outer cell membrane) of this Gram-negative bacterium is responsible for the much lower inactivation rates observed.⁷³ Although *M. smegmatis* does retain the Gram stain and therefore should be considered Gram-positive, the mycobacterial cell envelope contains elements of both Gram-positive and negative bacteria.⁷⁴ In addition, genome analysis indicates that mycobacteria might be more closely related to Gram-negative rather than Gram-positive bacteria.⁷⁵ Regardless, the unusually low cell wall permeability is undisputed and is the major reason for the relatively high resistance of mycobacteria to dry conditions, alkali, chemical disinfectants, therapeutic agents and their remarkable ability to survive these hostile conditions.^{74, 82} Despite the impermeable cell wall, we report here efficient inactivation of *M. smegmatis* with **4.4** at 20 μM concentration (based upon the porphyrin content). We even observed significantly improved (1-2 log units depending on the conditions) inactivation when compared to *E. coli*. Further, a dependence of the degree of

cell survival on the dark incubation time is apparent for *M. smegmatis*. Generally, it is agreed that the incubation time for standard dissolved PS does not influence the degree of bacterial inactivation because binding of the PS to the bacterial cell is fast.^{18, 70-72} Therefore, our finding is unusual and might be explained with the possible presence of endogenous mycobacterial cellulases. Cellulases are enzymes that hydrolyse cellulose.⁸³⁻⁸⁶ Among this enzyme class are endoglucanases, which are capable of interrupting the hydrogen-bonding network of crystalline cellulose leading to the separation of the individual cellulose strands, by contrast, exoglucanases hydrolyse the cellulose strands into smaller units of 2-4 glucose molecules. Whereas functional cellulases have been discovered in *Mycobacterium tuberculosis*,⁸⁷ a gene encoding functional cellulases has been identified for *M. smegmatis* (strain mc² 155) and other mycobacteria.⁸⁸ If *M. smegmatis* expresses extracellular cellulases, these enzymes might be able to partially degrade the photosensitizer **4.4** releasing smaller soluble units into the medium, which could be responsible for the observed increase of photodynamic inactivation with prolonged incubation times. Similar incubation time dependencies were not clearly observed when analyzing the PDI data for *E. coli* and *S. aureus* (Figure 4.10 A and C). Currently, we cannot exclude that similar incubation time dependencies exist at higher concentrations of **4.4** for *E. coli* and lower concentrations for *S. aureus*. However, to the best of our knowledge, *E. coli* and *S. aureus* are not known to express cellulases. More detailed studies are currently under way in our laboratory to address these questions.

Control experiments with the soluble porphyrin **3.1** (Table 4.4) indicate that levels of > 100 nM for *M. smegmatis*, 50 nM for *E. coli* and 10 nM for *S. aureus* in solution would

significantly reduce the viable cell count. Therefore, the presence of unbound porphyrin does need to be addressed when evaluating the data shown in Figure 4.10. UV-visible spectroscopic analysis of the supernatant of the CNC-Por (**4.4**) stock solution used in PDI experiments isolated by centrifugation (16,000 x g, 30 min) showed the presence of dissolved porphyrin species. According to this analysis, at most 88 nM porphyrin species were present in the supernatant in a typical PDI experiment, part of which could be attributed to unbound porphyrin. By comparison, 100 nM of **3.1** caused a reduction in viable cells of less than 1 log unit against *M. smegmatis*, while at 20 μ M CNC-Por (**4.4**) caused reductions in viable cells of up to 3-4 log units. Therefore, we can exclude unbound porphyrin to significantly contribute to the cell loss. For *E. coli*, we expect > 3 log units of inactivation (30 minutes illumination) if CNC-Por (**4.4**) indeed was contaminated with 50-100 nM of **3.1**, but photodynamic inactivation with 20 μ M **4.4** was \leq 2 log units. Consequently, we conclude that levels of unbound porphyrin contamination must be below 50 nM, and the porphyrin species detected in the supernatant are most likely due to small crystals of **4.4** that did not separate under the centrifugation conditions used. *S. aureus* is extremely sensitive to photodynamic inactivation with **3.1** (compare to Chapter 3). Even at 10 nM **3.1** viable cell loss of 3 log units (15 minutes illumination) were observed. In this case, we cannot exclude the possibility that < 50 nM of **3.1** contributed to the loss in cell viability observed during photodynamic inactivation with **4.4**.

In conclusion, we have developed a synthetic route for surface modification of cellulose nanocrystals with porphyrins using Click chemistry. The benchmark compound CNC-Por (**4.4**) was characterized by infrared and PFGSE-¹H-NMR spectroscopies of the

acetylated derivative as well as GPC analysis of the benzoylated derivative and TGA as proof of the covalent linkage between porphyrin and the cellulose polymer. Promising results were obtained in our investigation of the ability of **4.4** to photoinactivate bacteria. Three genera of bacteria, *S. aureus* (Gram-positive), *E. coli* (Gram-negative) and *M. smegmatis* (mycobacterium), were investigated. Five-six log unit reductions in viable cells were observed against *S. aureus*, 3-4 log units for *M. smegmatis* and 1-2 log units for *E. coli* using CNC-Por (**4.4**) in suspension at 20 μ M solution (based on the porphyrin concentration). Future studies will investigate the interaction between the porphyrin-cellulose photosensitizer and microbes in order to design PSs for use in photobactericidal materials. With cellulose as a bio-degradable as well as renewable resource along with the defined character and molecular control exhibited by the nanocrystalline cellulose surface, we anticipate value in the development of cellulose-porphyrin based conjugates for use in photobactericidal papers, fabrics and coatings for application in the healthcare and food preparation industries.

Experimental Methods

Materials and Methods. Buffer salts were purchased from Fisher Scientific, Middlebrook 7H9 Agar and 7H10 broth from BD Difco, LB broth Miller from EMD Chemicals and Tryptic Soy broth from Teknova. Unless otherwise specified, all other chemicals were obtained from commercial sources in the highest purity available. Ultra pure water used for all media and buffers was provided by an Easypure II system (Barnstead). UV-vis absorption measurements were performed on a Varian Cary 50 Bio instrument or a

Genesys 10 uv scanning UV-vis instrument from Thermo Electron Corp for single wavelength measurements. All procedures were carried out under commonly practiced sterile techniques. A Perkin Elmer Model 3110 atomic absorption spectrometer was used for determination of the Zn ion content of **4.4**. FTIR spectra were measured on a Thermo Nicolet NEXUS 670 FT-IR spectrophotometer. Spectra in the range of 4000-650 cm^{-1} were obtained with a resolution of 4 cm^{-1} by accumulating 64 scans. Thermal decomposition temperatures were determined using a TA Instrument TGAQ500 ramping 10 $^{\circ}\text{C}/\text{min}$ under N_2 purging. CNC samples were dried using a lyophilizing system from Labconco (Kansas City, Mo, USA). For Transmission Electron Microscopy (TEM), a suspension (0.01% w/v in water) of cellulose nanocrystals were deposited as drops on carbon-coated electron microscope grids, negatively stained with uranyl acetate and allowed to dry. The grids were observed with a Philips 400T microscope operated at an accelerating voltage of 120 kV.

Formation of Cellulose Nanocrystals (4.1). The cellulose nanocrystals were formed by acidic hydrolysis as reported in the literature.^{38, 89, 90} 2.0 g of cellulose pulp were obtained from Whatman #1 filter paper (98% α -cellulose, 80% crystallinity) and blended in a 10 Speed Osterizer[®] Blender. Hydrolysis of the resulting pulp was achieved after 3 hours at 100 $^{\circ}\text{C}$ using 100 mL of 2.5 M HBr and intermittent ultrasonication (5 min per hour, 50% power, Omni Ruptor 250 W ultrasonic homogenizer). After dilution with deionized water, the mixture was subjected to five washing/centrifugation cycles (5000 x g, 10 min, IEC Centra-CL3 Series) to remove excess acid and water soluble fragments. Once pH 4-5 was reached, the fine cellulose particles started to disperse into the aqueous supernatant. The polydisperse

cellulose contained in the turbid supernatant was collected and subjected to centrifugation at 15,000 x g for 60 min in a Sorvall[®] Superspeed centrifuge in order to remove ultra-fine particles. The sediment containing CNC with an average length of 100-400 nm was dried using a lyophilizing system.

Surface tosylation of CNC (4.2). Surface tosylated CNC was synthesized analogous to the method described by Rahn et al.⁹¹ 0.5 g of CNC (3.1 mmol glucosyl units) was suspended in pyridine (10 mL) and the mixture was cooled to 10 °C. Tosyl chloride (0.9 g, 5 mmol) was then added, and the reaction mixture was stirred for 2 days at room temperature. Addition of 100 mL ethanol to the reaction mixture resulted in a precipitate that was collected by filtration. The product was washed with ethanol (50 mL) and deionized water (50 mL) five times each, and freeze-dried, yielding **4.2**.

Surface azide bearing CNC-N₃ (4.3). Synthesis of the azide surface modified CNC (**4.3**) was conducted according to literature procedures with some modifications.^{43, 53, 92} 400 mg tosylated CNC was suspended in 20 mL of DMF, followed by careful addition of 400 mg sodium azide. The reaction mixture was stirred at 100 °C for 24 h. After precipitation through addition of 50 mL of deionized water and centrifugation, the product was washed five times with ethanol (50 mL) and five times with deionized water (50 mL). The resulting CNC-N₃ (**4.3**) was dialyzed against deionized water for 3 days and consequently freeze-dried. The degree of substitution was calculated from the elemental analysis (C 41.06%, H 6.35%, O 48.84%, N 3.75%) DS = 0.14.

Click reaction of CNC-N₃ (4.3) with porphyrin 3.1. Conditions for the Click reaction were adjusted from the literature.^{40, 53, 93, 94} 400 mg of CNC-N₃ (**4.3**) and 400 mg of porphyrin

3.1 were mixed in 30.0 mL of DMF (99.5% purity). Next, a mixture of 30 mg CuBr₂, 70 mg of ascorbic acid and 200 µl triethylamine in 1 mL DMF were added, and the reaction mixture was stirred vigorously for 5 min at room temperature, followed by stirring at 60 °C for 36 hours. The product was isolated by centrifugation and washed 3 times with ethanol and 3 times with water. For the photodynamic inactivation studies the final product was extensively washed to remove any unreacted porphyrin **3.1**, and isolated by 60 min centrifugation at 12,000 x g: 4 times with DMF, 3 times with 0.05 M acetic acid, 4 times with water and 3 times with ethanol. After washing, the CNC-Por (**4.4**) product was freeze-dried.

Acetylation of CNC-N₃ (4.3) and CNC-Por (4.4). For the PFGSE-NMR experiments, samples of CNC-N₃ (**4.3**) and CNC-Por (**4.4**) were acetylated to generate DMSO-soluble derivatives according to literature procedure with minor modification.⁹⁵⁻⁹⁷ 100 mg of the CNC-derivative was dissolved in 3 g 1-allyl-3-methylimidazolium chloride (about 3% w/w) at 80 °C for 12 hours. 315 µl acetic anhydride (5 mol/mol anhydrous glucose units) was added to the solution and the mixture was stirred for 2 h at 80 °C. The product was precipitated by addition of 30 mL deionized water and washed 7 times with water. The CNC-derivative was obtained after freeze-drying and residual water was removed under high vacuum.

Benzoylation of CNC compounds 4.3 and 4.4. 50 mg of the CNC compound **4.3** or **4.4** was dissolved in 1-allyl-3-methylimidazolium chloride (950 mg) in a 15 mL flask by first thoroughly dispersing the sample, followed by heating at 80 °C with magnetic stirring until the solution was transparent (about 4 hrs). Pyridine (330 µL, 3.7 mmol) was added, and the mixture was homogenized to form a uniform paste before being allowed to cool to room

temperature. Benzoyl chloride (380 μL , 3.3 mmol) was then added in one portion and the sample stirred for 3 hours at room temperature. The benzoylated product was precipitated by addition of a 1:3 mixture of deionized water and EtOH by vigorous stirring for 5 minutes, after which the precipitate was collected by filtration using a medium porosity sintered funnel. The collected product was washed with EtOH and triturated with MeOH at room temperature for 18 hours. The final products were collected by filtration and dried under vacuum to yield a green powder.

Gel permeation chromatography. GPC analysis was carried out with a Waters model ALC/GPC 204 (Waters Associates, Milford, MA) and 510 pump equipped a UV detector (210 nm). The analysis was conducted at 40 $^{\circ}\text{C}$ using THF as the eluent at a flow rate of 0.7 mL/min. 200 μL of a 1 mg/mL solution of the analyte in THF was injected onto two Ultrastragel columns (Styragel HR 1 and Styragel HR 5E, Waters) connected in series for analysis. Standard mono-disperse polystyrenes (molecular weight ranges from 0.82 to 1860 kg/mol) were used for calibration. The number- (M_n) and weight (M_w) average molecular weights were calculated using the Millenium 32 software.

Determination of porphyrin loading by atomic absorption. Atomic absorption was used to determine the concentration of Zn ions in samples of CNC-Por (**4.4**), which is equivalent to the porphyrin loading if complete metallation of the porphyrin is assumed. About 10 mg of thoroughly washed and lyophilized CNC-Por (**4.4**) was suspended in 10 mL 1 mol/L HCl in a volumetric flask. The solution was heated to 60 $^{\circ}\text{C}$ for 2 hours resulting in demetallation of the porphyrin. The zinc ion concentration was determined using the standard addition method: To each sample for the calibration curve (range of 0.01 mmol/L to 0.1

mmol/L Zn(OAc)₂ in 1 mol/L HCl) 1 mL of the demetallated CNC-Por stock solution was added for a total volume of 10 mL. Under these conditions, the response of the atomic absorption instrument containing a Zn lamp operated at 10 mA was linear. The zinc ion concentration of the sample was calculated from the Y-intercept and the slope of the calibration curve. Typical porphyrin loadings were in the range of ~0.2 μmol porphyrin/mg of CNC-Por (4.4). Determination of the Zn content was done in triplicate for each batch of 4.4 synthesized.

Pulsed-Field-Gradient, Spin-Echo NMR Spectroscopy.^{59, 98} Modification of the glucose-OH groups by acetylation rendered the CNC-Por compound sufficiently soluble in DMSO-*d*₆ to conduct NMR spectroscopic studies. Spectra were obtained at 25 °C on a Bruker Avance 500 MHz spectrometer (1996) with an Oxford Narrow Bore Magnet (1989), Dell Host Workstation and Red Hat Linux operation system with Topspin 2.1 software. The instrument is equipped with three-channel gradient control (GRASPIII), variable-temperature-, pre-cooling-, temperature stabilization- as well as three frequency channels with waveform memory and amplitude shaping units. ¹H-NMR diffusion measurements were conducted with a 5 mm triple axis gradient probe (ID500-5EB, Nalorac Cryogenic Corp) equipped with actively shielded gradient coils. The gradient strength was calibrated using literature values for water diffusion in ¹H₂O/²H₂O mixtures. The longitudinal eddy current (LED) pulse sequence was used in all diffusion experiments.^{61, 99} Ten gradient experiments were acquired for each dataset. The gradient strength was adjusted linearly from 5.3 to 47.7 G/cm and applied in y-direction while all other delays were held constant. The gradient pulse interval Δ was 10 ms, the gradient duration δ 5 ms with a recovery time of 6 ms. Acquisition

temperature was 24.5 °C. The attenuation of the signal intensities derived from the peak height of each experiment was used to generate Stejskal-Tanner plots to determine the diffusion coefficients. Diffusion coefficients were estimated by least square regression.

Photosensitizer stock solution. 1 mM stock solutions of photosensitizers in filter-sterilized ultrapure water were prepared based on the porphyrin content determined by atomic absorption spectroscopy in the case of **4.4**, and stored in the dark at -80 °C.

Bacterial strains and growth conditions. The bacterial strains *Mycobacterium smegmatis* mc² 155 (donated by Prof. William Jacobs, Albert Einstein College of Medicine, USA), *Escherichia coli* BL21(Dε3)pLysS (Stratagene, USA) and *Staphylococcus aureus* 29213 (donated by Prof. Christian Melander, North Carolina State University, USA) were used in this study. *M. smegmatis* was grown in 5 mL cultures in Middlebrook 7H9 media with ADS and 100 µg/mL cycloheximide as the antibiotic.¹⁰⁰ *E. coli* was cultured in LB broth Miller with 50 µg/mL chloramphenicol and 100 µg/mL ampicillin. *S. aureus* was grown in 5 mL cultures in Tryptic Soy Broth without antibiotics. The cells were incubated at 37 °C on an orbital shaker (500 rpm) until an optical density (OD₆₀₀) of 0.65-0.70 (*M. smegmatis* and *S. aureus*) or 0.33-0.40 (*E. coli*) at 600 nm, corresponding to a concentration of 1-3 10⁸ CFU/mL, was reached.

Incubation of cells with photosensitizer. The 5 mL culture with a concentration of 1-3 10⁸ CFU/mL was pelleted by centrifugation (10 min, 3716 x g) at room temperature, the supernatant discarded, and the cells were resuspended in a total volume of 5 mL PBS (170 mM NaCl, 3.4 mM KCl, 10.0 mM Na₂HPO₄, 1.8 mM KH₂PO₄, pH 7.2 with additional

0.05% Tween 80) and the appropriate volume of the photosensitizer stock solution. The cells were incubated between 5 and 60 minutes in the dark and agitated by a Vortex set to the lowest speed.

Illumination of cells. All photosensitization experiments were performed using a noncoherent light source, PDT light model LC122 (LumaCare, USA), and the fluence rate was measured with an Orion power meter (Orphir Optronics Ltd., Israel). 1 mL aliquots of the cell suspension in PBS were added to a sterile 24 well plate (BD Falcon, flat bottom) and illuminated with visible light (400-700 nm) with a fluence rate of 60 mW/cm² for the duration of 15 or 30 minutes (corresponding to fluences of 54 or 108 J/cm²) while magnetically stirred. 0.05% Tween-80 in the buffer was important to prevent excessive aggregation of the PS during the illumination process. After illumination, an aliquot was used for viability assays. All experiments were conducted in triplicate at a minimum.

Cell survival assay. 40 µL from the illuminated cell suspension was 1:10 serially diluted six times and plated on square plates (Middlebrook 7H10-ADS solid media for *M. smegmatis*, LB Broth Miller-Agar plates for *E. coli* and Tryptic Soy Broth-Agar plates for *S. aureus*) as described by Jett and coworkers.¹⁰¹ The plates were incubated at 37 °C in the dark for 48-60 h (*M. smegmatis*) or overnight (*E. coli* and *S. aureus*). The survival rate was determined from the ratio of CFU/mL of the illuminated solution and the dark control. Due to the plating technique employed, a maximum of a 6 log unit change in CFU/mL corresponding to ≥ 100 CFU/mL could be detected for an initial concentration of $1 \cdot 10^8$ CFU/mL. Survival rates of $< 0.0001\%$ could not be detected. The percentage of survival for samples for which the corresponding plates did not show any colonies was set to the

detection limit of 0.0001%. Samples with photosensitizer present but kept in the dark (dark control) and illuminated samples with CNC-N₃ (**4.3**) present (light control) served as controls. Statistical significance was assessed via a two-tailed, unpaired Student's t-test.

Acknowledgements

We would like to thank Prof. Dimitris S. Argyropoulos and Dr. Hasan Sadeghifar for fruitful collaboration on this project. Further, we thank Dr. Hanna S. Gracz for assistance with the PFGSE-NMR experiments.

REFERENCES

1. Klevens, R. M.; Edwards, J. R.; Richards, C. L.; Horan, T. c.; Gaynes, R. P.; Pollock, D. A.; Cardo, D. M., Estimating Health care-associated Infections and Deaths in U.S. Hospitals, 2002. In Prevention, C. f. D. C. a., Ed. Centers for Disease Control and Prevention: 2007; Vol. 122, pp 160.
2. Scott, R. D., The direct medical costs of healthcare-associated infections in U.S. hospitals and the benefits of prevention. In *Center for Disease Control and Prevention*, Centers for Disease Control and Prevention: 2009.
3. Sauvet, G.; Fortuniak, W.; Kazmierski, K.; Chojnowski, J., Amphiphilic block and statistical siloxane copolymers with antimicrobial activity. *Journal of Polymer Science Part A: Polymer Chemistry* **2003**, 41, (19), 2939.
4. Vigo, T. L., Advances in Antimicrobial Polymers and Materials. In *Biotechnology and Bioactive Polymers*, Gebelein, C. G.; Carraher, C. E., Eds. Plenum Press: New York, 1994; p 225.
5. Kenawy, E.-R.; Abdel-Hay, F. I.; El-Shanshoury, A. E.-R. R.; El-Newehy, M. H., Biologically active polymers. V. Synthesis and antimicrobial activity of modified poly(glycidyl methacrylate-co-2-hydroxyethyl methacrylate) derivatives with quaternary ammonium and phosphonium salts. *Journal of Polymer Science Part A: Polymer Chemistry* **2002**, 40, (14), 2384.
6. Kurt, P.; Wood, L.; Ohman, D. E.; Wynne, K. J., Highly Effective Contact Antimicrobial Surfaces via Polymer Surface Modifiers. *Langmuir* **2007**, 23, (9), 4719.
7. Cen, L.; Neoh, K. G.; Kang, E. T., Surface Functionalization Technique for Conferring Antibacterial Properties to Polymeric and Cellulosic Surfaces. *Langmuir* **2003**, 19, (24), 10295.
8. Krishnan, S.; Ward, R. J.; Hexemer, A.; Sohn, K. E.; Lee, K. L.; Angert, E. R.; Fischer, D. A.; Kramer, E. J.; Ober, C. K., Surfaces of fluorinated pyridinium block copolymers with enhanced antibacterial activity. *Langmuir* **2006**, 22, (26), 11255.
9. Viscardi, G.; Quagliotto, P.; Barolo, C.; Savarino, P.; Barni, E.; Fiscaro, E., Synthesis and surface and antimicrobial properties of novel cationic surfactants. *Journal of Organic Chemistry* **2000**, 65, (24), 8197.

10. Kanazawa, A.; Ikeda, T., Multifunctional tetracoordinate phosphorus species with high self-organizing ability. *Coordination Chemistry Reviews* **2000**, 198, (1), 117.
11. Liang, J.; Chen, Y.; Ren, X.; Wu, R.; Barnes, K.; Worley, S. D.; Broughton, R. M.; Cho, U.; Kocer, H.; Huang, T. S., Fabric Treated with Antimicrobial N-Halamine Epoxides. *Industrial & Engineering Chemistry Research* **2007**, 46, (20), 6425.
12. Eknoian, M. W.; Worley, S. D.; Bickert, J.; Williams, J. F., Novel antimicrobial N-halamine polymer coatings generated by emulsion polymerization. *Polymer* **1999**, 40, (6), 1367.
13. Bromberg, L.; Hatton, T. A., Poly(N-vinylguanidine): Characterization, and catalytic and bactericidal properties. *Polymer* **2007**, 48, (26), 7490.
14. Vigo, T. L., Manmade fibers: their origin and development. In *Manmade fibers: their origin and development*, Seymour, R. B.; Porter, R. S., Eds. Elsevier: Amsterdam, 1992; p 214.
15. Seymour, R. B.; Porter, R. S., Manmade fibers: their origin and development. **1993**.
16. Estevao, L. R. M.; Mendonca-Hagler, L. C. S.; Nascimento, R. S. V., Development of Polyurethane Antimicrobial Composites Using Waste Oil Refinery Catalyst. *Industrial & Engineering Chemistry Research* **2003**, 42, (24), 5950.
17. Ignatova, M.; Labaye, D.; Lenoir, S.; Strivay, D.; Jerome, R.; Jerome, C., Immobilization of Silver in Polypyrrole/Polyanion Composite Coatings: Preparation, Characterization, and Antibacterial Activity. *Langmuir* **2003**, 19, (21), 8971.
18. Jori, G., Inactivation of Pathogenic Microorganisms by Photodynamic Techniques: Mechanistic Aspects and Perspective Applications. *Anti-Infective Agents in Medicinal Chemistry* **2007**, 6, (2), 119.
19. Macdonald, I. J.; Dougherty, T. J., Basic principles of photodynamic therapy. *Journal of Porphyrins and Phthalocyanines* **2001**, 5, 105.
20. Bonnett, R., *Chemical aspects of photodynamic therapy*. Gordon and Breach Science Publishers: Amsterdam, The Netherlands, 2000.
21. Merkel, P. B.; Kearns, D. R., Radiationless decay of singlet molecular oxygen in solution. Experimental and theoretical study of electronic-to-vibrational energy transfer. *Journal of the American Chemical Society* **1972**, 94, (21), 7244.
22. Kummler, R. H.; Bortner, M. H., Production and Destruction Mechanism for O₂ (1δg) in the lower atmosphere. *Annals of the New York Academy of Sciences* **1970**, 171, (1), 273.

23. Midden, W. R.; Wang, S. Y., Singlet oxygen generation for solution kinetics: clean and simple. *Journal of the American Chemical Society* **1983**, 105, (13), 4129.
24. Bezman, S. A.; Burtis, P. A.; Izod, T. P. J.; Thayer, M. A., Photodynamic Inactivation of *E. coli* by Rose Bengal immobilized on Polystyrene Beads. *Photochemistry and Photobiology* **1978**, 28, (3), 325.
25. Dahl, T. A.; Robert Midden, W.; Hartman, P. E., Pure Singlet Oxygen Cytotoxicity for Bacteria. *Photochemistry and Photobiology* **1987**, 46, (3), 345.
26. Lucas, R.; Granet, R.; Sol, V.; Morvan, C. L.; Policar, C.; Riviere, E.; Krausz, P., Synthesis and cellular uptake of superparamagnetic dextran-nanoparticles with porphyrinic motifs grafted ob esterification. *e-Polymers* **2007**, 089.
27. Carvalho, C. M. B.; Alves, E.; Costa, L.; Tome, J. P. C.; Faustino, M. A. F.; Neves, M. G. P. M. S.; Tome, A. C.; Cavaleiro, J. A. S.; Almeida, A.; Cunha, A.; Lin, Z.; Rocha, J., Functional Cationic Nanomagnet - Porphyrin Hybrids for the Photoinactivation of Microorganisms. *ACS Nano* **2010**, 4, (12), 7133.
28. Wilson, M., Light-Activated Antimicrobial Coating for the Continuous Disinfection of Surfaces. *Infection Control and Hospital Epidemiology* **2003**, 24, (10), 782.
29. Sherrill, J.; Michielsen, S.; Stojiljkovic, I., Grafting of light-activated antimicrobial materials to nylon films. *Journal of Polymer Science Part A: Polymer Chemistry* **2003**, 41, (1), 41.
30. Bonnett, R.; Buckley, D. G.; Burrow, T.; Galia, A. B. B.; Saville, B.; Songca, S. P., Photobactericidal materials based on porphyrins and phthalocyanines. *Journal of Materials Chemistry* **1993**, 3, (3), 323.
31. Krouit, M.; Granet, R.; Krausz, P., Photobactericidal plastic films based on cellulose esterified by chloroacetate and a cationic porphyrin. *Bioorganic & Medicinal Chemistry* **2008**, 16, (23), 10091.
32. Krouit, M.; Granet, R.; Krausz, P., Photobactericidal films from porphyrins grafted to alkylated cellulose - synthesis and bactericidal properties. *European Polymer Journal* **2009**, 45, (4), 1250.
33. Bonnett, R.; Krysteva, M. A.; Lalov, I. G.; Artarsky, S. V., Water disinfection using photosensitizers immobilized on chitosan. *Water Research* **2006**, 40, (6), 1269.
34. Krouit, M.; Granet, R.; Branland, P.; Verneuil, B.; Krausz, P., New photoantimicrobial films composed of porphyrinated lipophilic cellulose esters. *Bioorganic & Medicinal Chemistry Letters* **2006**, 16, (6), 1651.

35. French, A. D.; Bertoniere, N. R.; Brown, R. M.; Chanzy, H.; Gray, D.; Hattori, K.; Glasser, W., *Kirk-Othmer Encyclopedia of Chemical Technology*. 5th ed.; John Wiley & Sons, Inc.: New York, 2004; Vol. 5.
36. Habibi, Y.; Lucia, L. A.; Rojas, O. J., Cellulose Nanocrystals: Chemistry, Self-Assembly, and Applications. *Chemical Reviews* **2010**, 110, (6), 3479.
37. Ranby, B. G., Fibrous macromolecular systems. Cellulose and muscle. The colloidal properties of cellulose micelles. *Discussions of the Faraday Society* **1951**, 11, 158.
38. Filpponen, I.; Argyropoulos, D. S., Regular Linking of Cellulose Nanocrystals via Click Chemistry: Synthesis and Formation of Cellulose Nanoplatelet Gels. *Biomacromolecules* **2010**, 11, (4), 1060.
39. Rostovtsev, V. V.; Green, L. G.; Fokin, V. V.; Sharpless, K. B., A Stepwise Huisgen Cycloaddition Process: Copper(I)-Catalyzed Regioselective 'Ligation' of Azides and Terminal Alkynes. *Angewandte Chemie International Edition* **2002**, 41, (14), 2596.
40. Tornøe, C. W.; Christensen, C.; Meldal, M., Peptidotriazoles on Solid Phase: [1,2,3]-Triazoles by Regiospecific Copper(I)-Catalyzed 1,3-Dipolar Cycloadditions of Terminal Alkynes to Azides. *Journal of Organic Chemistry* **2002**, 67, (9), 3057.
41. Vitz, J.; Erdmenger, T.; Schubert, U. S., Imidazolium Based Ionic Liquids as Solvents for Cellulose Chemistry. In *Cellulose Solvents: For Analysis, Shaping and Chemical Modification*, American Chemical Society: Vol. 1033, pp 299.
42. Swatloski, R. P.; Spear, S. K.; Holbrey, J. D.; Rogers, R. D., Dissolution of Cellulose with Ionic Liquids. *Journal of the American Chemical Society* **2002**, 124, (18), 4974.
43. Heinze, T.; Liebert, T., Unconventional methods in cellulose functionalization. *Progress in Polymer Science* **2001**, 26, (9), 1689.
44. Liebert, T.; Hänsch, C.; Heinze, T., Click Chemistry with Polysaccharides. *Macromolecular Rapid Communications* **2006**, 27, (3), 208.
45. Lahann, J., *Click Chemistry for Biotechnology and Material Science*. Wiley: Chichester, West Sussex, 2009.
46. Cimolai, N., MRSA and the environment: implications for comprehensive control measures. *European journal of clinical microbiology & infectious diseases: official publication of the European Society of Clinical Microbiology* **2008**, 27, (7), 481.
47. Neely, A. N.; Maley, M. P., Survival of Enterococci and Staphylococci on Hospital Fabrics and Plastic. *Journal of Clinical Microbiology* **2000**, 38, (2), 724.

48. Filpponen, I. The synthetic Strategies for Unique Properties in Cellulose Nanocrystals Materials. North Carolina State University, Raleigh, 2009.
49. Sugiyama, J.; Vuong, R.; Chanzy, H., Electron diffraction study on the two crystalline phases occurring in native cellulose from an algal cell wall. *Macromolecules* **1991**, 24, (14), 4168.
50. Elazzouzi-Hafraoui, S.; Nishiyama, Y.; Putaux, J.-L.; Heux, L.; Dubreuil, F.; Rochas, C., The Shape and Size Distribution of Crystalline Nanoparticles Prepared by Acid Hydrolysis of Native Cellulose. *Biomacromolecules* **2007**, 9, (1), 57.
51. Okita, Y.; Saito, T.; Isogai, A., Entire Surface Oxidation of Various Cellulose Microfibrils by TEMPO-Mediated Oxidation. *Biomacromolecules* 11, (6), 1696.
52. Nishiyama, Y.; Langan, P.; Chanzy, H., Crystal Structure and Hydrogen-Bonding System in Cellulose I β from Synchrotron X-ray and Neutron Fiber Diffraction. *Journal of the American Chemical Society* **2002**, 124, (31), 9074.
53. Zhang, J.; Xu, X.-D.; Wu, D.-Q.; Zhang, X.-Z.; Zhuo, R.-X., Synthesis of thermosensitive P(NIPAAm-co-HEMA)/cellulose hydrogels via "click" chemistry. *Carbohydrate Polymers* **2009**, 77, (3), 583.
54. Hasegawa, T.; Umeda, M.; Numata, M.; Li, C.; Bae, A.-H.; Fujisawa, T.; Haraguchi, S.; Sakurai, K.; Shinkai, S., 'Click chemistry' on polysaccharides: a convenient, general, and monitorable approach to develop (1 \rightarrow 3)- β -D-glucans with various functional appendages. *Carbohydrate Research* **2006**, 341, (1), 35.
55. Iha, R. K.; Wooley, K. L.; Nystrom, A. M.; Burke, D. J.; Kade, M. J.; Hawker, C. J., Applications of Orthogonal "Click" Chemistries in the Synthesis of Functional Soft Materials. *Chemical Reviews* **2009**, 109, (11), 5620.
56. Lambert, J. B.; Shurvell, H. F.; Lightner, D. A.; Cooks, R. G., *Organic Structural Spectroscopy*. Prentice-Hall, Inc.: Upper Saddle River, 2001.
57. Oh, S. Y.; Yoo, D. I.; Shin, Y.; Seo, G., FTIR analysis of cellulose treated with sodium hydroxide and carbon dioxide. *Carbohydrate Research* **2005**, 340, (3), 417.
58. Skoog, D. A., *Principles of Instrumental Analysis*. 6th ed.; Thomson Brooks/Cole: Belmont, CA, 2007.
59. Stejskal, E. O.; Tanner, J. E., Spin Diffusion Measurements: Spin Echoes in the Presence of a Time-Dependent Field Gradient. *The Journal of Chemical Physics* **1965**, 42, (1), 288.
60. Stilbs, P., Fourier transform pulsed-gradient spin-echo studies of molecular diffusion. *Progress in Nuclear Magnetic Resonance Spectroscopy* **1987**, 19, (1), 1.

61. Gibbs, S. J.; C. S. Johnson, J., A PFG-NMR Experiment for Accurate Diffusion and Flow Studies in the Presence of Eddy Currents. *Journal of Magnetic Resonance* **1991**, 93, 395.
62. Cohen, Y.; Avram, L.; Frish, L., Diffusion NMR Spectroscopy in Supramolecular and Combinatorial Chemistry: An Old Parameter—New Insights. *Angewandte Chemie International Edition* **2005**, 44, (4), 520.
63. Lauterbur, P. C., Image Formation by Induced Local Interactions: Examples Employing Nuclear Magnetic Resonance. *Nature* **1973**, 242, (5394), 190.
64. Bihan, D. L., *Perfusion and Diffusion Magnetic Resonance Imaging: Applications of functional MRI*. Raven Press: New York, 1995.
65. Gorman, C. B.; Smith, J. C.; Hager, M. W.; Parkhurst, B. L.; Sierzputowska-Gracz, H.; Haney, C. A., Molecular Structure - Property Relationships for Electron-Transfer Rate Attenuation in Redox-Active Core Dendrimers. *Journal of the American Chemical Society* **1999**, 121, (43), 9958.
66. Roberts, J. M.; Sierzputowska-Gracz, H.; Stejskal, E. O.; Osteryoung, J. G., Determination of Li⁺ Self-Diffusion Coefficients in an Aqueous Suspension of Sulfonated Polystyrene Latex by Pulsed-Field-Gradient, Spin-Echo NMR. *The Journal of Physical Chemistry B* **1998**, 102, (40), 7735.
67. Derrick, T. S.; McCord, E. F.; Larive, C. K., Analysis of Protein/Ligand Interactions with NMR Diffusion Measurements: The Importance of Eliminating the Protein Background. *Journal of Magnetic Resonance* **2002**, 155, (2), 217.
68. Bleicher, K.; Lin, M.; Shapiro, M. J.; Wareing, J. R., Diffusion Edited NMR: Screening Compound Mixtures by Affinity NMR to Detect Binding Ligands to Vancomycin. *The Journal of Organic Chemistry* **1998**, 63, (23), 8486.
69. Price, K.; Lucas, L.; Larive, C., Analytical applications of NMR diffusion measurements. *Analytical and Bioanalytical Chemistry* **2004**, 378, (6), 1405.
70. Hamblin, M. R.; Hasan, T., Photodynamic therapy: a new antimicrobial approach to infectious disease? *Photochemical & Photobiological Sciences* **2004**, 3, (5), 436.
71. Maisch, T.; Szeimies, R.-M.; Jori, G.; Abels, C., Antibacterial photodynamic therapy in dermatology. *Photochemical & Photobiological Sciences* **2004**, 3, (10), 907.
72. Wainwright, M., Photodynamic antimicrobial chemotherapy (PACT). *Journal of Antimicrobial Chemotherapy* **1998**, 42, (1), 13.
73. Hancock, R. E. W., Alterations in Outer Membrane Permeability. *Annual Review of Microbiology* **1984**, 38, (1), 237.

74. Brennan, P. J.; Nikaido, H., The Envelope of Mycobacteria. *Annual Review of Biochemistry* **1995**, 64, (1), 29.
75. Fu, L. M.; Fu-Liu, C. S., Is Mycobacterium tuberculosis a closer relative to Gram-positive or Gram-negative bacterial pathogens? *Tuberculosis* **2002**, 82, (2-3), 85.
76. Redl, F. X.; Lutz, M.; Daub, J., Chemistry of Porphyrin-Appended Cellulose Strands with a Helical Structure: Spectroscopy, Electrochemistry, and in situ Circular Dichroism Spectroelectrochemistry. *Chemistry – A European Journal* **2001**, 7, (24), 5350.
77. Holzer, W.; Penzkofer, A.; Redl, F. X.; Lutz, M.; Daub, J., Excitation energy density dependent fluorescence behaviour of a regioselectively functionalized tetraphenylporphyrin-cellulose conjugate. *Chemical Physics* **2002**, 282, (1), 89.
78. Ringot, C.; Sol, V.; Granet, R.; Krausz, P., Porphyrin-grafted cellulose fabric: New photobactericidal material obtained by "Click-Chemistry" reaction. *Materials Letters* **2009**, 63, (21), 1889.
79. Ringot, C.; Saad, N.; Granet, R.; Bressollier, P.; Sol, V.; Krausz, P., Meso-functionalized aminoporphyrins as efficient agents for photo-bactericidal surfaces. *Journal of Porphyrins and Phthalocyanines* **2010**, 14, 925.
80. Feese, E.; Ghiladi, R. A., Highly efficient in vitro photodynamic inactivation of Mycobacterium smegmatis. *Journal of Antimicrobial Chemotherapy* **2009**, 64, (4), 782.
81. Navarre, W. W.; Schneewind, O., Surface proteins of gram-positive bacteria and mechanisms of their targeting to the cell wall envelope. *Microbiology And Molecular Biology Reviews* **1999**, 63, (1), 174.
82. Trias, J.; Benz, R., Permeability of the cell wall of Mycobacterium smegmatis. *Molecular Microbiology* **1994**, 14, (2), 283.
83. Ghose, T. K., Measurement Of Cellulase Activities. *Pure And Applied Chemistry* **1987**, 59, (2), 257.
84. Gilkes, N. R.; Henrissat, B.; Kilburn, D. G.; Miller, R. C.; Warren, R. A. J., Domains In Microbial Beta-1,4-Glycanases - Sequence Conservation, Function, And Enzyme Families. *Microbiological Reviews* **1991**, 55, (2), 303.
85. Beguin, P., Molecular-Biology Of Cellulose Degradation. *Annual Review Of Microbiology* **1990**, 44, 219.
86. Beguin, P.; Aubert, J. P., The Biological Degradation Of Cellulose. *Fems Microbiology Reviews* **1994**, 13, (1), 25.

87. Varrot, A.; Leydier, S.; Pell, G.; Macdonald, J. M.; Stick, R. V.; Henrissat, B.; Gilbert, H. J.; Davies, G. J., Mycobacterium tuberculosis Strains Possess Functional Cellulases. *Journal of Biological Chemistry* **2005**, 280, (21), 20181.
88. Mba Medie, F.; Ben Salah, I.; Drancourt, M.; Henrissat, B., Paradoxical conservation of a set of three cellulose-targeting genes in Mycobacterium tuberculosis complex organisms. *Microbiology* 156, (5), 1468.
89. Araki, J.; Wada, M.; Kuga, S.; Okano, T., Influence of surface charge on viscosity behavior of cellulose microcrystal suspension. *Journal of Wood Science* **1999**, 45, (3), 258.
90. Araki, J.; Wada, M.; Kuga, S.; Okano, T., Flow properties of microcrystalline cellulose suspension prepared by acid treatment of native cellulose. *Colloids and Surfaces A: Physicochemical and Engineering Aspects* **1998**, 142, (1), 75.
91. Rahn, K.; Diamantoglou, M.; Klemm, D.; Berghmans, H.; Heinze, T., Homogeneous synthesis of cellulose p-toluenesulfonates in N,N-dimethylacetamide/LiCl solvent system. *Die Angewandte Makromolekulare Chemie* **1996**, 238, (1), 143.
92. Tim, L.; Claudia, H.; Thomas, H., Click Chemistry with Polysaccharides. *Macromolecular Rapid Communications* **2006**, 27, (3), 208.
93. Hasegawa, T.; Umeda, M.; Numata, M.; Fujisawa, T.; Haraguchi, S.; Sakurai, K.; Shinkai, S., Click Chemistry on Curdlan: A Regioselective and Quantitative Approach to Develop Artificial β -1,3-Glucans with Various Functional Appendages. *Chemistry Letters* **2006**, 35, (1), 82.
94. Hasegawa, T.; Umeda, M.; Numata, M.; Li, C.; Bae, A.-H.; Fujisawa, T.; Haraguchi, S.; Sakurai, K.; Shinkai, S., 'Click chemistry' on polysaccharides: a convenient, general, and monitorable approach to develop (1 \rightarrow 3)-[β]-d-glucans with various functional appendages. *Carbohydrate Research* **2006**, 341, (1), 35.
95. Cao, Y.; Wu, J.; Meng, T.; Zhang, J.; He, J.; Li, H.; Zhang, Y., Acetone-soluble cellulose acetates prepared by one-step homogeneous acetylation of cornhusk cellulose in an ionic liquid 1-allyl-3-methylimidazolium chloride (AmimCl). *Carbohydrate Polymers* **2007**, 69, (4), 665.
96. Wu, J.; Zhang, J.; Zhang, H.; He, J.; Ren, Q.; Guo, M., Homogeneous Acetylation of Cellulose in a New Ionic Liquid. *Biomacromolecules* **2004**, 5, (2), 266.
97. Schlufte, K.; Schmauder, H.-P.; Dorn, S.; Heinze, T., Efficient Homogeneous Chemical Modification of Bacterial Cellulose in the Ionic Liquid 1-N-Butyl-3-methylimidazolium Chloride. *Macromolecular Rapid Communications* **2006**, 27, (19), 1670.

98. Morris, K. F.; Johnson, C. S., Diffusion-ordered two-dimensional nuclear magnetic resonance spectroscopy. *Journal of the American Chemical Society* **1992**, 114, (8), 3139.
99. Zeng, L.; Stejskal, E. O., Characterization of a Polypropylene/Super-Absorbent Web by NMR Diffusion Studies. *Applied Spectroscopy* **1996**, 50, 1402.
100. Larsen, M., Some Common Methods in Mycobacterial Genetics. In *Molecular Genetics of Mycobacteria*, Hatfull, G. F., Ed. ASM Press: Washington DC, 2000; pp 313.
101. Bradley D. Jett, K. L. H., Mark M. Huycke, and Michael S. Gilmore, Simplified Agar Plate Method for Quantifying Viable Bacteria. *BioTechniques* **1997**, 23, (4), 648.

CHAPTER 5

Towards Small Molecule Model Complexes of the KatG Active Site

Abstract

This Chapter describes the synthesis and characterization of first generation small molecule model complexes of the KatG active site in an effort to gain understanding of the failure of KatG to activate isoniazid, the most commonly prescribed anti-TB drug. KatG, native to *M. tuberculosis*, is a bifunctional heme metalloprotein possessing both catalase ($\text{H}_2\text{O}_2 \rightarrow \text{H}_2\text{O} + \frac{1}{2} \text{O}_2$) and peroxidase ($2 \text{AH} + \text{H}_2\text{O}_2 \rightarrow 2\text{A}\cdot + 2 \text{H}_2\text{O}$) activities. We have synthesized two tetraarylporphyrins, TMPyPFe^{II} (**5.1**) and TMImpFe^{II} (**5.2**), containing an appended imidazole or pyridine tether, respectively. ¹H-NMR studies in CD₂Cl₂ and THF-*d*₈ revealed pyrrole resonances consistent with a high spin ferrous center, confirming coordination of the imidazole and pyridine ligands to the iron center. Low temperature ¹H-NMR spectroscopic monitoring of the reaction of TMImpFe^{II} and TMPyPFe^{II} with dioxygen showed formation of low spin complexes which we ascribed as ferric superoxo adducts, Fe^{III}-(O₂⁻). Upon warming, decomposition occurred, yielding Fe^{III}-OH complexes. The spectroscopic data collected may serve as a reference for more elaborate model complexes of the KatG active site.

Introduction

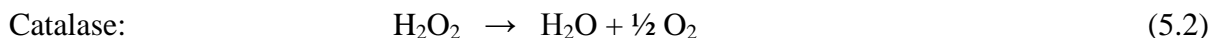
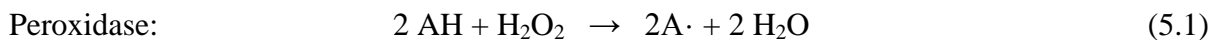
Metalloprotein structure-function relationships are heavily investigated in bioinorganic chemistry, especially in light of the numerous and indispensable roles metal ions play in biological systems, including: i) dioxygen transport (hemoglobin, myoglobin, hemocyanin, hemerythrin), ii) electron transfer ('blue' copper proteins, plastocyanin, rubredoxins and ferredoxins, cytochrome *c*), iii) elimination of reactive oxygen intermediates (dismutases), iv) oxidation/reduction reactions (galactose oxidase, ascorbate oxidase, bleomycin, ribonucleotide reductase, cytochrome *c* oxidase), v) oxidation by oxygen transfer to a substrate (lipoxygenase, soluble and particulate methane monooxygenases, cytochrome P450, tyrosinase), and vi) structure (Zn).¹⁻⁹

One approach in bioinorganic chemistry is the modeling of metalloenzyme active sites using synthetic small molecule analogs. Such chemistry can contribute to our understanding of metalloproteins by targeting aspects of structure, spectroscopy, and mechanism, which through model complexes can be investigated in great detail. The major advantage of small molecule model systems is attributed to the ability to conduct detailed investigations under conditions unattainable in biological systems, such as a wide temperature and pH range, organic media or high pressure. The importance of biomimetic systems to aid in the interpretation of data obtained from the natural systems is well established, as many metalloprotein models of myoglobin/hemoglobin, cytochrome P450 and others have been studied extensively.¹⁰

The catalase peroxidase, KatG, is of particular interest to our laboratory. In addition to studies on a variety of mutants of the natural enzyme in our group,¹¹ we attempt to use

model complexes of the KatG active site to elucidate structure-function relationships and reactivity in KatG.

Structure of KatG. KatG is a bifunctional hemoprotein belonging to Class I of the peroxidase superfamily (plants, fungi, bacteria), catalyzing reactions of type (5.1) and (5.2).¹²



KatGs have a high sequence homology to peroxidases, and thus possess significant peroxidase activity (5.1). However, KatGs have no sequence homology with any known catalase despite having high catalytic activity. The latter reactivity has been correlated to the presence of the Met-Tyr-Trp crosslink in the KatG active site.^{13, 14} Several crystal structures of KatG from different organisms have been published in recent years: *Haloarcula marismortui*,¹⁵ *Burkholderia pseudomallei*¹⁶ and *M. tuberculosis*.¹⁷ Figure 5.1 shows the KatG active site of *M. tuberculosis*.¹⁷

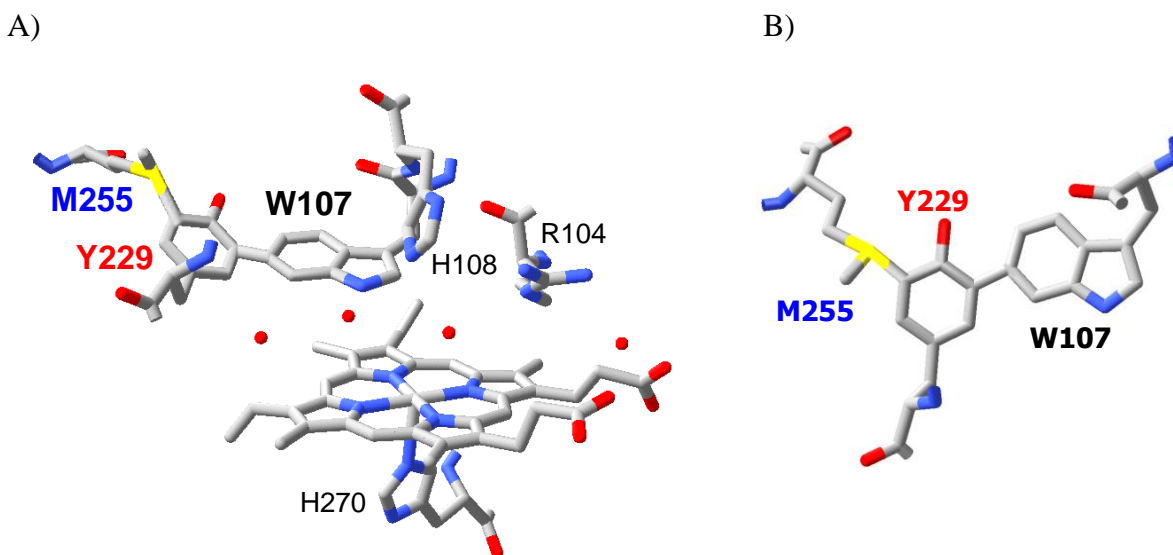


Figure 5.1: Crystal structures of A) the KatG active site of *M. tuberculosis*, and B) the Met-Tyr-Trp crosslink. Coordinates were obtained from the Protein Data Bank (entry 1S1J).¹⁷

KatGs are heme enzymes which, on the distal side of the heme, contain a covalent linkage of Methionine 255, Tyrosine 229 and Tryptophan 107 (*M. tuberculosis* numbering) as a common structural characteristic. On the proximal side, the heme iron is coordinated by a histidine axial base typically observed in peroxidases.¹⁸ Covalent crosslinks can be found in a growing number of metalloenzymes such as in cytochrome *c* oxidase (His240-Tyr244),^{19, 20} catalase HPII (His392-Tyr415)²¹ or galactose oxidase (Tyr272-Cys228).^{22, 23} Due to the presence of these modified amino acids, which display altered redox and pK_a properties, the enzyme chemistry is essentially impacted.^{24, 25} Formation of the crosslink in KatG is believed to occur by metal-mediated autocatalytic processes. Although mechanisms for the formation of the Met-Tyr-Trp crosslink have been proposed, these are still speculative and unable to be confirmed in the enzyme.^{26, 27} We believe that small molecule studies will prove useful in

determining the mechanism of formation of such crosslinks *in vitro* and to correlate to findings *in vivo*.

Role of KatG in anti-tuberculosis treatment. Isonicotinyl hydrazine (INH) or ‘Isoniazid’, first discovered in 1952,²⁸ is the most commonly prescribed anti-TB drug.²⁹ The mechanism of action of INH is not understood in detail to date. However, the consensus opinion is that INH, a prodrug, is activated *in vivo* by KatG, a catalase-peroxidase enzyme native to *M. tuberculosis*. The isonicotinoyl acyl radical produced consequently forms an INH-NADH adduct (Figure 5.2).³⁰⁻³²

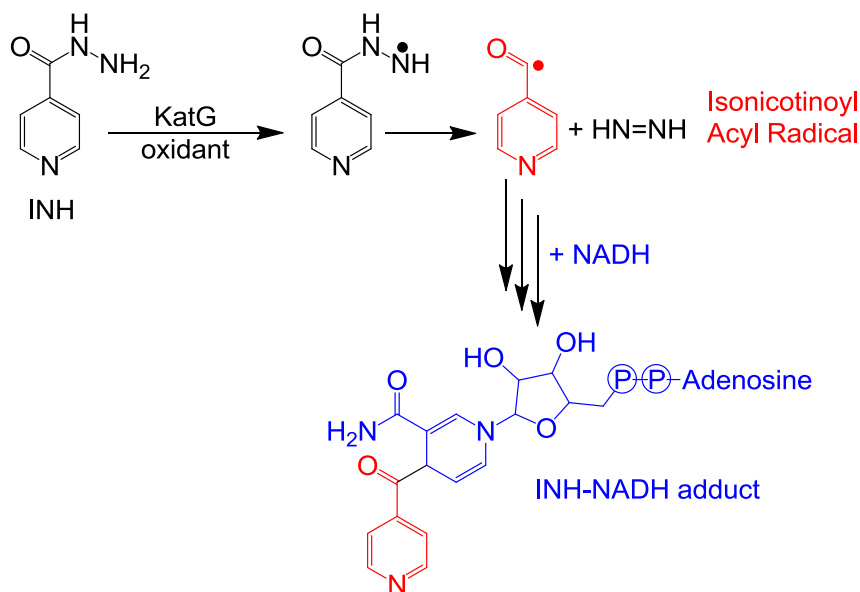


Figure 5.2: Activation of INH by KatG.

Ultimately, the INH-NADH adduct leads to inhibition of mycolic acid synthesis by blocking the enoyl acyl-carrier-protein reductase (InhA) active site. Inhibition of InhA results

in a weakened, mycolic acid deficient mycobacterial cell wall leading to cell death. Isoniazid is bactericidal for rapidly dividing *M. tuberculosis*, but only bacteriostatic for dormant bacteria. Therefore, resistance can develop quickly if INH is not used in conjunction with other anti-TB drugs, which eradicate mycobacteria in a low metabolic state.

The origin of isoniazid drug-resistance can be traced back to deletions or point mutations in the *katG* gene.³³⁻³⁵ Despite intensive studies, drug-resistance and the mechanism of isoniazid activation in KatG are not fully understood to date. Therefore, more studies are necessary to elucidate structure-function relationships in KatG and explain its failure to activate isoniazid in drug-resistant variants.

Ghiladi et al. recently suggested several possible pathways for the activation of INH by KatG (Figure 5.3, blue, green and red cycles).³⁵ Wild type KatG turned over INH in a peroxidase-like cycle (A→B→F). For INH-resistant mutants of KatG (Arg104Leu, His108Gln, Ser315Thr), variations in the catalytic cycle were discovered (Figure 5.3, green and blue cycles). Upon addition of superoxide by pulse radiolysis to the resting enzyme, the formation of Compound III [(KatG)Fe^{III}-(O₂⁻)] was observed by UV-visible spectroscopy, but in the presence of INH, Compound II was formed immediately. The conversion of Compound III to Compound II formally requires two electrons. Therefore, three one-electron reductions incorporating INH were suggested to complete the cycle (G→H→I→F, red). This type of reactivity, however, was only observed with wild type KatG and not with drug-resistant mutants. From these *in vitro* studies, the authors hypothesized that the Compound III pathway (Figure 5.3, red) plays an important role in distinguishing INH susceptible wild

type KatG from INH resistance mutants in their ability to catalyze INH-NADH adduct formation.

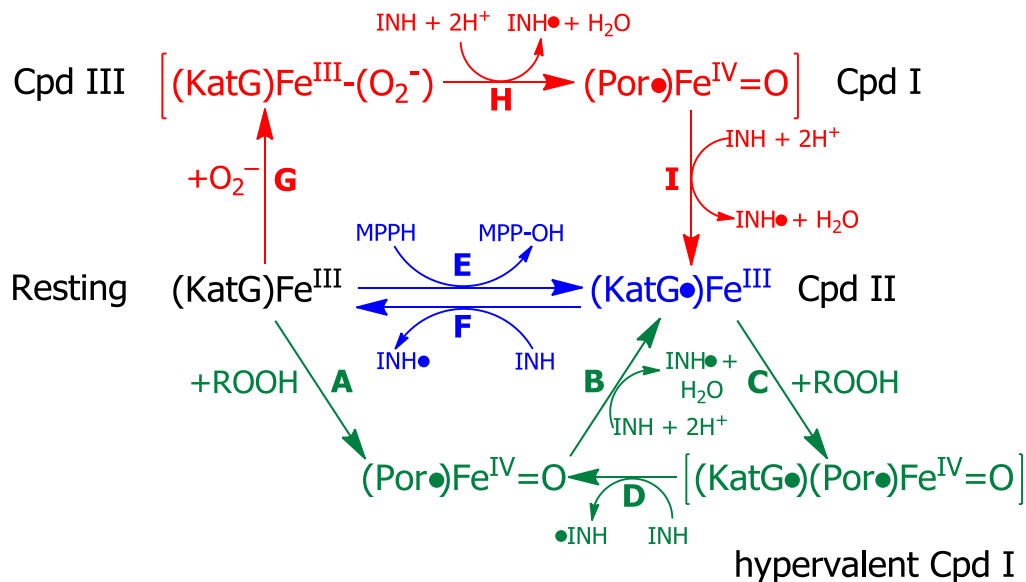


Figure 5.3: Proposed mechanism for the activation of isoniazid by KatG (Reprinted with permission from Ref [35]. Copyright 2005 American Chemical Society).

Small molecule model complexes will prove helpful in determining the validity of the proposed superoxide pathway (Figure 5.3, red) for INH activation. There are four possible routes for generating Compound III in hemoproteins: i) reaction of the ferric enzyme with superoxide (pulse radiolysis), ii) reaction of the ferric enzyme with excess H_2O_2 , iii) reaction of the ferrous enzyme with dioxygen, and iv) reacting Compound II with H_2O_2 . Using synthetic small molecule model complexes, generation of Compound III is typically achieved by reacting the ferrous heme with dioxygen at low temperature.^{2, 36} To date, there are no published synthetic models addressing the KatG active site incorporating a mimic for the

crosslinked species. Therefore, we have begun to synthesize a series of 1st generation small molecule analogs of the active site (Figure 5.4). The model complexes are based on *meso*-tetraarylporphyrins, which have been used extensively as scaffolds for mimics of simpler metalloprotein active sites such as hemoglobin.² We chose to synthesize 1st generation model complexes containing an *ortho*-phenyl tethered axial base considering related systems published in the literature. Original N-donor tethered heme systems connected through the β -pyrrole positions were synthesized by Traylor and co-workers.³⁷⁻³⁹ Momenteau and co-workers investigated similar tethered heme complexes containing histidine bound through a β -pyrrole propionic side chain.⁴⁰ Although much insight could be gained from such systems, an apparent problem is the formation of intermolecular dimers where the N-donor histidine coordinates to the iron of a second heme complex due to the orientation of the tether in the porphyrin plane.⁴⁰ On the contrary, attachment of the tether at the *ortho* position in *meso*-tetraarylporphyrins such as in **5.1** and **5.2** directs the tether towards the center of the heme, therefore increasing the likelihood of intramolecular coordination of the N-donor substituent (Figure 5.4). Many model complexes representing cytochromes c, b, and a₃ by Walker, and multitethered “picket fence porphyrins” by Collman and co-workers, utilize this principle.⁴¹⁻⁴⁵ More recent heme enzyme mimics by Collman, Karlin and Naruta of the cytochrome c oxidase active site also exploit the positioning of *ortho*-phenyl substituents over the porphyrin plane.⁴⁶⁻⁵² While this work was ongoing, reactivity towards oxygen of a very similar model complex to **5.2** also based on the 5,10,15-trimesityl-20-(2-nitrophenyl)porphyrin has been reported by Naruta and co-workers.⁵³ They presented detailed characterization of a low-spin ferric hydroperoxo complex, which is a commonly

proposed key intermediate in catalytic cycles of monooxygenase and peroxidase enzymes. Formation of the hydroperoxide complex was achieved by protonation from a high-spin η^2 -peroxo ferric complex and alternatively by one electron reduction of the ferric superoxide form in the presence of a proton source. This example demonstrates the versatility and reactivity of such simple model complexes in mimicking heme enzyme intermediates which are otherwise difficult to study.

For the more elaborate KatG model systems, the main features of the targeted model complexes include a donor axial base on the proximal side of the prosthetic heme group, and a novel model or precursor peptide for the crosslinked amino acids on the distal side (2nd generation). For the initial 1st generation model complexes, the influence of the axial base was investigated. Spectroscopic data obtained from these simpler molecules will be used as reference for data collected from more elaborate model complexes.

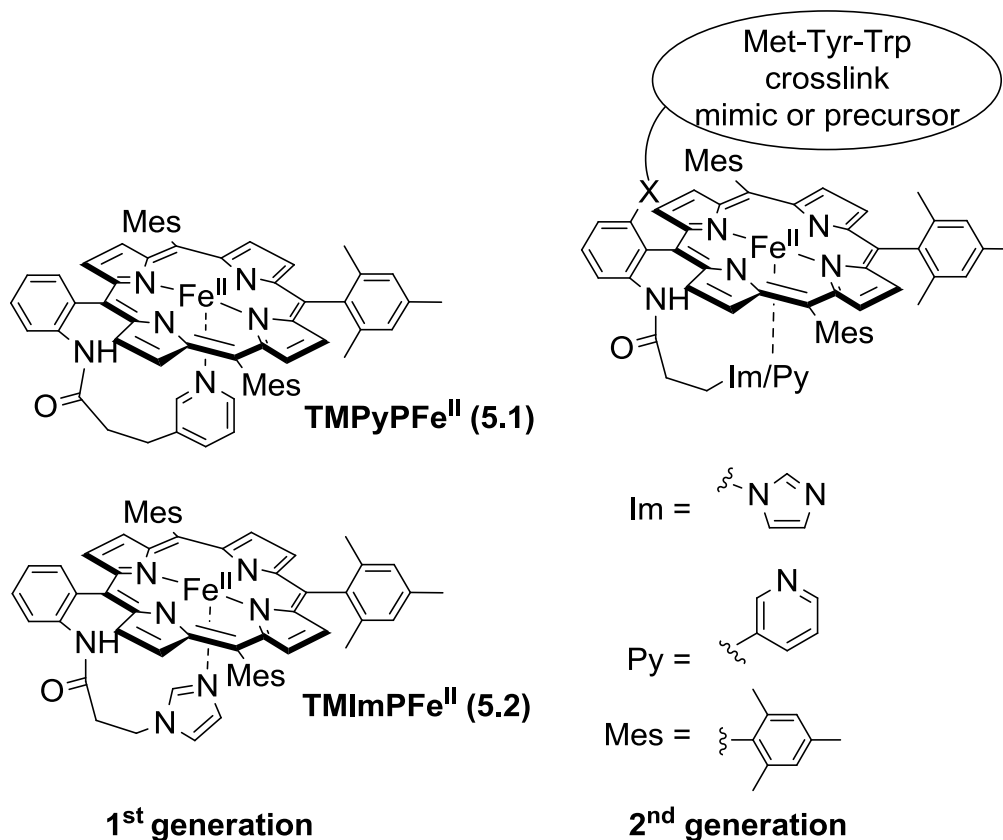


Figure 5.4: Target model complexes of the KatG active site.

Results

The porphyrin scaffold is based on an A₃B porphyrin. Mesityl substituents were selected to provide enough steric bulk to prevent μ -oxo dimer (PorFe^{III}-O-Fe^{III}Por) formation of the model complexes after exposure of the ferrous heme to air.^{54, 55} We chose to synthesize a pyridine tethered tetraarylporphyrin (**5.1**), because of its known stability and coordination to the central iron atom.^{2, 56, 57} Furthermore, 3-(3-Pyridinyl)propionic acid is commercially

available, eliminating additional steps to synthesize an adequate tether. The tether was appended to the porphyrin scaffold by amide bond formation resulting in **5.1**. We also synthesized an imidazole tethered variation **5.2** with an analogous strategy mimicking the natural histidine coordination of the heme more closely. Imidazole tethered heme model complexes are known to be sensitive to air and light, complicating their isolation and purification.^{50, 57-59}

Figure 5.5 shows the synthetic route to the two first generation model complexes **5.1** and **5.2**. The parent porphyrin, 5-(2-nitrophenyl)-10,15,20-tris(2,4,6-trimethylphenyl)-porphyrin (**5.3**), was synthesized in the first step by a statistical condensation of the corresponding aldehydes and pyrrole using the Lindsey method.⁶⁰ A ratio of 3:2 of mesitaldehyde to 2-nitrobenzaldehyde with a 2 h reaction time was found to yield **5.3** as the major organic product with only minor amounts of tetramesitylporphyrin and other porphyrin side products. The reaction has been scaled up to produce 1.2-1.5 g batches of 5-(2-nitrophenyl)-10,15,20-tris(2,4,6-trimethylphenyl)porphyrin and 200-300 mg of tetramesitylporphyrin simultaneously. The product was purified twice by column chromatography on alumina with mixtures of CH₂Cl₂/hexanes. Reduction of the nitro group of **5.3** to an amine was achieved by using tin(II) chloride as the reducing agent in the biphasic solvent system aqueous HCl/CHCl₃.^{61, 62} Complete conversion of the starting material was observed, eliminating a chromatographic purification step. Simple recrystallization of the isolated porphyrin **5.4** resulted in almost quantitative yields. The axial pyridine base was appended to the porphyrin by amide bond formation. 3-(3-Pyridinyl)propionic acid, obtained commercially, was converted to the corresponding propionyl chloride using thionyl chloride,

which was immediately reacted with porphyrin **5.4** in a THF/DMF mixture. Porphyrin **5.5** was obtained in 77% yield after chromatographic purification and recrystallization.^{46, 47} The insertion of iron(II) into the porphyrin was first attempted with FeCl₂·4 H₂O in refluxing DMF under argon atmosphere.⁶³ The high temperature over several hours decomposed the starting material and no desired product was observed. Consequently, the solvent was changed to THF and the iron-complexed porphyrin **5.5** was successfully isolated.^{46, 47} Chromatographic purification of the product proved tedious and had to be carried out several times to remove traces of side products (some μ -oxo dimer formation was observed by UV-visible spectroscopy) and starting material. Yields between 60 and 70% were obtained. Model complex **5.1** was obtained by reduction of **5.5** using sodium hydrosulfite as the reducing agent in degassed solvents under inert atmosphere. The organic solvent was evaporated and **5.1** was stored at -40 °C in the glovebox without further purification.

Tethering of 3-(1-*H*-imidazol-1-yl)propionyl acid to porphyrin **5.4** proved to be more challenging. Employing the conditions used for the formation of **5.5** did not result in any product. However, application of conditions developed by Collman et al. in sodium acetate buffered acetic acid with dropwise addition of 3-(1-*H*-imidazol-1-yl)propionyl chloride to the porphyrin solution afforded **5.6** in 56% yield.⁵⁸ During aqueous work up of the reaction mixture a decomposition product developed explaining the modest yield. According to the mass difference observed in MALDI-TOF mass spectrometry and ¹H-NMR spectroscopic analyses, this side product eliminated imidazole from the tether. Such decomposition has been reported previously, and is most likely due to a photosensitized reaction of imidazole with dioxygen.⁵⁹ However, porphyrin **5.6** appeared to be stable upon isolation and storage in

the freezer. The yield was not significantly improved by conducting the work up of the reaction in the dark and with degassed solutions. Metallation and reduction to the ferrous model complex **5.2** was achieved under conditions described for the pyridine tethered model complex **5.1**. Porphyrin **5.2** was stored at -40°C in the glovebox after isolation.

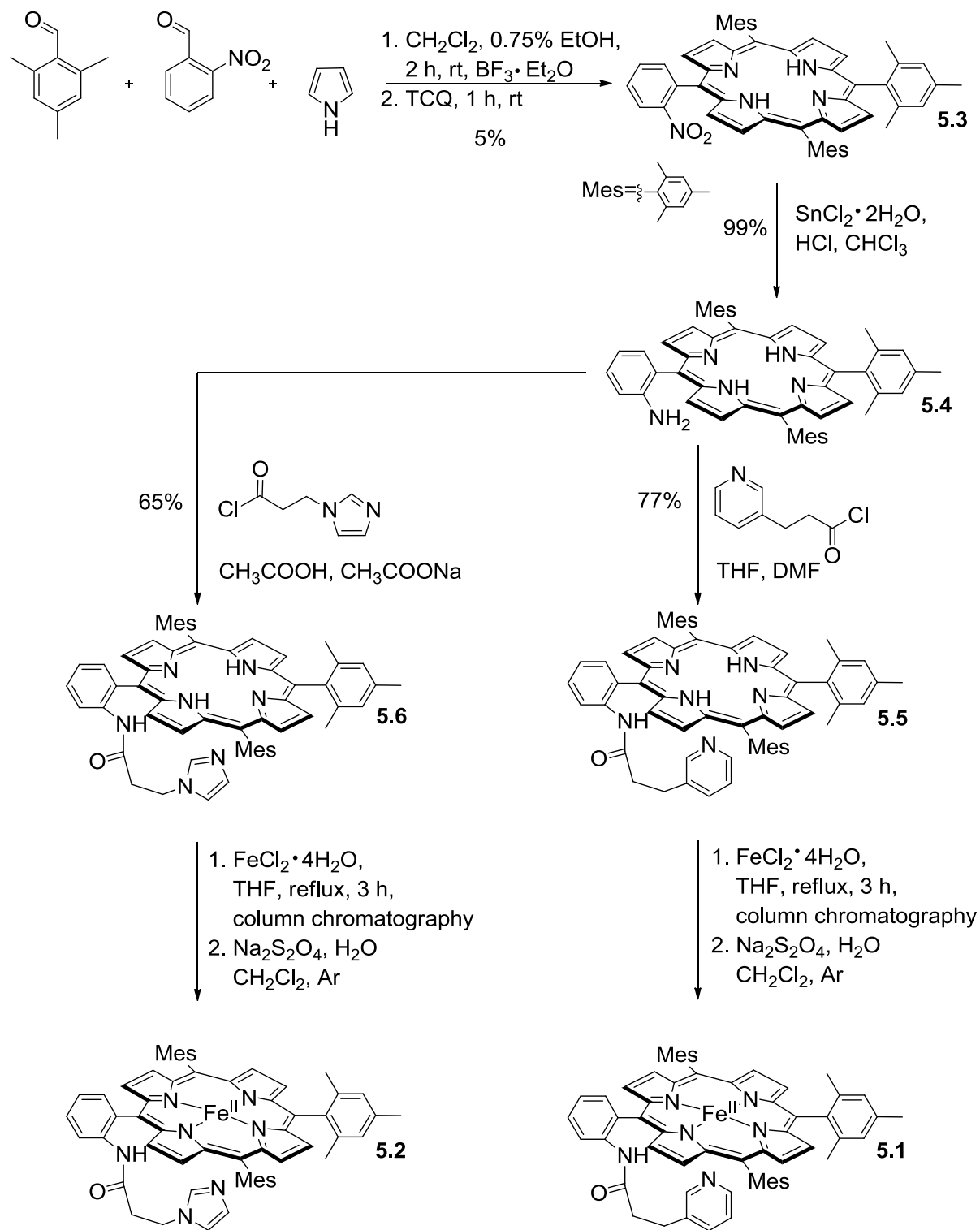


Figure 5.5: Synthesis of model complexes **5.1** and **5.2**.

¹H-NMR studies at room temperature. ¹H- and ²H-NMR spectra of heme model complexes have been investigated in great detail in the past 30 years.^{2, 63-66} Therefore, the chemical shifts of the β -pyrrole hydrogens on the porphyrin periphery have been established as a tool to reliably identify the oxidation and spin state of the complexed iron. Table 5.1 lists some commonly found chemical shifts for the pyrrolic hydrogens at room and low temperature.

Table 5.1: Chemical shifts for β -pyrrole hydrogens in heme complexes^{65, 66}

Complex type ^a	Coordination	Chemical shift in ppm	
		Room temperature	Low temperature
Fe(II), HS S=2	5	30-60	40-85
Fe(II), LS S=0	5 and 6	9	9
Fe(II), IS S=1	4	4-5	
Fe(III), HS S=5/2	5 and 6	70-80	100-120
Fe(III), LS S=1/2	5 and 6	< 0	< -25
Fe(III), IS S=3/2	5		-20
Fe(III)-(O ₂ ⁻), LS S=0		-	9-10
Fe(III)-(O ₂) ²⁻		60	
Fe(IV)=O			2-4
Fe(III)-O-Fe(III)		14	14
Fe(III)-(O ₂ ²⁻)-Fe(III)		-	15-17

^a HS: high spin, LS: low spin, IS: intermediate spin, S: spin quantum number

The room temperature ^1H -NMR spectra of model complex **5.1** in weakly coordinating solvents such as THF (Figure 5.6 A) and acetone (Figure 5.6 B) show peaks between 40 and 50 ppm, which is indicative of a high spin ferrous (5 or 6 coordinate) center, where either the solvent or the axial tether is coordinated to the iron (Table 5.1). In CD_2Cl_2 , a non-coordinating solvent, the peaks in the paramagnetic region (40 ppm, Figure 5.6 C) indicate coordination of the nitrogen atom of the tether to the Fe(II) center, resulting in a high spin Fe(II) complex. A four coordinate complex would be expected to have intermediate spin with pyrrolic resonances at 4-5 ppm, which is not observed in CD_2Cl_2 .

^1H -NMR spectra of **5.2** in weakly coordinating solvents (THF- d_8 , Figure 5.7 A; acetone, Figure 5.7 B) also reveal several sets of peaks between 40 and 65 ppm, which are indicative of a high spin ferrous center. Currently, a detailed assignment of individual signals in the paramagnetic region is not clear. Analysis of the ^2H -NMR spectra of β -pyrrole deuterated analogs will help to understand the origin of these signals. Signals in the paramagnetic region are conserved in the non-coordinating solvent CD_2Cl_2 (Figure 5.7 C), also indicating coordination of the nitrogen atom contained in the imidazole-bearing tether to the metal center.

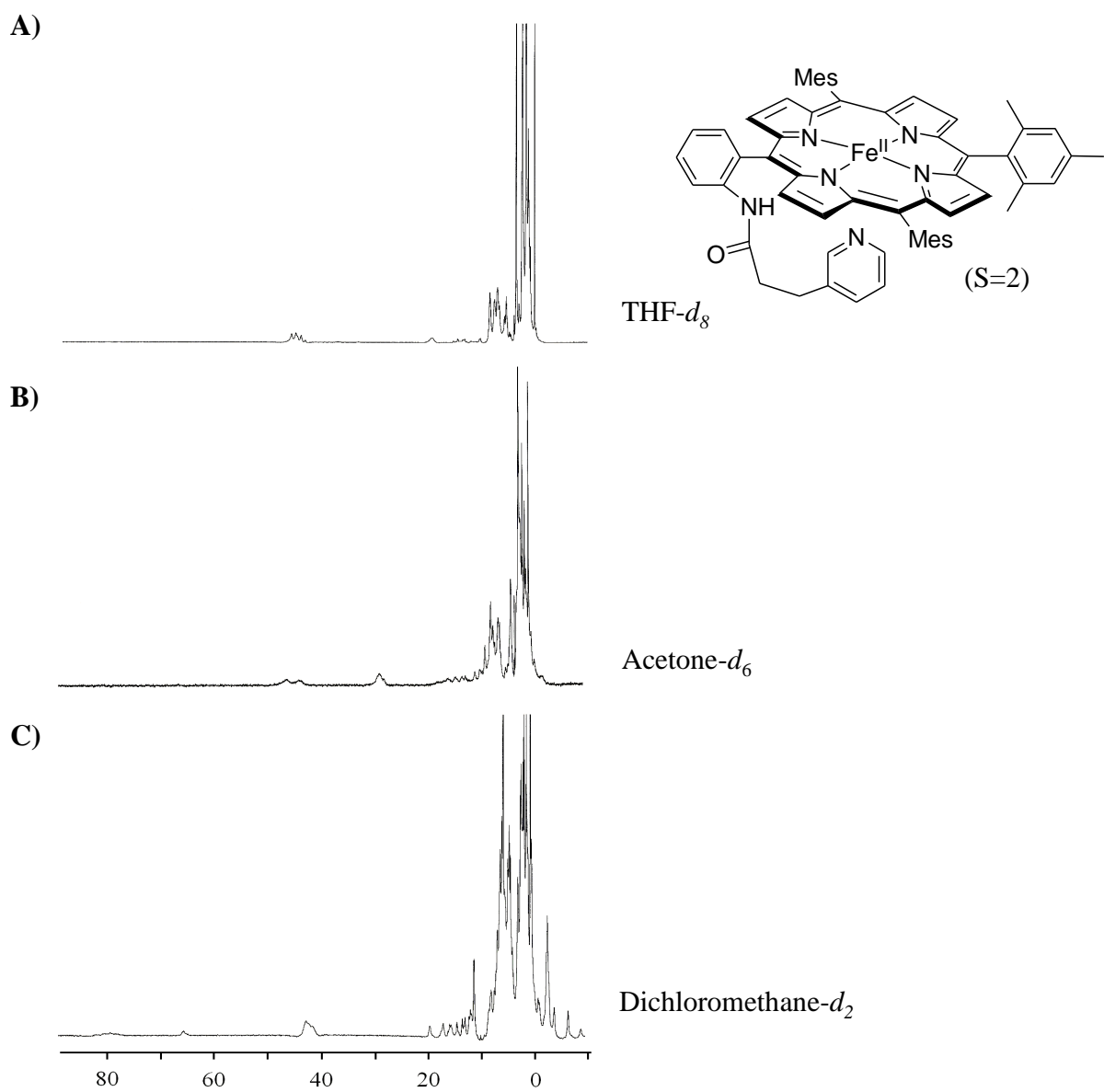


Figure 5.6: $^1\text{H-NMR}$ spectra of $\text{TMPyPFe}^{\text{II}}$ (**5.1**) in several solvents at room temperature.

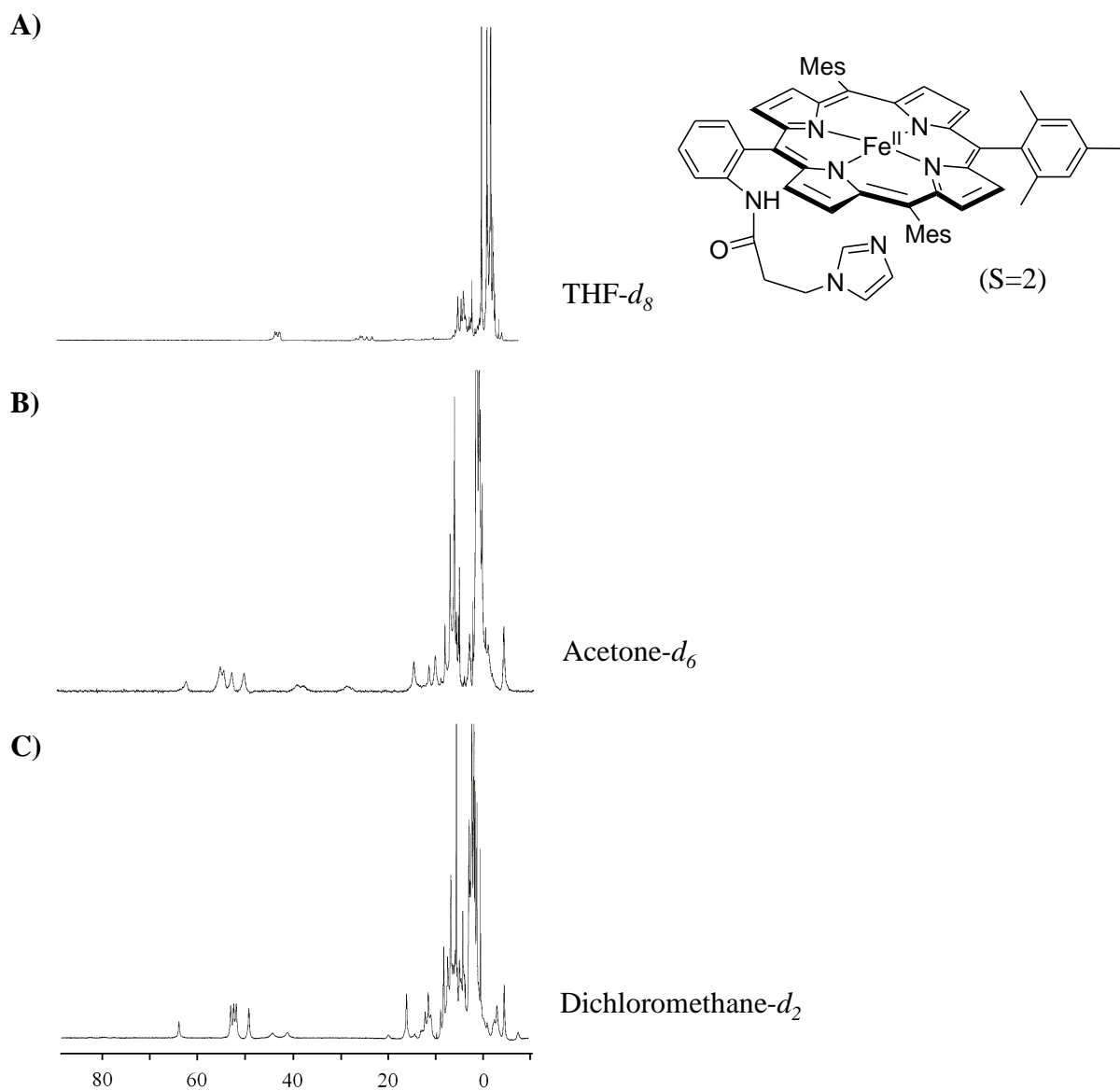


Figure 5.7: $^1\text{H-NMR}$ spectra of TMImpPFe^{II} (**5.2**) in several solvents at room temperature.

Low Temperature ¹H-NMR studies of oxygen adducts. According to the Curie law, the contact and dipolar contributions to the chemical shift are both dependent upon the magnetic susceptibility χ , which is inversely proportional to the temperature per equation 5.3,

$$M = \chi \cdot H = C \cdot H \cdot T^{-1} \quad (5.3)$$

wherein, M represents magnetization, C is the Curie constant, H denotes the magnetic field strength and T is the temperature. Therefore, the chemical shifts of the β -pyrrole hydrogens will shift in a temperature-dependent manner (Table 5.1), as discussed below.

Compounds **5.1** and **5.2** and their respective dioxygen adducts were investigated at low temperature (-80 °C) by ¹H-NMR spectroscopy (Figures 5.8 and 5.9). In THF, the pyrrole resonances, which had been observed around 40 ppm for **5.1** (Figure 5.6 A) and 50-60 ppm for **5.2** (Figure 5.7 A) at room temperature, were shifted downfield to 84/72 ppm (Figure 5.8 A) and 90/66 ppm (Figure 5.9 A), respectively. These shifts are assigned to originate from 5 or 6 coordinate ferrous hemes, where the axial ligands are THF solvent and/or the nitrogen atom of the tethered ligand. Addition of dioxygen resulted in a diamagnetic species (Figure 5.8 B and 5.9 B, pyrrole-H ~9-10 ppm, Table 5.1), which was assigned as the low spin ferric superoxo adduct, Fe(III)-(O₂⁻). Upon warming, the pyrrole resonances shifted to 116/108 ppm for **5.1** (Figure 5.8 C) and 115 ppm for **5.2** (Figure 5.9 C) at -80 °C. The shift can be explained by O-O bond cleavage yielding Fe(III)-OH decomposition products (HS, S=5/2). It appears that the mesityl meso-substituents on the porphyrin periphery add sufficient steric hindrance to prevent the formation of μ -oxo dimer species ($\delta_{\text{pyrrole}} = 14\text{-}15$ ppm, RT and -80 °C, Table 5.1). Our observations are consistent with other published heme dioxygen studies.^{2, 63, 64}

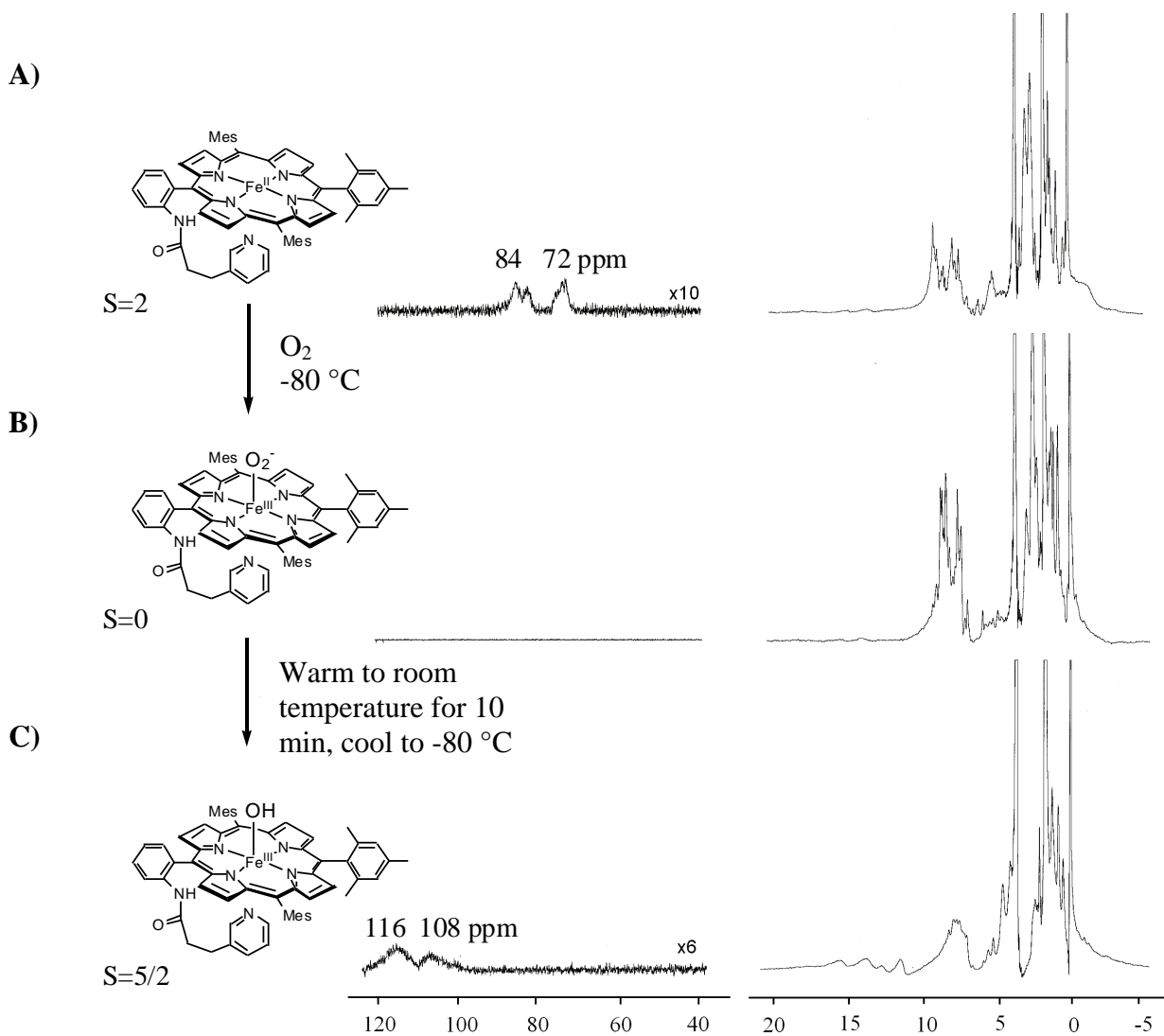


Figure 5.8: ^1H -NMR spectra of A) TmPyPFe^{II} (**5.1**), B) its dioxygen adduct, and C) the ferric-hydroxy decomposition product in THF- d_8 , -80°C .

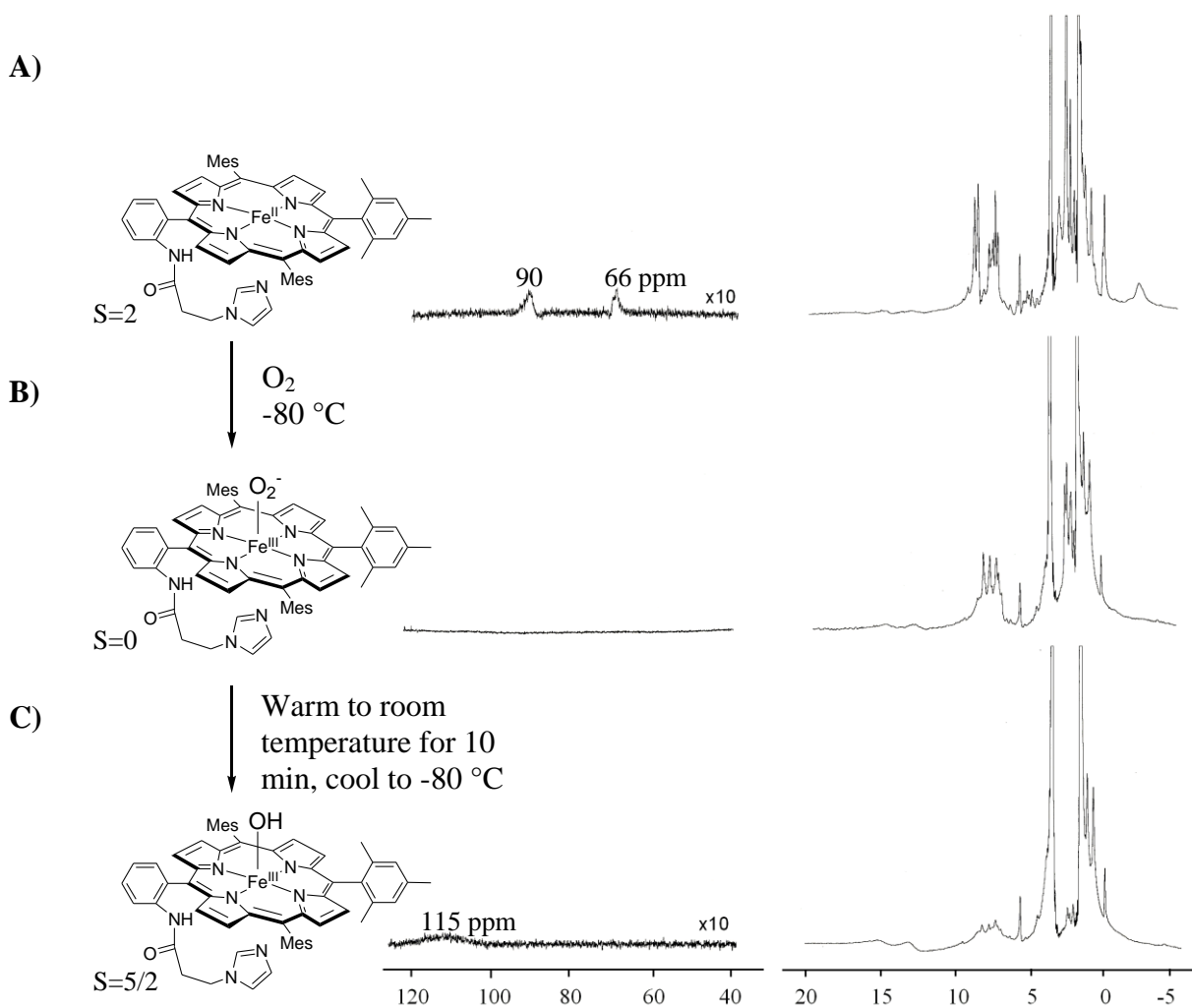


Figure 5.9: ^1H -NMR spectra of A) TMImpFe^{II} (**5.2**), B) its dioxygen adduct, and C) the ferric-hydroxy decomposition product in THF- d_8 , -80°C.

Synthesis of β -pyrrole-deuterated porphyrins. It is apparent that the $^1\text{H-NMR}$ spectra of **5.1** or **5.2** change from representing paramagnetic to diamagnetic species after addition of dioxygen, but detailed peak assignments of the β -pyrrole hydrogens in the diamagnetic region for the dioxygen adduct are not clear due to the complexity of the proton signals. β -Pyrrole deuterated analogs of **5.1** and **5.2**, and their respective dioxygen adducts, would yield vastly simpler $^2\text{H-NMR}$ spectra that would allow verification of the assignment of the signals formed from TMPyPFe(II) and TMImpFe(II) after reaction with dioxygen at $-78\text{ }^\circ\text{C}$ as the diamagnetic Fe(III)-superoxo adducts.

We have begun the synthesis of β -pyrrole deuterated model complexes of **5.1** and **5.2**. In a first attempt, the ethanol co-solvent (CH_2Cl_2 containing 0.75% EtOH) during porphyrin condensation was replaced with ethanol- d_1 (Figure 5.10).⁶⁷ Under these conditions an average of 25% β -pyrrole deuteration was observed by $^1\text{H-NMR}$ spectroscopy, yielding **5.3- d_2** . The level of deuteration was conserved during the reduction step with SnCl_2 in conc. HCl/CHCl_3 to **5.4- d_2** . Metallation of the reduced porphyrin with iron showed a peak at 80 ppm in the $^2\text{H-NMR}$ spectrum (Figure 5.11). However, it was concluded that 25% deuteration might not be sufficient to record quality $^2\text{H-NMR}$ spectra at low temperature, where peaks are more broadened. Therefore, we investigated a route to fully ($> 90\%$) β -pyrrole deuterated porphyrin analogs starting with pyrrole- d_5 (Figure 5.12).

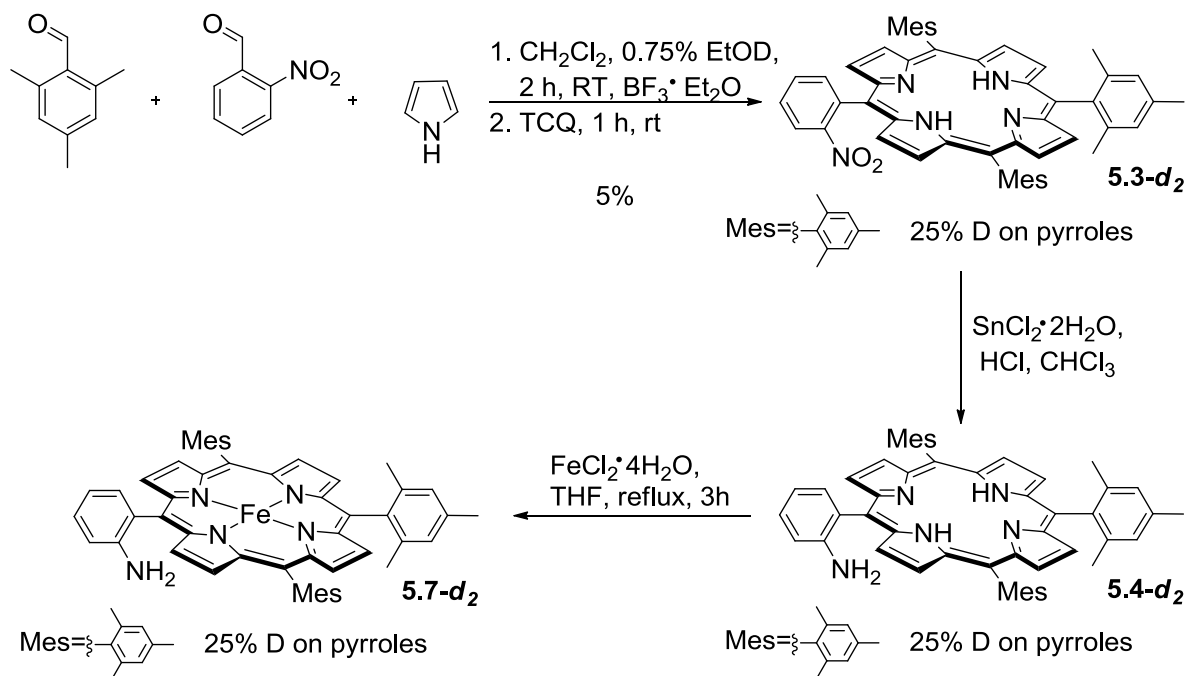


Figure 5.10: Synthesis of partially β -pyrrole deuterated porphyrin analogs.

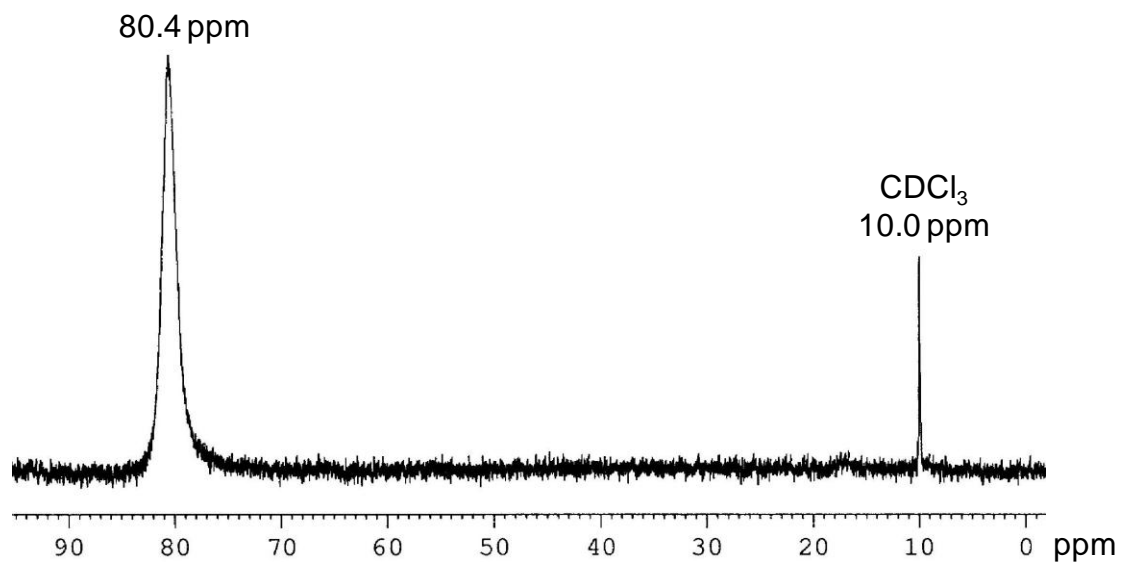


Figure 5.11: ^2H -NMR spectrum of **5.7- d_2** in CHCl_3 .

Efficient synthesis of pyrrole- d_5 was achieved following a protocol reported by Dolphin and coworkers.⁶⁸ Treatment of pyrrole with acetic acid- d_1 in deuterium oxide for 8 h in the dark yielded 70-80 % deuteration, and 95-97% if the reaction was conducted twice. Formation of fully deuterated 2-nitrophenyl porphyrin (**5.3- d_8**) was successful under conditions used previously (Figure 5.12). The reduction of the nitro group of **5.3- d_8** was also successful and no significant loss in deuterium was observed.

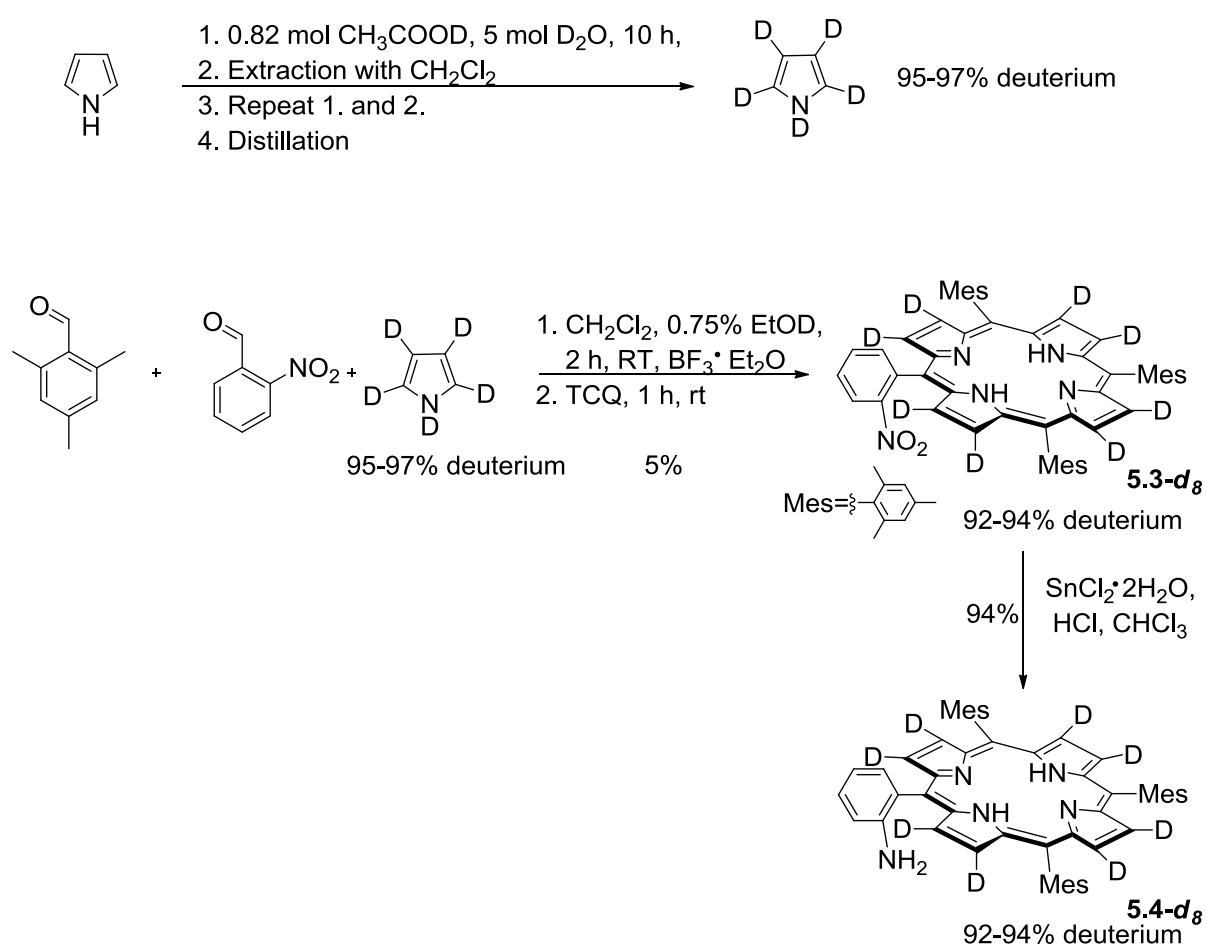


Figure 5.12: Route to fully β -pyrrole deuterated porphyrins, **5.3- d_8** and **5.4- d_8** .

Summary and Outlook

Simple, 1st generation model complexes containing an appended pyridine or imidazole tether were synthesized in good yields. The iron complexed compounds were investigated by ¹H-NMR spectroscopy and it was shown that the tethered pyridine/imidazole coordinates to the complexed iron in a non-coordinating solvent. Whether the complexation is intra- or intermolecular could be investigated by UV-visible spectroscopic dilution experiments.⁶⁹

Further, the dioxygen adducts of the reduced form of the model complexes **5.1** and **5.2** were investigated by ¹H-NMR spectroscopy at low temperature. Diamagnetic species (judged by the disappearance of signals in the paramagnetic region) were detected upon bubbling air through the ferrous heme complex solution, corresponding to the formation of putative Fe(III)-(O₂⁻) adducts. ²H-NMR spectra may reveal the exact chemical shift of the pyrrole hydrogens/deuteriums and confirm the assignment. Towards this goal, a synthetic route to fully β -pyrrole deuterated porphyrin analogs of **5.1** and **5.2** involving *d*₅-pyrrole has been identified.⁶⁸ The oxygen adducts of **5.1** and **5.2** are not stable at room temperature and decompose to Fe(III)-OH species which are unambiguously identified by the pyrrole resonances 100-120 ppm at -78 °C.⁷⁰

The model complexes **5.1** and **5.2** serve as reference compounds for more elaborate systems which more closely relate to the structural components in the KatG active site. The future goals of this project are the synthesis of 2nd generation model complexes (also including water soluble variations based on approaches described in Chapter 3) which are expected to shed some light into:

- (1) Formation of the Met-Tyr-Trp crosslink in the active site
- (2) The reactivity of ferric superoxo complexes in order to investigate possible INH activation pathways (Figure 5.3)

Study of the Met-Tyr-Trp crosslink formation with peptide tethered model complexes.

The Met-Tyr-Trp crosslink (Figure 5.1 B) has been identified in several catalase-peroxidases, such as in KatG from *Bulkholderia pseudomallei*,¹⁶ *Synechocystis* PCC 6803,⁷⁰ and *M. tuberculosis*,¹⁷ but knowledge of the mechanism of crosslink autocatalytic formation is scarce. There is also little literature precedent on covalent bond formation between tyrosine and tryptophan or tyrosine and methionine amino acid side chains in metalloproteins. To the best of our knowledge, there is no published record of a Met-Tyr crosslink besides the one in KatG species. However, there are several reports on Cys-Tyr crosslinks, e.g. in galactose oxidase from *Dactylium dendroides*²³ or catalase-1 from *Neurospora crassa*.⁷¹ Poulos and co-workers identified a Tyr-Trp crosslink (C-N bond) in the His52Tyr mutant of cytochrome c peroxidase.⁷²

Ghiladi et al. have recently isolated and quantified the Met-Tyr-Trp crosslink of *M. tuberculosis* by digestion of the enzyme.^{26, 27} By investigating several variants with mutations in the crosslink region, some insight into the crosslink formation was gained, which led to the proposal of the mechanism shown in Figure 5.13.²⁷

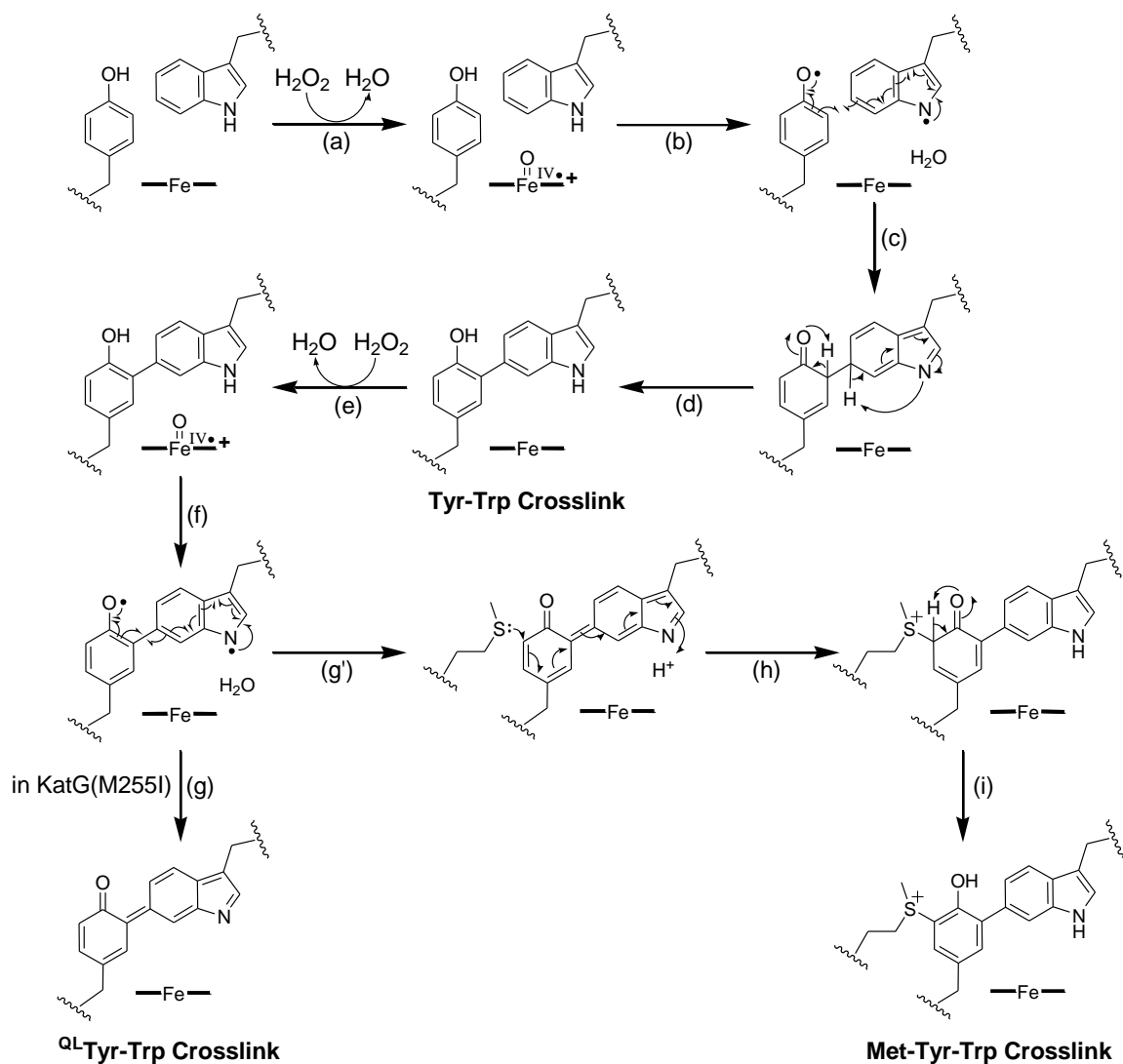


Figure 5.13: Proposed mechanism for formation of the Met-Tyr-Trp crosslink in KatG (Reprinted with permission from Ref [27]. Copyright 2005 American Chemical Society).

They suggested that Compound I ($\text{Fe}^{\text{IV}}=\text{O}$, Por $\cdot+$), formed with peracetic acid *in vitro* or hydrogen peroxide *in vivo*, is the two-electron oxidized species initiating crosslink formation by simultaneous oxidation of the tyrosine and tryptophan amino acid side chains (Figure 5.13, steps a and b). This is plausible because both tyrosine and tryptophan residues

are within the spatial threshold for long range electron transfer.¹⁷ The *in vitro* formed one-electron oxidized Compound II species ($\text{Fe}^{\text{IV}}=\text{O}$) was not able to initiate crosslink formation. The second covalent bond in the crosslink is formed consecutively after renewed Compound I formation (step e). In the Met255Ile mutant, which does not contain methionine in the active site, a quinone-like (QL) crosslink was isolated and characterized (step f and g).²⁷ In wild type KatG, it has been proposed that the S-C bond is formed by nucleophilic attack of the quinone-like intermediate by the sulfur atom (steps h and i). This mechanism is further supported by the observation that no crosslink was found in mutants lacking tyrosine or tryptophan (Tyr122Phe and Trp249Phe in KatG from *Synechocystis*) in the active site.¹⁴ However, mutation of methionine (Met255Ile in KatG from *M. tuberculosis*) still allowed formation of the Tyr-Trp crosslink, indicating that this bond is formed first and that formation of the Met-Tyr bond is contingent upon coupling of tyrosine and tryptophan.²⁷

Investigations including synthetic small molecule model complexes under conditions unattainable for enzymes, e.g. low temperature experiments, might help in further identifying intermediates and clarifying the mechanism involved in the crosslink formation. Therefore, we propose to synthesize KatG model complexes featuring both an axial base (pyridinyl or imidazolyl) and a short peptide tether including tryptophan, tyrosine and/or methionine side chains (Figure 5.13). The peptide tether can be obtained by standard solid phase peptide synthesis.⁷³ We suggest porphyrin-peptide linkage through an amide bond or using click chemistry similar to the methodology described in Chapter 3. After successful synthesis, these 2nd generation model complexes (as well as their dioxygen adducts) will be characterized by low temperature ¹H- and ²H-NMR as well as UV-visible spectroscopies. If

crosslink formation in such model complexes can be initiated, its development can be investigated with, for example, UV-visible stopped-flow spectroscopy and freeze-quench techniques. We will strive to observe or indirectly find evidence for some of the proposed steps in the suggested mechanism (Figure 5.12). Along these lines, we will investigate the addition of radical scavengers to the reaction such as TEMPO. Products can be analyzed with a combination of HPLC and ESI-mass spectrometry as reported in the literature. Furthermore, reactions including radical spin traps, e.g. phenyl-butyl-nitrone or other spin traps suitable for oxygen or nitrogen based radicals, will allow for studies of trapped intermediates by EPR spectroscopy.^{74, 75}

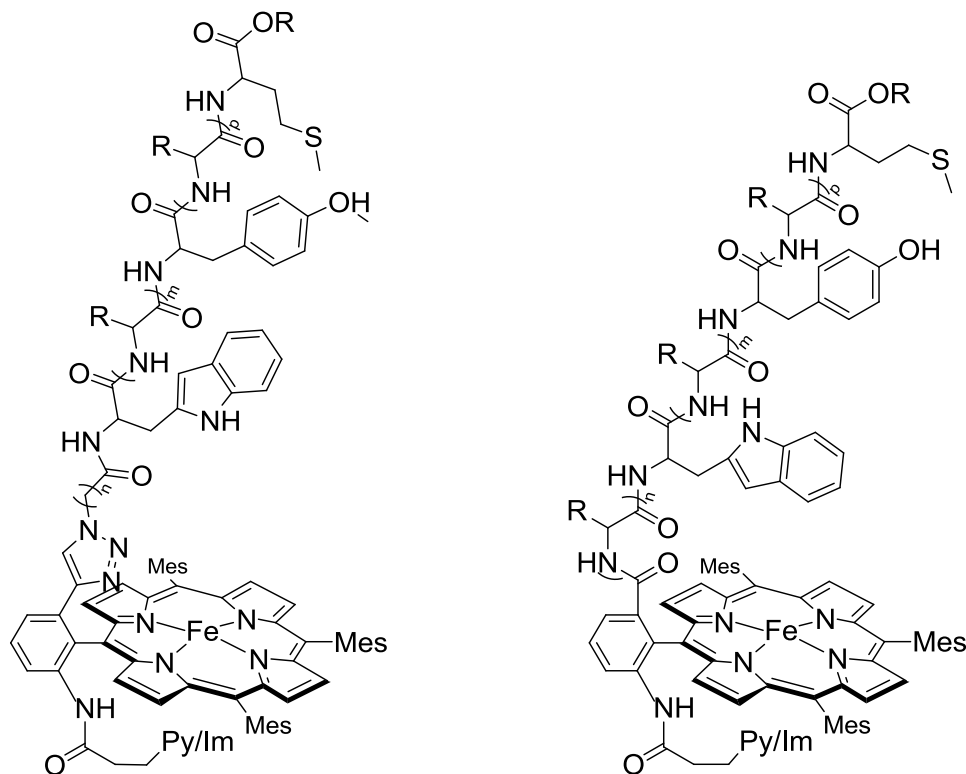


Figure 5.14: Planned 2nd generation model complexes.

Reactivity of Ferric Superoxo Complexes. Ghiladi et al. were able to propose several mechanisms for the activation of INH by KatG for wild type and INH resistant mutation variants. They concluded that the Compound III pathway (Figure 5.3, red) plays an important role in distinguishing INH susceptible wild type KatG from INH resistance mutations in their ability to catalyze INH-NADH adduct formation. The only intermediates observed for this pathway were Compound III [Fe(III)-(O₂⁻)] and Compound II [Fe(IV)=O]. Conversion from Compound III to Compound II formally requires two electrons, which are proposed to be delivered by two one-electron oxidations of INH. To find evidence for the validity of this mechanism, we propose to investigate the ferric-superoxo adducts of compounds **5.1** and **5.2** as well as the suggested 2nd generation model complexes (Figures 5.14) towards their ability to utilize INH as an electron donor for catalytic turnover. By comparing reactivity studies of **5.1** and **5.2** to 2nd generation model complexes, we might shed some light into the reactivity of ferric superoxo species of KatG towards substrate oxidation.

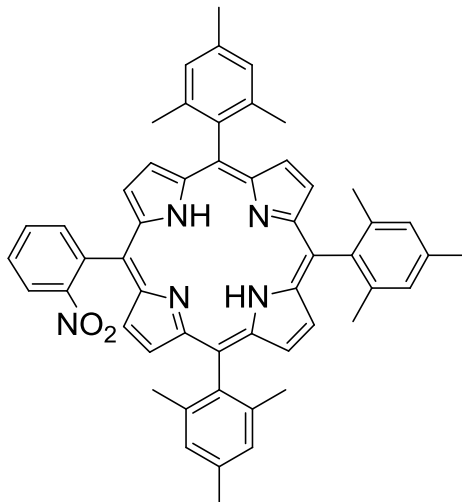
Experimental Methods

Material and Methods. Reagents and solvents were purchased from commercial sources and were of reagent quality. Dichloromethane and THF were dried with a MBraun solvent purifier. Preparation and handling of air-sensitive materials were carried out under an argon atmosphere using standard Schlenk technique. Solvents and solutions were deoxygenated by either repeated freeze-pump-thaw cycles, or by bubbling argon (10-20 min) directly through the solution. Solid air-sensitive samples were stored, handled and samples

for NMR spectroscopy were prepared in a MBraun LabMaster 130 (< 1 ppm O₂, < 1 ppm H₂O) glovebox under nitrogen atmosphere.

¹H-NMR spectra were measured on a Varian Mercury 300 or 400 MHz NMR spectrometer. ²H-NMR spectra were recorded on a Varian Gemini spectrometer at 46 MHz. All spectra were recorded in 5 mm o. d. NMR tubes, and chemical shifts are reported in δ values calibrated by the solvent peak with shifts referenced downfield from TMS. Mass spectrometric analysis was conducted on a Bruker Daltonics Omniflex MALDI-TOF MS and Agilent Technologies 5975 GC/MS (EI).

Variable temperature NMR studies. NMR solvents were degassed prior to use. In the glovebox, a solution containing 10-20 mg of the porphyrin to be investigated in 1 mL deuterated solvent was prepared and transferred to a 5 mm o.d. NMR tube with screw-cap septum top (Wilmad Glass). ¹H-NMR spectra were recorded at room temperature before cooling to the desired temperature. Addition of dioxygen at low temperature was carried out in the following manner: the NMR tube was removed from the spectrometer, placed in a dry ice/acetone bath, and using a syringe 3 mL of air was bubbled gently and directly through the solution by piercing the septum cap with a long syringe needle. Referencing of the spectra was performed as described above for each given temperature.



5-(2-Nitrophenyl)-10,15,20-tris-(2,4,6-trimethylphenyl)porphyrin 5.3.

1.2 L of dry dichloromethane, 9 mL ethanol (0.75%), 10.3 mL (70 mmol) mesitaldehyde, 6.3 g (47 mmol) 2-nitrobenzaldehyde and 8.1 mL (117 mmol) pyrrole were added to a 2 L 3-neck flask. The solution was deoxygenated with argon for 10 minutes. After the addition of 3.4 mL (28 mmol) $\text{BF}_3 \cdot \text{Et}_2\text{O}$ in the dark, the solution was stirred for 2 hours under inert gas atmosphere. 4 mL triethylamine and 14 g (88 mmol) of tetrachlorobenzoquinone were added and the solution was stirred for another 2 hours exposed to air. The dark green reaction mixture was then filtered through silica gel in a fritted filter funnel with dichloromethane as the eluent. The solvent was reduced to a volume of about 100 mL. The crude reaction mixture was brought to dryness in the presence of 70 mL of neutral alumina. For the chromatographic purification, the material was divided onto two columns with alumina as the stationary phase and hexane/dichloromethane 6:1 as the eluent. After the side product, tetramesitylporphyrin, had eluted from the column, the polarity of the solvent was increased to hexane/dichloromethane 4:1. The product fraction was chromatographed again under the same conditions. After recrystallization from hexane/dichloromethane 1.3 g (2.48 mmol, 5%)

of 5-(2-nitrophenyl)-10,15,20-tris(2,4,6-trimethylphenyl)porphyrin was isolated as purple crystals. $^1\text{H-NMR}$ (300 MHz, CDCl_3 , RT) δ 8.6 (d, 2H, $J^3 = 5$ Hz, β -pyrrole), 8.6 (s, 4H, β -pyrrole), 8.5 (d, 2H, $J^3 = 5$ Hz, β -pyrrole), 8.4 (dd, 1H, $J^3 = 7$ Hz, $J^4 = 2$ Hz), 8.1 (dd, 1H, $J^3 = 7$ Hz, $J^4 = 2$ Hz), 7.9 (m, 2H), 7.3 (br s, 6H, mesityl arom. H), 2.6 (s, 9H, mesityl- CH_3), 1.9 (s, 3H, mesityl- CH_3), 1.8 (s, 6H, mesityl- CH_3), 1.8 (s, 6H, mesityl- CH_3), 1.8 (s, 3H, mesityl- CH_3), -2.5 ppm (br, 2H, NH); UV-vis (CHCl_3 , RT, ϵ in $10^3 \cdot \text{M}^{-1} \text{cm}^{-1}$) λ_{max} 419 (324.3), 515 (16.1), 549 (4.9), 591 (4.8), 647 nm (1.9); MALDI-TOF MS m/z 786.0 ($\text{C}_{53}\text{H}_{48}\text{N}_5\text{O}_2$, $[\text{M}+\text{H}]^+$); R_f (silica, hexane: CH_2Cl_2 1:1) 0.4.

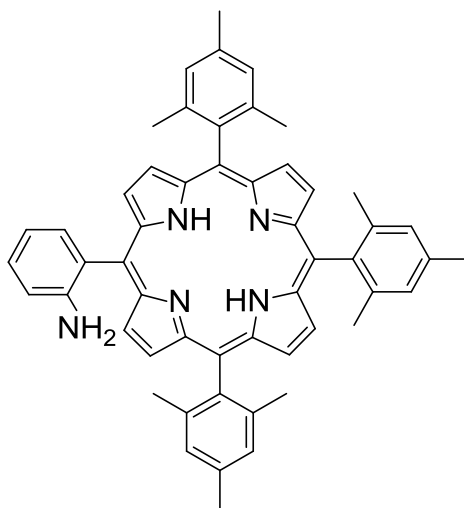
5-(2-Nitrophenyl)-10,15,20-tris-(2,4,6-trimethylphenyl)porphyrin 5.3-d₂.

Synthesis was analogous to the procedure described for **5.3** but EtOH was substituted with EtOD for the reaction solvent. Yield 4%. $^1\text{H-NMR}$ (400 MHz, CDCl_3 , RT) δ 8.7 (m, 2H, β -pyrrole), 8.6 (s, 2.3H, β -pyrrole), 8.5 (m, 1.5H, β -pyrrole), 8.5 (dd, 1H, $J^3 = 7$ Hz, $J^4 = 2$ Hz), 8.2 (dd, 1H, $J^3 = 7$ Hz, $J^4 = 2$ Hz), 7.9 (m, 2H), 7.3 (m, 6H, mesityl arom. H), 2.6 (s, 9H, mesityl- CH_3), 1.9-1.8 (several s, 18H, mesityl- CH_3), -2.5 ppm (br, 2H, NH); MALDI-TOF MS m/z 787.6 ($\text{C}_{53}\text{H}_{45}\text{D}_2\text{N}_5\text{O}_2$, $[\text{M}]^+$); R_f (silica, hexane: CH_2Cl_2 1:1) 0.4.

5-(2-Nitrophenyl)-10,15,20-tris-(2,4,6-trimethylphenyl)porphyrin 5.3-d₈.

Deuterated **5.3-d₈** was synthesized by the same procedure as described under for **5.3** using d_5 -pyrrole and 1.2 L DCM with 0.75% EtOD as the solvent. Yield 5%. $^1\text{H-NMR}$ (400 MHz, CDCl_3 , RT) δ 8.7-8.6 (3 s, 0.5H, β -pyrrole), 8.5 (m, 1H, $J = 2$ Hz), 8.2 (m, 1H), 7.9 (m, 2H), 7.3 (m, 6H, mesityl arom. H), 2.6 (s, 9H, mesityl- CH_3), 1.9-1.8 (several s, 18H, mesityl-

CH₃), -2.5 ppm (br, 2H, NH); MALDI-TOF MS *m/z* 793.1 (C₅₃H₃₉D₈N₅O₂, [M]⁺); R_f (silica, hexane:CH₂Cl₂ 1:1) 0.4.



5-(2-Aminophenyl)-10,15,20-tris-(2,4,6-trimethylphenyl)porphyrin 5.4.

718 mg (3.18 mmol) tin(II)chloride in 20 mL conc. HCl were dissolved in a 100 mL 3-neck flask. 500 mg (0.64 mmol) of the nitroporphyrin **5.3** was dissolved in about 25 mL chloroform and added to the flask. The solution turned bright green/blue. The mixture was stirred vigorously for 2 h at RT, then 50 min at 65-70 °C. Afterwards, the solution was cooled to 0 °C in an ice bath and neutralized with about 30 mL of ammonium hydroxide. The solution was stirred for 10 minutes and poured into a separatory funnel. The organic phase was extracted 3 times with brine and dried over Na₂SO₄. Recrystallization from hexane/dichloromethane gave 478 mg (0.63 mmol, 99%) of 5-(2-aminophenyl)-10,15,20-tris(2,4,6-trimethylphenyl)porphyrin as dark purple crystals. ¹H-NMR (300 MHz, CDCl₃, RT) δ 8.8 (d, 2H, *J*³ = 5 Hz, β-pyrrole), 8.6 (d, 2H, *J*³ = 5 Hz, β-pyrrole), 8.6 (s, 4H, β-pyrrole), 7.8 (dd, 1H, *J*³ = 7 Hz, *J*⁴ = 2 Hz), 7.6 (dd, 1H *J*³ = 7 Hz, *J*⁴ = 2 Hz), 7.3 (br, s, 6H,

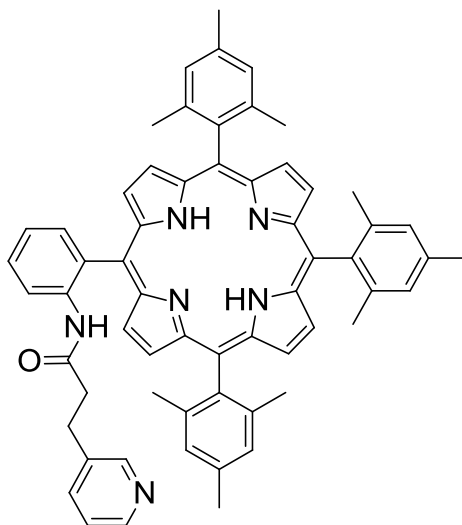
mesityl arom. H), 7.1 (m, 2H), 3.6 (br s, 2H, NH₂), 2.6 (s, 9H, mesityl-H), 1.8 (s, 9H, mesityl-H), 1.9 (s, 9H, mesityl-H), -2.5 ppm (s, 2H, NH); UV-vis (CHCl₃, RT, ϵ in 10³ M⁻¹cm⁻¹) λ_{max} 418 (328.5), 514 (16.2), 547 (4.5), 589 (4.8), 645 nm (2.1); MALDI-TOF MS m/z 755 (C₅₃H₄₉N₅, [M]⁺); R_f (silica, hexane:CH₂Cl₂ 1:1) 0.3.

5-(2-Aminophenyl)-10,15,20-tris-(2,4,6-trimethylphenyl)porphyrin 5.4-d₂.

Synthesis was analogous to the procedure described for **5.4**. Yield 99%. ¹H-NMR (400 MHz, CDCl₃, RT) δ 8.8 (d, 1.5H, $J^3 = 4.4$ Hz, β -pyrrole), 8.6 (d, 1.5H, $J^3 = 4.4$ Hz, β -pyrrole), 8.6 (s, 3H, β -pyrrole), 7.8 (dd, 1H, $J^3 = 7.2$ Hz, $J = 2.0$ Hz), 7.6 (dd, 1H, $J^3 = 7.2$ Hz, $J^4 = 2.0$ Hz), 7.3 (br s, 6H, mesityl arom. H), 7.1 (m, 2H), 3.6 (br s, 2H, NH₂), 2.6 (s, 9H, mesityl-H), 1.84 (s, 9H, mesityl-H), 1.80 (s, 9H, mesityl-H), -2.6 ppm (s, 2H, NH); MALDI-TOF MS m/z 757.7 (C₅₃H₄₇D₂N₅, [M]⁺); R_f (silica, hexane:CH₂Cl₂ 1:1) 0.3.

5-(2-Aminophenyl)-10,15,20-tris-(2,4,6-trimethylphenyl)porphyrin 5.4-d₈.

Synthesis was analogous to the procedure described for **5.4**. Yield 80%. ¹H-NMR (400 MHz, CDCl₃, RT) δ 8.8-8.6 (3 m, 0.6H, β -pyrrole), 7.8 (d, 1H, $J^3 = 7.2$ Hz), 7.6 (m, 1H), 7.3 (br s, 6H, mesityl arom. H), 7.1 (m, 2H), 3.6 (br s, 2H, NH₂), 2.6 (s, 9H, mesityl-H), 1.84 (s, 9H, mesityl-H), 1.81 (s, 9H, mesityl-H), -2.6 ppm (s, 2H, NH); MALDI-TOF MS m/z 763.1 (C₅₃H₄₁D₈N₅, [M]⁺); R_f (silica, hexane:CH₂Cl₂ 1:1) 0.3.



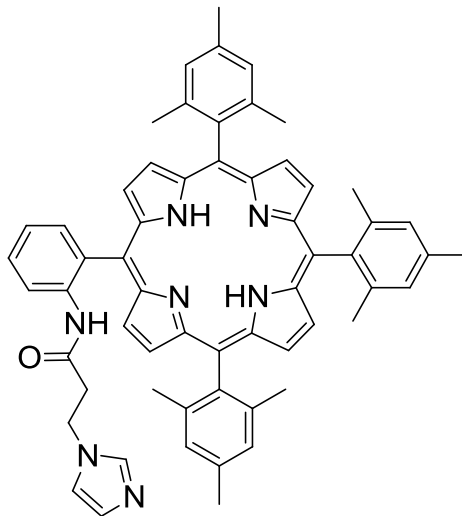
5-{2-[3-(Pyridin-3-yl)propionyl]aminophenyl}-10,15,20-tris-(2,4,6-trimethylphenyl)porphyrin 5.5.

360 mg (2.38 mmol) 3-(3-pyridinyl)propionic acid was dissolved in 5 mL (69.0 mmol) thionyl chloride under argon in a dry 100 mL 3-neck flask equipped with a reflux condenser. The reaction mixture was heated to 60-70 °C for 3.5 hours. The solvent was evaporated *in vacuo* and the 3-pyridinepropionyl chloride was dried under high vacuum for 20-30 minutes. In another dry 100 mL 2-neck flask, 600 mg (0.4 mmol) of porphyrin **5.4** was dissolved in 25 mL dry THF under argon atmosphere. After addition of 0.6 mL of triethylamine, the propionyl chloride, dissolved in 15 mL dry DMF, was added dropwise to the porphyrin solution. The reaction mixture was stirred at RT until TLC analysis showed consumption of the starting material (3 h). 15 mL of water was added dropwise to precipitate the porphyrin. The aqueous solution was decanted, the porphyrin redissolved in 40 mL of dichloromethane and dried over Na₂SO₄. The product was purified by repeated column chromatography on alumina with dichloromethane/hexane/methanol 400:200:5 as the eluent.

The reaction yielded 543 mg (0.61 mmol, 77%) of **5.5** as purple crystals. $^1\text{H-NMR}$ (400 MHz, CDCl_3 , RT) δ 8.7 (s, 4H, β -pyrrole), 8.6 (s, 4H, β -pyrrole), 8.1 (m, 1H), 7.9 (m, 2H), 7.8 (t, 1H, $J^3 = 7$ Hz), 7.4 (t, 1H, $J^3 = 7$ Hz), 7.3 (br, s 6H, mesityl arom. H), 6.8 (m, 3H), 2.6 (s, 9H, mesityl- CH_3), 2.4 (t, 3H, $J^3 = 8$ Hz, CH_2 -tether), 1.8-1.7 (three s, 18H, mesityl- CH_3), 1.6 (t, 3H, $J^3 = 8$ Hz, CH_2 -tether), -2.6 ppm (s, 2H, NH); UV-vis (CHCl_3 , RT, ϵ in $10^3 \text{ M}^{-1}\text{cm}^{-1}$) λ_{max} 305 (14.2), 369 (22.3), 419 (420.0), 514 (18.4), 549 (5.4), 646 nm (2.4); MALDI-TOF MS m/z 889.6 ($\text{C}_{61}\text{H}_{56}\text{N}_6\text{O}$, $[\text{M}]^+$); R_f (alumina, hexane: CH_2Cl_2 :MeOH 4:6:0.2) 0.2.

*5-{2-[3-(Pyridin-3-yl)propionyl]aminophenyl}-10,15,20-tris-(2,4,6-trimethylphenyl)porphyrin **5.5-d₂**.*

Synthesis was analogous to the procedure described for **5.5** and **5.4-d₂** was used as a substrate. Yield 87%; $^1\text{H-NMR}$ (400 MHz, CDCl_3 , RT) δ 8.8 (m, 6H, β -pyrrole), 8.2 (m, 1H), 8.1 (d, $J^3=7$ Hz, 1H), 8.0 (s, 1H), 7.9 (t, 1H, $J^3 = 7$ Hz), 7.6 (t, 1H, $J^3 = 7$ Hz), 7.4 (br s, 6H, mesityl arom. H), 7.0 (m, 3H), 6.8 (m, 1H), 2.7 (s, 9H, mesityl- CH_3), 2.6 (t, 3H, $J^3 = 8$ Hz, CH_2 -tether), 2.0-1.9 (three s, 18H, mesityl- CH_3), 1.7 (t, 3H, $J^3 = 8$ Hz, CH_2 -tether), -2.5 ppm (s, 2H, NH); $^{13}\text{C-NMR}$ (100 MHz, CDCl_3 , RT) δ 169.8, 149.5, 147.6, 139.6 (C overlapping), 139.5, 139.3, 138.6, 138.15, 138.10, 135.6, 135.5, 135.2, 131.5, 131.4-129.4 (br, β -C porphyrin), 129.7, 128.1, 128.0, 123.2, 123.1, 39.9, 28.0, 22.0 (C overlapping), 21.7 ppm; MALDI-TOF MS m/z 890.8 ($\text{C}_{61}\text{H}_{54}\text{D}_2\text{N}_6\text{O}$, $[\text{M}]^+$); R_f (alumina, hexane: CH_2Cl_2 :MeOH 4:6:0.2) 0.2.

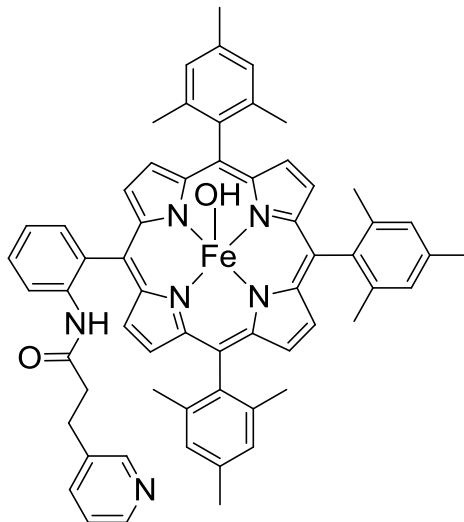


5-[2-[3-(1H-Imidazol-1-yl)propionyl]aminophenyl]-10,15,20-tris-(2,4,6-trimethylphenyl)-porphyrin **5.6**.

300 mg (2.13 mmol) 3-(1H-imidazol-1-yl)propionyl acid was dissolved in 3 mL (41.0 mmol) thionyl chloride under argon in a dry 100 mL 3-neck flask equipped with a reflux condenser. The reaction mixture was heated to 60-70 °C for 2 hours. The solvent was evaporated *in vacuo* and the 3-(1H-imidazol-1-yl)propionyl chloride was dried under high vacuum for 20-30 minutes. The acid chloride and 537 mg (0.7 mmol) porphyrin **5.4** were dissolved in a total volume of 115 mL glacial acetic acid. A solution of sodium acetate (590 mg in 12 mL H₂O) was added over a period of 3 h under inert atmosphere in the dark. The reaction solution was stirred for 3 more hours, after which it was diluted in CH₂Cl₂ in a separatory funnel and extracted with degassed water and sat. NaHCO₃. The organic phase was dried over Na₂SO₄ and the solvent was removed under reduced pressure. The crude product was purified by column chromatography on silica with CH₂Cl₂:NEt₃ (100:0.1) increasing to CH₂Cl₂:NEt₃:MeOH (100:0.1:1.5) to elute the product fraction. A second column under the

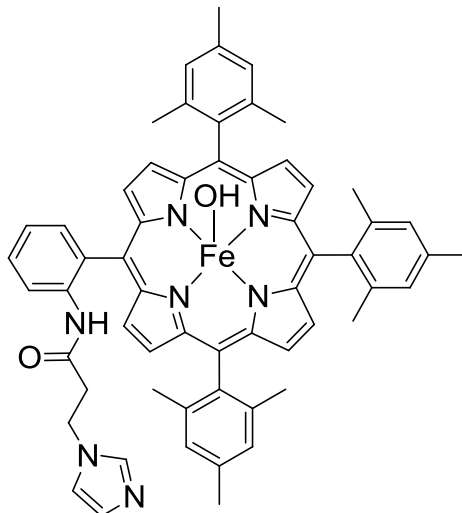
same conditions was necessary to obtain a pure product. After recrystallization from CH₂Cl₂/heptane, 350 mg (0.4 mmol, 56%) of **5.6** were isolated as a purple solid. ¹H-NMR (300 MHz, CDCl₃, RT) δ 8.7-8.6 (m, 8H, β-pyrrole), 8.0 (dd, 1H, $J^3 = 7$ Hz, $J^4 = 1$ Hz), 7.8 (td, 1H, $J^3 = 7$ Hz, $J^4 = 1$ Hz), 7.5 (td, 1H, $J^3 = 7$ Hz, $J = 1$ Hz), 7.3 (s, 6H, mesityl arom. H), 7.1 (s, 1H), 6.8 (s, 1H), 6.7 (s, 1H), 6.4 (s, 1H), 3.8 (t, 2H, $J^3 = 6$ Hz, CH₂-tether), 2.6 (s, 9H, mesityl-CH₃), 1.8 (s, 18H, mesityl-CH₃), 1.7 (t, 2H, $J^3 = 6$ Hz, tether CH₂), -2.5 (br, s, 2H, NH); UV-vis (CH₂Cl₂, RT) λ_{max} 373, 419, 515, 548, 590, 645 nm; MALDI-TOF MS m/z 878 (C₅₉H₅₅N₇O, [M]⁺); R_f (silica, CH₂Cl₂:MeOH:NEt₃ 100:1.5:0.1) 0.2.

Insertion of Iron. Under argon atmosphere, 0.16 mmol of the unmetallated porphyrin was placed in a dry 100 mL 3-neck flask equipped with a reflux condenser and air-free dropping funnel, which was charged with 20 mL dry THF. The THF was deoxygenated for 15 minutes and added to the porphyrin. The solution was heated to reflux, 480 mg (2.45 mmol) FeCl₂·4 H₂O was added, and refluxed for 5 additional hours. After the solution had cooled to room temperature, 5-10 mL of 1 mol/l NaOH was added and stirring was continued for 30 minutes. The organic phase was extracted twice with 1 mol/l NaOH and once with deionized water. The organic phase was dried over Na₂SO₄ followed by concentration to minimal volume. The crude reaction mixture was purified by column chromatography.



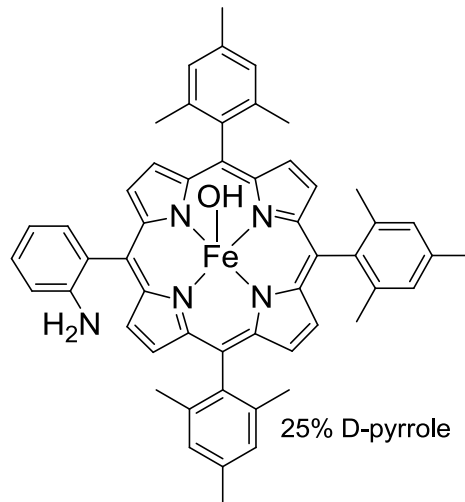
5-{2-[3-(Pyridine-3-yl)propionyl]aminophenyl}-10,15,20-tris-(2,4,6-trimethylphenyl)-porphyrin iron(III) hydroxide 5.5.

Purification: alumina, 100:2:0.1 CH₂Cl₂:MeOH:NEt₃. Yield: 65%. ¹H-NMR (400 MHz, THF, RT) δ 80 ppm (β-pyrrole-H); UV-vis (CHCl₃, RT, ε in 10³ M⁻¹cm⁻¹) λ_{max} 577 (0.8), 419 (115.1), 334 nm (32.1); MALDI-TOF MS m/z = 942.9 (C₆₁H₅₄N₆O₁Fe, [M-OH]⁺); R_f (alumina,CH₂Cl₂: MeOH:NEt₃ 100:1:0.1) 0.2.



5-[2-[3-(1H-Imidazol-1-yl)propionyl]aminophenyl]-10,15,20-tris-(2,4,6-trimethylphenyl)-porphyrin iron(III) hydroxide **5.6**.

Purification: alumina, 100:2:0.1 CH₂Cl₂:MeOH:NEt₃. Yield: 62%. ¹H-NMR (400 MHz, THF, RT) δ 82 ppm (β-pyrrole-H); UV-vis (CHCl₃, RT) λ_{max} 636 (sh), 580, 417, 333 nm; MALDI-TOF MS m/z = 931.0 (C₅₉H₅₅N₇O₁Fe, [M-OH]⁺); R_f (alumina, CH₂Cl₂: MeOH:NEt₃ 100:2:0.1) 0.1.

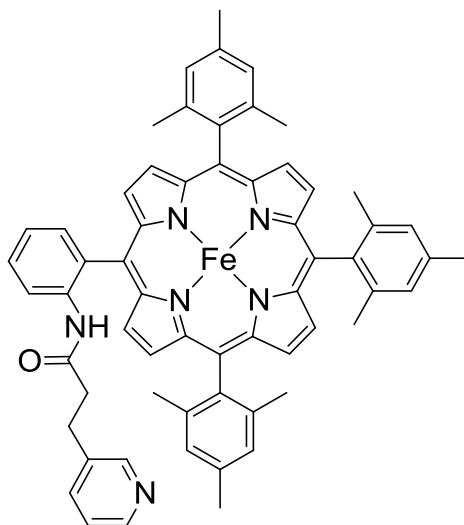


5-(2-Aminophenyl)-10,15,20-tris-(2,4,6-trimethylphenyl)porphyrin iron (III) 5.7-d₂.

Purification: alumina, 100:2:0.1 CH₂Cl₂:MeOH:NEt₃. Yield 75%. ²H-NMR (400 MHz, RT): CDCl₃, δ 80 ppm (β-pyrrole-D); LDI-TOF MS m/z = 811.8 (C₅₃H₄₅D₂N₅Fe, [M-OH]⁺).

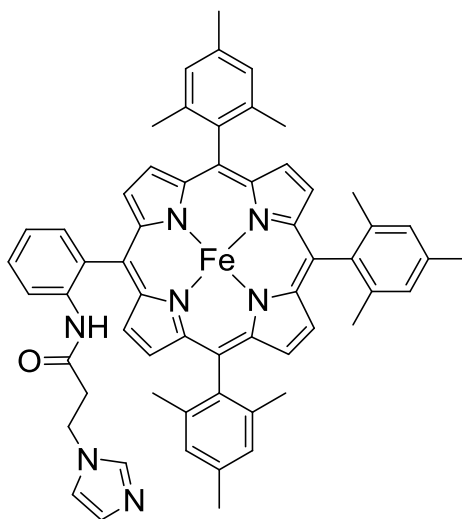
Reduction procedure generating the Fe(II) complexes 5.1 and 5.2.

Under Ar, to a solution of the porphyrin (0.1-0.2 mmol) dissolved in 80 mL deoxygenated CH₂Cl₂ was added 40 mL of 1 mol/L sodium hydrosulfite in deoxygenated water. The two solutions were agitated with Ar bubbling for 30 minutes to ensure complete mixing. The color of the organic phase changed from red-brown to intensely red. After separation of the two layers, the organic one was allowed to slowly pass through a Schlenk filter tube over which was packed a small plug of anhydrous sodium sulfate. The solvent was removed *in vacuo* and the Fe(II) complexes **5.1** and **5.2** were isolated and subsequently stored at -40 °C under inert atmosphere.



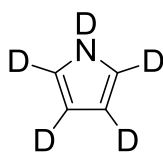
5-{2-[3-(Pyridine-3-yl)propionyl]aminophenyl}-10,15,20-tris-(2,4,6-trimethylphenyl)porphyrin iron(II) 5.1.

Yield 95%. $^1\text{H-NMR}$ (400 MHz, RT): THF, δ 47-43 (β -pyrrole-H); DCM, δ 40-43 (β -pyrrole-H); acetone, δ 47-43 ppm (β -pyrrole-H); MALDI-TOF MS $m/z = 942.9$ ($\text{C}_{61}\text{H}_{54}\text{N}_6\text{OFe}$, $[\text{M}]^+$).



5-{2-[3-(1H-Imidazol-1-yl)propionyl]aminophenyl}-10,15,20-tris-(2,4,6-trimethylphenyl)-porphyrin iron(II) **5.2**.

Yield 95%. $^1\text{H-NMR}$ (400 MHz, RT): THF, δ 45-43 (β -pyrrole-H); DCM, δ 65, 54-52 (β -pyrrole-H), 50 (β -pyrrole-H); acetone, δ 63, 55 (β -pyrrole-H), 53 (β -pyrrole-H), 51 ppm (β -pyrrole-H); MALDI-TOF MS $m/z = 931.3$ ($\text{C}_{59}\text{H}_{54}\text{N}_7\text{OFe}$, $[\text{M}+\text{H}]^+$).



Pyrrole-d₅.

A solution of 50 g (0.747 mol) pyrrole in 47 mL (0.82 mol) acetic acid- d_1 and 100 mL (5.0 mol) deuterium oxide were stirred at room temperature over night in the dark. 300 mL of DCM were added and the suspension was neutralized with potassium carbonate. After filtration, the solvent was removed *in vacuo* and the reaction was repeated. After 2 cycles the

crude product was purified by vacuum distillation. 37 g (0.513 mol, 70%) of pyrrole-*d*₅ was isolated. ²H-NMR (46 MHz, CHCl₃, RT) δ 8.3 (br, s, 1D, ND), 6.8 (s, 2D), 6.2 ppm (s, 2D); GC EI-MS m/z 72 (C₅D₅N, [M]⁺).

REFERENCES

1. Holm, R. H.; Kennepohl, P.; Solomon, E. I., Structural and Functional Aspects of Metal Sites in Biology. *Chemical Reviews* **1996**, 96, (7), 2239.
2. Momenteau, M.; Reed, C. A., Synthetic Heme-Dioxygen Complexes. *Chemical Reviews* **1994**, 94, (3), 659.
3. Niederhoffer, E. C.; Timmons, J. H.; Martell, A. E., Thermodynamics of oxygen binding in natural and synthetic dioxygen complexes. *Chemical Reviews* **1984**, 84, (2), 137.
4. Meunier, B.; de Visser, S. I. P.; Shaik, S., Mechanism of Oxidation Reactions Catalyzed by Cytochrome P450 Enzymes. *Chemical Reviews* **2004**, 104, (9), 3947.
5. Solomon, E. I.; Sundaram, U. M.; Machonkin, T. E., Multicopper Oxidases and Oxygenases. *Chemical Reviews* **1996**, 96, (7), 2563.
6. Solomon, E. I.; Szilagyi, R. K.; DeBeer George, S.; Basumallick, L., Electronic Structures of Metal Sites in Proteins and Models: Contributions to Function in Blue Copper Proteins. *Chemical Reviews* **2004**, 104, (2), 419.
7. Ortiz de Montellano, P. R., Hydrocarbon Hydroxylation by Cytochrome P450 Enzymes. *Chemical Reviews* **2009**, 110, (2), 932.
8. Riley, D. P., Functional Mimics of Superoxide Dismutase Enzymes as Therapeutic Agents. *Chemical Reviews* **1999**, 99, (9), 2573.
9. Baik, M.-H.; Newcomb, M.; Friesner, R. A.; Lippard, S. J., Mechanistic Studies on the Hydroxylation of Methane by Methane Monooxygenase. *Chemical Reviews* **2003**, 103, (6), 2385.
10. Messerschmidt, A.; Huber, R.; Poulos, T.; Wieghardt, K., *Handbook of Metalloenzymes*. John Wiley & Sons, Ltd.: West Sussex, 2001; Vol. 2.
11. Cade, C. E.; Dlouhy, A. C.; Medzihradzky, K. F.; Salas-Castillo, S. P.; Ghiladi, R. A., Isoniazid-resistance conferring mutations in Mycobacterium tuberculosis KatG: Catalase, peroxidase, and INH-NADH adduct formation activities. *Protein Science* **19**, (3), 458.
12. Smulevich, G.; Jakopitsch, C.; Droghetti, E.; Obinger, C., Probing the structure and bifunctionality of catalase-peroxidase (KatG). *Journal of Inorganic Biochemistry* **2006**, 100, (4), 568.

13. Jakopitsch, C.; Ivancich, A.; Schmuckenschlager, F.; Wanasinghe, A.; Poltl, G.; Furtmuller, P. G.; Ruker, F.; Obinger, C., Influence of the Unusual Covalent Adduct on the Kinetics and Formation of Radical Intermediates in *Synechocystis* Catalase Peroxidase: A stopped-flow and EPR characterization of the Met275, TYyr249, and Arg439 variants. *Journal of Biological Chemistry* **2004**, 279, (44), 46082.
14. Jakopitsch, C.; Auer, M.; Ivancich, A.; Ruker, F.; Furtmuller, P. G.; Obinger, C., Total Conversion of Bifunctional Catalase-Peroxidase (KatG) to Monofunctional Peroxidase by Exchange of a Conserved Distal Side Tyrosine. *Journal of Biological Chemistry* **2003**, 278, (22), 20185.
15. Yamada, Y.; Fujiwara, T.; Sato, T.; Igarashi, N.; Tanaka, N., The 2.0 Å crystal structure of catalase-peroxidase from *Haloarcula marismortui*. *Nature Structural & Molecular Biology* **2002**, 9, (9), 691.
16. Carpena, X.; Loprasert, S.; Mongkolsuk, S.; Switala, J.; Loewen, P. C.; Fita, I., Catalase-peroxidase KatG of *Burkholderia pseudomallei* at 1.7 Å resolution. *Journal of Molecular Biology* **2003**, 327, (2), 475.
17. Bertrand, T.; Eady, N. A. J.; Jones, J. N.; Jesmin; Nagy, J. M.; Jamart-Gregoire, B.; Raven, E. L.; Brown, K. A., Crystal Structure of *Mycobacterium tuberculosis* Catalase-Peroxidase. *Journal of Biological Chemistry* **2004**, 279, (37), 38991.
18. Welinder, K. G., Superfamily of plant, fungal and bacterial peroxidases. *Current Opinion in Structural Biology* **1992**, 2, 388.
19. Ostermeier, C.; Harrenga, A.; Ermler, U.; Michel, H., Inaugural Article: Structure at 2.7 Å resolution of the *Paracoccus denitrificans* two-subunit cytochrome c oxidase complexed with an antibody FV fragment. *Proceedings of the National Academy of Sciences* **1997**, 94, (20), 10547.
20. Yoshikawa, S.; Shinzawa-Itoh, K.; Nakashima, R.; Yaono, R.; Yamashita, E.; Inoue, N.; Yao, M.; Fei, M. J.; Libeu, C. P.; Mizushima, T.; Yamaguchi, H.; Tomizaki, T.; Tsukihara, T., Redox-Coupled Crystal Structural Changes in Bovine Heart Cytochrome c Oxidase. *Science* **1998**, 280, (5370), 1723.
21. Bravo, J.; Fita, I.; Ferrer, J. C.; Ens, W.; Hillar, A.; Switala, J.; Loewen, P. C., Identification of a novel bond between a histidine and the essential tyrosine in catalase HPII of *Escherichia coli*. *Protein Science* **1997**, 6, (5), 1016.
22. Ito, N.; Phillips, S. E. V.; Yadav, K. D. S.; Knowles, P. F., Crystal Structure of a Free Radical Enzyme, Galactose Oxidase. *Journal of Molecular Biology* **1994**, 238, (5), 704.

23. Ito, N.; Phillips, S. E. V.; Stevens, C.; Ogel, Z. B.; McPherson, M. J.; Keen, J. N.; Yadav, K. D. S.; Knowles, P. F., Novel thioether bond revealed by a 1.7Å crystal structure of galactose oxidase. *Nature* **1991**, 350, (6313), 87.
24. Proshlyakov, D. A.; Pressler, M. A.; DeMaso, C.; Leykam, J. F.; DeWitt, D. L.; Babcock, G. T., Oxygen Activation and Reduction in Respiration: Involvement of Redox-Active Tyrosine 244. *Science* **2000**, 290, (5496), 1588.
25. Mate, M. J.; Sevinc, M. S.; Hu, B.; Bujons, J.; Bravo, J.; Switala, J.; Ens, W.; Loewen, P. C.; Fita, I., Mutants That Alter the Covalent Structure of Catalase Hydroperoxidase II from *Escherichia coli*. *Journal of Biological Chemistry* **1999**, 274, (39), 27717.
26. Ghiladi, R. A.; Knudsen, G. M.; Medzihradzky, K. F.; de Montellano, P. R. O., The Met-Tyr-Trp Cross-link in *Mycobacterium tuberculosis* Catalase-peroxidase (KatG): Autocatalytic Formation and effect on Enzyme Catalysis and Spectroscopic Properties. *Journal of Biological Chemistry* **2005**, 280, (24), 22651.
27. Ghiladi, R. A.; Medzihradzky, K. F.; Ortiz de Montellano, P. R., Role of the Met-Tyr-Trp cross-link in *Mycobacterium tuberculosis* catalase-peroxidase (KatG) as revealed by KatG(M255I). *Biochemistry* **2005**, 44, (46), 15093.
28. Fox, H. H., The Chemical Approach to the Control of Tuberculosis. *Science* **1952**, 116, (3006), 129.
29. Zhang, Y., The magic bullets and tuberculosis drug targets. *Annual Review of Pharmacology and Toxicology* **2005**, 45, (1), 529.
30. Rozwarski, D. A.; Grant, G. A.; Barton, D. H.; nbsp; R; Jacobs, W. R., Jr.; Sacchettini, J. C., Modification of the NADH of the Isoniazid Target (InhA) from *Mycobacterium tuberculosis*. *Science* **1998**, 279, (5347), 98.
31. Lei, B.; Wei, C.-J.; Tu, S.-C., Action Mechanism of Antitubercular Isoniazid. Action by *Mycobacterium tuberculosis* KatG, Isolation, and characterization of InhA inhibitor. *Journal of Biological Chemistry* **2000**, 275, (4), 2520.
32. Martin Wilming, K. J., Spontaneous Formation of the Bioactive Form of the Tuberculosis Drug Isoniazid. *Angewandte Chemie International Edition* **1999**, 38, (17), 2588.
33. Rouse, D. A.; DeVito, J. A.; Li, Z.; Byer, H.; Morris, S. L., Site-directed mutagenesis of the katG gene of *Mycobacterium tuberculosis*: effects on catalase-peroxidase activities and isoniazid resistance. *Molecular Microbiology* **1996**, 22, (3), 583.
34. Wei, C.-J.; Lei, B.; Musser, J. M.; Tu, S.-C., Isoniazid Activation Defects in Recombinant *Mycobacterium tuberculosis* Catalase-Peroxidase (KatG) Mutants Evident in InhA Inhibitor Production. *Antimicrobial Agents and Chemotherapy* **2003**, 47, (2), 670.

35. Ghiladi, R. A.; Medzihradzky, K. F.; Rusnak, F. M.; Ortiz de Montellano, P. R., Correlation between isoniazid resistance and superoxide reactivity in mycobacterium tuberculosis KatG. *Journal of the American Chemical Society* **2005**, 127, (38), 13428.
36. Collman, J. P.; Boulatov, R.; Sunderland, C. J.; Fu, L., Functional Analogues of Cytochrome c Oxidase, Myoglobin, and Hemoglobin. *Chemical Reviews* **2004**, 104, (2), 561.
37. Chang, C. K.; Traylor, T. G., Solution behavior of a synthetic myoglobin active site. *Journal of the American Chemical Society* **1973**, 95, (17), 5810.
38. Chang, C. K.; Traylor, T. G., Synthesis of the Myoglobin Active Site. *Proceedings of the National Academy of Sciences of the United States of America* **1973**, 70, (9), 2647.
39. Traylor, T. G.; Chang, C. K.; Geibel, J.; Berzinis, A.; Mincey, T.; Cannon, J., Syntheses and NMR characterization of chelated heme models of hemoproteins. *Journal of the American Chemical Society* **1979**, 101, (22), 6716.
40. Momenteau, M.; Rougee, M.; Loock, B., Five-Coordinate Iron-Porphyrin as a Model for the Active Site of Hemoproteins. *European Journal of Biochemistry* **1976**, 71, (1), 63.
41. Collman, J. P.; Gagne, R. R.; Halbert, T. R.; Marchon, J. C.; Reed, C. A., Reversible oxygen adduct formation in ferrous complexes derived from a picket fence porphyrin. Model for oxymyoglobin. *Journal of the American Chemical Society* **1973**, 95, (23), 7868.
42. Collman, J. P.; Gagne, R. T.; Reed, C. A., Paramagnetic dioxygen complex of iron(II) derived from a picket fence porphyrin. Further models for hemoproteins. *Journal of the American Chemical Society* **1974**, 96, (8), 2629.
43. Walker, F. A.; Simonis, U., Iron Porphyrin Chemistry. In *Encyclopedia of Inorganic Chemistry*, 2nd ed.; King, R. B., Ed. John Wiley & Sohns, Ltd: Chichester, 2005; Vol. IV, p 2390.
44. Safo, M. K.; Gupta, G. P.; Walker, F. A.; Scheidt, W. R., Models of the cytochromes b. Control of axial ligand orientation with a hindered porphyrin system. *Journal of the American Chemical Society* **1991**, 113, (15), 5497.
45. Walker, F. A.; Reis, D.; Balke, V. L., Models of the cytochromes b. 5. EPR studies of low-spin iron(III) tetraphenylporphyrins. *Journal of the American Chemical Society* **1984**, 106, (23), 6888.
46. Kopf, M. A.; Karlin, K. D., Dioxygen Reactivity of Reduced Heme and Heme-Copper Complexes Utilizing Tetraarylporphyrinates Tethered with Both a Pyridyl Axial Ligand and N,N-Bis[2-(2-pyridyl)ethyl]amine Chelate. *Inorganic Chemistry* **1999**, 38, (22), 4922.

47. Kim, E.; Shearer, J.; Lu, S.; Moenne-Loccoz, P.; Helton, M. E.; Kaderli, S.; Zuberbuhler, A. D.; Karlin, K. D., Heme/Cu/O₂ Reactivity: Change in Fe^{III}-(O₂²⁻)-Cu^{II} Unit Peroxo Binding Geometry Effected by Tridentate Copper Chelation. *Journal of the American Chemical Society* **2004**, 126, (40), 12716.
48. Liu, J.-G.; Naruta, Y.; Tani, F., A Functional Model of the Cytochrome c Oxidase Active Site: Unique Conversion of a Heme-μ-peroxo-CuII Intermediate into Heme- superoxo/CuI. *Angewandte Chemie* **2005**, 117, (12), 1870.
49. Collman, J. P.; Ghosh, S.; Dey, A.; Decreau, R. A.; Yang, Y., Catalytic Reduction of O₂ by Cytochrome c Using a Synthetic Model of Cytochrome c Oxidase. *Journal of the American Chemical Society* **2009**, 131, (14), 5034.
50. Collman, J. P.; Fu, L.; Herrmann, P. C.; Zhang, X., A Functional Model Related to Cytochrome c Oxidase and Its Electrocatalytic Four-Electron Reduction of O₂. *Science* **1997**, 275, (5302), 949.
51. Collman, J. P.; Devaraj, N. K.; Decreau, R. A.; Yang, Y.; Yan, Y.-L.; Ebina, W.; Eberspacher, T. A.; Chidsey, C. E. D., A Cytochrome c Oxidase Model Catalyzes Oxygen to Water Reduction Under Rate-Limiting Electron Flux. *Science* **2007**, 315, (5818), 1565.
52. Collman, J. P.; Dey, A.; Decreau, R. A.; Yang, Y.; Hosseini, A.; Solomon, E. I.; Eberspacher, T. A., Interaction of nitric oxide with a functional model of cytochrome c oxidase. *Proceedings of the National Academy of Sciences* **2008**, 105, (29), 9892.
53. Liu, J.-G.; Ohta, T.; Yamaguchi, S.; Ogura, T.; Sakamoto, S.; Maeda, Y.; Naruta, Y., Spectroscopic Characterization of a Hydroperoxo-Heme Intermediate: Conversion of a Side-On Peroxo to an End-On Hydroperoxo Complex. *Angewandte Chemie International Edition* **2009**, 48, (49), 9262.
54. Cheng, R. J.; Latos-Grazynski, L.; Balch, A. L., Preparation and characterization of some hydroxy complexes of iron(III) porphyrins. *Inorganic Chemistry* **1982**, 21, (6), 2412.
55. Latos-Grazynski, L.; Cheng, R. J.; La Mar, G. N.; Balch, A. L., Oxygenation patterns for substituted meso-tetraphenylporphyrin complexes of iron(II). Spectroscopic detection of dioxygen complexes in the absence of amines. *Journal of the American Chemical Society* **1982**, 104, (22), 5992.
56. Collman, J. P.; Broring, M.; Fu, L.; Rapta, M.; Schwenninger, R.; Straumanis, A., Novel Protecting Strategy for the Synthesis of Porphyrins with Different Distal and Proximal Superstructures. *Journal of Organic Chemistry* **1998**, 63, (23), 8082.
57. Collman, J. P.; Rapta, M.; Broring, M.; Raptova, L.; Schwenninger, R.; Boitrel, B.; Fu, L.; L'Her, M., Close Structural Analogues of the Cytochrome c Oxidase Fe_{a3}/Cu_B Center

Show Clean $4e^-$ Electroreduction of O_2 to H_2O at Physiological pH. *Journal of the American Chemical Society* **1999**, 121, (6), 1387.

58. Collman, J. P.; Broring, M.; Fu, L.; Rapta, M.; Schwenninger, R., Imidazole Acid Chlorides: Preparation and Application in the Syntheses of Biomimetic Heme Models. *Journal of Organic Chemistry* **1998**, 63, (23), 8084.

59. Collman, J. P.; Brauman, J. I.; Doxsee, K. M.; Halbert, T. R.; Bunnenberg, E.; Linder, R. E.; LaMar, G. N.; Del Gaudio, J.; Lang, G.; Spartalian, K., Synthesis and characterization of "tailed picket fence" porphyrins. *Journal of the American Chemical Society* **1980**, 102, (12), 4182.

60. Lindsey, J. S.; Schreiman, I. C.; Hsu, H. C.; Kearney, P. C.; Marguerettaz, A. M., Rothmund and Adler-Longo reactions revisited: Synthesis of tetraphenylporphyrins under equilibrium conditions. *J. Org. Chem.* **1987**, 52, (5), 82.

61. Bettelheim, A.; White, B. A.; Raybuck, S. A.; Murray, R. W., Electrochemical polymerization of amino-, pyrrole-, and hydroxy-substituted tetraphenylporphyrins. *Inorg. Chem.* **1987**, 26, (7), 1009.

62. Bookser, B. C.; Bruce, T. C., Syntheses of quadruply two- and three-atom, aza-bridged, cofacial bis(5,10,15,20-tetraphenylporphyrins). *J. Am. Chem. Soc.* **1991**, 113, (11), 4208.

63. Ghiladi, R. A. Dioxygen reactivity of small molecule synthetic analogues for the the active sites of heme and copper containing enzymes. The Johns Hopkins University, Baltimore, 2001.

64. Ghiladi, R. A.; Kretzer, R. M.; Guzei, I.; Rheingold, A. L.; Neuhold, Y. M.; Hatwell, K. R.; Zuberbuhler, A. D.; Karlin, K. D., $(F_8TPP)Fe^{II}/O_2$ Reactivity Studies $\{F_8TPP = \text{Tetrakis}(2,6\text{-difluorophenyl})\text{porphyrinate}^{(2-)}\}$: Spectroscopic (UV-Visible and NMR) and Kinetic Study of Solvent-Dependent $(Fe/O_2 = 1:1 \text{ or } 2:1)$ Reversible O_2 -Reduction and Ferryl Formation. *Inorganic Chemistry* **2001**, 40, (23), 5754.

65. Walker, F. A., Proton NMR and EPR Spectroscopy of Paramagnetic Metalloporphyrins. In *The Porphyrin Handbook*, Kadish, K. M.; Smith, K. M.; Guillard, R., Eds. Academic Press: San Diego, 2000; Vol. 5, pp 81.

66. Walker, F. A.; Simonis, U., Proton NMR Spectroscopy of Model Hemes. In *NMR of Paramagnetic Molecules*, Berliner, L. J.; Reuben, J., Eds. Plenum Press: New York, 1993; Vol. 12, pp 133.

67. Gross, Z.; Kaustov, L., New efficient routes for the preparation of deuterated tetraarylporphyrins. *Tetrahedron Letters* **1995**, 36, (21), 3735.

68. Fajer, J.; Borg, D. C.; Forman, A.; Felton, R. H.; Vegh, L.; Dolphin, D., ESR studies of porphyrin p-cations: the $^2A_{1u}$ and $^2A_{2u}$ states. *Annals of the New York Academy of Sciences* **1973**, 206, 349.
69. Berto, T. C.; Praneeth, V. K. K.; Goodrich, L. E.; Lehnert, N., Iron-Porphyrin NO Complexes with Covalently Attached N-Donor Ligands: Formation of a Stable Six-Coordinate Species in Solution. *Journal of the American Chemical Society* **2009**, 131, (47), 17116.
70. Jakopitsch, C.; Kolarich, D.; Petutschnig, G.; Furtmüller, P. G.; Obinger, C., Distal side tryptophan, tyrosine and methionine in catalase-peroxidases are covalently linked in solution. *FEBS Letters* **2003**, 552, (2-3), 135.
71. Díaz, A.; Horjales, E.; Rudiño-Piñera, E.; Arreola, R.; Hansberg, W., Unusual Cys-Tyr Covalent Bond in a Large Catalase. *Journal of Molecular Biology* **2004**, 342, (3), 971.
72. Bhaskar, B.; Immoos, C. E.; Shimizu, H.; Sulc, F.; Farmer, P. J.; Poulos, T. L., A Novel Heme and Peroxide-dependent Tryptophan-tyrosine Cross-link in a Mutant of Cytochrome c Peroxidase. *Journal of Molecular Biology* **2003**, 328, (1), 157.
73. Chan, W. C.; White, P. D., *Fmoc solid phase peptide synthesis: a practical approach*. Oxford University Press: Oxford; New York, 2000.
74. Barr, D. P.; Gunther, M. R.; Deterding, L. J.; Tomer, K. B.; Mason, R. P., ESR Spin-trapping of a Protein-derived Tyrosyl Radical from the Reaction of Cytochrome c with Hydrogen Peroxide. *Journal of Biological Chemistry* **1996**, 271, (26), 15498.
75. Reinke, L. A.; Moore, D. R.; Sang, H.; Janzen, E. G.; Kotake, Y., Aromatic hydroxylation in PBN spin trapping by hydroxyl radicals and cytochrome P-450. *Free Radical Biology and Medicine* **2000**, 28, (3), 345.

APPENDIX

X-Ray Crystallography of 3.1 – Details on disorders

Pyridinium Disorder. The N-methyl pyridinium group bound to the C10 meso carbon exhibited an orientational disorder which can be described as a rotation about the C10-C29 bond vector. The angle between the disordered aromatic rings is 38.8°. The normalized occupancy for the major component refined to 0.696(7). A number of restraints were necessary to keep the refined parameters physically reasonable.

Iodide disorder. The sites for anions I2 and I3 were each disordered over 2 sites, designated I2' and I3'. The normalized occupancy for the major components for I2 and I3 refined to values 0.84(2) and 0.649(18) respectively. The distance between the I2 and I2' sites was 0.47 Å and 0.44 Å for the I3 and I3' sites.

Solvent Disorder. In the lattice there were three CHCl₃ molecules as well as a fractionally occupied methanol molecule of solvation which exhibited various types of disorders. The first solvent site (containing carbon C1S) exhibited an orientational disorder which can be described as a rotation about the C1S-C11 bond axis, giving rise to two different positions for Cl2 and Cl3, denoted as Cl2' and Cl3'. The major component refined to an occupancy of 0.665(10).

The second CHCl₃ of solvation exhibited disorder over two different positions in the unit cell with only atom Cl4 being common to both positions of the molecule. The carbon sites C2S and C2S' were 2.64 Å apart. The normalized occupancy for the major component refined to a value of 0.712(4).

The third CHCl₃ was also distributed over two positions in the lattice and in addition, the secondary position also occupied by a partial MeOH molecule. It was presumed that the

occupancy of the MeOH molecule and the primary chloroform site for were identical. This means, that when the chloroform molecule occupied the secondary site, there was no methanol in the lattice, and when the primary chloroform site was occupied the methanol molecule was also present. The chloroform sites shared in common only the atomic position occupied by Cl8. The carbon centers C3S and C3S' were 2.43 Å apart. The normalized occupancy of the major component refined to a value of 0.590(5).

The final difference map showed relatively large peaks (approximately $3 \text{ e}^-/\text{\AA}^3$) in the vicinity of the solvent molecules. However, a sensible chemical model was not apparent, and therefore any atomic density which may have been represented by the peaks were left out of the final model.

Copyright Permissions

Figure 1.1.

© Copyright World Health Organization (WHO), 2011. All Rights Reserved.

The information in the various pages of the WHO web site is issued by the World Health Organization for general distribution. The information presented is protected under the Berne Convention for the Protection of Literature and Artistic works, under other international conventions and under national laws on copyright and neighboring rights. Extracts of the information in the web site may be reviewed, reproduced or translated for research or private study but not for sale or for use in conjunction with commercial purposes. Any use of information in the web site should be accompanied by an acknowledgment of WHO as the source, citing the uniform resource locator (URL) of the article. Reproduction or translation of substantial portions of the web site, or any use other than for educational or other non-commercial purposes, require explicit, prior authorization in writing. Applications and enquiries should be addressed to the programme responsible for the page used.

Figure 1.3.

AMERICAN CHEMICAL SOCIETY LICENSE TERMS AND CONDITIONS

Feb 19, 2011

This is a License Agreement between Elke Feese ("You") and American Chemical Society ("American Chemical Society") provided by Copyright Clearance Center ("CCC"). The license consists of your order details, the terms and conditions provided by American Chemical Society, and the payment terms and conditions.

License Number	2605520088207
License Date	Feb 10, 2011
Licensed content publisher	American Chemical Society
Licensed content publication	Chemical Reviews
Licensed content title	Bioinorganic Photochemistry: Frontiers and Mechanisms
Licensed content author	Konrad Szaciłowski et al.
Licensed content date	Jun 1, 2005
Volume number	105
Issue number	6
Type of Use	Thesis/Dissertation
Format	Print and Electronic
Portion	Table/Figure/Micrograph
Number of Table/Figure/Micrographs	3

Author of this ACS article	No
Title of the thesis / dissertation	Development of Novel Photosensitizers for
Photodynamic Inactivation of Bacteria	
Expected completion date	Mar 2011
Estimated size(pages)	200

Figure 1.5.

I, the copyright holder of this work, hereby publish it under the following licenses: Permission is granted to copy, distribute and/or modify this document under the terms of the GNU Free Documentation License, Version 1.2 or any later version published by the Free Software Foundation; with no Invariant Sections, no Front-Cover Texts, and no Back-Cover Texts. A copy of the license is included in the section entitled *GNU Free Documentation License*.

Figure 1.8.

NATURE PUBLISHING GROUP LICENSE
TERMS AND CONDITIONS

Feb 19, 2011

This is a License Agreement between Elke Feese ("You") and Nature Publishing Group ("Nature Publishing Group") provided by Copyright Clearance Center ("CCC"). The license consists of your order details, the terms and conditions provided by Nature Publishing Group, and the payment terms and conditions.

License Number	2605491094221
License date	Feb 10, 2011
Licensed content publisher	Nature Publishing Group
Licensed content publication	Nature Reviews Microbiology
Licensed content title	Bacterial cell shape
Licensed content author	Matthew T. Cabeen and Christine Jacobs-
Wagner	
Licensed content date	Aug 1, 2005
Volume number	3
Issue number	8
Type of Use	reuse in a thesis/dissertation
Requestor type	academic/educational
Format	print and electronic
Portion	figures/tables/illustrations

Number of figures/tables/illustrations	1
High-res required	no
Figures	Figure 2 in original
Author of this NPG article	no
Title of your thesis / dissertation	Development of Novel Photosensitizers for
Photodynamic Inactivation of Bacteria	
Expected completion date	Mar 2011
Estimated size (number of pages)	200

Figure 1.9.

JOHN WILEY AND SONS LICENSE
TERMS AND CONDITIONS

Feb 19, 2011

This is a License Agreement between Elke Feese ("You") and John Wiley and Sons ("John Wiley and Sons") provided by Copyright Clearance Center ("CCC"). The license consists of your order details, the terms and conditions provided by John Wiley and Sons, and the payment terms and conditions.

License Number	2605491504075
License date	Feb 10, 2011
Licensed content publisher	John Wiley and Sons
Licensed content publication	Biopolymers
Licensed content title	Mode of action of linear amphipathic α -helical
antimicrobial peptides	
Licensed content author	Ziv Oren, Yechiel Shai
Licensed content date	451
End page	463
Type of use	Dissertation/Thesis
Requestor type	University/Academic
Format	Print and electronic
Portion	Figure/table
Number of figures/tables	1
Original Wiley figure/table number(s)	Figure 1
Will you be translating?	No

Figures 2.1, 2.2, 2.3 and Tables 2.1, 2.2, 2.4.

OXFORD UNIVERSITY PRESS LICENSE
TERMS AND CONDITIONS

Feb 26, 2011

This is a License Agreement between Elke Feese ("You") and Oxford University Press ("Oxford University Press") provided by Copyright Clearance Center ("CCC"). The license consists of your order details, the terms and conditions provided by Oxford University Press, and the payment terms and conditions.

License Number	2605500812174
License date	Feb 10, 2011
Licensed content publisher	Oxford University Press
Licensed content publication	Journal of Antimicrobial Chemotherapy
Licensed content title	Highly efficient in vitro photodynamic inactivation of Mycobacterium smegmatis
Licensed content author	Elke Feese, Reza A. Ghiladi
Licensed content date	10/01/2009
Type of Use	Thesis/Dissertation
Title of your work	Development of Novel Photosensitizers for Photodynamic Inactivation of Bacteria

Figure 3.1.

AMERICAN CHEMICAL SOCIETY LICENSE
TERMS AND CONDITIONS

Feb 26, 2011

This is a License Agreement between Elke Feese ("You") and American Chemical Society ("American Chemical Society") provided by Copyright Clearance Center ("CCC"). The license consists of your order details, the terms and conditions provided by American Chemical Society, and the payment terms and conditions.

License Number	2605510107914
License Date	Feb 10, 2011
Licensed content publisher	American Chemical Society
Licensed content publication	Chemical Reviews
Licensed content title	Cellulose Nanocrystals: Chemistry, Self- Assembly, and Applications
Licensed content author	Youssef Habibi et al.
Licensed content date	Jun 1, 2010
Volume number	110

Issue number	6
Type of Use	Thesis/Dissertation
Format	Print and Electronic
Portion	Table/Figure/Micrograph
Number of Table/Figure/Micrographs	8
Author of this ACS article	No
Order reference number	6
Title of the thesis / dissertation	Development of Novel Photosensitizers for
Photodynamic Inactivation of Bacteria	
Expected completion date	Mar 2011
Estimated size(pages)	200

Figure 5.3.

AMERICAN CHEMICAL SOCIETY LICENSE
TERMS AND CONDITIONS

Feb 26, 2011

This is a License Agreement between Elke Feese ("You") and American Chemical Society ("American Chemical Society") provided by Copyright Clearance Center ("CCC"). The license consists of your order details, the terms and conditions provided by American Chemical Society, and the payment terms and conditions.

License Number	616641355647
License Date	Feb 26, 2011
Licensed content publisher	American Chemical Society
Licensed content publication	Journal of the American Chemical Society
Licensed content title	Correlation between Isoniazid Resistance and
Superoxide Reactivity in Mycobacterium tuberculosis KatG	
Licensed content author	Reza A. Ghiladi et al.
Licensed content date	Sep 1, 2005
Volume number	127
Issue number	
Type of Use	Thesis/Dissertation
Format	Print and Electronic
Portion	Table/Figure/Micrograph
Number of Table/Figure/Micrographs	1
Author of this ACS article	No
Title of the thesis / dissertation	Development of Novel Photosensitizers for
Photodynamic Inactivation of Bacteria	
Expected completion date	Mar 2011
Estimated size(pages)	200

Figure 5.13.

AMERICAN CHEMICAL SOCIETY LICENSE
TERMS AND CONDITIONS

Feb 26, 2011

This is a License Agreement between Elke Feese ("You") and American Chemical Society ("American Chemical Society") provided by Copyright Clearance Center ("CCC"). The license consists of your order details, the terms and conditions provided by American Chemical Society, and the payment terms and conditions.

License Number	2605511227072
License Date	Feb 10, 2011
Licensed content publisher	American Chemical Society
Licensed content publication	Biochemistry
Licensed content title	Role of the Met–Tyr–Trp Cross-Link in Mycobacterium tuberculosis Catalase-Peroxidase (KatG) As Revealed by KatG(M255I)†
Licensed content author	Reza A. Ghiladi et al.
Licensed content date	Nov 1, 2005
Volume number	44
Issue number	46
Type of Use	Thesis/Dissertation
Requestor type	Not specified
Format	Print and Electronic
Portion	Table/Figure/Micrograph
Number of Table/Figure/Micrographs	11
Author of this ACS article	No
Title of the thesis / dissertation	Development of Novel Photosensitizers for Photodynamic Inactivation of Bacteria
Expected completion date	Mar 2011
Estimated size(pages)	200